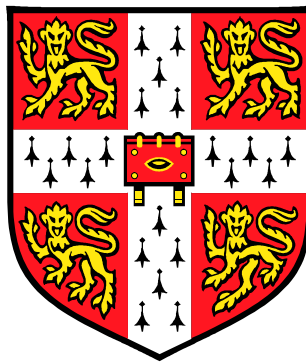




# ***Critical Current Anisotropy in High Temperature Superconductors***

*John Hay Durrell*

Jesus College  
Cambridge



A dissertation submitted for the degree of Doctor of Philosophy at the  
University of Cambridge

April 2001

## **Table of Contents**

<b>1. INTRODUCTION .....</b>	<b>1</b>
1.1. BACKGROUND.....	1
1.2. SUBJECT AND AIMS .....	2
1.3. OVERVIEW OF THIS THESIS.....	3
1.4. BIBLIOGRAPHY .....	4
<b>2. FLUX LINES AND CRITICAL CURRENTS IN SUPERCONDUCTORS.....</b>	<b>5</b>
2.1. THEORETICAL BASIS OF SUPERCONDUCTIVITY .....	5
2.2. MAGNETIC FIELDS IN SUPERCONDUCTORS .....	7
2.3. FLUX LINE PINNING .....	12
2.4. FLUX LINES IN ANISOTROPIC SUPERCONDUCTORS .....	21
2.5. BIBLIOGRAPHY .....	27
<b>3. SAMPLE PREPARATION AND EXPERIMENTAL TECHNIQUES .....</b>	<b>30</b>
3.1. THIN FILM HIGH $T_c$ SUPERCONDUCTORS .....	30
3.2. SAMPLE PREPARATION .....	37
3.3. FILM CHARACTERISATION .....	40
3.4. MEASUREMENT RIG.....	43
3.5. CONCLUSION.....	51
3.6. BIBLIOGRAPHY .....	51
<b>4. CRITICAL CURRENTS IN VICINAL YBCO FILMS .....</b>	<b>54</b>
4.1. PREVIOUS EXPERIMENTAL MEASUREMENTS.....	54
4.2. SAMPLE AND MEASUREMENT DETAILS.....	69
4.3. $J_c(\theta)$ MEASUREMENTS.....	71
4.4. $J_c(\phi)$ MEASUREMENTS.....	80
4.5. $J_c(B)$ MEASUREMENTS .....	83
4.6. FIB INVESTIGATION OF TRACK WIDTH EFFECT.....	84
4.7. DISCUSSION .....	85
4.8. CONCLUSION.....	86
4.9. BIBLIOGRAPY.....	87
<b>5. MEASUREMENTS ON DE-OXYGENATED VICINAL YBCO FILMS .....</b>	<b>90</b>

5.1. INTRODUCTION .....	90
5.2. SAMPLE PREPARATION AND CHARACTERISATION.....	93
5.3. RESULTS .....	95
5.4. DISCUSSION .....	99
5.5. CONCLUSIONS.....	100
5.6. BIBLIOGRAPHY .....	100
<b>6. CRITICAL CURRENT MEASUREMENTS ON <i>c</i>-AXIS FILMS .....</b>	<b>102</b>
6.1. INTRODUCTION .....	102
6.2. SAMPLE DETAILS .....	108
6.3. RESULTS AND DISCUSSION .....	110
6.4. CONCLUSION.....	116
6.5. BIBLIOGRAPHY .....	117
<b>7. CRITICAL CURRENT ANISOTROPY IN THIN FILM <math>\text{Bi}_2\text{Sr}_2\text{CaCu}_2\text{O}_{8-x}</math>.....</b>	<b>118</b>
7.1. THE FLUX LINE LATTICE IN BSCCO .....	118
7.2. SAMPLE DESCRIPTION.....	121
7.3. RESULTS .....	124
7.4. DISCUSSION .....	131
7.5. CONCLUSION.....	133
7.6. BIBLIOGRAPHY .....	134
<b>8. CONCLUSIONS AND FURTHER WORK.....</b>	<b>136</b>
8.1. CONCLUSIONS.....	136
8.2. FURTHER WORK .....	137
8.3. BIBLIOGRAPHY .....	138
<b>APPENDIX A - LIST OF SAMPLES STUDIED .....</b>	<b>139</b>
<b>APPENDIX B – DIAGRAMS OF THE MEASUREMENT GEOMETRY .....</b>	<b>140</b>
<b>APPENDIX C – PUBLICATIONS .....</b>	<b>141</b>

***Declaration***

I declare that, except where otherwise stated, this dissertation is the result of my own work and includes nothing which is the outcome of work done in collaboration. No part of this dissertation has been submitted at Cambridge or any other University for a degree, diploma or other qualification. (c) John Durrell 2001.

John Durrell

Cambridge

April 2001

## **Acknowledgements**

My acknowledgments must, naturally, start with expressing my profound thanks to my supervisor Professor Jan E. Evetts. Needless to say without his guidance, good humour and confidence during this work it would not exist. I am grateful for having had the opportunity to work in such a well-balanced and friendly research group.

I should express my appreciation to the Interdisciplinary Research Centre in Superconductivity and the Department of Materials Science and Metallurgy for the award of a research council grant, financial support in my fourth year and the provision of experimental facilities.

Dr Peter Berghuis introduced me to the experimental techniques required and helped considerably with my understanding of all things flux related. His particular sense of humour and, most importantly, stoicism in the face of experimental adversity proved invaluable.

Although he is no longer a member of the group, I owe a significant debt to Robert Herzog who built the first incarnation of the two-axis goniometer, both for his attention to detail and willingness to provide technical support on the occasions when all seemed lost. Without his help it would have been impossible to modernise the computer control of the rig.

I am grateful to Zoe Barber who, as the academic responsible for the group thin film deposition lab, ensured that I was well supplied with experimental samples from the group's facilities. Within the group, I would like to thank Ed Tarte, Gary Gibson, Annette Bramley and Lawrence Mechin for growing me superconducting samples, and for introducing me to thin film deposition. Noel Rutter was kind enough to perform X-Ray measurements on some of my samples and provide many hours of stimulating discussion.

I am grateful to Mark Blamire for access to the clean room facilities used to pattern my chips. I should like to thank Gavin Burnell and Wilfred Booij for helping me with the black art of thin film processing.

I am grateful to Matthew Dodgson for taking the time to discuss various aspects of Chapter 7 with me.

Through the European Community 'SUPERCURRENT' programme I was fortunate to be able to enter into a fruitful collaboration with the applied physics group of the Johannes Kepler Universität, Linz. I would like to express my thanks to Roman Rössler, Johannes Pedarnig and Professor Dieter Bäuerle both for supplying samples and engaging in invaluable discussions about this work. I am indebted to another member of the SUPERCURRENT

collaboration, Christian Jooss, of the University of Göttingen, both for the MO measurements he performed on several of my samples and for very illuminating discussions of my results.

I am grateful to Peter Czerwinka of the university of Nottingham for providing me with an anti-phase boundary rich sample.

I should like to express my appreciation for financial support from the Cambridge Philosophical Society which enabled an extension to the time available to me for experimental work. I am also grateful to Jesus College for assistance towards the cost of attending IWCC9-99.

Needless to say I owe a debt of gratitude to many other people, including Philip McBrien, Richard Moseley, Neil Todd, Cliff Elwell, Rachel Speaks, Robert Kinsey, Dolores Vasquez-Navarro, Mike Hogg, Bernard Zeimetz, Lawrence Wright, Robert Hadfield, Ashish Garg, Maria Glew, Moon-Ho Jo, Rumen Tomov, Bartek Glowacki, Andreas Diaz, Gary Chapman and Nadia Stelmashenko.

I would also like to thank Diana for her unstinting support over the past three years. Finally, I am grateful to my parents for their indulgence over 7 expensive years!

## Summary

After nearly 15 years of research effort, High Temperature Superconductors (HTS) are finding a wide range of practical applications. A clear understanding of the factors controlling the current carrying capacity of these materials is a prerequisite to their successful technological development. The critical current density ( $J_c$ ) in HTS is directly dependent on the structure and pinning of the Flux Line Lattice (FLL) in these materials.

This thesis presents an investigation of the  $J_c$  anisotropy in HTS. The use of thin films grown on off  $c$ -axis (vicinal) substrates allowed the effect of current directions outside the cuprate planes to be studied. With this experimental geometry Berghuis, *et al.* (Phys. Rev. Lett. **79**, *12*, pg. 2332) observed a striking *flux channelling* effect in vicinal  $\text{YBa}_2\text{Cu}_3\text{O}_{7-\delta}$  (YBCO) films. By confirming, and extending, this observation, it is demonstrated that this is an intrinsic effect. The results obtained, appear to fit well with the predictions of a field angle dependent cross-over from a three dimensional rectilinear FLL to a kinked lattice of strings and pancakes. The pinning force density for movement of strings inside the cuprate planes is considerably less than that on vortex pancake elements. When the FLL is entirely string-like this reduced pinning leads to the observed channelling minima. It is observed that anti-phase boundaries enhance the  $J_c$  in vicinal YBCO films by strongly pinning vortex strings.

The effect on the FLL structure cross-over of increasing anisotropy has been elucidated using de-oxygenated vicinal YBCO films. Intriguingly, the counter intuitive prediction that the range of applied field angle for which the kinked lattice is fully developed reduces with increasing anisotropy, appears to be confirmed.

Although vortex channelling cannot be observed in  $c$ -axis YBCO films, the pinning force density for vortex string channelling has been extracted by observing string dragging. By studying the effect of rotating the applied field at a constant angle to the cuprate planes, it is possible to observe the cross-over into the string pancake regime in  $c$ -axis films. In the 3D region, the observed behaviour is well explained by the anisotropic Ginzburg-Landau model. Measurements were also made on thin films of the much more anisotropic  $\text{Bi}_2\text{Sr}_2\text{CaCu}_2\text{O}_{8+x}$  material, grown on vicinal substrates. The absence of any flux channelling effect and clear adherence to the expected Kes-Law behaviour in the observed  $J_c$  characteristics does not provide evidence for the existence of the predicted 'crossing lattice' in  $\text{Bi}_2\text{Sr}_2\text{CaCu}_2\text{O}_{8+x}$ .

*“Owl explained about flux pinning and creep. He had explained this to Pooh and Christopher Robin once before, and had been waiting ever since for a chance to do it again, because it is a thing you can easily explain twice before anybody knows what you are talking about”*

Blatter *et al.* (1994) Rev. Mod. Phys. **66** (4) pp 1129, with apologies to A.A. Milne

# 1. Introduction

## 1.1. Background

Nearly 15 years after the discovery of the family of cuprate based high temperature superconductors (HTS) an increasing number of practical applications of these materials are appearing (Moore 1999, Evetts, *et al.* 2000). This is due to the considerable research effort centred on solving the myriad technological problems associated with the commercialisation of HTS. This technological progress has gone hand in hand with a deeper physical understanding of the behaviour of HTS. For example, the main limit to large engineering critical current densities in continuous conductors is the presence of high angle grain boundaries. Thus a thorough understanding of the physics of weak links in HTS superconductors has a direct bearing on the application of HTS.

HTS are significantly different to conventional (LTS) superconductors<sup>◇</sup>. The nature of the electron pairing is still not clear, except that it appears not to be the *s*-wave phonon interaction found in LTS materials (Tsuei, *et al.* 2000). HTS exhibit large anisotropies in both their physical and superconducting properties, and large values of the Ginzburg-Landau parameter  $\kappa$  ( $\sim 100$ ). The second critical field for HTS materials can be almost an order of magnitude higher than that found in LTS (LTS magnets can now reach  $\sim 22$  T at 4.2 K whereas  $\text{YBa}_2\text{Cu}_3\text{O}_{7-\delta}$  has an upper critical field of at least 80 T). In spite of these differences the magnetic behaviour of HTS may be described using the rich theoretical structure stemming from the Ginzburg-Landau phenomenological theory (Blatter, *et al.* 1994). G-L theory has been extended to both the case of a homogenous yet anisotropic superconductor (Blatter 1992) and to that of two-dimensional superconducting layers with Josephson coupling between them (Lawrence and Doniach 1970).

The compound  $\text{YBa}_2\text{Cu}_3\text{O}_{7-\delta}$  is one of the most promising for commercial applications. It is the least anisotropic and has a high  $H_{c2}$ . In addition it suffers to a much lesser degree than most HTS to the suppression of the practical upper critical field due to the irreversibility effect. It behaves neither purely as a layered two dimensional material nor as a homogenous

---

<sup>◇</sup> Superconductivity has recently been reported at  $\sim 39$  K in  $\text{MgB}_2$ . It is as yet unclear whether this material has more in common with HTS or represents a conventional superconductor with an unusually high  $T_c$ .

anisotropic superconductor. It is the rich behaviour of the Flux Line Lattice in  $\text{YBa}_2\text{Cu}_3\text{O}_{7-\delta}$  that this thesis seeks to elucidate.

## 1.2. Subject and Aims

$\text{YBa}_2\text{Cu}_3\text{O}_{7-\delta}$  (YBCO) exhibits distinct differences in the structure of its flux line lattice compared to more anisotropic superconductors. For example in  $\text{Bi}_2\text{Sr}_2\text{CaCu}_2\text{O}_{8+x}$  (BSCCO 2212) only the component of the field perpendicular to the cuprate layers affects the critical current density (Schmitt, *et al.* 1991). This is not the case in YBCO where the critical current is found to depend on both the inclination of the magnetic field with respect to the cuprate planes,  $\theta$ , and the rotation of the field about the  $c$ -axis,  $\phi$ , (Nishizaki, *et al.* 1993). It has been suggested (Blatter, *et al.* 1994) that there is a cross-over in YBCO between an anisotropic lattice of Abrikosov vortices to a kinked lattice regime consisting of joined ‘string’ and ‘pancake’ vortices respectively perpendicular to and parallel to the cuprate planes. This cross-over is expected to be both temperature and field angle dependent.

If the FLL structure is dependent on the angle between the applied field and the cuprate planes this has the important consequence that a scaling law based purely on one model of the FLL will not describe the variation in  $J_c$  over the entire angular range. This cross-over can be investigated by making high resolution measurements of the critical current behaviour in YBCO.

The analysis of such results can be greatly assisted by using an experimental system where the applied current is not parallel to the crystal axes. Indeed, it has been shown that effects completely masked in  $c$ -axis films may be investigated using thin films grown on mis-cut (vicinal) substrates (Berghuis, *et al.* 1997). For convenience such films are referred to as ‘vicinal’ films in this thesis.

The proposed FLL structure cross-over in YBCO is dependent on the anisotropy of its superconducting parameters. It is possible to adjust this anisotropy by reducing the oxygen doping. This reduces the  $T_c$  of the material and increases its anisotropy. Measurements on de-oxygenated YBCO should shed light on this relationship.

The aim of this thesis is therefore to elucidate the structure of and pinning forces on the Flux Line Lattice in HTS. This is achieved through measurements of the variation of the transport critical current density with temperature, magnetic field magnitude and magnetic field direction.

### **1.3. Overview of this Thesis**

An introduction to the theory of superconductivity is presented in Chapter 2. The extension of the Ginzburg-Landau theory to the cases of layered and anisotropic superconductors is discussed.

In Chapter 3 the film growth and experimental techniques used to collect the data presented in this thesis are described. The LabVIEW based measurement system implemented by the author for this work is described. The use of such an automated measurement system allows large amount of accurate and meaningful data to be collected in much less time than is required for manual techniques. This has allowed a much larger range of experimental parameters to be explored than would otherwise have been possible. Additionally every  $J_c$  value is determined from a current versus voltage ( $IV$ ) characteristics providing considerable improvement in accuracy over criterion tracking or resistive methods of determining  $J_c$ .

Chapter 4 concerns measurements performed on YBCO thin films grown on tilted vicinal substrates. When the direction of current flow is tilted away from the crystal axes it becomes much easier to separate different contributions to the pinning of and Lorentz force on the Flux Line Lattice. As has been previously discussed, this allows effects to be explored that are obscured if measurements are performed on  $c$ -axis orientated films. The critical current behaviour and thus the Flux Line Lattice (FLL) is explored at a range of fields, temperatures and field orientations. This allows the flux channelling effect and, more broadly, the cross-over from the Abrikosov FLL to the string/pancake FLL to be studied.

Measurements on de-oxygenated vicinal films are described in Chapter 5. As YBCO is de-oxygenated its anisotropy increases. This effect of this on both the position of the FLL structure cross-over and the magnitude of the vortex string channelling effect is investigated.

In Chapter 6 measurements on  $c$ -axis oriented films are described. The effect of changing the Lorentz force direction at a constant field angle, and thus constant FLL structure, is studied. From these measurements it is possible to indirectly observe flux line channelling and deduce a vortex string pinning force density. Measurements on  $c$ -axis films underline the observation that no one angular scaling model described the entire range of angular behaviour in YBCO.

In Chapter 7, to provide a contrast, results on vicinal films of the highly anisotropic BSCCO material are described. These are shown to be qualitatively different from the behaviour of de-oxygenated YBCO. These results are compared to the results of the crossing lattice model (Koshelev 1999).

## **1.4. Bibliography**

- Berghuis, P., E. DiBartolomeo, G. A. Wagner and J. E. Evetts (1997). Phys. Rev. Lett. **79**(12): 2332-2335.
- Blatter, G., M. V. Feigelman, V. B. Geshkenbein, A. I. Larkin and V. M. Vinokur (1994). Rev. Mod. Phys. **66**(4): 1125-1388.
- Blatter, G., Geshkenbein, V.B. and Larkin, A.I. (1992). Phys. Rev. Lett. **68**(6): 875-878.
- Evetts, J. E. and B. A. Glowacki (2000). Supercon. Sci. Technol. **13**(5): 443-447.
- Koshelev, A. E. (1999). Physical Review Letters **83**(1): 187-190.
- Lawrence, W. E. and S. Doniach (1970). Proceedings of the 12th International Conference on Low Temperature Physics, Kyoto, Keigaku, Tokyo.
- Moore, T. (1999). Epri Journal **24**(1): 8-15.
- Nishizaki, T., F. Ichikawa, T. Fukami, T. Aomine, T. Terashima and Y. Bando (1993). Physica C **204**(3-4): 305-314.
- Schmitt, P., P. Kummeth, L. Schultz and G. Saemannschenko (1991). Phys. Rev. Lett. **67**(2): 267-270.
- Tsuei, C. C. and J. R. Kirtley (2000). Rev. Mod. Phys. **72**(4): 969-1016.

## 2. Flux Lines and Critical Currents in Superconductors

*This Chapter reviews basic superconductivity theory, the phenomenological Ginzburg-Landau theory describing fields in superconductors, and the extension of Ginzburg-Landau theory to anisotropic and layered superconductors. The majority of the material described was developed to describe the behaviour of conventional superconductors, but is equally applicable to high  $T_c$  materials. Theories describing the behaviour of the flux line lattice in the presence of a tilted external field are reviewed.*

### 2.1. Theoretical Basis of Superconductivity

#### 2.1.1. Basic Properties

A superconducting material exhibits zero-resistance below a *critical temperature* ( $T_c$ ). This property was first noted at 4.2 K in resistivity measurements on mercury by Kammerling Onnes (1911). In the absence of impurity scattering a conventional metal would also be expected to exhibit no resistance at 0 K. The phenomenon of superconductivity exhibits further characteristic properties indicating that it is a distinct thermodynamic state.

Meissner noted that when a superconductor is cooled magnetic flux is expelled from the bulk of the sample (Meissner and Ochsenfeld 1933). A purely ‘zero-resistance’ material would not be expected to do this, moreover such a material would be expected to set up currents to prevent the internal flux changing with variation in the magnitude of the external field. Additionally, superconductivity is observed to be suppressed with the application of an external field (Onnes 1914) above a certain critical value  $H_c$ . The value of  $H_c^*$ , the thermodynamic *critical field*, can be defined in terms of the difference between the free energy densities of the normal and superconducting states. Equation (2.1) is valid for a long thin superconductor in a parallel field; other geometries are discussed in section 2.2.3:

$$\frac{\mu_0 H_c^2(T)}{2} = f_n(T) - f_s(T) \quad (2.1)$$

---

\* In this thesis  $\mathbf{H}$  denotes the macroscopic vector field and the quantity  $\mathbf{B}$  is the average macroscopic flux density related by  $\mathbf{B} = \mu_0 \mathbf{H}$  in free space. The quantity  $\mathbf{h}$  is used to denote the microscopic flux density.

This observation implies a limitation on the current carrying capacity of the superconducting state. Only a finite current can be carried in a superconducting wire; since at the *critical current* ( $I_c$ ) the *self field* generated by a current flowing in a wire will exceed  $H_c$  at the surface of the wire. The value of  $I_c$  is given by Silsbee's rule, where  $r$  is the radius of the wire:

$$I_c = 2\pi r H_c \quad (2.2)$$

### 2.1.2. The London Model

Two equations describing electrodynamics in superconductors were proposed by F. and H. London (1935a). This model is not derived from physical principles, but rather justified from observations of behaviour, it is therefore a phenomenological theory.

London (1935b) postulated that the supercurrent is carried by *superelectrons*. Defining  $m$  to be the mass of the superelectrons,  $e$  their charge and  $\langle \mathbf{v}_s \rangle$  their mean velocity and given a magnetic vector potential  $\mathbf{A}$  the canonical momentum  $\langle \mathbf{p} \rangle$  is given by equation (2.3). For the ground state of the superelectrons it is postulated that the canonical momentum is zero.

$$\langle \mathbf{p} \rangle = m\mathbf{v}_s + e\mathbf{A} \quad (2.3)$$

If it is assumed that this ground state persists the equation

$$\mathbf{v}_s = -e\mathbf{A}/m \quad (2.4)$$

may be written. Given a superelectron number density  $n_s$  the supercurrent density  $\mathbf{J}_s$  may be derived:

$$\mathbf{J}_s = n_s e \langle \mathbf{v}_s \rangle = -n_s e^2 \mathbf{A}/m \quad (2.5)$$

From the definition of the vector potential  $\text{curl}\mathbf{A}=\mathbf{B}$  and with no electrostatic potential  $\mathbf{E} = -\partial\mathbf{A}/\partial t$ . By choosing a specific gauge, the 'London gauge' where  $\text{div}\mathbf{A}=0$  and  $\text{div}\mathbf{J}=0$ , equation (2.5) may be rewritten to give the London equations where the London parameter,  $\Lambda$ , is given by  $\Lambda=m/n_s e^2$ :

$$\mathbf{h} = -\text{curl}(\Lambda\mathbf{J}_s) \quad (2.6)$$

$$\mathbf{E} = \frac{\partial}{\partial t}(\Lambda\mathbf{J}_s) \quad (2.7)$$

Equation (2.7) states that in a constant electric field  $\mathbf{E}$ , the current density of the superconducting electrons  $\mathbf{J}_s$  will increase continuously. This equation thus expresses the zero-resistance property of superconductors.

Neglecting any currents other than the supercurrent, using the Maxwell equation  $\mu_0\mathbf{J}_s=\text{curl}\mathbf{h}$  with equation (2.6), and substituting  $\lambda_L^2=m/\mu_0 n_s e^2$  leads to the equation describing screening in superconductors:

$$\nabla^2 \mathbf{h} - \frac{1}{\lambda_L^2} \mathbf{h} = 0 \quad (2.8)$$

Equation (2.8) may be solved in one dimension to give the following equation for the local penetration of an external magnetic field into a superconductor:

$$h(x) = h_0 e^{-x/\lambda_L} \quad (2.9)$$

The London penetration depth,  $\lambda_L$ , is therefore the characteristic length for the penetration of magnetic field into a superconductor..

### 2.1.3. BCS Theory

The Bardeen, Cooper and Schrieffer (BCS) theory (Bardeen, *et al.* 1957) is a complete quantum mechanical description of superconductivity. The details of the theory are complex and only applies to conventional low  $T_c$  superconductors (LTS). Consequently, only an outline of the theory will be discussed here. Crucially, the London model can be shown to be a limiting case of the BCS theory (Schrieffer and Tinkham 1999) and the Ginzburg-Landau phenomenological theory described in section 2.2.1 can be derived from it (Gor'kov 1959).

The BCS theory attributes the supercurrent to Cooper electron pairs. The electron pairs form due to interactions with vibrations, phonons, in the lattice of the superconductor. The exact nature of the pairing interaction in HTS has not been determined. This interaction gives rise to an attractive potential between pairs of electrons. The electron pairs occupy a condensed momentum state in which the Cooper pairs all have the same pair momentum  $p = \hbar s$ , where  $s$  represents the momentum due to the supercurrent. Furthermore each pair occupies a volume characterised by the BCS coherence length  $\xi_0$ . The BCS theory is discussed fully in several reference works: (Bardeen 1992, Tinkham 1996)

## 2.2. Magnetic Fields in Superconductors

### 2.2.1. The Ginzburg-Landau Phenomenological Theory

Landau (1937) developed a general theory of phase transitions, from which he extrapolated a theory for the superconducting-normal phase transition. Landau argued that the transition from the normal to the superconducting state occurred when the free energy of the superconducting phase drops below that of the normal phase. He also noted that phase transitions often depend on some ordering parameter. Thus the free energy density should be some function of an ordering parameter, the form of this dependence giving the order of the phase transition.

Ginzburg and Landau developed Landau's original theory by postulating a superconducting order parameter (Ginzburg and Landau 1950). An order parameter based on the superconducting charge carrier number density  $n_p$  was suggested. They defined the proposed order parameter  $\Psi(\mathbf{r})$  by normalising it so that

$$\int_{-\infty}^{\infty} \Psi \Psi^* dV = n_p \quad (2.10)$$

where the superscript '\*' indicates a complex conjugate. They also introduced the concept that the free energy might also depend on the derivative of  $\Psi$  in space. By minimising their postulated free-energy equation, where  $\alpha$  and  $\beta$  are functions of  $T$ ,  $F_n$  the normal state free energy,  $B_E$  the externally applied field and  $\epsilon$  is a constant,

$$F = F_n + \int_V \alpha \Psi^* \Psi + \frac{1}{2} \beta (\Psi^* \Psi)^2 + \epsilon \left| \nabla \Psi - \frac{2e}{i\hbar} \mathbf{A} \Psi \right|^2 dV + \int \frac{1}{2\mu_0} (B - B_E)^2 dV \quad (2.11)$$

with respect to small changes in  $\Psi$  and with respect to the magnetic field the two *Ginzburg-Landau equations* may be obtained. The first equation is an energy eigenvalue equation for all points inside a superconductor:

$$\frac{1}{2m} (-i\hbar \nabla + 2e\mathbf{A})^2 \Psi + (\alpha + \beta \Psi^* \Psi) \Psi = 0 \quad (2.12)$$

The second equation describes the current density in terms of a quantum mechanical probability density flow:

$$\mathbf{J}_s = \frac{ie\hbar}{m} (\Psi^* \nabla \Psi - \Psi \nabla \Psi^*) - \frac{4e^2}{m} \mathbf{A} \Psi \Psi^* \quad (2.13)$$

Ginzburg and Landau also introduced a boundary condition which states that at the edge of a superconductor:

$$i\hbar \nabla \Psi + 2e\mathbf{A} \Psi = 0 \quad (2.14)$$

From equations (2.12) and (2.13) two characteristic lengths may be extracted. The Ginzburg-Landau penetration depth,  $\lambda$ , is given by the following equation:

$$\lambda = \sqrt{\frac{m\beta}{4\mu_0 e^2 |\alpha|}} \quad (2.15)$$

and the Ginzburg-Landau coherence length,  $\xi$ , by:

$$\xi = \sqrt{\frac{\hbar^2}{2m|\alpha|}} \quad (2.16)$$

The Ginzburg-Landau penetration depth is, like the London penetration depth discussed in section 2.1.2, a characteristic length for the decay of magnetic field in a superconductor. The

coherence length  $\xi$  is a characteristic length for the decay of small perturbations in the superconducting order parameter  $\Psi$ . The coherence length may also be thought of as a characteristic length describing the spatial extent of the superconducting charge carriers.

### 2.2.2. Type II Superconductivity

Solutions of the Ginzburg-Landau equations fall into two groups depending on the sign of the energy of the normal state–superconducting state interface. Abrikosov (1957) noted that for values of the *Ginzburg-Landau parameter*,  $\kappa = \lambda/\xi$ , less than  $1/\sqrt{2}$  the surface energy is positive and the Meissner effect is observed. Such materials are termed Type I superconductors.

For values of  $\kappa$  greater than  $1/\sqrt{2}$  Abrikosov predicted that magnetic flux would be expected to penetrate into the superconductor in the form of filaments. As the surface energy in this case is negative the lowest energy state is that with the longest normal-superconducting boundary. The equilibrium state thus consists of large number of filaments each containing one flux quantum:

$$\Phi_0 = \frac{h}{2e} \quad (2.17)$$

These materials are termed Type II superconductors.

Type II superconductors exhibit Type-I like superconducting behaviour up to a first critical field  $H_{c1}$ . Above this field flux penetrates into the material, the flux lines (or *flux vortices*) are screened by induced supercurrents. Above a second critical field,  $H_{c2}$ , all superconducting behaviour is suppressed. The second critical field is reached where the areas of normal material associated with each *flux vortex* overlap.

### 2.2.3. The Intermediate State

Although the shortest possible normal-superconducting boundary is energetically favourable in Type I superconductors, it is possible to observe an *intermediate* state in Type I superconductors where flux penetrates the superconductor. If a Type I superconductor is not in the form of a plate parallel to the field, flux may penetrate even though the applied field is less than the thermodynamic critical field  $H_c$ . These *demagnetising* effects are due to compression of flux lines, the local field at the surface of the sample exceeding  $H_c$ . The applied field is not, however, sufficient to maintain the entire volume in the normal state. Experimentally, the superconducting material is seen to contain interpenetrating regions of normal and superconducting states

The demagnetising factor  $\eta$  can be shown to be  $1/3$  for a sphere and  $1$  for an infinite plate perpendicular to the field. For applied fields such that  $1-\eta < H/H_c < 1$  a sample will contain alternating normal and superconducting regions. The intermediate state may also be observed in current carrying wires subject to a self field.

#### 2.2.4. The Flux Line

Each flux line that nucleates in a Type II superconductor is surrounded by a circulating current which screens the rest of the superconductor. It is these circulating currents that give rise to the term flux vortex. The screening currents, and the local field  $\mathbf{h}$ , extend over the characteristic length  $\lambda$ . The superconducting order parameter falls to zero with a characteristic length  $\xi$ .

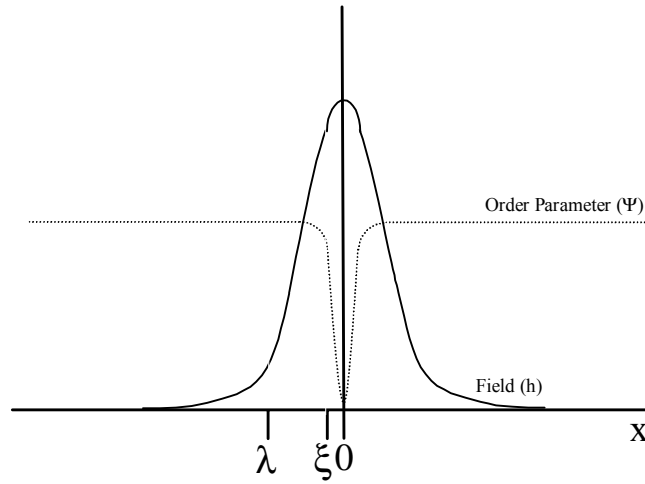


Figure 2.1 Cross section of a flux vortex showing the spatial variation of  $\mathbf{h}$  and  $\Psi$ .

In the limit of large values of  $\kappa$  it can be assumed that the vortex possesses a normal state core of diameter  $\xi$ . In this high  $\kappa$  limit the order parameter will, if the vortices are widely spaced, be  $\sim 1$  outside the vortex cores. This regime is termed the *London limit* since the London equations may be used to describe the behaviour of the superconductor outside the core. This limit is particularly applicable for the HTS materials which exhibit large values of  $\kappa$ .

Given the London limit it is possible to write an equation describing the variation of the microscopic field  $\mathbf{h}$  outside the core due to an isolated vortex. Equation (2.6) is modified to include a term to account for the flux in the vortex (Tinkham, 1996), where  $\mathbf{z}$  is a unit vector along the axis of the vortex and  $\int \delta(\mathbf{r}) d\mathbf{r} = 1$  inside the core:

$$\Lambda \text{curl} \mathbf{J} + \mathbf{h} = \hat{\mathbf{z}} \Phi_0 \delta(\mathbf{r}) \quad (2.18)$$

From this an equation may be derived giving  $\mathbf{h}(\mathbf{r})$ . The spatial dependence of  $\mathbf{h}(\mathbf{r})$  is  $e^{-r/\lambda}$  as  $|r| \rightarrow \infty$  and  $\ln(\lambda/r)$  for  $\xi \ll |r| \ll \lambda$ .

When considering the critical field at which flux lines first nucleate into a Type II superconductor,  $H_{c1}$ , it is essential to know the line energy associated with each flux vortex. At  $H_{c1}$  the free energy of the system does not change when a vortex is introduced. The line energy of the vortex must therefore be equal to the magnetic energy associated with the vortex. An equation for  $H_{c1}$  in terms of the line energy of the vortex  $\varepsilon_{\text{core}}$  may then be written:

$$H_{c1} = \frac{\varepsilon_{\text{core}}}{\mu_0 \Phi_0} \quad (2.19)$$

The line energy of the vortex may be considered to consist of contributions from the microscopic field energy and the kinetic energy of the currents, continuing the London approximation, the energy due to the normal core is neglected. This gives the following approximation for the line energy:

$$\varepsilon = \frac{\mu_0 \Phi_0 H_c}{\sqrt{2\kappa}} \ln \kappa \quad (2.20)$$

Thus neglecting the core energy  $H_{c1}$  is:

$$H_{c1} = \frac{H_c}{\sqrt{2\kappa}} \ln \kappa \quad (2.21)$$

Including the energy due to the core, it can be shown that an extra factor of 0.08 is introduced into this equation. This approximation is good for values of  $\kappa$  larger than about 20 and breaks down for  $\kappa < 4$ .

The upper critical field,  $H_{c2}$ , is the point at which the nucleation of superconducting regions occurs, it is given by the following expression:

$$\mu_0 H_{c2} = \Phi_0 / 2\pi\xi^2 \quad (2.22)$$

$H_{c2}$  may equally be calculated for Type I superconductors: it is lower than  $H_c$  and it is possible in very perfect samples to show that the onset of bulk superconductivity does not occur until the applied field drops below  $H_{c2}$ . Further, higher, critical fields  $H_{c3}$  and  $H_{c4}$  may be defined to account for surface (Saint-James and de Gennes 1963) and corner effects respectively.

### 2.2.5. The Flux Line Lattice

As the applied field on a superconductor is raised above  $H_{c1}$  more and more flux vortices are expected to enter the material. As each vortex generates a microscopic field of the same orientation it will experience a repulsive potential from its neighbours.

In a homogeneous isotropic superconductor it may be shown that the *flux line lattice* (FLL) adopts a hexagonal structure. In anisotropic superconductors different FLL structures are observed (Kogan and Clem 1992).

As the lattice structure is known the nearest neighbour lattice spacing,  $a_0$ , may be calculated. The flux vortex number density is simply  $n_v=B/\Phi_0$ . Each vortex line accounts for  $1/n_v=a_0^2\sqrt{3}/2$  of area. Thus we can write an equation for the flux density in terms of  $a_0$ .

$$B = \frac{2\Phi_0}{\sqrt{3}a_0^2} \quad (2.23)$$

By reference to equation (2.22), it can be seen that at the upper critical field the vortex spacing is of the order of  $\xi$ .

This calculation is true only in the absence of an applied transport current. Since  $\mathbf{J}=\text{curl}\mathbf{H}$ , such a current must have a field associated with it. This leads, in most cases, to a vortex density gradient across the material. In certain geometries, such as the Corbino disk (Campbell and Evetts 1972), the superconductor cannot support a flux density gradient and the transport current leads to curvature of the flux lines.

## 2.3. Flux Line Pinning

### 2.3.1. The Critical State Model

The discussion in the previous section concentrated on the basic structure of the FLL in the mixed state. In real materials the behaviour of the mixed state is greatly affected by the phenomenon of *flux pinning*. If the superconducting material contains defects which perturb the order parameter or the penetration depth the flux line lattice can adopt a lower energy state by distorting so as to accommodate the potentials due to these *pinning centres*.

Pinning has a significant effect on the entry of flux into a Type II superconductor by opposing the motion of flux into a bulk superconductor. The balance between flux pinning and the external magnetic pressure is described by the *critical state model* (Bean, 1962).

In the Bean model any change in external applied field will be screened by induced currents in the surface of the superconducting sample. If the local current at the surface exceeds a certain critical current  $J_c$  the flux enters a flux flow state (see section 2.3.5) and flux enters the sample until equilibrium is restored or the entire sample supports  $J_c$ . This latter state is termed the critical state as all external changes in field will then result in a change in the internal flux gradient. An externally induced current can be considered in terms of the field generated. The force balance equation may thus be written:

$$\left|(\mathbf{B} \times (\nabla \times \mathbf{H}))\right| = BJ_c(B) \quad (2.24)$$

Using the critical state model it is, therefore, possible to deduce the maximum average critical current density of a superconducting sample,  $J_c$ , from magnetisation measurements.

Equation (2.24) is widely applicable but there are cases where it does not apply. If the approximation  $\mu_0 B = H$  is no longer valid, such as at low applied fields,  $B$  becomes a function of the thermodynamic field  $H$ . Currents parallel to  $B$  lead to  $\mathbf{J} \times \mathbf{B} = 0$ , and a *force free* configuration, this is discussed later. Finally, as discussed later, currents in a superconductor can slowly decay due to *flux creep* changing the current and field profile in the sample away from the critical state.

### 2.3.2. Flux Lines and Transport Currents

In this section the pinning of flux vortices under the influence of a transport current is considered. It is assumed that the sample is fully penetrated containing the same flux vortex density throughout, corresponding to an externally applied field  $\mathbf{B}_a$ . This approximation is reasonable for a thin film in a perpendicularly applied field.

From Lorentz's law, in the presence of a transport current  $\mathbf{J}$ , an individual flux vortex will experience a driving force given by (2.25) where  $\mathbf{f}_l$  is the Lorentz force on an individual vortex and the flux vortices are orientated in the  $z$  direction:

$$\mathbf{f}_l = \mathbf{J} \times \Phi_0 \hat{\mathbf{z}} \quad (2.25)$$

As  $B = n_v \Phi_0$  the force per unit volume,  $F_l = n_v \mathbf{f}_l$ , on the flux line lattice is given by

$$\mathbf{F} = \mathbf{J} \times \mathbf{B} \quad (2.26)$$

In the absence of pinning the flux lines will be driven through the material leading to dissipation as discussed in section 2.3.5. If we represent the pinning forces on the lattice as an average force density, at the critical current the Lorentz force density will be just equal to the pinning force density on the lattice  $F_p$ . A force balance equation may then be written where  $\mathbf{J}_c$  is the *critical current density*:

$$F_p = |\mathbf{J}_c \times \mathbf{B}| \quad (2.27)$$

It is important to note that this equation gives the average pinning force density in the material, it is not always possible to write an equivalent equation for an individual vortex. The relation of the bulk pinning force density to local pinning forces is discussed in section 2.3.4. One special case of (2.27) occurs if the applied field is parallel to the current direction. The product  $\mathbf{J} \times \mathbf{B}$  will be zero. This implies that there is no Lorentz force and that  $J_c$  will be infinite. A complete description of this '*force free*' regime (Walmsley 1972) is difficult to achieve. Experimentally a finite  $J_c$  is observed in the force free regime, this stems from helical instabilities in the FLL (Brandt 1995 pg 1514). It is, therefore, possible to define a longitudinal critical current density. When this current is exceeded the FLL enters a complex,

dynamic, state which has been observed experimentally (Timms and Walmsley 1976, Walmsley and Timms 1977, Blamire and Evetts 1985).

### 2.3.3. Sources of Pinning

It is possible to divide pinning centres into two groups depending on whether they arise from interactions with the core ( $\xi$  dependent) or the screening currents ( $\lambda$  dependent). In both cases the FLL is distorted so as to accommodate pinning sites, in order to minimise the overall free energy of the system. Pinning where the order parameter falls to zero over defects of a size similar to  $\xi$  is termed core pinning. An example of this would be a cylinder defect of radius  $\xi$ . Magnetic pinning arises from interactions between the screening currents and defects with lengths of the order of  $\lambda$ . An example of magnetic pinning would be that due to variations in the thickness of a thin film. In HTS materials, except for  $B_a \sim B_{c1}$ , the screening currents and associated fields overlap leading to a relatively uniform local magnetic field compared to the isolated vortex case. Magnetic pinning is therefore less important than core pinning.

In oxide superconductors it is possible to produce high quality single crystals where the pinning is weak compared to that found in thin films. In such crystals the pinning is predominately due to randomly distributed point defects. In these materials the pinning is successfully described by the collective pinning model outlined in the next section. Thin film samples, as a consequence of the growth technique, have a high density of strong pinning centres and thus much larger critical current values. There are several types of strong pinning in thin films such as anti-phase boundaries, twin planes, dislocations and surface features. In the case of the HTS material YBCO, Dam and co-workers have recently provided convincing evidence (Huijbregtse, *et al.* 2000, Dam, *et al.* 1999) that dislocations are the dominant form of pinning centres in YBCO thin films. In vicinal YBCO films containing a high density of anti-phase boundaries an enhancement of  $J_c$  of almost an order of magnitude is observed (Jooss, *et al.* 1999, Jooss, *et al.* 2000). Pinning by twin boundaries has been widely reported (Roas, *et al.* 1990). In contrast to weak random pinning potentials, these types of pinning centre are strong and correlated.

### 2.3.4. Summing Pinning Forces

Having defined a pinning force density, the question arises of the relation between the assembly of individual pinning potentials, each exerting a certain force on the FLL, and the total average pinning force density as deduced from critical current measurements. It is useful to define two types of pinning. In the weak pinning limit, discussed below, the FLL is subject to a large number of weak pinning centres but the short range order of the lattice is preserved.

In the strong pinning limit the flux lattice is disordered with each flux line being individually pinned.

Where the pinning is weak the *collective pinning* model (Larkin and Ovchinnikov 1979) can describe the effect of random weak pinning centres on the FLL. Larkin noted that it is not possible to pin a completely rigid and periodic FLL with a random distribution of pinning sites. Pinning occurs only when the flux lines move out of the equilibrium position in order to accommodate pinning centres. In the Larkin-Ovchinnikov collective pinning model the lattice is considered as a series of flux bundles with a characteristic size defined by  $R_c$  perpendicular to the field and  $L_c$  parallel to it. The flux lattice is considered to be regular within each volume. Each flux bundle may then be considered to be pinned in place. From this model the following equation for the pinning force is derived:

$$F_p = \left( \frac{nf_p^2}{V_c} \right)^{1/2} \quad (2.28)$$

where  $f_p$  is the pinning force associated with each of the pinning centres,  $n$  the pinning centre density,  $F_p$  the volume pinning force density and  $V_c$  the collective pinning volume.

In the limit of a soft, i.e. easily distorted, vortex lattice and a high density of pinning centres the pinning volume can reduce to the size of an individual vortex. It then becomes meaningful to write a force balance equation for individual vortex lines. The total pinning force density may then be expressed as the sum of the pinning force on each vortex. This leads to

$$F = n_v f_p \quad (2.29)$$

where  $n_v$  is the vortex density and  $f_p$  is the average pinning force per unit length on each vortex line.

In the case of thin film YBCO it can be assumed that the pinning is strong and that at least some of the pinning centres are correlated. Correlated pinning centres can, as discussed above, pin an entirely rigid FLL. This is evident from large values of critical current observed in thin film samples. The FLL in the presence of strong random pinning centres is not ordered, being akin to an amorphous solid. In this regime the collective pinning model's appeal to localised order is moot and the approximation of (2.29) is valid.

### 2.3.5. Flux Flow

When the Lorentz force density exceeds the pinning force density flux lines will move through the superconductor. If the  $E$  versus  $J$  ( $EJ$ ) characteristic of a superconductor is measured above  $J_c$  a linear  $EJ$  relationship is observed, assuming no flux creep (see section

2.3.6). From this a flux flow resistivity,  $\rho_f$ , may be defined as  $E = \rho_f J$ . The flux flow resistivity is smaller than, but related to, the normal state, ohmic, resistance of the material.

For uniform vortex motion the dissipation per unit volume is given by  $\mathbf{J} \cdot \mathbf{E}$ , this should be equal to the product of the Lorentz force and the flux flow velocity  $(\mathbf{J} \times \mathbf{B}) \cdot \mathbf{v}$ . Thus we can derive that:

$$\mathbf{E} = \mathbf{B} \times \mathbf{v} \quad (2.30)$$

(Josephson 1962). If a drag coefficient per unit length of vortex, independent of velocity,  $\eta$ , is defined the average dissipation is given by:

$$\mathbf{J} \cdot \mathbf{E} = n_v \eta \langle v^2 \rangle \quad (2.31)$$

Here  $n_v$  is the vortex number density. Combining (2.30) and (2.31) gives:

$$E = \frac{\Phi_0 B}{\eta} J \quad (2.32)$$

allowing  $\rho_f$  to be identified as  $\Phi_0 B / \eta$ . This EJ characteristic is depicted in figure 2.2.

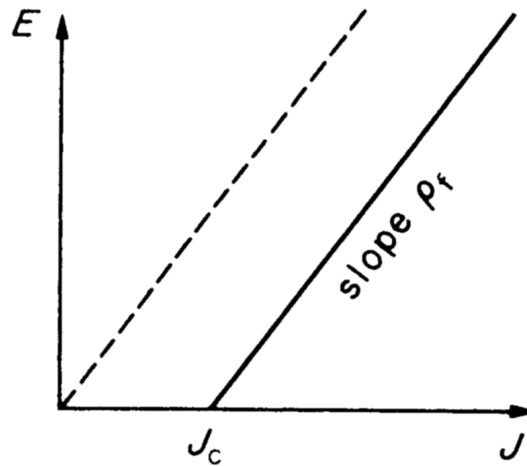


Figure 2.2 Critical current transition with and without pinning. Pinning shifts the point at which the flux lines move from  $J=0$  to  $J=J_c$ .

Bardeen and Stephen (1965) developed a model relating the flux flow resistivity to the ohmic resistivity. They commenced by assuming a flux line with a normal core of radius  $\xi$  and that the flux line moves slowly enough to be considered as being in quasi equilibrium. The properties of the superconducting phase may then be treated outside the core, using the London equations.

As the London equations apply, outside the core the local electric field at the edge of the core can be calculated. This is found to be everywhere constant, perpendicular to the direction of motion and given by  $E_{\text{core}} = v B_{c2}$ . As the field lines must be continuous and no charge is present in the core the field in the core is constant and equal to  $E_{\text{core}}$ . The equation for the dissipation

per unit length of core  $\pi\xi^2 E_{\text{core}}^2/\rho_n$  may then be written. Bardeen and Stephen assumed that an equal contribution to dissipation is due to normal currents flowing outside the core. The dissipation in a core is equal to the work done in moving the core against the flux flow viscosity, so  $JE=\eta v$ . The flux drag coefficient  $\eta$  is therefore equal to  $\Phi_0 B_{c2}/\rho_n$ . Finally, we can deduce the Bardeen-Stephen relation between the normal state resistivity,  $\rho_n$ , and  $\rho_f$ :

$$\rho_f = \rho_n B/B_{c2} \quad (2.33)$$

This correctly predicts that at  $B_{c2}$   $\rho_f = \rho_n$ .

### 2.3.6. Thermally Activated Flux Motion

The critical current transition shown in Figure 2.2 is sharply defined. However, if  $E$  versus  $J$  characteristics on real type II materials are measured the transition is found to be curved. In addition a current set up in a ring of Type II material will decay, albeit slowly and with a logarithmic time dependence. This phenomenon of *flux creep* is attributed to a thermally activated rearrangement of flux lines from a metastable configuration to one with lower energy.

Anderson *et al.* (1964) proposed a creep model for flux lines moving between adjacent pinning points due to thermal activation. The jump rate is postulated as having an exponential dependence on the thermal energy of the form given in equation (2.34) where  $U$  is the barrier energy and  $\omega_0$  a characteristic frequency for hopping attempts.

$$R = \omega_0 e^{\frac{-U}{kT}} \quad (2.34)$$

Anderson and Kim suggested a form for the barrier energy,  $U$ , of the form

$$U = U_0 \left( 1 \pm \frac{J}{J_c} \right) \quad (2.35)$$

This corresponds to a sawtooth shaped potential energy diagram. The sign in the equation changes depending on whether movement with or against the Lorentz force is being considered. Movement with the Lorentz force is easier than movement opposing it, as is shown in Figure 2.3.

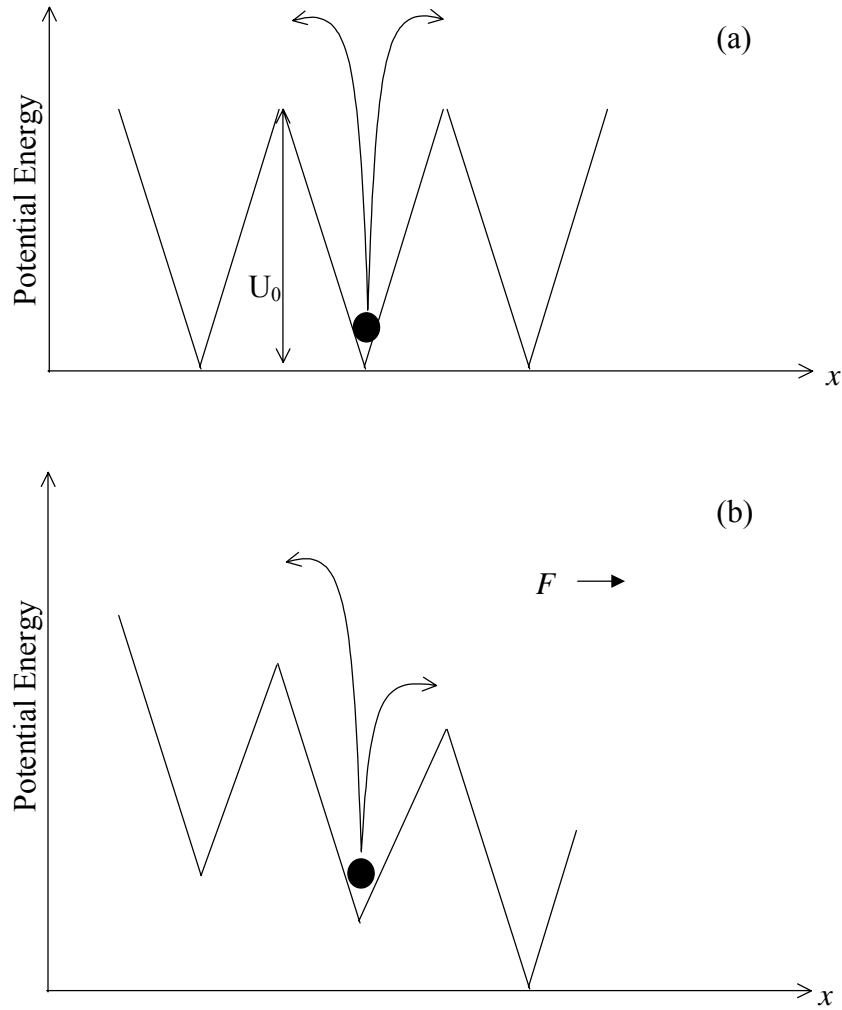


Figure 2.3 The change in the potential energy environment of a flux line in an arbitrary potential without (a) and with (b) a Lorentz force being present.

The difference in jump rates for motion against or with the Lorentz force gives rise to a net jump rate in the direction of the Lorentz force.

$$R = \omega_0 e^{\frac{-U_0}{kT}} \sinh\left(\frac{U_0 J}{kTJ_c}\right) \quad (2.36)$$

A consequence of flux creep is that field trapped in a Type-II material will decay. This effect has been shown experimentally (Kim, *et al.* 1962) to have a logarithmic dependence with time. In most low- $T_c$  materials flux creep is almost negligible except in the vicinity of  $T_c$ .

Flux creep has the practical effect of making the definition of  $J_c$  in terms of an experimentally measured  $EJ$  characteristic imprecise. In practical measurements a voltage criterion (equivalent to a certain  $E$  field in a given length of conductor) is used to define the *criterion critical current*  $J_{c1}$  as shown in Figure 2.4.

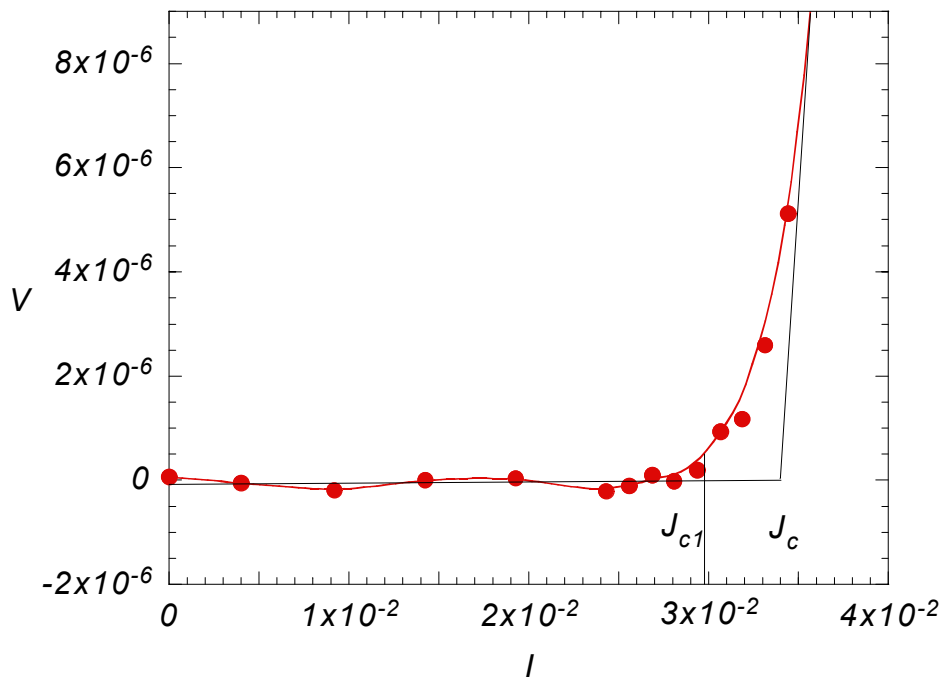


Figure 2.4 An IV curve (red) measured on a 500  $\mu\text{m}$  long YBCO current track (sample 200630) showing flux creep and  $J_{c1}$  defined using a voltage criterion of  $5 \times 10^{-7}$  V. For comparison the definition of  $J_c$  for an idealised creep free IV characteristic (black) is also shown.

Obtaining a relation between  $J_c$  and  $J_{c1}$  requires a model for the behaviour and structure of the FLL. Several such models have been proposed each predicting a different form of the  $U(j)$  dependence. This is discussed further in the next section.

In some HTS materials, most notably BSCCO, a linear  $EJ$  characteristic is observed for currents well below the critical current transition. This phenomenon is termed Thermally Activated Flux Flow (Griessen 1992).

### 2.3.7. The Flux Vortex Phase Diagram

If magnetisation measurements are made on a sample of HTS it is possible to observe ‘reversible’ magnetic properties at fields significantly smaller than the second critical field. This field is termed the irreversibility field and is a function of temperature  $B_{\text{irr}}(T)$ . The line on a  $B$  versus  $T$  phase diagram that defines this transition between the irreversible and reversible magnetisation states is termed the irreversibility line. Above the irreversibility line flux appears not to be trapped and no critical state behaviour is observed; nor is there a difference between field cooled and zero field cooled magnetisation.

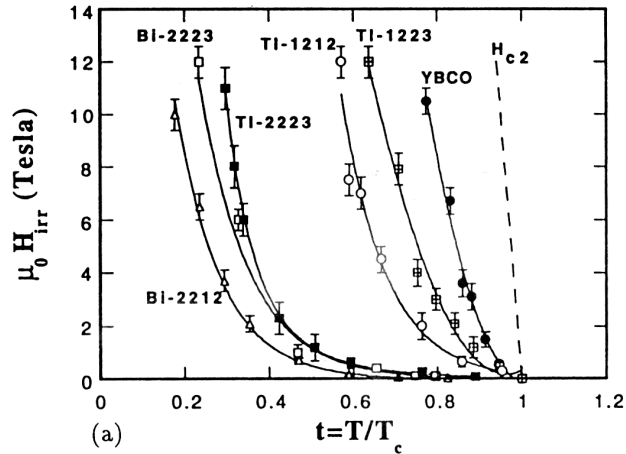


Figure 2.5 Irreversibility lines for various HTC materials (Johnson, *et al.* 1994)

The position of the irreversibility line is profoundly dependent on the nature and density of pinning centres in a material. One practical consequence of this is that identifying  $H_{c2}$  with the onset of dissipation can greatly underestimate its value.

Also linked to the FLL structure is the phase of the vortex matter. In the limit of high pinning density a thermodynamic transition between a disordered solid and a vortex liquid has been observed in resistivity-temperature measurements (Crabtree, *et al.* 2000). The disordered vortex solid/vortex liquid transition shown in Figure 2.6 has been associated with the irreversibility line. The irreversibility line lies between the melting transition and  $H_{c2}$ . The type of vortex matter is expected to be reflected in the current dependence of the activation energy for flux creep.

In low pinning density materials, such as high quality de-twinned single crystal YBCO, further thermodynamic transitions have been identified within the solid and liquid phases. Figure 2.6 shows some of these on a phase diagram.

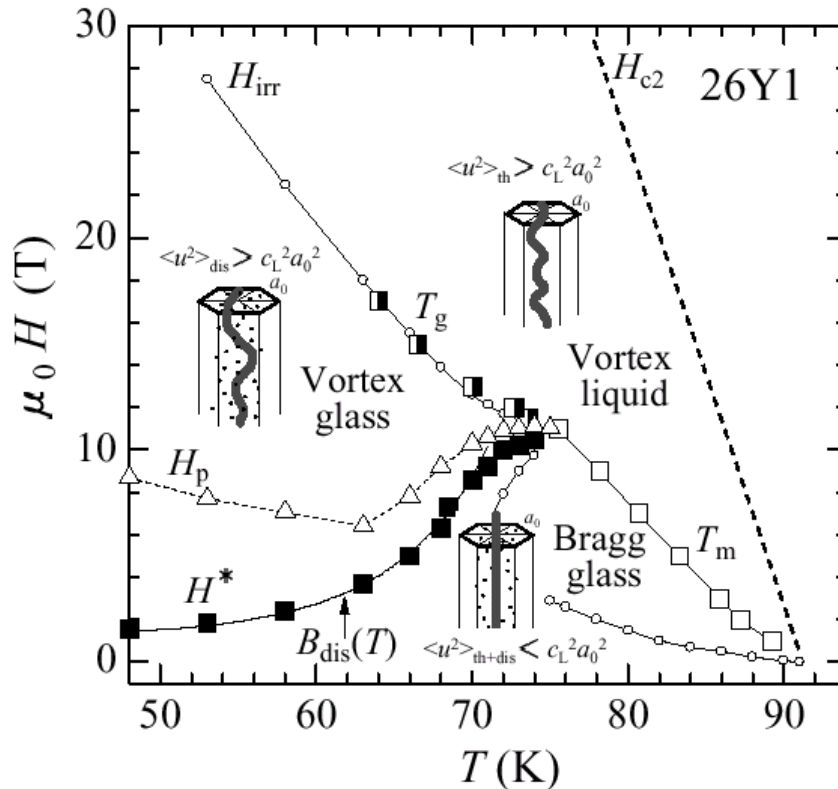


Figure 2.6 A zoology of possible types of vortex matter in de-twinned YBCO (From Nishizaki, *et al.* 2000).

The exact form and behaviour of the vortex matter in the weak pinning limit is the subject of considerable ongoing research. Both resistivity transitions and  $EJ$  characteristics are studied carefully for changes in the flux creep activation energy, discussed in Section 2.3.7, which may indicate higher order thermodynamic transitions. The type of vortex solid has been predicted to depend on the nature of the pinning centres with a ‘Boson-Glass’ predicted on the basis of planar disorders (Nelson and Vinokur 1992) and a ‘vortex-glass’ on the basis of point pinning centres (Feigel'man, *et al.* 1989). Where the Anderson-Kim model predicts an exponentially small  $E$  far below  $J_c$  these models predict  $E=0$ .

Berghuis *et al.* (1996) carefully studied  $EJ$  characteristics measured on strongly pinned thin films and found that the vortex glass model gave the best fit for current densities well below  $J_c$ . Given the similar predictions of the models it is very difficult to distinguish between them on the basis of  $EJ$  characteristics measured on thin films.

## 2.4. Flux Lines in Anisotropic Superconductors

### 2.4.1. Anisotropic Ginzburg-Landau Theory

In contrast to the majority of LTS superconductors the HTS materials all exhibit significant anisotropy in both their crystallographic and superconducting properties. The three

crystallographic axes in HTS materials are the  $a$  and  $b$  axes, in the cuprate planes, and the  $c$ -axis directed normal to the planes. (This is discussed further in Chapter 3). In the case of the oxide superconductors the  $a$ - $b$  anisotropy is usually small enough to be neglected, and the material may be treated as being uniaxial. The anisotropy between the parameters in the  $a$ - $b$  plane and the  $c$ -axis is very large (Datta 1992).

The isotropic Ginzburg-Landau theory described in section 2.2.1 can be extended to deal with superconducting materials where the superconducting parameters (such as  $\xi$  and  $\lambda$ ) are not isotropic. The material anisotropy is introduced by defining a charge carrier mass tensor (Kogan and Clem 1992). The mass tensor has the values  $m_{ab}$  in the  $a$  and  $b$  directions and  $m_c$  in the  $c$ -axis direction. It is then possible to write an anisotropic version of equation (2.11) and obtain G-L equations in terms of the superconducting parameters for the crystallographic directions  $\lambda_{ab}$ ,  $\lambda_c$ ,  $\xi_{ab}$  and  $\xi_c$ .

The mass in the  $a$ - $b$  plane is denoted  $m_{ab}$  and that in the  $c$ -axis direction  $m_c$ . A G-L mass anisotropy parameter  $\varepsilon$  may then be introduced with  $\varepsilon^2 = (m_{ab}/m_c)$ . For convenience some authors also define a reciprocal anisotropy parameter  $\gamma = 1/\varepsilon$ .

$$\varepsilon = \frac{1}{\gamma} = \frac{\lambda_{ab}}{\lambda_c} = \frac{\xi_c}{\xi_{ab}} = \sqrt{\frac{m_{ab}}{m_c}} \quad (2.37)$$

The following general angular dependence of superconducting properties is predicted on the basis of anisotropic Ginzburg Landau theory:

$$\varepsilon_\theta^2(\theta) = \varepsilon^2 \cos^2 \theta + \sin^2 \theta \quad (2.38)$$

Equation (2.38) is effectively a scaling law for the angular dependent properties of an anisotropic uniaxial superconductor.

It is important to note that equation (2.38) is only applicable to a homogenous anisotropic superconductor. In addition an observed physical quantity may not scale as (2.38) if, for example the pinning is also anisotropic. A flux line tilted about the  $a$ -axis would be expected to have an elliptical core with one axis  $\xi_{ab}$  and the other equal to  $\varepsilon_\theta \xi_{ab}$ . A flux line lying along the  $b$ -axis is depicted in Figure 2.7

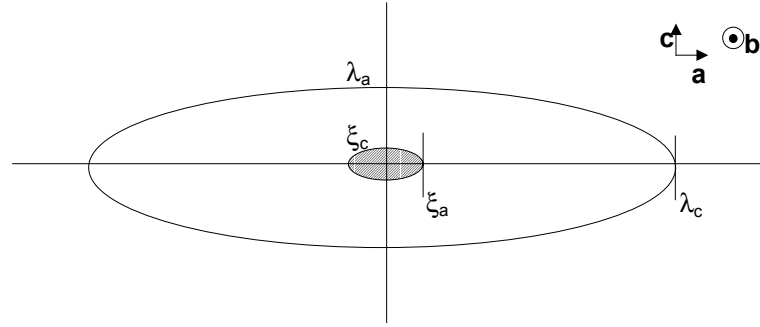


Figure 2.7 A flux line laying along the  $b$  axis in a HTS material.

Having obtained values for the superconductivity parameters in the crystallographic axis directions and a scaling law it is possible to write anisotropic versions of the equations defining the field dependent behaviour of the superconductor. For example the angular dependence of the second critical field in terms of that for a field parallel to the  $c$ -axis is given by equation (2.39).

$$B_{c2}(\theta) = \frac{B_{c2}^c}{\varepsilon_\theta} \quad (2.39)$$

#### 2.4.2. The Lawrence-Doniach Model for Layered Superconductors

The anisotropic G-L theory assumes a homogenous material. However the HTS materials, with the possible exception of YBCO, can often be better pictured as sheets of 2D G-L superconductor separated by non-superconducting layers. The Lawrence Doniach model is expected to apply if the interlayer spacing,  $d$ , is of the order of, or larger than the  $c$ -axis coherence length,  $\xi_c$ . The coupling between layers is expected to be that of a stack of extended Josephson junctions.

Clem (Clem 1991, Clem 1998) considered the form of the vortex lines in a two dimensional superconductor for a field directed along the  $c$ -axis. The form of the vortex inside each sheet of superconductor reduces to a flat core surrounded by screening currents inside the superconducting layer. This two-dimensional flux element is termed a *flux pancake*. The flux contained by the pancake is directed along the  $c$ -axis of the material. By calculating the attractive potentials due to the magnetic fields surround each pancake Clem showed that the individual pancakes will tend to align themselves into stacks. The dissolution of these stacks at temperatures near to  $T_c$  is one proposed cause of the irreversibility line in BSCCO.

When a field applied along the  $a$ - $b$  planes on a two dimensional superconductor, *Josephson-Vortices*, or *vortex strings*, are nucleated (Blatter, *et al.* 1994). These are, in many ways, similar to conventional Abrikosov vortices. However, the order parameter is not suppressed completely to zero at the centre of the vortex. The dimensions of the region of suppressed

order parameter is characterised by the length,  $d$ , in the  $c$ -axis direction and  $d/\epsilon$  in the planes.

Figure 2.8 is a schematic of a Josephson vortex aligned with the  $b$ -axis:

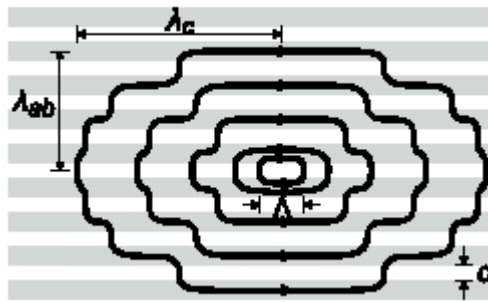


Figure 2.8 Currents flowing round a Josephson vortex lying along the  $b$ -axis. The width of the order parameter perturbation at the core is given by  $\Lambda=d/\epsilon$ .

For a tilted applied field in the 2D model both pancakes and strings are expected to be present, this is discussed in later chapters. The precise configuration of each vortex line is expected to be highly dependent on the intrinsic anisotropy of the superconducting material.

#### 2.4.3. Angular Applied Fields in Anisotropic Superconductors

The study of fields applied at an angle to the  $c$ -axis is essential for the investigation of the nature of the flux line lattice in HTS materials. In this section three possible models of a tilted flux line are discussed.

In section 2.4.1 an angular scaling law for the Ginzburg-Landau parameters was given. The case of a tilted Abrikosov vortex in an anisotropic material may therefore be considered with the aid of equation (2.38). The elliptical nature of the core of a vortex tilted about the  $a$ -axis is shown in Figure 2.9:

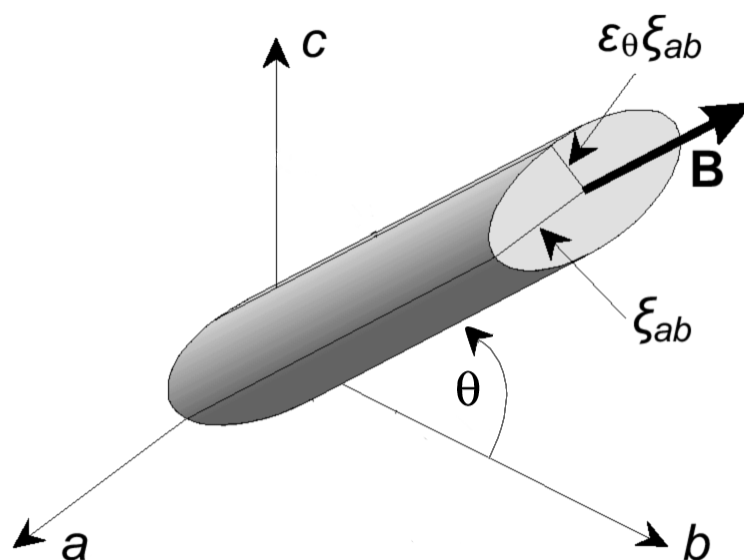


Figure 2.9 A tilted vortex core in a uniaxial anisotropic superconductor

From Figure 2.9 it can be observed that when the core is parallel to the  $c$ -axis  $\epsilon_0$  is equal to one and the core is circular. The same principle can be applied to determining the extent of the screening currents.

A complication arises when considering such tilted vortices in a thin film, where  $\lambda$  may easily be larger than the film thickness and at the surface the screening currents are constrained. This will tend to prevent flux lines at small applied fields in thin slabs tilting with the applied field (Brandt 1993). This would suggest that the  $J_c(B)$  behaviour in this regime will be entirely dependent on the  $c$ -axis component of the applied field.

At  $B \gg B_{c1}$  (which is a wide range in HTS materials) the fields due to adjacent vortices will overlap. In the  $a$ - $b$  plane  $\lambda$  is typically 150nm (Datta 1992) whilst the nearest neighbour lattice spacing at 0.5 T is, by equation (2.23), 69 nm. This means that variations in the local field,  $h$ , and screening currents are reduced. Thus, while an isolated flux vortex may not be tilted, a lattice of closely spaced vortices may be tilted. Thus as the applied field tends towards  $H_{c2}$  the flux lines in the material are increasingly aligned with the external field (Clem 1999).

If the flux line consists of joined flux pancake and vortex string elements *kinked* vortex lines may be formed (Bulaevskii, *et al.* 1992, Blatter, *et al.* 1994 pg 1286, Brandt 1995, pg. 1486), as shown in Figure 2.10. The field component parallel to the  $a$ - $b$  planes is carried by Josephson vortices localised in the intercalated layers. The  $c$ -axis component is carried by the flux pancakes.

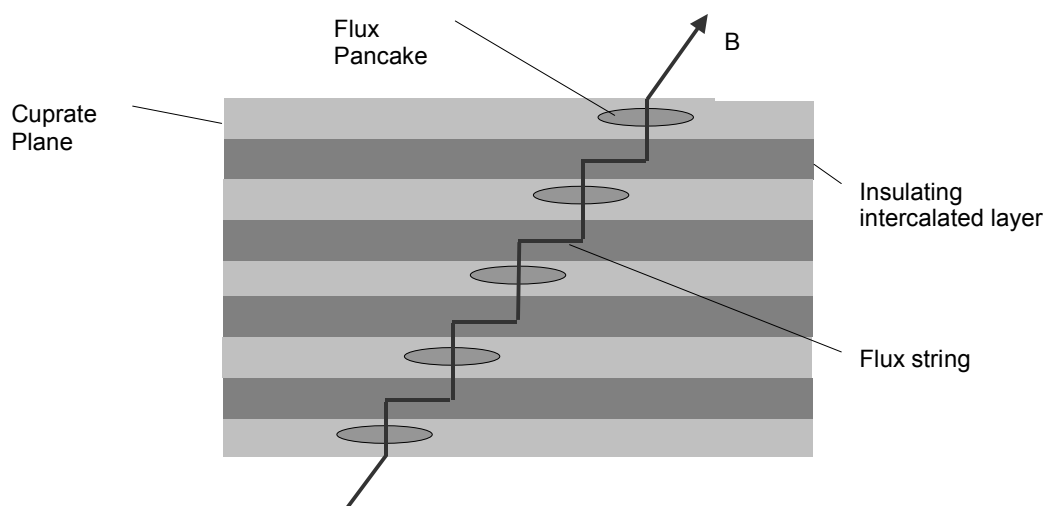


Figure 2.10 A kinked vortex line in a layered superconductor

The final FLL state discussed here is the *crossing lattice*. As with the kinked vortex line it consists of both pancake and string elements. The elements are not, however, joined in contiguous lines. The Josephson strings form a dilute highly anisotropic lattice and the vortex

pancakes align themselves through their mutual magnetic attraction into stacks (Bulaevskii, *et al.* 1992, Koshelev 1999). More pancakes appear along Josephson strings due to attraction between the two vortex elements. This structure, which is expected for highly anisotropic HTS materials, has been imaged using a scanning hall probe (Dodgson 2000).

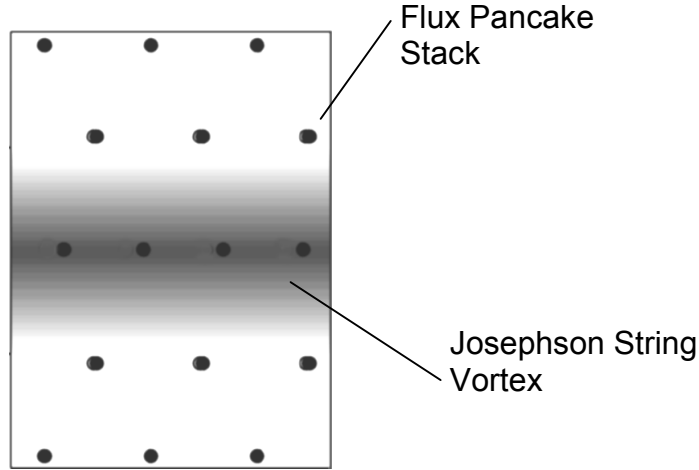


Figure 2.11 View along the  $c$ -axis of the crossing lattice showing the increase in pancake density over a Josephson vortex (Koshelev 1999).

#### 2.4.4. Lattice Structure Cross-Over in YBCO

The particular form of the FLL clearly depends on the anisotropy of the particular HTS under consideration. For the relatively isotropic HTS material  $\text{YBa}_2\text{Cu}_3\text{O}_{7-\delta}$  an angularly dependent cross-over from the Abrikosov lattice to a kinked vortex lattice has been predicted.

Blatter *et al.* (1994), pg. 1286, predicts a cross-over from continuous vortex lines to kinked vortex lines. Intermediate between the two states is a distorted lattice. The nature of the vortex state depends on the ratio between the coherence length and the interlayer spacing  $d/\xi_{ab}(t)$ , the anisotropy parameter  $\epsilon$  and the angle between the applied field and the cuprate planes (Berghuis, *et al.* 1997). The coherence length is proportional to  $1/\sqrt{1-t}$  near  $T_c$ , where  $t$  is the reduced temperature  $T/T_c$ . For values of  $\theta$  less than  $\theta_1$  the distorted state develops where

$$\tan(\theta_1) = d/\xi_{ab}(t) \quad (2.40)$$

This state becomes fully developed at  $\theta_2$  where

$$\tan(\theta_2) = \epsilon \quad (2.41)$$

This cross-over is suppressed at a temperature  $T_{cr}$  where the  $c$ -axis coherence length  $\epsilon\xi_{ab}(t)$  is greater than  $d/\sqrt{2}$ . In YBCO  $\epsilon \sim 0.2$  (Farrell, *et al.* 1988, Dolan, *et al.* 1989, Farrell, *et al.* 1990)  $d = 0.8$  nm (Cava, *et al.* 1987) and  $\xi_{ab}(0) \sim 1.6$  nm (Welp, *et al.* 1989). From this we obtain  $\theta_1 = 35^\circ$  and  $\theta_2 = 11^\circ$  at  $t=0$ . Berghuis *et al.* estimated  $T_{cr} = 80$  K. Interestingly while  $\theta_1$  will have

a  $T$  dependence  $\theta_2$  is equal to  $\epsilon$  which does not. At  $\theta=0^\circ$  the vortex lines will be *locked in* (Feinberg, 1990) to the cuprate planes and the FLL will, in principle, consist entirely of vortex strings.

## 2.5. Bibliography

- Abrikosov, A. A. (1957). Zh. Eksperim. i Teor. Fiz. **32**: 1442.
- Anderson, P. W. and Y. B. Kim (1964). Rev. Mod. Phys. **36**: 39.
- Bardeen, J. (1992). Superconducting Materials: BCS and Phenomenological Theories. Concise Encyclopedia of Magnetic and Superconducting Materials. J. E. Evetts. Oxford, Pergamon
- Bardeen, J. and M. J. Stephen (1965). Phys. Rev. A **140**: 1197.
- Bardeen, S., L. N. Cooper and J. R. Schrieffer (1957). Phys. Rev **108**: 1175.
- Bean, C. P. (1962). Phys. Rev. Lett. **8**: 250.
- Berghuis, P., E. DiBartolomeo, G. A. Wagner and J. E. Evetts (1997). Phys. Rev. Lett. **79**(12): 2332-2335.
- Berghuis, P., R. Herzog, R. E. Somekh, J. E. Evetts, R. A. Dayle, F. Baudenbacher and A. M. Campbell (1996). Physica C **256**: 13.
- Blamire, M. G. and J. E. Evetts (1985). Philosophical Magazine B. **51**(4): 421-438.
- Blatter, G., M. V. Feigelman, V. B. Geshkenbein, A. I. Larkin and V. M. Vinokur (1994). Rev. Mod. Phys. **66**(4): 1125-1388.
- Brandt, E. H. (1993). Phys. Rev. B **48**(9): 6699-6702.
- Brandt, E. H. (1995). Rep. Prog. Phys. **58**(11): 1465-1594.
- Bulaevskii, L. N., M. Ledvij and V. G. Kogan (1992). Phys. Rev. B **46**(1): 366-380.
- Campbell, A. M. and J. E. Evetts (1972). Critical Currents in superconductors. London, Taylor and Francis.
- Cava, R. J., B. Batlogg, R. B. Vandover, D. W. Murphy, S. Sunshine, T. Siegrist, J. P. Remeika, E. A. Rietman, S. Zahurak and G. P. Espinosa (1987). Phys. Rev. Lett. **58**(16): 1676-1679.
- Clem, J. R. (1991). Phys. Rev. B **43**(10 PtA): 7837-7846.
- Clem, J. R. (1998). Supercon. Sci. Technol. **11**(10): 909-914.
- Clem, J.R. (1999). Personal Communication.
- Crabtree, G. W., W. K. Kwok, R. J. Olsson, G. Karapetrov, L. M. Paulius, A. Petrean, V. Tobos and W. G. Moulton (2000). J. Supercon. **13**(5): 741-748.

- Dam, B., J. M. Huijbregtse, F. C. Klaassen, R. C. F. van der Geest, G. Doornbos, J. H. Rector, A. M. Testa, S. Freisem, J. C. Martinez, B. Stauble-Pumpin and R. Griessen (1999). Nature **399**(6735): 439-442.
- Datta, T. (1992). Oxide Superconductors: Physical Properties. Concise Encyclopedia of Magnetic and Superconducting Materials. J. E. Evetts. Oxford, Pergamon
- Dodgson, M. (2000) Personal Communication.
- Dolan, G. J., F. Holtzberg, C. Feild and T. R. Dinger (1989). Phys. Rev. Lett. **62**(18): 2184-2187.
- Farrell, D. E., J. P. Rice, D. M. Ginsberg and J. Z. Liu (1990). Phys. Rev. Lett. **64**(13): 1573-1576.
- Farrell, D. E., C. M. Williams, S. A. Wolf, N. P. Bansal and V. G. Kogan (1988). Phys. Rev. Lett. **61**(24): 2805-2808.
- Feigel'man, M. V., V. B. Geshkenbein and V. M. Vinokur (1989). Phys. Rev. Lett. **63**: 2303.
- Ginzburg, V. L. and L. D. Landau (1950). Zh. Eksperim. i Teor. Fiz. **20**: 1064.
- Gor'kov, L. P. (1959). Zh. Eksperim. i Teor. Fiz. **36**: 1918.
- Griessen, R. (1992). Flux Creep Phenomena. Concise Encyclopedia of Magnetic and Superconducting Materials. J. E. Evetts. Oxford, Pergamon: 145
- Huijbregtse, J. M., B. Dam, R. C. F. van der Geest, F. C. Klaassen, R. Elberse, J. H. Rector and R. Griessen (2000). Phys. Rev. B **62**(2): 1338-1349.
- Johnson, J. D., D. N. Zheng and A. M. Campbell (1994). Critical Currents in High Temperature Superconductors. IRC Research Review. Y. Liang, IRC, Cambridge University
- Jooss, C., R. Warthmann and H. Kronmuller (2000). Phys. Rev. B **61**(18): 12433-12446.
- Jooss, C., R. Warthmann, H. Kronmuller, T. Haage, H. U. Habermeier and J. Zegenhagen (1999). Phys. Rev. Lett. **82**(3): 632-635.
- Josephson, B. D. (1962). Phys. Lett. **1**: 251-253.
- Kim, Y. B., C. F. Hempsted and A. R. Strnad (1962). Phys. Rev. Lett. **9**: 306.
- Kogan, V. G. and J. R. Clem (1992). Anisotropy in Superconducting Materials. Concise Encyclopedia of Magnetic and Superconducting Materials. J. E. Evetts. Oxford, Pergamon
- Koshelev, A. E. (1999). Phys. Rev. Lett. **83**(1): 187-190.
- Landau, L. D. (1937). Phys. Z. Sowjet **11**: 545.
- Larkin, A. I. and Ovchinnikov (1979). J. Low Temp. Phys. **34**: 409.
- London, F. (1935). Proc. Roy. Soc. **A152**: 24.

- London, F. and H. London (1935). Proc. Roy. Soc. **A149**: 71.
- Meissner, W. and R. Ochsenfeld (1933). Naturwissenschaften **21**: 787.
- Nelson, D. R. and V. M. Vinokur (1992). Phys. Rev. Lett. **68**: 2398.
- Nishizaki, T. and N. Kobayashi (2000). Supercon. Sci. Technol. **13**(1): 1-11.
- Onnes, H. K. (1911). Leiden Comm. **120b, 122b, 124c**.
- Onnes, H. K. (1914). Commun. Phys. Lab. Univ. Leiden **221e**.
- Roas, B. L., L. Schultz and G. Saemannishenko (1990). Phys. Rev. Lett. **64**(4): 479.
- Saint-James, D. and P. G. de Gennes (1963). Phys. Lett. **7**: 306.
- Schrieffer, J. R. and M. Tinkham (1999). Rev. Mod. Phys. **71**(SPI/1): S313-S317.
- Timms, W. E. and D. G. Walmsley (1976). J Phys F **6**(11): 2107-18.
- Tinkham, M. (1996). Introduction to Superconductivity. New York, Mc Graw Hill.
- Waldram, J. (1996). Superconductivity of Metals and Cuprates. London, Institute of Physics Publishing.
- Walmsley, D. G. (1972). J. Phys. F: Metal Physics **2**(3): 510-28.
- Walmsley, D. G. and W. E. Timms (1977). J. Phys. F **7**(11): 2373-80.
- Welp, U., W. K. Kwok, G. W. Crabtree, K. G. Vandervoort and J. Z. Liu (1989). Phys. Rev. Lett. **62**(16): 1908-1911.

### 3. Sample Preparation and Experimental Techniques

*To perform transport critical current measurements on oxide superconductors a suitable measurement system and grain boundary free samples are required. Epitaxially grown thin films provide a very convenient system in which well orientated current tracks can be easily defined. This chapter describes the growth and preparation of the superconducting samples measured for this work and the two-axis 8 T cryogenic goniometer system used to perform transport critical current measurements.*

#### 3.1. Thin Film High $T_c$ Superconductors

##### 3.1.1. Overview

The use of thin films to obtain practical and well controlled samples of superconductor was well established long before the discovery of High  $T_c$  superconducting oxides (HTS). Thin film deposition is itself a mature technology having been in use for over 150 years (Ohring 1992). Despite the properties of early bulk HTS samples being dominated by grain boundary effects it was possible to study the intrinsic critical current properties of these new materials by preparing thin epitaxial films. Indeed some of the first practical measurements of transport critical current were observed using such thin films (Somekh, *et al.* 1987).

Thin film samples of superconductor do not act simply as very thin single crystals: thin films exhibit larger values of the critical current density,  $J_c$ , due to a larger defect density; the difference between the surface of the film and the interface with the substrate can give rise to ‘surface pinning’ effects (Berghuis, *et al.* 1996) and the geometry of a thin film current track means it has a larger demagnetising factor than bulk samples. In addition, thin film samples are of the order of 200nm thick, the same length scale as the superconducting penetration depth  $\lambda$  (Datta 1992) which can complicate measurements in small, tilted fields as discussed in Section 2.4.3. Although good quality thin films are epitaxial, they are not single grained, and the orientation of the  $a$  and  $b$  axes rotate by 90 degrees over the film giving rise to ‘twin’ boundaries which can act as strong pinning centres (Roas, *et al.* 1990).

Using lithography on a thin film it is relatively straightforward to define a small bar of superconducting material (e.g.  $10\mu\text{m}\times 100\mu\text{m}\times 200\text{nm}$ ), the electrical properties of which are conveniently measured using a four terminal resistance technique. Such a thin sample will

have low values of the absolute critical current,  $I_c$ , which greatly simplifies the performance of accurate, low noise measurements.

### 3.1.2. Structure of HTS

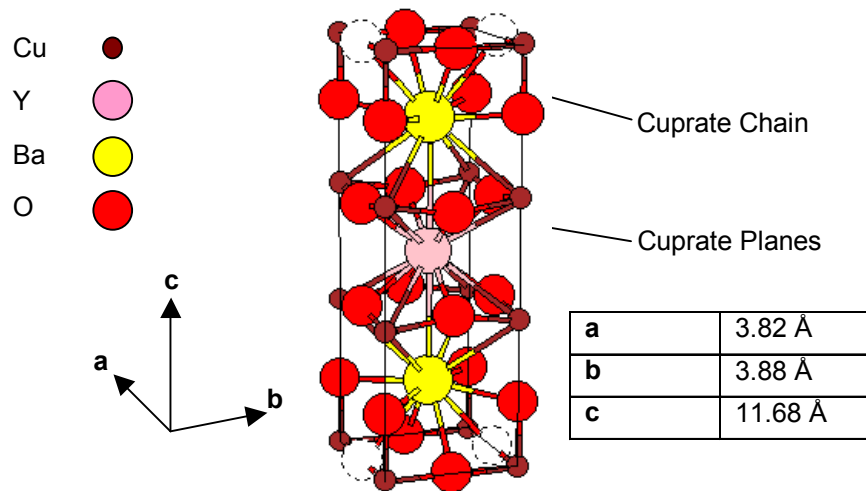


Figure 3.1 A unit cell of  $YBa_2Cu_3O_7$ . Although in the diagram all the oxygen sites in the chains are shown filled the oxygen content of the material can be varied by removing oxygen from the cuprate chains. This strongly affect the superconducting transition temperature ( $T_c$ )

The crystal structure of a representative HTS, YBCO, is shown in Figure 3.1. The three crystallographic directions are, by convention, referred to as the  $a$  [100],  $b$  [010] and  $c$  [001] axes. The superconducting charge carriers are thought to arise in the  $a$ - $b$  cuprate planes with the blocking layers acting as a charge reservoir. This planar structure is common to all the perovskite high  $T_c$  superconductors (Waldram 1996).

The superconducting properties of the material are poorer, in terms of  $J_c$ , in the  $c$ -axis direction. For this reason most thin films grown are ‘ $c$ -axis films’ in which the  $c$ -axis [001] of the material grows normal to the surface of the substrate. This is preferable for many applications as a uniform high critical current is obtained for currents flowing in the plane of the film surface.

Some studies have been performed on  $a$ -axis films, where the  $a$ -axis is normal to the surface of the film (Herzog 1997). In  $a$ -axis films the superconducting properties in the plane of the film are highly anisotropic; currents flowing in the  $a$ -axis direction show a  $J_c$  similar to  $c$ -axis films whereas the  $J_c$  value for currents flowing in the  $c$ -axis direction are lower. Intermediate between these two types of films are those grown on *vicinal* substrates. A vicinal substrate is polished so that the [001] axis is at an angle,  $\theta_v$ , to the surface normal of the film. By varying the vicinal angle the superconducting anisotropy in the plane of the surface of the material may be altered. Figure 3.2 illustrates these three film types:

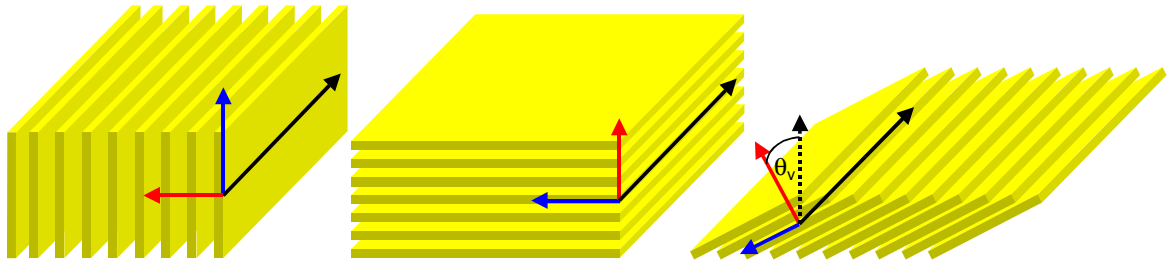


Figure 3.2 This diagram illustrates a-axis, c-axis and vicinal films. The a (blue), b (black) and c (red) –axis directions are indicated. The vicinal angle,  $\theta_v$ , is the angle between the c-axis and a vector normal to the surface of the film.

The development of HTS films grown on vicinal substrates has had three main aims. Firstly it is hoped that the smooth *step-flow* growth seen in vicinal films gives rise to a higher quality film surface morphology (Mechin, *et al.* 1998), secondly it is possible to examine the behaviour of a current flowing at a specific angle to the crystal lattice rather than parallel to one of the crystallographic axes (Berghuis, *et al.* 1997), this is not possible using a bulk single crystal. Finally, in the highly anisotropic material  $Tl_2Ba_2CaCu_2O_8$ , the intrinsic Josephson effect between cuprate planes has been observed. This was achieved by patterning a short, narrow current track so the current must flow in the weakly coupled c-axis direction to cross between cuprate planes (Chana, *et al.* 2000).

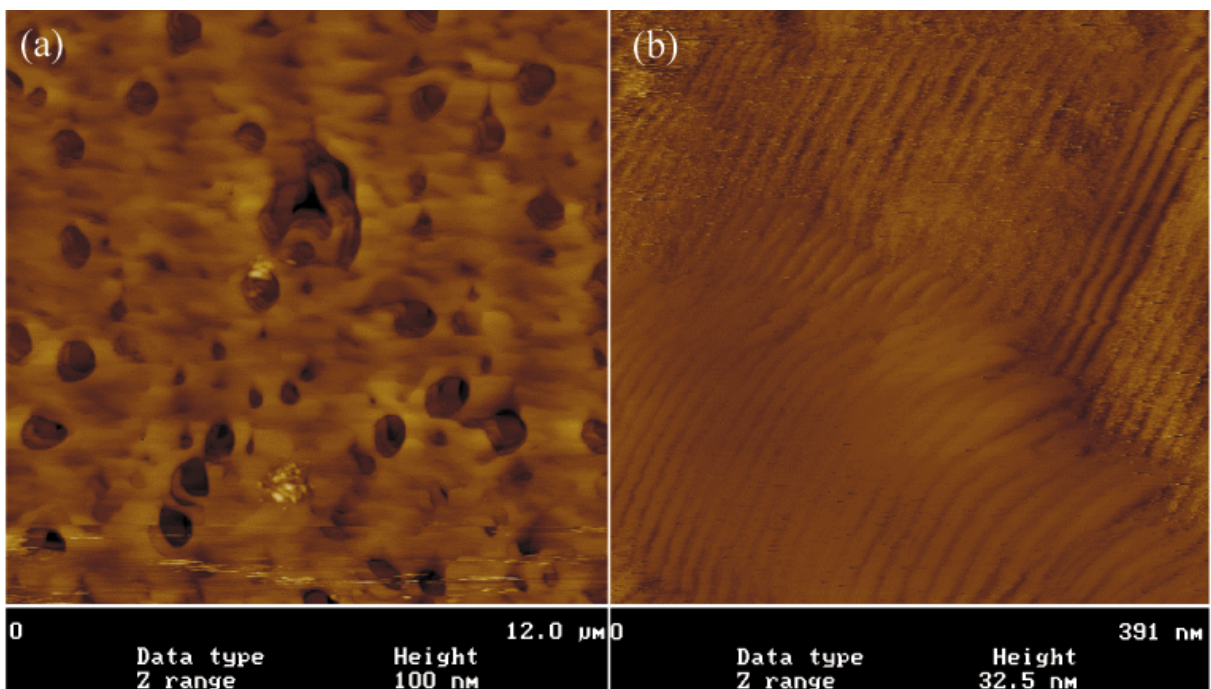


Figure 3.3 Atomic force microscopy (a) and scanning tunnelling microscopy (b) images of a de-oxygenated 6 degree vicinal YBCO film (sample 8722). The right hand image, at a higher resolution, shows characteristic step-flow growth. The film was grown using DC sputtering.

Figure 3.3 shows images of the surface of a de-oxygenated film (sample 8722) grown on a 6° off-axis vicinal substrate. Using Atomic Force Microscopy (AFM) and at a 12 micron scale it

can be seen that the film surface exhibits numerous defects, such as pinholes, however at a higher resolution, using Scanning Tunnelling Microscopy (STM), the step-flow terraces can be clearly observed. The form of the step-flow growth can be seen clearly in Figure 3.4, a projection of Figure 3.3b. The AFM technique is discussed further in Section 3.3.

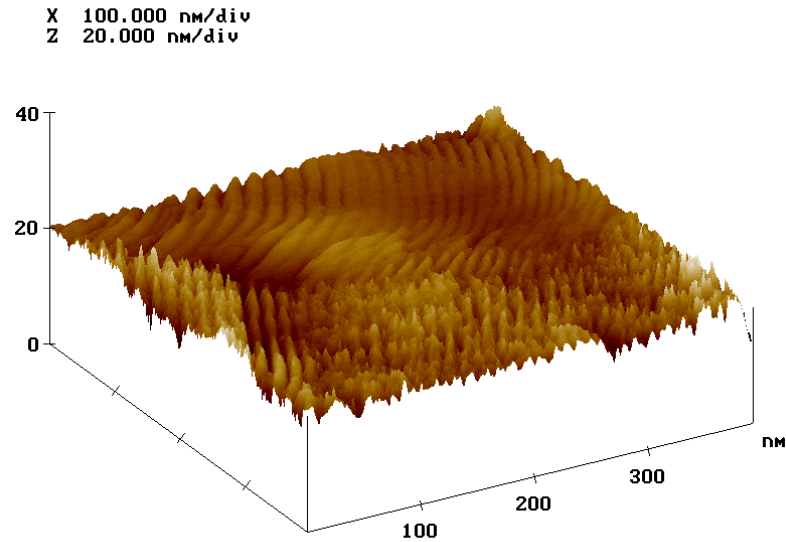


Figure 3.4 Pseudo 3D projection of the STM image shown in Figure 3.3b

### 3.1.3. Overview of HTS Thin Film Deposition

The two superconducting oxides studied in this thesis are  $\text{YBa}_2\text{Cu}_3\text{O}_{7-\delta}$  (YBCO) and  $\text{Ba}_2\text{Sr}_2\text{CaCu}_2\text{O}_{8+x}$  (BSCCO 2212). Considerably more research effort has been devoted to the growth of epitaxial YBCO films than BSCCO films. In general it is more challenging to obtain good quality BSCCO 2212 films, however the basic principles behind deposition are the same. The high quality (Rossler, *et al.* 2000) BSCCO 2212 films for this thesis were prepared by laser ablation, DC sputtering can also be employed (Raffy, *et al.* 1988, Raffy, *et al.* 1989). Difficulties arise mainly due to problems in avoiding contamination from the  $\text{Ba}_2\text{Sr}_2\text{Ca}_2\text{Cu}_2\text{O}_{10+x}$  (BSCCO 2223) and other phases.

As discussed, the extensive existing understanding of thin film deposition techniques meant that a range of candidate techniques were initially available for preparing films of HTS. By comparison to the deposition of conventional low  $T_c$  superconductors (LTS) some specific considerations constrain the range of suitable deposition techniques for oxide superconductors (Somekh, *et al.* 1992). Depositing HTS materials requires temperatures which are a large fraction of the material's melting point (typically 0.7-0.85) and the process is highly sensitive

to, amongst other factors, temperature and the oxygen concentration. In addition to ensure epitaxial growth the substrate must be a good lattice match to the HTS.

Two commonly used methods for preparing thin film samples are pulsed laser ablation (PLD) and DC sputtering. These methods were employed to grow the thin films measured for this Thesis. Both these techniques can produce films with  $T_c > 90\text{K}$  exhibiting high critical current densities. In general sputtering provides films with smoother surfaces as it is not prone to droplet formation on the surface of the film. However, in the measurements made for this thesis no systematic difference between the critical current behaviour of high quality PLD films and high quality sputtered films was observed.

Other techniques that can be used to prepare thin films of HTS include Metalorganic Chemical Vapour Deposition (MOCVD) (Berry, *et al.* 1988), E-beam evaporation and Liquid Phase Epitaxy (LPE) (Schneemeyer, *et al.* 1988). LPE, where the superconductor crystallises from precursors dissolved in a flux, has been the subject of considerable research effort as it seems suitable for the production of continuous lengths of conductor.

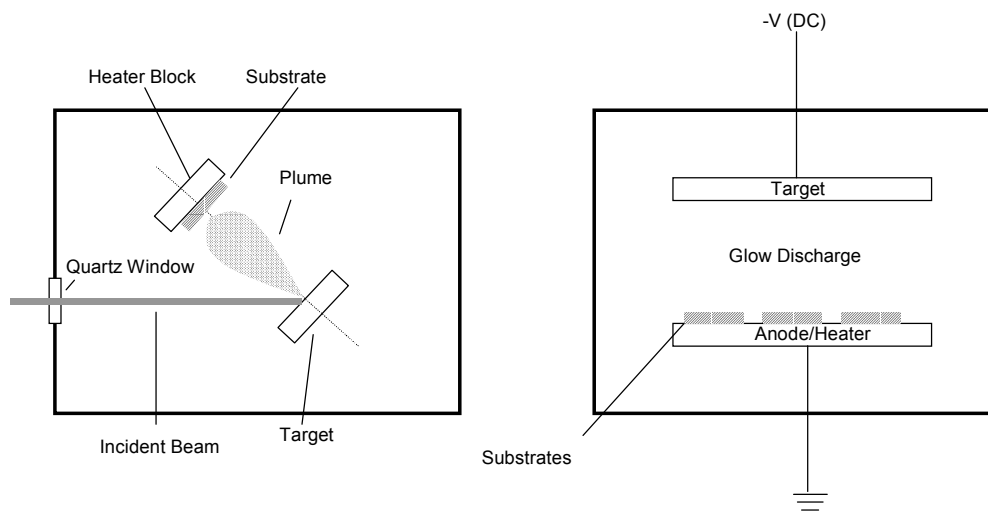


*Figure 3.5 Simplified schematic of a PLD system (left) and a DC sputtering system (right). After Ohring (1992).*

In a PLD system a laser is fired repeatedly at a stoichiometric target, the substrate is positioned in the resultant plume of ablated material and growth results. There are many parameters in optimising a Pulsed Laser Deposition (PLD) system among which the most critical are pulse repetition rate, beam energy, substrate temperature and the oxygen partial pressure during deposition.

In DC sputtering systems, a sputtering gas, such as argon, is first ionised. Positive Ar ions are accelerated towards the target, which is held at a negative potential with respect to the

substrate holder. Neutral atoms are then removed from the target via momentum transfer. These atoms travel through the discharge and are deposited on the substrate.

The systems shown in Figure 3.5 are *on-axis* deposition systems, *off-axis* deposition systems are also employed. In an off-axis system the substrate is tilted with respect to the target. Off-axis laser ablation can produce films with a very smooth surface (Santiso, *et al.* 1998).

Commonly used substrates for YBCO deposition (with the lattice mismatch) are SrTiO<sub>3</sub> (1.2%), LaAlO (2.6%) and MgO (8%). The best lattice matches are obtained with gallates such as PrGaO<sub>3</sub> (0.02%), however these materials are relatively costly. MgO has a low dielectric constant which makes it a good choice for films grown for microwave applications, the large lattice mismatch does not preclude the growth of good quality films. LaAlO<sub>3</sub> films exhibit clear twins and SrTiO<sub>3</sub> is a good general purpose substrate. There are many other perovskite materials with similar lattice matches (Somekh, *et al.* 1992).

The temperature range employed has a strong effect on film growth, a temperature of 650-750 °C tends to produce *a*-axis orientated films, although if morphologically clean *a*-axis films are required, a template layer is grown at this temperature and growth is completed at a higher temperature (Linker, *et al.* 1992). At 750-830 °C growth tends to be *c*-axis orientated with characteristic 'spiral' growth patterns. On vicinal substrates a slightly higher temperature is required for optimal film properties, vicinal films have also been found to be much more sensitive to small substrate temperature variations (Gibson 2000). It has also been shown that vicinal films are sensitive to substrate surface preparation (Haage, *et al.* 1997). While the films measured for this thesis did not exhibit them, it appears that films grown on annealed substrates can exhibit anti-phase boundaries leading to enhanced pinning and thus higher critical current values (Habermeier, *et al.* 1998).

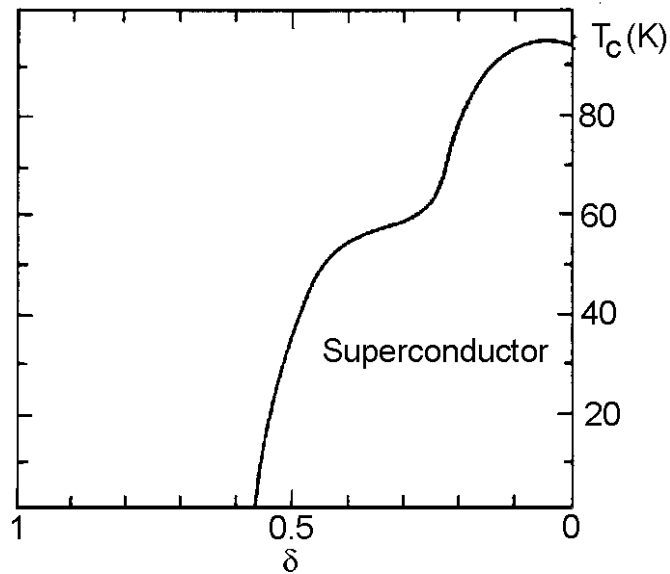


Figure 3.6 Variation of  $T_c$  with oxygenation in  $YBa_2Cu_3O_{7-\delta}$  (Cyrot and Pavuna 1995)

After film growth, an oxygenation step is required to obtain optimum properties. The film is annealed under oxygen in order to ensure optimum oxygen doping and thus the highest possible  $T_c$ . The optimum doping is with  $\delta=0.07$ . Figure 3.6 shows the variation of  $T_c$  with oxygenation. The annealing step can be carried out at a lower oxygen pressure if de-oxygenated films are required. It is possible, as shown in Figure 3.7, to predict what conditions are required to give a particular oxygenation. When de-oxygenating the films measured for this work it was not found possible to reliably produce films with a particular value of  $\delta$ . The de-oxygenation of YBCO is discussed further in Chapter 5.

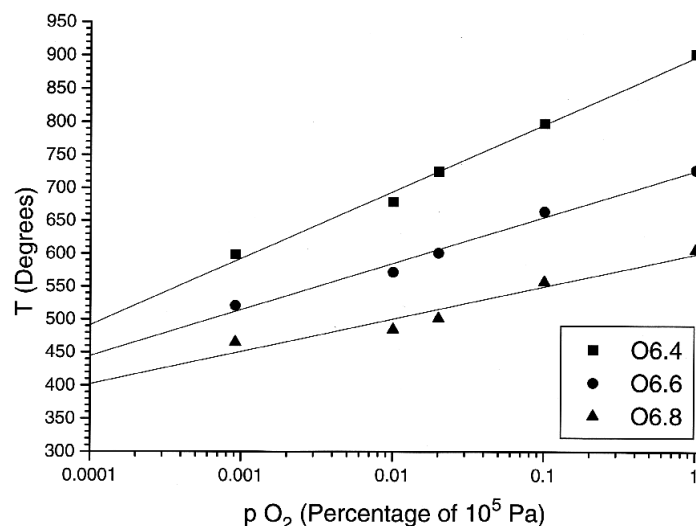


Figure 3.7 Plot showing predicted equilibrium oxygenation values for varying combinations of temperature and pressure. (Vazquez-Navarro 1998, Vazquez-Navarro, et al. 2000)

## **3.2. Sample Preparation**

### **3.2.1. Sources of Films Studied in this Thesis**

Appendix A lists the samples studied for this work. Most of these films were prepared by my colleagues in the IRC in Superconductivity in Cambridge, Dr E. Tarte, Dr A. Bramley, Dr V. Tsaneva and Dr G. Gibson. Some of the films were provided by Mr R. Rössler and Dr J Pedarnig of the Department of Applied Physics at the Johannes-Kepler Universität Linz. Films studied with numbers in the range 8000-9999 were deposited using an off-axis DC sputtering system (Mechin, *et al.* 1998). Films in the Y and Z series were deposited in Cambridge using an off and an on-axis laser ablation system respectively. Finally films 210600 and 200630 were provided by the University of Linz having been prepared by on-axis laser ablation. BSCCO films identified as L1,L2 and L3 were also deposited in Linz using laser ablation (Zahner, *et al.* 1998, Rossler, *et al.* 2000).

### **3.2.2. Contacts**

Good quality electrical contacts are an absolute prerequisite to successful measurements. In most cases, it was found that where it was impossible to obtain low noise results, that this was due to high contact resistances. Previous experiments carried out using the apparatus described here employed e-beam evaporated Au/Ag contacts (Herzog 1997), and this technique was used for sample 8722. However, it was found experimentally that contacts ex-situ sputtered using a lift off process could carry up to 0.5A without the need for contact annealing. An additional advantage was that the lift-off method did not require the use of a metal contact mask with the consequent risk of scratching samples.

Contacts were deposited before patterning. First 2  $\mu\text{m}$  of Hoechst AZ1529 resist was spun onto the chip and baked for one minute at 100 °C. The chip was then exposed to UV light through a negative mask of the contact pad pattern, using a projection lithography system. As fine features are not required in this process the resist was over exposed (4 minutes) to ensure that the developer was easily removed. This was especially important at the edge of the chip where the resist is thicker.

Once exposed the pattern was developed in a 4:1 diluted proprietary developer solution for about 30 s. By observing changing interference fringes on the surface during developing it was possible to accurately perform this step, thus minimising the contact between the surface of the film and the developer solution. This is important since the surface of YBCO may become passivated by contact with water. As the resolution required was low no step to improve the lift-off was required. When lift-off processes are performed on small features the

resist is often treated with chlorobenzine to generate an overhang at the edge of the remaining resist.

After drying in compressed air, layers of silver and gold were deposited using magnetron sputtering (roughly 150nm layers of each). The use of an Au/Ag bilayer has previously proven to give good quality contacts (Herzog 1997). After soaking in acetone the remaining photoresist was removed along with the unwanted sections of the Au/Ag layer.

### 3.2.3. Patterning

The majority of films prepared were patterned using broad beam Argon ion-milling which, although not essential for 10 micron features, results in a current track with sharply defined edges.

Two image masks used were used, these were designed for use with vicinal films and feature perpendicular tracks to allow the properties of the film both transverse **T** and parallel **L** to the vicinal steps to be examined. For 12x3 mm substrates a pattern (CAM 24) with 6 10x100 micron tracks, 3 **T** and 3 **L**, was used as shown in Figure 3.8. A pattern for 10x10 mm substrates (IRC 194) provided 2 **T** and 1 **L** track at widths of 20, 10 and 5 microns.

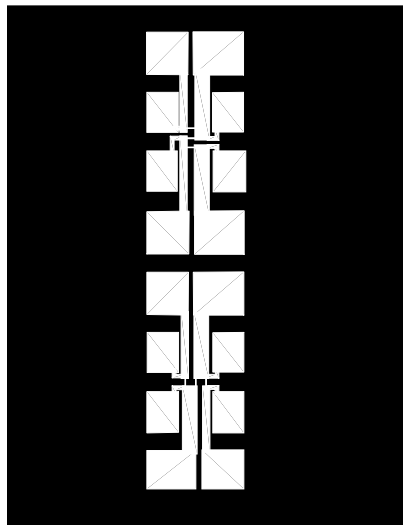


*Figure 3.8 An example of a lithographic mask pattern. The pattern, drawn using a CAD program, is transferred to a chromed quartz plate. (Mask CAM 24)*

In order to pattern a film, it was first cleaned using acetone both in an ultrasound bath and using an airbrush. A 2  $\mu\text{m}$  layer of Hoechst AZ1529 photoresist was then applied and baked for 1 minute at 100°C. The mask pattern was then transferred to the photoresist using a projection lithography system. A 45 second exposure of UV light gave satisfactory results. The exposed developer was then removed in a 4:1 concentration of the resist manufacturer's proprietary developer.

When patterning films grown on vicinal substrates it is essential to ensure that the current tracks are well aligned in relation to the vicinal direction. Using the mask aligner it proved possible to carefully align the pattern edge with the edge of the sample. In this way it proved possible to achieve rotational alignment errors of less than  $0.5^\circ$ .

Ion milling, using Ar-ions, was employed to transfer the desired pattern from the photoresist to the YBCO film. In an ion-milling system an ion gun directs ionised Argon towards the sample. The incident ions ablate both the exposed YBCO and the photoresist. This technique is not selective, however the layer of photoresist is much thicker than the YBCO film and is milled more slowly. In the system used, YBCO was milled at approximately 12 nm per minute with a  $0^\circ$  beam incidence angle. Ion-milling was found to give very satisfactory clean tracks which outweighed the slightly increased complexity of the process. Ion milling has been used successfully to produce tracks in YBCO as thin as  $0.2 \mu\text{m}$  (Schneider, *et al.* 1993). The alternative approach using orthophosphoric acid to perform the etching results in a less well defined track edge. Figure 3.9 shows a section of a Ar-ion patterned film.

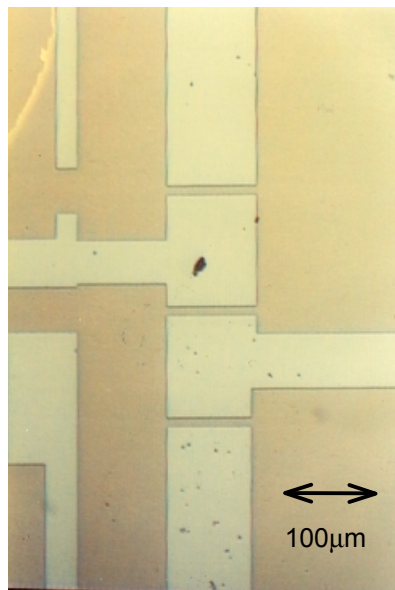


*Figure 3.9 A track patterned transferred onto a YBCO film grown on a vicinal substrate, the edge of a contact pad is visible in the top left of the image.*

### 3.3. Film Characterisation

#### 3.3.1. X-Ray

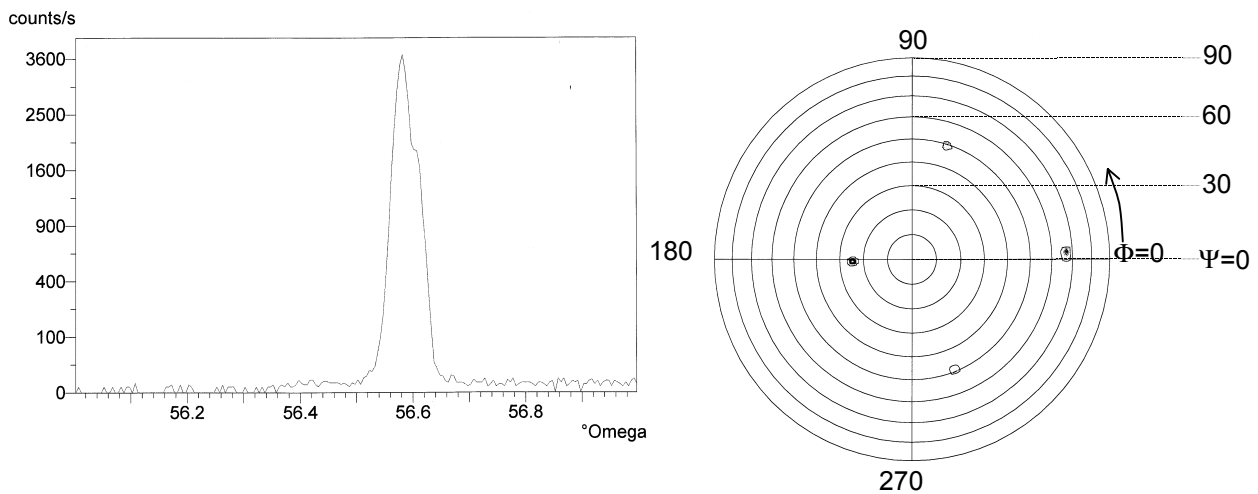


Figure 3.10 (005) Rocking curve (left) and (103) pole figure (right) for a YBCO film grown on a 20 degree miscut substrate. The rocking curve shows that the film is well aligned and the pole figure shows that the film has indeed grown with the desired orientation. (Data courtesy N. Rutter).

Having deposited a film, it is of course essential to ensure that the desired well aligned epitaxial growth has occurred. Rocking curves were taken from representative samples from the batches measured. In general, rocking curves taken from films grown on vicinal substrates were slightly less well aligned than the best  $c$ -axis films. Figure 3.10a shows data from film Z334B with a FWHM of about  $0.4^\circ$ . Sample Z334B was grown using PLD, sputtered vicinal films have been found to exhibit similar values for the FWHM, a very good quality  $c$ -axis film will have a FWHM value of around  $0.2^\circ$  (Mechin, *et al.* 1998).

In order to confirm that the films had grown with the same tilt angle as the substrates pole figures were obtained using a four-circle X-ray diffractometer. These measurements confirm the in-plane alignment of the film. As an example Figure 3.10b shows the pole figure from a  $20^\circ$  off axis film. There is no indication from the pole figure of any  $c$ -axis growth.

#### 3.3.2. AFM Imaging

Atomic Force Microscopy is a powerful tool for assessing the morphological quality of films. A Digital Instruments Nanoscope III was used in tapping mode to obtain AFM images of at least one film in each batch measured. The AFM was operated in 'Tapping Mode'. In this technique the probe is oscillated at a constant frequency as the AFM head scans across the surface. The amplitude of oscillation of the tip varies as it moves nearer to the surface of the film, this change is used as feedback to control the sample-tip distance and deduce the surface

height of the film. In addition the AFM used could be employed as an STM. Here the AFM head is replaced with a mechanically pulled PtIr tip held at a potential of a few hundred mV above ground. As the tip closes with the surface of the sample, which is connected to ground, a tunnelling current flows which provides measure of the tip-sample distance.

Figure 3.3a was taken using Tapping Mode AFM and Figure 3.3b is an example of an STM image. It was possible to confirm the existence of the characteristic step flow growth steps in the YBCO vicinal films measured. In general AFM measurements revealed that it was difficult to obtain vicinal films with as high a quality as the best *c*-axis films. Even the best films exhibited pin-hole defects or outgrowths, as shown in Figure 3.11.

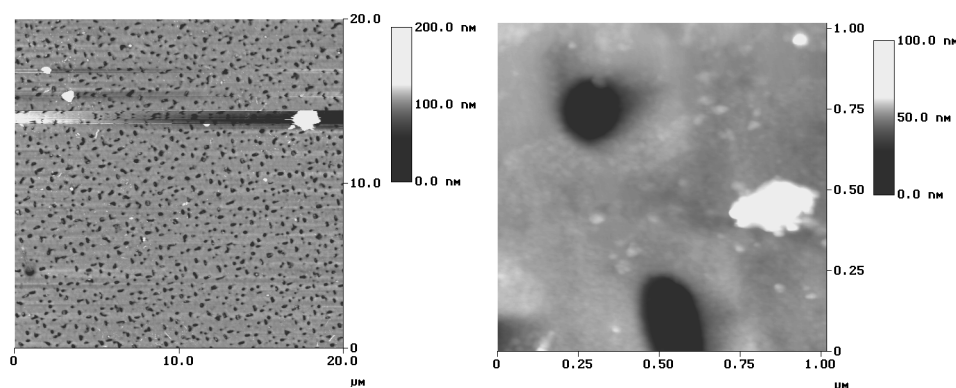


*Figure 3.11 AFM images of a 6 degree vicinal YBCO film (Z323) grown by on-axis PLD, showing characteristic pin hole defects.*

The AFM employed was well calibrated in the *z*-axis, a maximum error of +/- 2 nm was observed imaging 180nm deep pits on a calibration sample. The AFM could therefore be used to obtain film thickness by measuring the height of chemically etched steps.

### 3.3.3. $T_c$ Measurements

In order to measure the critical transition temperature of the thin films,  $T_c$ , a four point resistance technique was used employing a probe dipped into an He storage dewar. When measuring de-oxygenated films, the transition temperature gives an indication of the average film oxygenation, as shown in Figure 3.6. The transition curve for an unpatterned, de-oxygenated 6° vicinal film is shown in Figure 3.12. More accurate *R-T* curves on patterned tracks, and *R-T* curves in field were obtained using the measurement apparatus described in section 3.4.

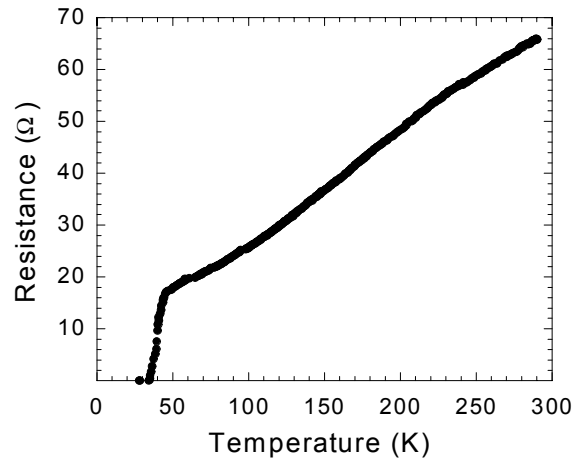


*Figure 3.12 A resistance versus temperature plot for a de-oxygenated YBCO film (8722) grown on a  $6^\circ$  vicinal substrate.*

The probe consists of a copper block with a platinum resistance temperature sensor embedded within. The film is contacted by an array of spring loaded Pogo® contacts set in a tufnol block. The contact block clamps the sample to the copper block ensuring good thermal contact between the temperature sensor and the sample.

The probe is cooled by lowering it slowly into the cold helium vapour in the neck of a standard helium transport dewar. Data acquisition is automatically performed by a program written in the graphical programming language LabVIEW (Kirkman and Buksh 1992) by the author. As the probe is cooled, the measurement system continually measures the resistance of the film and the temperature sensing element using a standard four wire technique. The resistance of the platinum sensor is converted to a temperature using the calibration supplied by the manufacturer. The temperature sensing element does not produce meaningful readings at temperatures below  $\sim 40$  K. To limit the amount of data recorded to manageable proportions a new point is only recorded when it is outside a user defined ellipse around the previous point.

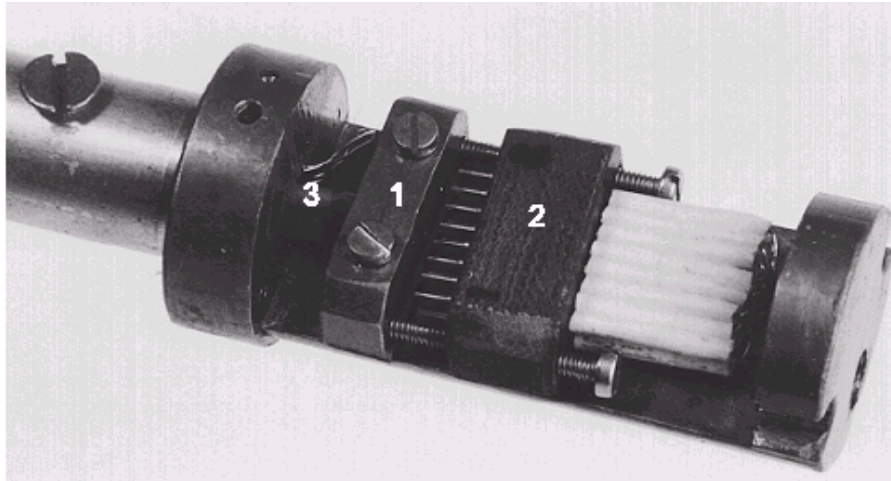


*Figure 3.13.  $T_c$  probe sample holder showing copper block containing temperature sensor (1), pogo pin holder (2), and wiring (3).*

All the fully oxygenated samples measured for this thesis had  $T_c > 90\text{K}$  (zero resistance) and  $< 0.5\text{ K}$  wide. This is not as good as can be routinely achieved using  $c$ -axis films (Herzog 1997), however superconducting film growth on vicinal substrates is a less well developed technique.

### **3.4. Measurement Rig**

#### **3.4.1. Goniometer**

To study the angular dependence of critical current on field, it is important to be able to rotate the field in two axes rather than just one. The experiments described in this thesis were therefore, performed using a high resolution two-axis goniometer (Figure 3.14). The goniometer employed was built and designed by R. Herzog (Herzog and Evetts 1994, Herzog 1997).

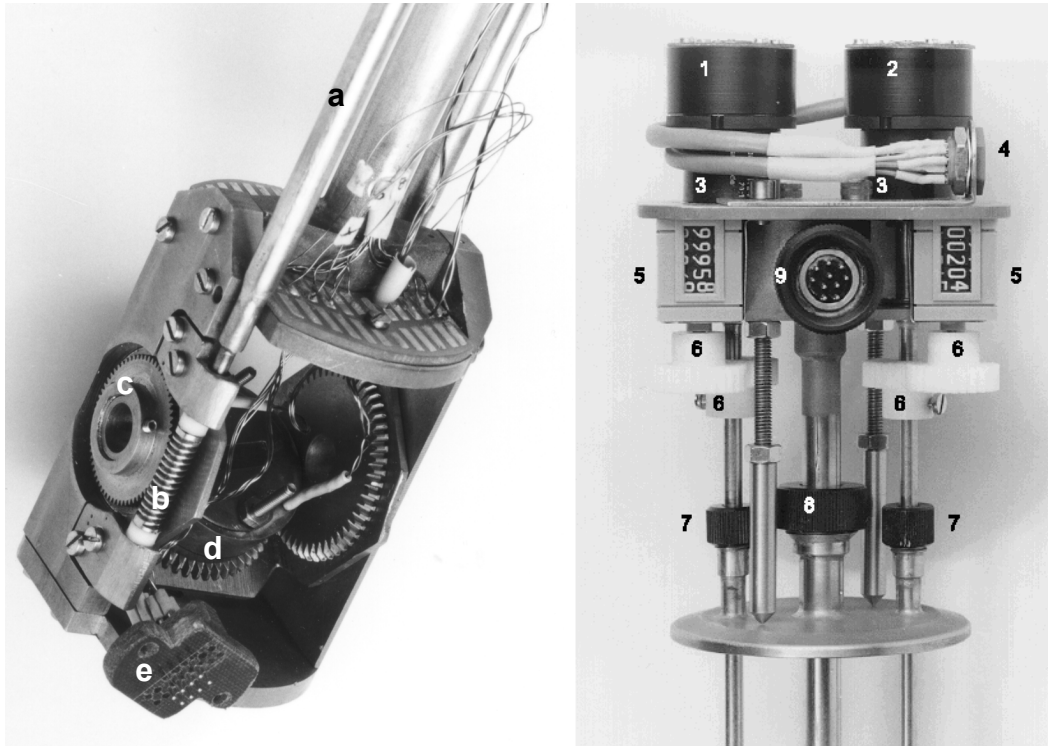


Figure 3.14 Goniometer sample space (left) and head (right). The left figure shows the drive shafts (a), worm gears (b), drive gear (c), copper block containing temperature sensor and heater element (d) and the tufnall block in which the Pogo contacts are mounted (e). On the right is shown the drive motors for  $\theta_e$  (1) and  $\phi_e$  (2) rotation, reduction gearing (3), position indicators (5) and the compression glands round the support and drive shafts (7,8). The probe is gas tight, this allows it to be used in the flow cryostat.

The goniometer allows the copper block, against which the sample is held by spring loaded contact pins, to be tilted ( $\theta_e$ ). The copper block may be rotated ( $\phi_e$ ). These axes of rotation are illustrated in Figure 3.15. It should be noted that the axis of  $\phi_e$  rotation tilts with  $\theta_e$ . Due to the arrangement of the gearing if rotation in  $\theta_e$ , with  $\phi_e$  held constant, is desired the second,  $\phi_e$ , drive shaft must be rotated the same number of steps as the block is tilted.

The motors are driven by a microstepping controller which allows the motors to be positioned with a high degree of angular resolution, one degree of rotation requires  $2166\frac{2}{3}$  motor steps. In use the stepper motor controller is itself remotely operated by a computer which takes care of translating a desired  $\theta_e$ ,  $\phi_e$ , position into the number of motor steps required from the current position. The computer provides motor on/standby, direction and step signals for each motor to the controller in the form of TTL level digital signal lines.

The goniometer control system is open-loop, in that there is no position feedback to the control software to ensure that the desired position has been reached. In operation, to provide manual verification that the system is working correctly, the computer displays the position which it records the stage as being at. This can be compared to the position indicators

mounted on the head of the probe. The accuracy of the system in use is therefore limited by the accuracy to which these counters may be read,  $\pm 0.1^\circ$ .

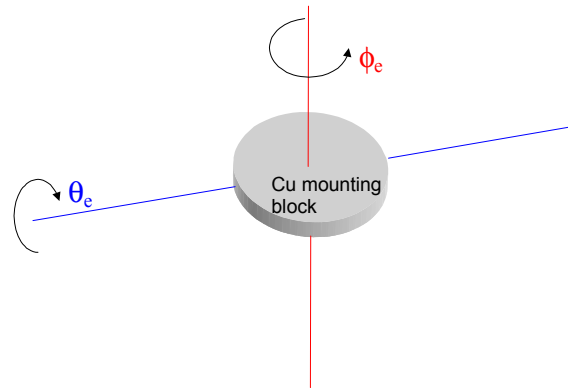


*Figure 3.15 Axes of rotation of the sample holder.*

For measurements on *c*-axis films the angles describing the rotation of the stage  $\phi_e$  and  $\theta_e$  can be easily be used to obtain the angle of the applied magnetic field with respect to the crystal axes of the superconducting sample. It is simple to define the tilt of the magnetic field  $\theta$  as being the angle between the field and the cuprate planes. This can be directly obtained from  $\theta_e$ . The angle  $\phi_e$  then gives the angle of rotation of the magnetic field about the *c*-axis with respect to the current direction.

When a film grown on a vicinal substrate is considered, the geometry becomes considerably more complex. Figure 3.16 shows a section of a current track in a vicinal film. We again define  $\theta$  and  $\phi$ , which give the direction of the applied field with respect to the crystal structure of the tilted thin film.  $\theta$  is the angle between the field and the cuprate planes,  $\theta=0^\circ$  corresponds to the field parallel to the planes.  $\phi$  represents rotation of the plane in which the field is tilted. The angle  $\phi=0^\circ$  is defined as being when the magnetic field is rotated in the same plane as the vicinal tilt.

At  $\phi_e=0^\circ$  converting from  $\theta_e$  to  $\theta$  is simple,  $\theta_v$  must be subtracted and  $\phi_e=\phi=0^\circ$ . This is not true for other values of  $\phi_e$ . For example, a scan in  $\theta_e$  with  $\phi_e=90^\circ$  will not be perpendicular to the crystal structure when the applied field is parallel to the surface normal. The maximum discrepancy is  $\theta_v$ .

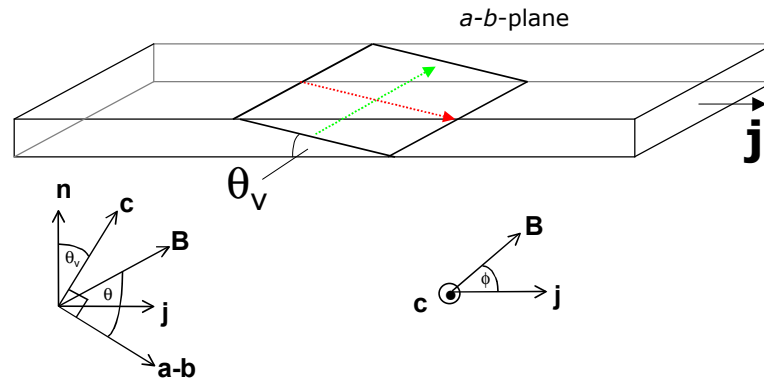


Figure 3.16 A cross section of a current track showing the direction of the field at  $\theta=0^\circ$ ,  $\phi=0^\circ$  (red) and  $\theta=0^\circ$ ,  $\phi=90^\circ$  (green). The vicinal angle  $\theta_v$  is the angle between the surface normal  $\hat{n}$  and the c-axis of the material.

The geometry of the magnetic field orientation dependent critical current measurements is discussed further in Chapters 4 and 6.

### 3.4.2. Sample Mounting

Contact to the sample was effected using Pogo® pins. To ensure that differential contraction at cryogenic temperatures did not cause loss of contact indium pads were placed between the pogo pins and the Au/Ag contact pads. Occasionally a small amount of silver paste was used to hold the indium pads in place during mounting.

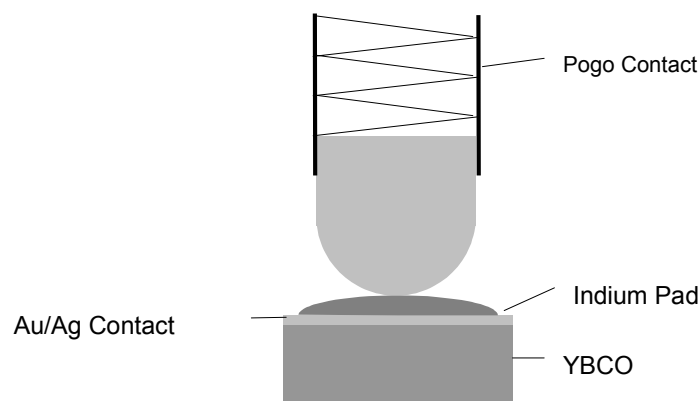


Figure 3.17 Contact between a pogo pin and a superconducting sample.

The probe was wired throughout with copper wire. Initially low thermal Cd alloy solder had been used for joints. However empirically it was found that standard 60/40 Sn/Pb solder gave just as satisfactory results with fewer health and safety concerns.

### 3.4.3. Cryostat

In use the goniometer is mounted in a variable temperature insert placed in the bore of a 8T superconducting magnet. Figure 3.18 shows the basic layout of the cryostat. In use a diaphragm pump creates a vacuum in the sample space which draws in cold helium liquid

through a needle valve. The helium boils and a stream of cold gas flows over the goniometer. The heating element in the copper block allows a temperature controller (Oxford Instruments ITC 4) to maintain the sample at a constant temperature. In use a temperature ripple of less than 30mK is regularly achieved which is similar to the measurement accuracy of the sensor.

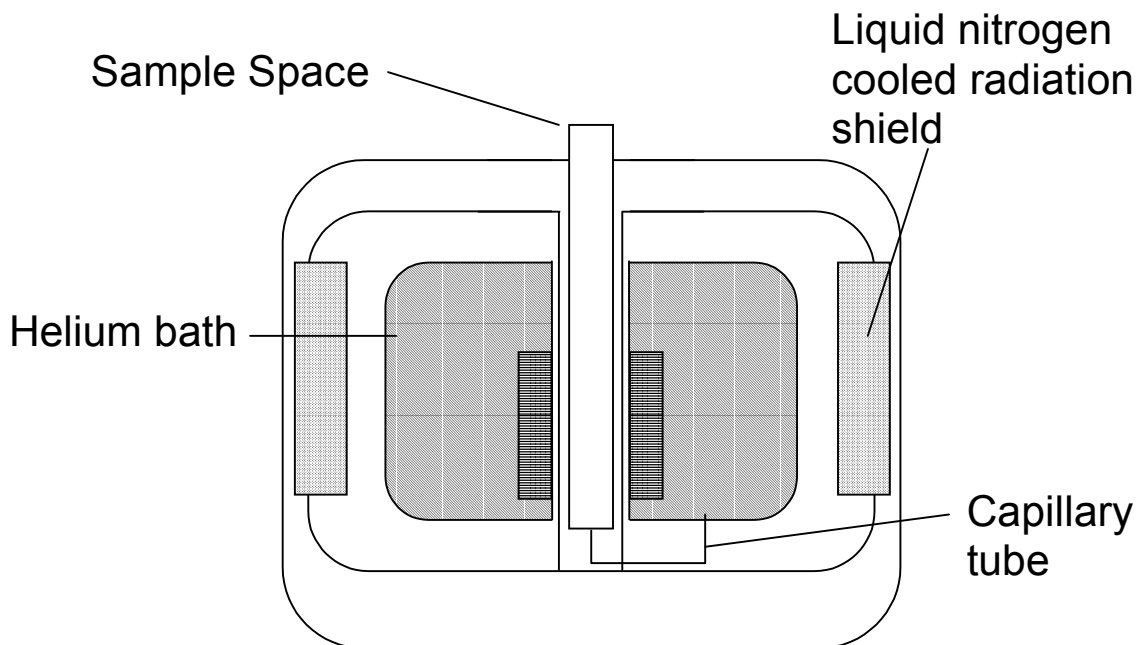


Figure 3.18 Schematic diagram of cryostat. For clarity the needle valve, magnet wiring and supports are omitted.

The temperature of the copper block is measured using a Lakeshore Cryotronics Cernox<sup>TM</sup> resistance sensor (Brandt, *et al.* 1999). The sensor is fitted into a flush fitting aperture in the copper block, as recommended by the manufacturer silicon grease was used to ensure good thermal contact. This has similar field insensitivity to a carbon-glass temperature sensor but allows useful readings to be obtained over the range 3K to 300K rather than 3K to 100K typical for Carbon-Glass sensors. The sensor is excited using a constant voltage source and the controller measures its conductance, the non-linearity in the response of the sensor is eliminated using a breakpoint table stored in the controller. The manufacturer's quoted accuracy of the sensor is  $\pm 35$  mK, however given the extra uncertainty introduced by the breakpoint table and the manufacturer's quoted worst case long term drift of  $\pm 25$  mK/year (over two years of operation since calibration) it is considered that the sensor is accurate to  $\pm 50$  mK. A second, carbon-glass temperature sensor allows the temperature at the base of the sample space to be ascertained.

The magnet system is economical in operation, 30 l of liquid helium often being sufficient for a week of measurements. The system was prone to icing of the helium capillary tube to

which no long term solution was found other than warming the cryostat up to room temperature periodically and flushing with dry He gas.

#### 3.4.4. Measurement Apparatus

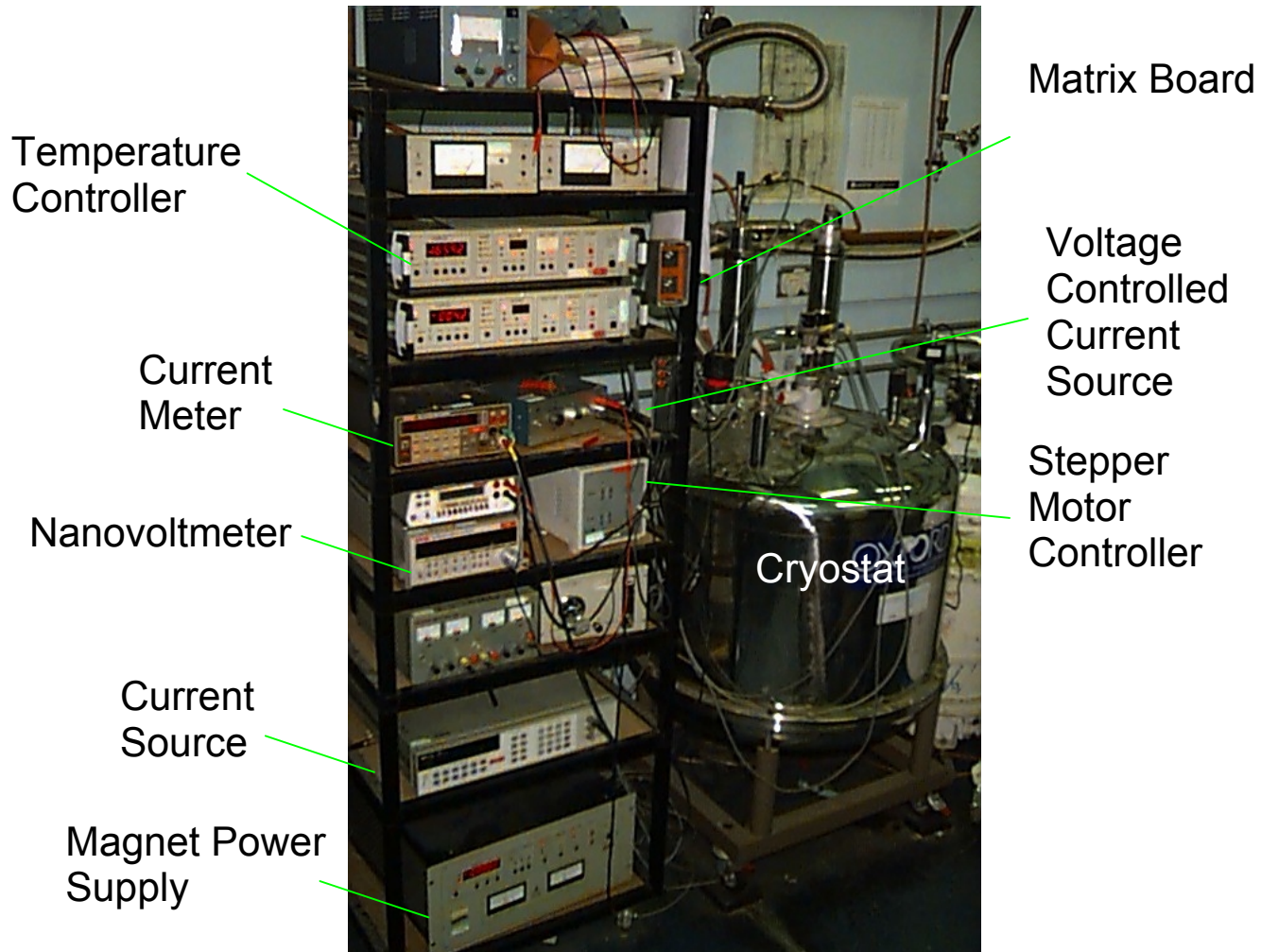


Figure 3.19 Physical layout of the experimental apparatus.

Four terminal resistance measurements on the sample were made using a HP8250A universal source to drive a current through the sample. For currents above 100mA a voltage controlled current source was controlled by the universal source, this provided currents up to 1A. The current flowing through the sample was independently measured using a Keithley model 199 DMM. A Keithley model 182 nanovoltmeter was used to measure the voltage developed in the sample. The built in digitally synthesized filter of the nanovoltmeter was used to obtain the lowest noise readings. When in use this requires at least 8 seconds to be allowed between readings, to allow the voltage value to settle.

Once DC offsets had been eliminated average noise levels of less than  $1 \times 10^{-8}$  V were measured, with this in mind a voltage criterion of  $5 \times 10^{-8}$  V was chosen to determine critical current. On a typical 500  $\mu\text{m}$  long track this corresponds to an electric field of  $1 \times 10^{-4}$  V/m.

The same configuration also allowed both resistance/temperature and resistance/field measurements to be made. A matrix board allowed the current and voltage pairs to be connected to any combination of the 12 pogo pins in the tufnol block. Figure 3.20 shows a block diagram of the measurement system.

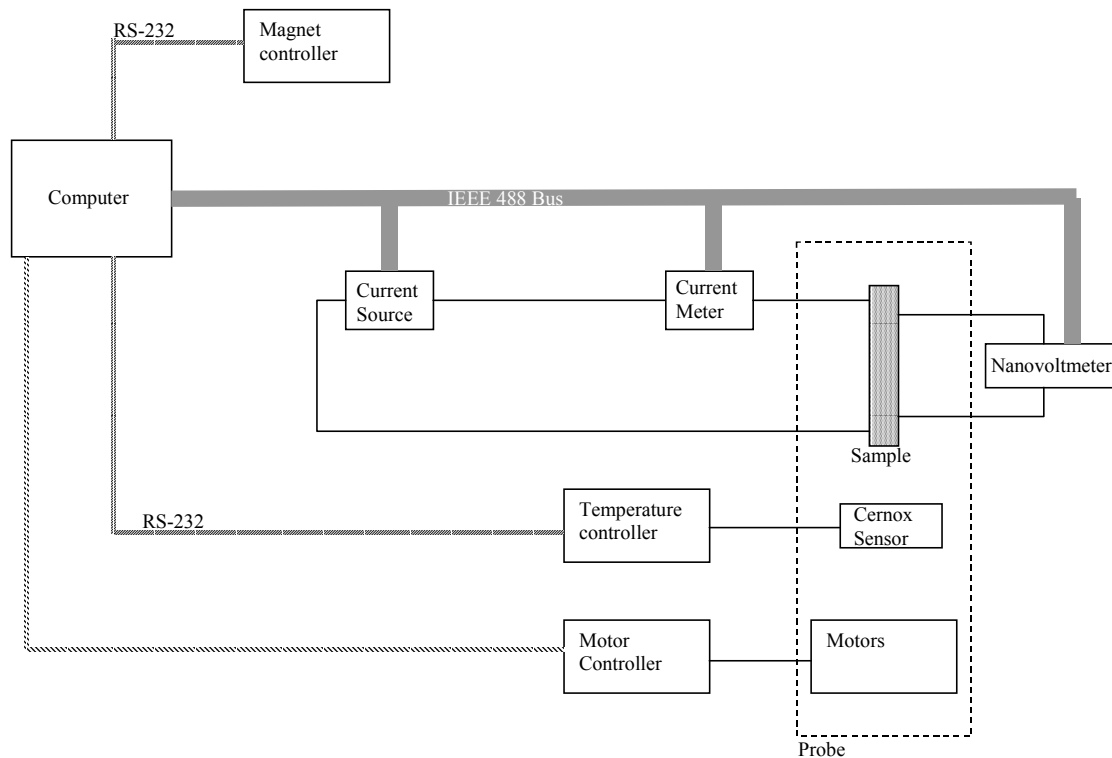


Figure 3.20. Block diagram of the measurement system.

### 3.4.5. Software

Computerised data logging is essential to high resolution angular  $J_c$  measurements, however if this is combined with computer control of the experiment it is possible to obtain a large number of data sets. As initially constructed the physical apparatus described above was automated in the language ASYST using an IBM 80386 computer with limited memory capacity Herzog (1997). In order to provide more measurement flexibility, extended provision for unattended operation and greater reliability, the measurement system was reimplemented in the LabView data acquisition language by the author. The data acquisition software was written from scratch although some library routines were employed for communication with measurement equipment. The software controlling the stepper motors was closely modelled on that written in ASYST by Herzog (1997).

The slow performance of the original computer necessitated that some of aspects of the measurement process be devolved to embedded controllers in the measurement equipment.

For example the current source autonomously performed current sweeps. The system becomes much more flexible and easy to debug if the central computer performs all the data processing.

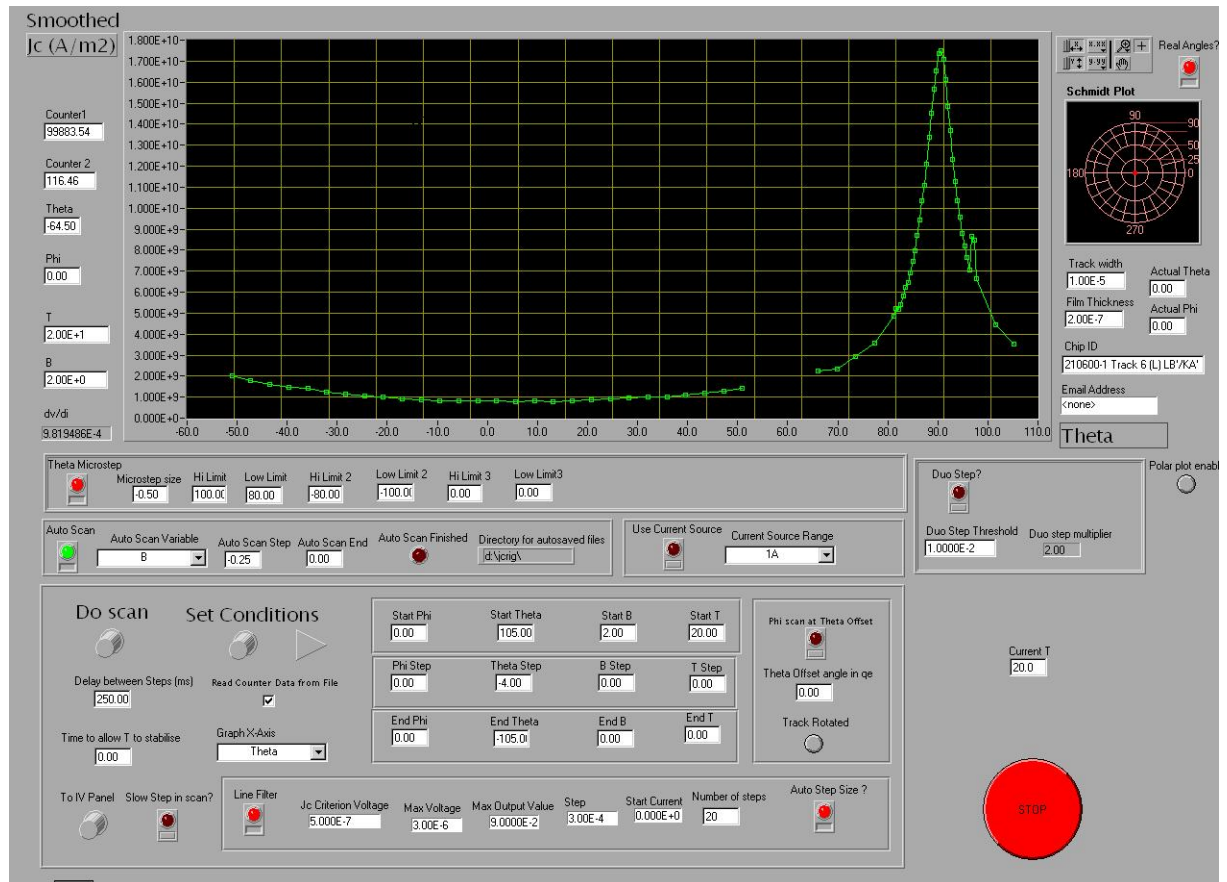


Figure 3.21 Screen shot of the front control panel of the LABVIEW application written by the author.

The measurement rig is capable of making a resistance or  $V/I$  measurement at any point in the experimental parameter space:  $(-8 < B < 8T)$ ,  $(4.2K < T < 300K)$ ,  $(-120^\circ < \theta < 120^\circ)$  and  $(0^\circ < \phi < 90^\circ)$ . This allows  $R(T)$ ,  $R(B)$ ,  $J_c(B)$ ,  $J_c(T)$ ,  $J_c(\theta)$  and  $J_c(\phi)$  measurements to be made.

For each datum point required the computer sets the required environmental parameters in accordance with scan settings requested by the user.

Resistance values are measured by a commutating technique. A user specified current is applied in the forward and reverse directions and the voltage recorded. In this way any zero offset may be eliminated.

If an  $IV$  curve is required the current is then stepped either in predefined increments or in increments determined from the last measured  $IV$  curve and the number of data points per curve desired by the user. During the measurement the current is increased by predetermined steps, at each step the voltage is recorded. When the recorded voltage exceeds a user-defined

value, usually two or three times the selected voltage criterion, the measurement is terminated and the computer continues to the next set of experimental parameters.

From the curve the critical current is determined by fitting a smoothed polynomial function to the measured data points. The value of the current at the voltage criterion may then be easily deduced. The use of a smoothing function has the additional advantage that a few 'rogue' data points do not result in erroneous critical current values being calculated. This is especially important when the program is using the last measured value of the critical current to determine the current step to use in the next measurement.

The use of these safeguards allows a large number, perhaps up to 20, of scans to be pre-configured and the apparatus left to perform them. The current status of the measurement can be viewed on any remote computer over the web and the entire system can be remotely controlled from a workstation with suitable software installed. In addition critical failures can be notified to the user via a SMS message to a mobile phone. This final feature was important since the apparatus is complex and exhibits many varied failure modes.

### **3.5. Conclusion**

The growth of the superconducting thin films used in this thesis and their patterning into experimental samples has been described. The availability of films grown on vicinal substrates and access to a high resolution two axis probe are almost a absolute prerequisite to the study of the angular dependence of critical currents in superconducting thin films. Intrinsically the experimental configuration is very flexible, the development of a control system in the modular LabVIEW program allows this to be fully exploited and provides reliable unattended operation. The flexibility of the system has allowed it to be used essentially unmodified in a separate research program on the magnetic field dependent behaviour of low angle grain boundaries in YBCO (Hogg, *et al.* 2001).

### **3.6. Bibliography**

- Berghuis, P., F. Baudenbacher, R. Herzog, R. Somekh, A. M. Campbell, J. E. Evetts and G. Wirth (1996). Proc. 8th IWCC in Superconductors, World Scientific, Singapore.
- Berghuis, P., E. DiBartolomeo, G. A. Wagner and J. E. Evetts (1997). Phys. Rev. Lett. **79**(12): 2332-2335.
- Berry, A. D., D. K. Gaskill, R. T. Holm, E. J. Cukauskas, R. Kaplan and R. L. Henry (1988). Appl. Phys. Lett. **52**(20): 1743-1745.
- Brandt, B. L., D. W. Liu and L. G. Rubin (1999). Rev. of Sci. Instr. **70**(1): 104-110.

- Chana, O. S., A. R. Kuzhakhmetov, P. A. Warburton, D. M. C. Hyland, D. Dew-Hughes, C. R. M. Grovenor, R. J. Kinsey, G. Burnell, W. E. Booij, M. G. Blamire, R. Kleiner and P. Muller (2000). Appl. Phys. Lett. **76**(24): 3603-3605.
- Cyrot, M. and D. Pavuna (1995). Introduction to Superconductivity and High- $T_c$  materials. Singapore, World Scientific.
- Datta, T. (1992). Oxide Superconductors: Physical Properties. Concise Encyclopedia of Magnetic and Superconducting Materials. J. E. Evetts. Oxford, Pergamon
- Gibson, G. (2000). Private Correspondance.
- Haage, T., J. Zegenhagen, J. Q. Li, H. U. Habermeier, M. Cardona, C. Jooss, R. Warthmann, A. Forkl and H. Kronmuller (1997). Phys. Rev. B. **56**(13): 8404-8418.
- Habermeier, H. U., T. Haage, J. Zegenhagen, R. Warthmann and C. Jooss (1998). Supercon. Sci. Technol. **11**(10): 929-934.
- Herzog, R. (1997). Critical Currents in YBCO thin films. Materials Science and Metallurgy, University of Cambridge.
- Herzog, R. and J. E. Evetts (1994). Rev. Sci. Instr. **65**(11): 3574-3576.
- Hogg, M. J., F. Kahlmann, E. J. Tarte, Z. H. Barber and J. E. Evetts (2001). Appl. Phys. Lett. **78**(10): 1433-1435.
- Kirkman, I. W. and P. A. Buksh (1992). Rev. Sci. Instr. **63**(1): 869-872.
- Linker, G., E. Brecht, J. Geerk, O. Meyer, B. Rauschenbach, J. Reiner, J. Remmel, C. Ritschel and W. R. L. (1992). Growth of a-axis orientated YBaCuO and EuBaCuO thin films. High Temperature Superconductor thin Films. L. Corraera. Amsterdam, North-Holland
- Mechin, L., P. Berghuis and J. E. Evetts (1998). Physica C **302**(2-3): 102-112.
- Ohring, M. (1992). The Materials Science of Thin Films, Academic Press, San Diego: xix-xx, 79
- Raffy, H., S. Labdi, A. Vaures, J. Arabski, S. Megtert and J. Perriere (1989). Physica C **162**: 613-614.
- Raffy, H., A. Vaures, J. Arabski, S. Megtert, F. Rochet and J. Perriere (1988). Solid State Comm. **68**(2): 235-238.
- Roas, B. L., L. Schultz and G. Saemannishenko (1990). Phys. Rev. Lett. **64**(4): 479.
- Rossler, R., J. D. Pedarnig, D. Bauerle, E. J. Connolly and H. W. Zandbergen (2000). Appl. Phys. a **71**(3): 245-247.
- Santiso, J., A. Moya and F. Baudenbacher (1998). Supercon.Sci. Technol. **11**(5): 462-466.

- Schneemeyer, L. F., R. B. Vandover, S. H. Glarum, S. A. Sunshine, R. M. Fleming, B. Batlogg, T. Siegrist, J. H. Marshall, J. V. Waszczak and L. W. Rupp (1988). Nature **332**(6163): 422-424.
- Schneider, J., H. Kohlstedt and R. Wordenweber (1993). Appl. Phys. Lett. **63**(17): 2426-2428.
- Somekh, R. E., Z. H. Barber and J. E. Evetts (1992). Oxide Superconductors: Thin-Film Deposition. Concise Encyclopedia of Magnetic and Superconducting Materials. J. E. Evetts. Oxford, Pergamon: 431-440
- Somekh, R. E., M. G. Blamire, Z. H. Barber, K. Butler, J. H. James, G. W. Morris, E. J. Tomlinson, A. P. Schwarzenberger, W. M. Stobbs and J. E. Evetts (1987). Nature **326**(6116): 857-859.
- Vazquez-Navarro, M. D. (1998) Personal Communication.
- Vazquez-Navarro, M. D., A. Kursumovic and J. E. Evetts (2000). Boletin De La Sociedad Espanola De Ceramica Y Vidrio **39**(3): 213-216.
- Waldram, J. (1996). Superconductivity of Metals and Cuprates. London, Institute of Physics Publishing: 222-229
- Zahner, T., R. Stierstorfer, R. Rossler, J. D. Pedarnig, D. Bauerle and H. Lengfellner (1998). Physica C **298**(1-2): 91-94.

## 4. Critical Currents in Vicinal YBCO Films

*The transport critical current density,  $J_c$ , in  $YBa_2Cu_3O_{7-\delta}$  (YBCO) varies with the orientation of the applied magnetic field. This dependence implies that there is a variation in the structure and pinning of the flux line lattice (FLL) with orientation of the applied magnetic field. The anisotropy of the FLL itself is due to the anisotropy and layered structure of YBCO. Most measurements of critical current densities in thin films to date have been performed on films where the  $c$ -axis grows normal to the film surface. With such 'c-axis' films, the analysis of the magnetic field angle dependence of  $J_c$  is complicated. The effects of extrinsic contributions to the angular field dependence of  $J_c$ , such as the measurement geometry and disposition of pinning centres are convoluted with those intrinsically due to the anisotropy of the material. As a consequence of this, it is difficult to distinguish between proposed FLL structure models on the basis of angular critical current density measurements on  $c$ -axis films. Films grown on mis-cut (vicinal) substrates have a reduced measurement symmetry and thus provide a greater insight into the critical current anisotropy. In this chapter previous descriptions of the magnetic field angle dependence of  $J_c$  in YBCO are reviewed. Measurements on YBCO thin films grown on a range of off-axis substrates are presented and the results interpreted in terms of the structure and dimensionality of the FLL in YBCO. There is strong evidence for a field angle and temperature dependent transition in the structure of the flux line lattice. As a consequence no one scaling law can, by itself, describe the observed critical current anisotropy.*

### 4.1. Previous Experimental Measurements

#### 4.1.1. Background

Measurements of the resistive transition, in a magnetic field applied at different angles to the cuprate planes, provides the simplest means of studying the field angle dependent properties of the flux line lattice (FLL) in YBCO. Such measurements indicate a broadening in the resistive transition with increasing applied field in both measurements on single crystals (Iye, *et al.* 1988, Palstra, *et al.* 1989) and thin single crystal films (Iye, *et al.* 1990). These results indicate that the broadening is thermal activation dependent, suggesting that it is due to

thermally activated flux creep. As is discussed in Chapter 2, flux creep is closely linked to the structure adopted by the FLL. Evidence for anisotropy of the FLL is apparent from the increased broadening of the resistive transition with a magnetic field applied parallel to the  $c$ -axis, as compared to that observed with fields applied parallel to the  $a$ - $b$  planes. In measurements on YBCO, Iye *et al.* (1989) found that the anisotropic Ginzburg-Landau (G-L) scaling equation (2.38) described the variation of  $B_{c2}$  with field angle. This provided evidence that the FLL in YBCO can be described using anisotropic G-L theory (Section 2.4.1). In contrast, measurements on  $\text{Bi}_2\text{Sr}_2\text{CaCu}_2\text{O}_{8+x}$  (BSCCO) showed that, in this material, the broadening of the resistive transition was exclusively dependent on the  $c$ -axis component of the magnetic field. ( $J_c$  and  $RT$  measurements on films of BSCCO grown on mis-cut substrates are presented in Chapter 7). There is, therefore, evidence from resistive transition measurements that the behaviour of the FLL in YBCO is different from that in BSCCO.

Initially prepared bulk samples of YBCO were polycrystalline and exhibited fairly low critical current densities,  $J_c$ . In YBCO grain boundaries can have a severely detrimental effect on  $J_c$ . Such weak links are one of the main technological challenges to practical conductor development. If the intrinsic behaviour of the FLL is to be studied this complication must be eliminated, requiring single crystal samples.

Critical current measurements on single crystals revealed that a  $J_c$  of almost  $5 \times 10^{10} \text{ Am}^{-2}$  could be supported intra-granularly in YBCO (Yeshurun, *et al.* 1989). The anisotropy between the  $a$ - $b$  planes and  $c$ -axis directions also became apparent in critical current density measurements (Dinger, *et al.* 1987). Samples prepared as thin films deposited on single crystal substrates were found to exhibit significantly larger critical current densities than single crystal samples (Chaudhari, *et al.* 1987). This is due to the high density of strong pinning sites found in thin films. These strong pinning sites have been shown to be predominantly due to dislocations (Dam, *et al.* 1999, Huijbregtse, *et al.* 2000).

Early determinations of  $J_c$  in single crystals were made using magnetisation measurements. Deducing the vortex structure from such measurements is complicated by the need to find both the demagnetising factor for a particular sample and models describing the way flux penetrates into and current flows in the sample (Herzog 1997). In contrast, determining the resistive transition from transport measurements allows a direct determination of  $J_c$ , although, as shown in Figure 2.4, a small uncertainty is introduced by flux creep. While transport measurements are now made routinely on single crystals, it is difficult to restrict the path current takes with respect to the crystal lattice. In contrast, thin films grown on single crystal substrates provide a very convenient and controllable experimental system. Additionally, with

a thin film sample it is simple to obtain a current path with a cross sectional area sufficiently small that the absolute magnitude of the critical current,  $I_c$ , is reasonably small. The contacts used in the measurements described in this work provided useful results for currents below  $\sim 1$  A.

#### 4.1.2. Angular Measurements on *c*-axis Thin Films of YBCO

Given the anisotropy and layered structure in YBCO, Tachiki and Takahashi (1989b) considered the effect of the intrinsically layered structure on pinning of the FLL. At  $t=0$ , where  $t$  is the reduced temperature  $T/T_c$ , the *c*-axis coherence length  $\xi_c$  is approximately 0.2 nm and thus the vortex core in YBCO is smaller than the layer spacing,  $d$ , which in YBCO is  $\sim 1.2$  nm.

As YBCO consists of superconducting layers alternating with blocking layers a flux vortex parallel to the *a-b* plane moving in the *c*-axis direction would experience strong modulation of the order parameter. The condensation energy for a vortex localised in the non-superconducting blocking layers is less than that for a vortex in a  $\text{CuO}_2$  plane. This gives rise to an *intrinsic pinning* force which acts to pin vortices into the blocking layers. For the case where the core size in the *c*-axis direction, effectively equal to twice the *c*-axis coherence length  $\xi_c$  in a large  $\kappa$  material, becomes equal to  $d$  Tachiki and Takahashi predicted that the intrinsic pinning effect would disappear. As the temperature rises, the coherence length will increase, near  $T_c$   $\xi_c(t)/\xi_c(0) = 1/\sqrt{1-t}$ . The core diameter ( $2\xi_c$ ) becomes equal to the layer spacing at about 70 K.

At temperatures near  $T_c$  therefore the intrinsic pinning effect is expected to disappear. However the predicted *intrinsic pinning peak* in the critical current density will not necessarily disappear when  $T > \sim 70$  K and the vortex core extends over more than one layer. As has been discussed in section 2.4.3, the core of an Abrikosov vortex parallel to the blocking layers is anisotropic. The vortex core is shorter along the *c*-axis direction than along the *a-b* plane since  $\xi_c = \epsilon \xi_{ab}$  (Figure 2.7). Smaller core sizes are associated with stronger pinning force densities. The anisotropic Ginzburg-Landau (G-L) model, therefore, also predicts that vortices parallel to the *a-b* planes are more strongly pinned against motion in the *c*-axis direction than the *a-b* direction.

Roas *et al.* (1990) performed measurements of the angular dependence of  $J_c$  in YBCO thin films. These measurements were made by varying the angle,  $\theta$ , between the cuprate planes and the applied magnetic field. The magnetic field was tilted about an axis parallel to  $\mathbf{J}$ . As  $\mathbf{B}$  and  $\mathbf{J}$  are then always perpendicular the magnitude of the Lorentz force density is  $JB$ . In this

geometry, at constant field, the critical current is proportional to the bulk pinning force density  $F_p$ . A more detailed discussion of the geometry of measurements on  $c$ -axis films is given in Chapter 6 of this thesis.

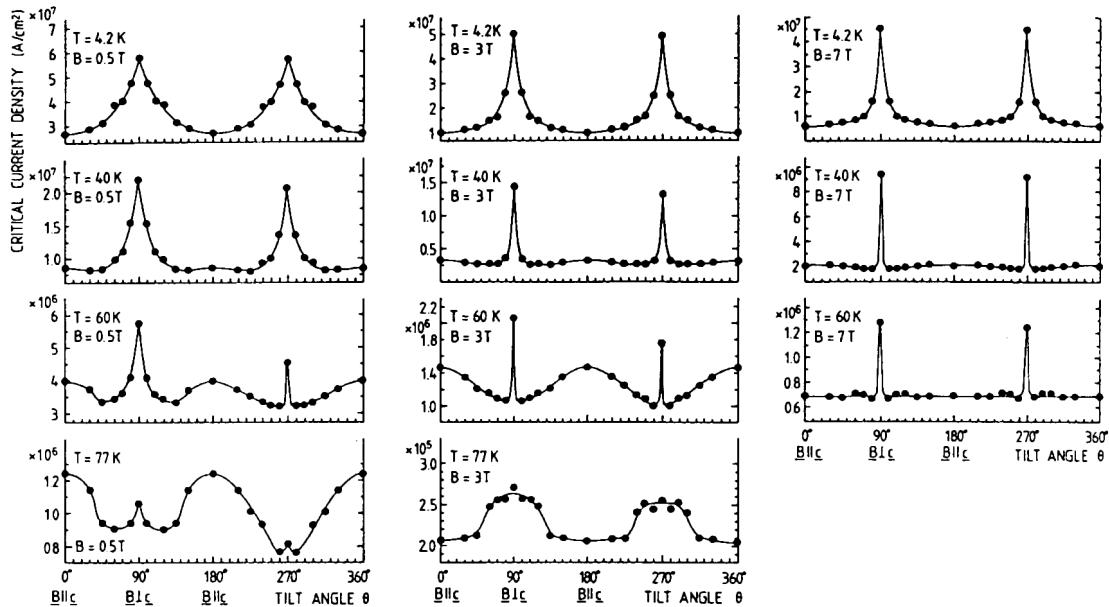


Figure 4.1  $J_c(\theta, \phi=0^\circ)$  as published by Roas *et al.* (1990) Note that in these plots  $\theta=0^\circ$  corresponds to a field parallel to the  $c$ -axis.

In the Roas *et al.* results reproduced in Figure 4.1 two main features can be observed. The peaks in the critical current density when the magnetic field is parallel to the cuprate planes are unmistakable. These peaks may be identified with the intrinsic pinning effect suggested by Tachiki and Takahashi. An enhancement of  $J_c$  is also observed for fields parallel to the  $c$ -axis. Roas *et al.* attributed this feature to pinning by twin boundaries in the film. Pinning by twin boundaries has also been observed in single crystals [Kaiser, 1991 #344]. The comparison of the Roas *et al.* results to any particular angular scaling law is limited by the relatively coarse resolution of the measurements. For instance in several plots the peak is inferred from a single data point.

Roas *et al.* patterned current paths at various orientations in the plane of the film to confirm that no in plane anisotropy could be observed. Given that twinning is prevalent in thin films the results from any current track would tend to be averaged out over several twins.

#### 4.1.3. Flux Line Lattice Models in YBCO

In this section previous  $J_c(\theta)$  measurements on YBCO are reviewed. Most authors have chosen to present their observations as supporting one or other of the models of the FLL

discussed in Chapter 2. These models are briefly reviewed in the context of the experimental data.

### The ‘Kes Law’

Several models have been proposed to relate the observed  $J_c(\theta)$  anisotropy in YBCO to the structure of the FLL. An elegant and simple possible model is the *Kes law* model. Kes *et al.* (1990) noted that in BSCCO the highly anisotropic layered structure would seem similar to the layered two dimensional model considered by Lawrence and Doniach (1970). The Kes model states that only the  $c$ -axis component of the applied magnetic field affects the critical current density, this leads to the following scaling law (if  $\theta=0^\circ$  is defined as field parallel to the  $a$ - $b$  planes):

$$J_c(B, \theta) = J_c(B \sin \theta, \theta=90^\circ) \quad (4.1)$$

The material is effectively ‘magnetically transparent’ for fields applied parallel to the  $a$ - $b$  planes. This model was developed for and has been found to well describe the behaviour in BSCCO.  $J_c(\theta)$  behaviour in BSCCO is discussed in Chapter 7.

Clem (1991) extended this model and predicted that in BSCCO the flux lines consist of stacks of two-dimensional vortices localised inside the  $a$ - $b$  planes. Each vortex element has screening currents flowing round it in the  $a$ - $b$  plane, these vortex elements are termed pancake vortices. The pancake vortices are, in a highly anisotropic material, magnetically attracted to those in the cuprate planes above and below and so line up to produce stacks. In less anisotropic materials the pancake vortices are also coupled by Josephson string vortices (Clem 1998) and may form tilted stacks.

Jakob, *et al.* (1993) reported that the Kes scaling law fitted results well for both BSCCO and YBCO. A study of the results shown in Figure 4.2 indicate that this ‘fit’ is markedly better for BSCCO than YBCO at  $t \sim 0.8$ . Jakob, *et al.* attributed the breakdown in the scaling law to the reduced intrinsic pinning at higher temperatures. The peak at  $\theta=0^\circ$  in the two dimensional model is not, however, due to intrinsic pinning, it is due to the zero vortex pancake density at that angle in any applied field. If field applied parallel to the cuprate planes interacts with the supercurrent, the material is no longer ‘magnetically transparent’ for fields parallel to the  $a$ - $b$  planes.

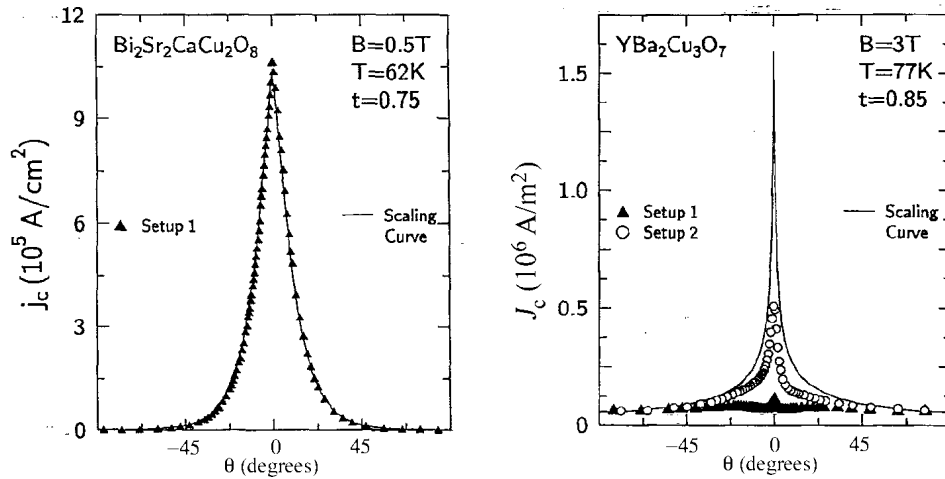


Figure 4.2 Fit to the Kes scaling law observed by Jakob *et al.* (1993) on BSCCO (left) and YBCO (right). Setup 1 corresponds to  $\phi=0^\circ$  and Setup 2 to  $\phi=90^\circ$ .

The Kes model requires that any field directed along the  $a$ - $b$  planes and any rotation of the field in plane at constant  $\theta$  has no effect on  $J_c$ . This is not observed to be the case in YBCO (Ravi Kumar, *et al.* 1994, Herzog 1997).

Nonetheless at low temperatures the Kes law can appear to give a reasonable fit to the data. A temperature dependent cross-over from a two-dimensional model to a three dimensional Ginzburg-Landau model has been proposed to explain this (Schalk, *et al.* 1992, Schalk, *et al.* 1993, Hosseinali, *et al.* 1994).

While YBCO is indeed anisotropic, experimental evidence simply does not support modelling it as a purely two dimensional superconductor. The unmodified Kes scaling law does not successfully describe the behaviour of the FLL in YBCO.

### The Tachiki and Takahashi model

Tachiki and Takahashi (1989a, 1993) developed their theory of intrinsic pinning into a *kinked vortex* model. In this model the flux lines consist of elements parallel and perpendicular to the cuprate planes.

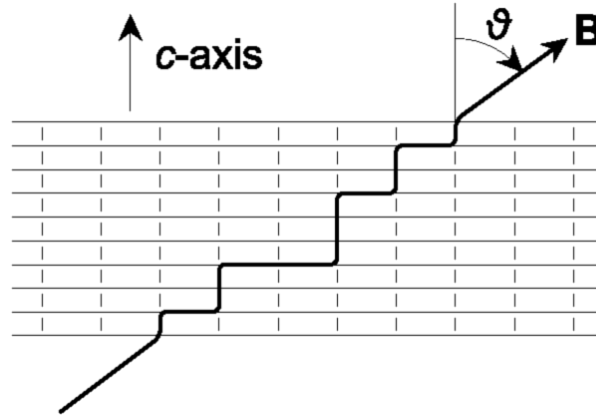


Figure 4.3 A tilted flux line according to the Tachiki and Takahashi model

The forces on the two different components of the vortex line (parallel to and perpendicular to the planes) are treated separately. The in plane segments are strongly intrinsically pinned while other pinning mechanisms pin the plane crossing elements. They predicted the following angular dependence for  $J_c$ .

$$J_c(\theta) = \text{smaller of} \left[ \begin{array}{l} J_c(0^\circ) \\ \frac{J_c(90^\circ)}{\sqrt{\cos\theta}} \end{array} \right] \quad (4.2)$$

Several authors reported broad agreement with this model, for example (Nishizaki, *et al.* 1991a, Nishizaki, *et al.* 1991b, Aomine, *et al.* 1994) . However no authors observed the predicted lock-in plateau.

#### Anisotropic G-L model

As has been discussed in the previous section the anisotropic G-L theory may also account for the intrinsic pinning peak. Blatter (1992) developed the following general scaling law, discussed in Chapter 2:

$$\varepsilon_\theta^2(\theta) = \varepsilon^2 \cos^2 \theta + \sin^2 \theta \quad (2.37)$$

which may be applied to the angular dependence of  $J_c$ . This gives the following dependence for the angular field dependence of  $J_c$ .

$$J_c(B, \theta) = J_c(\varepsilon_\theta B, \theta = 90^\circ) \quad (4.3)$$

This of course assumes that the vortex pinning force density has no angular dependence. A vortex core which extends over several layers may still be subject to a small intrinsic pinning potential in addition to the change in the pinning potential due to the changing anisotropy of the core. This may lead to larger pinning forces, and thus a larger value of  $J_c$ , at  $\theta=0^\circ$  than that predicted by Equation (4.3).

## Discussion

On the basis of extensive measurements of the magnetic field angle dependence of  $J_c$  Herzog (1997) compared the predications of the Kes law model and the G-L model. Herzog found that the anisotropic G-L model provided a poor fit to the observed data especially close to  $\theta=0^\circ$ . He concluded that the Kes model provided the best fit to the data he obtained. Nonetheless significant deviations from the predictions of this model were observed which Herzog attributed to coupling between the pancakes by Josephson string vortices rather than simple magnetic attraction. Pancake coupling in less anisotropic materials has been considered by Clem (1998). As such a structure is not purely 2D, the Kes law will not apply and the Josephson string vortices can interact with the supercurrent. This lattice of *kinked* vortex lines is however clearly distinct from a lattice of rectilinear Abrikosov vortices.

As has been described in Section 2.4.4 a model combining the kinked lattice model and the G-L model has been proposed (Berghuis, *et al.* 1997, Blatter, *et al.* 1994, pg. 1286). This cross-over model explicitly takes into account the fact that in YBCO the  $c$ -axis coherence length is of the order of the interlayer spacing for a relatively wide range of temperatures. Additionally, this model considers that the effect of the layered structure is less significant for a vortex parallel to the  $c$ -axis that for one close to the  $a$ - $b$  planes.

Broadly, therefore, the cross-over model predicts the anisotropic G-L model will apply for large values of  $\theta$ . When the applied field is close to parallel to the  $a$ - $b$  planes the flux line will become similar to the kinked model of Takahashi and Takishi. The flux line elements, however, are different depending on their orientation. Clem pancake vortices occupy the superconducting layers whilst Josephson vortices lie along the blocking layers. Two critical angles are introduced,  $\theta_1$  and  $\theta_2$  which are defined in Equations 2.40 and 2.41. It is predicted that below  $\theta_1$  the flux lines are distorted and below  $\theta_2$  the lines are kinked.

It is clear from previously published literature and the extensive measurements in Herzog (1997) that neither the anisotropic G-L model, the Kes model or the kinked vortex model successfully describes the angular dependence of  $J_c$  at all temperatures. The cross-over model may be able to reconcile the sometimes conflicting evidence available, although at the expense of relinquishing the search for a simple angular scaling law for critical current behaviour. It remains, however, the case that the main difficulty with distinguishing between these models on the basis of  $J_c(\theta)$  measurements is that all the models predict a peak in  $J_c$  near  $\theta=0^\circ$ . This is reflected in the range of opinions in the published literature. Clearly an ideal

experiment would show a clear signature of one model or another. Measurements on films grown on off-axis substrates are one way that this may be achieved.

#### 4.1.4. Angular Measurements on Vicinal Films

The definitions of the magnetic field tilt,  $\theta$ , and rotation,  $\phi$ , angles in the measurements on YBCO films grown on vicinal substrates are given in Figure 4.4. Here, these angles are defined with respect to the cuprate planes and the direction of the miscut. The angle  $\theta$  is that between the applied field and the superconducting planes whilst the angle  $\phi$  denotes rotation of the field about the  $c$ -axis. The angle  $\theta=0^\circ$  corresponds to field applied parallel to the cuprate planes and  $\theta=90^\circ$  to field perpendicular to the planes. At  $\phi=0^\circ$  as  $\theta$  varies field is swept in the direction of the tilt whereas  $\phi=90^\circ$  corresponds to field swept perpendicular to the tilt direction. These angles are shown in Figure 4.4.

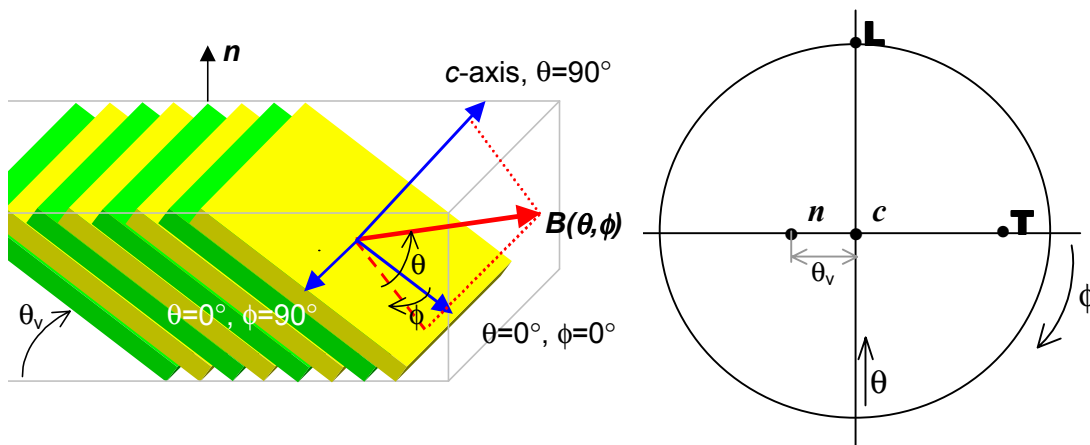


Figure 4.4 On the left is shown the geometry of a measurement on a vicinal film. The right hand diagram is a pole figure showing the definitions of  $\theta_v$ ,  $\theta$  and  $\phi$  and the direction of current flow in **T** and **L** tracks. Also shown are the vectors,  $\mathbf{n}$ , normal to the surface of the film and the  $c$ -axis direction.

In the case of a vicinal film the direction in which the current track is patterned becomes significant as the film no longer exhibits in-plane isotropy. Following the convention introduced by Haage, *et al.* (1997) tracks cut parallel to the vicinal steps are labelled **L** and those crossing the vicinal steps are labelled **T**. Higher critical currents and smaller normal state resistivities are observed in the **L** direction compared to the **T** direction where the current must cross between  $a$ - $b$  planes (Haage, *et al.* 1997, Mechin, *et al.* 1998). A cross section of a **T** track is shown in Figure 4.5.

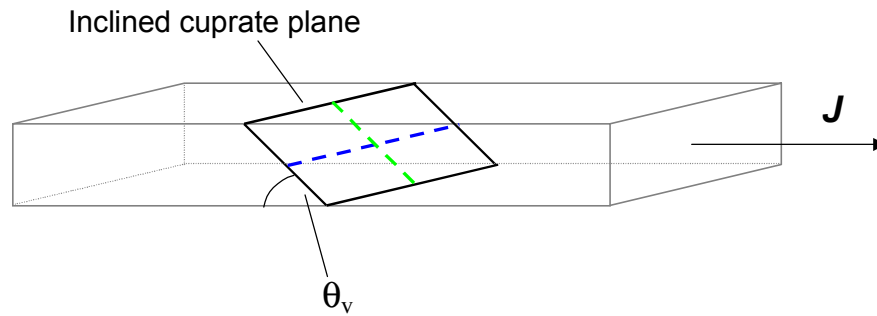


Figure 4.5 Cross-section of a **T** track showing the orientation of the vicinal steps. The green and blue lines indicate the orientation of the applied field at  $(\theta=0^\circ, \phi=0^\circ)$  and  $(\theta=0^\circ, \phi=90^\circ)$  respectively.

Measurements of the angular dependence of  $J_c$  in films grown on vicinal substrates have been performed by Berghuis *et al.* (1997). In these measurements, carried out on films grown on a  $6^\circ$  mis-cut substrate, a pronounced minimum is observed in  $J_c$  when the applied field is applied parallel to the  $a$ - $b$  planes. This is shown below in Figure 4.6.

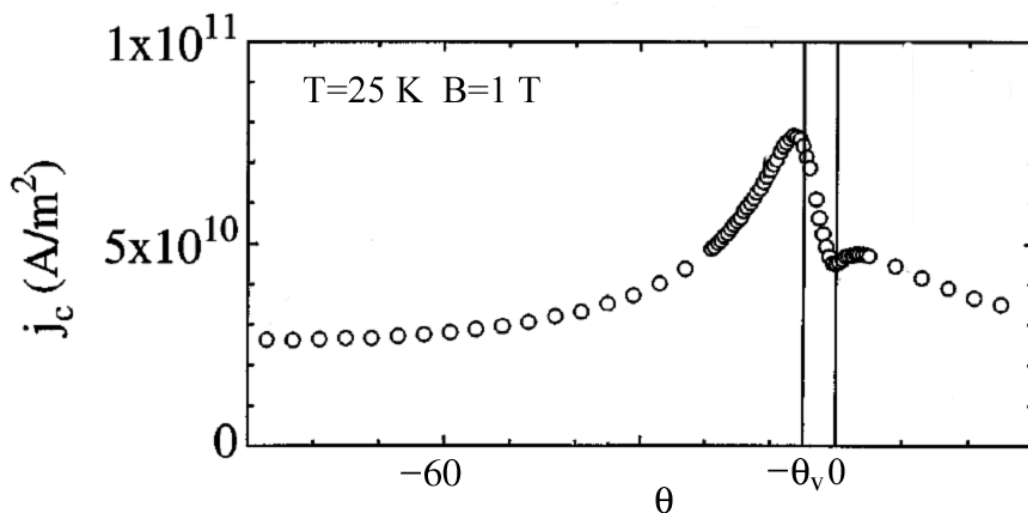


Figure 4.6 Berghuis *et al.* (1997) vicinal film  $J_c(\theta)$  results for a current flowing in a **T** track on a YBCO film grown on a  $6^\circ$  mis-cut substrate. The peak at  $-\theta_v$  is associated with the force free geometry ( $J||B$ ), the minimum at  $\theta=0^\circ$  is where the applied field is parallel to the  $a$ - $b$  planes.

The measurements shown in Figure 4.6 were carried out with  $\phi=0^\circ$ . The minimum appears when  $\theta=0^\circ$ , that is when the applied field is parallel to the cuprate planes. At this angle, there is a force directed along the  $a$ - $b$  planes on the vortex strings, as shown in Figure 4.7.

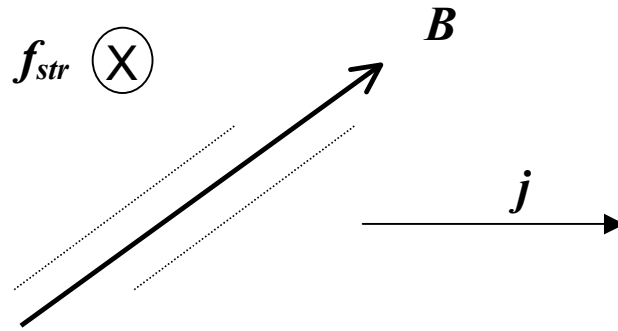


Figure 4.7 A vortex string at  $\theta=0^\circ$   $\phi=0^\circ$ . There is a Lorentz force on the string directed into the page of magnitude  $j\phi_0 \sin\theta_v$ . The dotted lines represent the orientation of the  $a$ - $b$  planes. The  $\phi=90^\circ$  geometry is shown in Figure 4.9

Any intrinsic pinning will tend to restrict flux lines to one blocking layer, but will not prevent them moving through the layer. The results therefore provide evidence of intrinsic *flux channelling*. In a  $c$ -axis film a Lorentz force is never directed inside the  $a$ - $b$  planes, whatever the direction of the applied field.

Berghuis interpreted this sharp variation in the vortex pinning force density results in terms of the cross-over into the string/pancake regime described by Blatter *et al.* (1994). In optimally oxygenated YBCO for  $\theta < 11^\circ$  the FLL is expected to change from consisting of elliptically cored Abrikosov vortices to consisting of kinked string/pancake vortex elements. At the lock-in angle,  $\theta=0^\circ$ , the flux pancakes disappear and a minimum in  $J_c$  is observed. This observation would tend to suggest that the pinning force per unit length on flux string elements is less than that on the pancake elements. This interpretation is supported by the observation that the vortex channelling minimum disappears at temperatures above that,  $T_{cr}$ , at which it is suggested that the anisotropic Abrikosov lattice persists at all angles of the applied magnetic field. This interpretation is supported by the data shown in Figure 4.8 as it can be seen that the characteristic channelling effect disappears with increasing temperature.

As discussed in Chapter 2, the transition to the string pancake lattice is not sharply defined, Blatter *et al.*, predicted that for  $\theta_2 > \theta > \theta_1$  the flux lines will be distorted rather than rectilinear or kinked. Unlike  $\theta_2$  the value of  $\theta_1$  is temperature dependent. In YBCO, at  $t=0$ ,  $\theta_1=35^\circ$ .

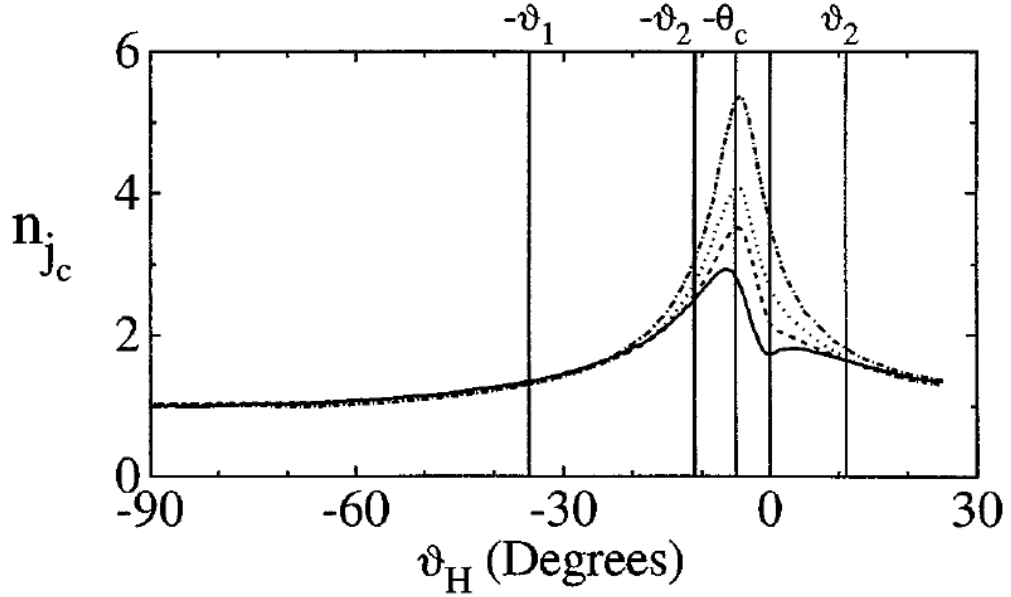


Figure 4.8 Data obtained by Berghuis *et al.* (1997) showing the temperature dependence of the channelling effect. The critical current data has been scaled so that  $n_{j_c} = J/J_c(90^\circ)$ . From bottom to top,  $J_c(\theta)$  behaviour is shown at 25 K, 40 K, 60 K and 76 K.

Berghuis noted that in the kinked vortex model the force on the individual vortex elements (strings and pancakes) must be separately considered. By writing an equation for the force balance on an individual vortex line<sup>†</sup> which is entirely composed of string elements Berghuis was able to extract a value for the string pinning force per unit length on a string.

$$f_{p, \text{str}} = j_c \phi_0 \sin \alpha \quad (4.4)$$

Here  $j_c$  is the critical current density,  $f_{p, \text{str}}$  is the pinning force on the vortex string,  $\phi_0$  is the flux quantum and  $\alpha$  is the angle between the vortex string and the current. In this case the flux line is only entirely string like when  $\alpha = \theta_v$ .

If the strong pinning assumption is valid then the pinning force density is given by  $F_{p, \text{str}} = n_v f_{p, \text{str}}$  (where  $n_v$  is the number density of vortices per unit area). From the definition of  $B$  we know that  $B = n_v \phi_0$ . The bulk equivalent of Equation (4.4) may then be written:

$$F_{p, \text{str}} = J_c B \sin \alpha \quad (4.5)$$

<sup>†</sup> This requires the assumption that the pinning is strong so that writing a force balance equation for an individual vortex line is meaningful. Hence the use of  $j_c$  to represent the *local* critical current density. To estimate  $f_{p, \text{str}}$  from transport measurements the assumption that  $j_c = J_c$  must be made.

The results published by Berghuis *et al.* (1997) only consider  $J_c(\theta)$  measurements made at  $\theta=0^\circ$ . Berghuis also noted, in unpublished results, that it is possible to observe a channelling dip in  $\phi=90^\circ$  measurements. In this geometry the field is always perpendicular to the strings. The total Lorentz force density on the strings is therefore  $J_c B$ . However, this force can be resolved into two components, one strongly pinned by intrinsic pinning and the other directed along the  $a$ - $b$  planes, this is depicted in Figure 4.9. This component is opposed by the string pinning force, if the intrinsic pinning is strong the vortex strings will be channelled. In this case the string pinning force density would in principle also be given by Equation (4.5).

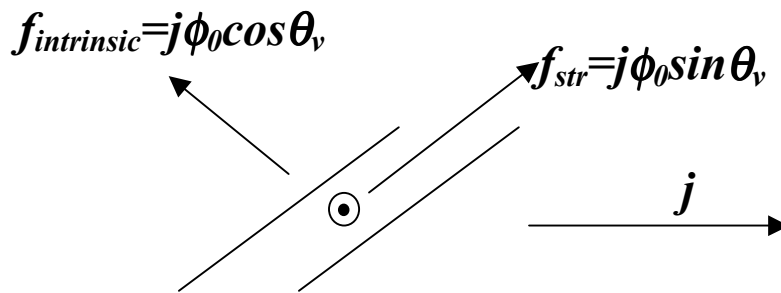


Figure 4.9 Lorentz force components on a vortex string at  $\theta=0^\circ$ ,  $\phi=90^\circ$ .

Measurements on vicinal films also allow surface pinning to be distinguished from intrinsic pinning (Berghuis, *et al.* 1996). No vortex channelling is observed in measurements on  $\perp$  cut tracks, since at no point is there a resolved component of the Lorentz force pushing the vortex strings along the  $a$ - $b$  planes. However, the position of the intrinsic pinning peak would be expected to be shifted by  $\theta_v$  from that observed in  $c$ -axis films. The position at which lock-in occurs is then no longer the same as the angle at which the applied field is parallel to the film surface. This allows surface pinning to be distinguished from intrinsic pinning, surface pinning can be identified as a shift in the expected intrinsic pinning peak. Berghuis *et al.* (1996) observed that surface pinning was significant only at low fields and high temperatures ( $B < 0.25$  T for  $T > 50$ K). Outside this regime it is reasonable to assume that the  $\theta$  dependence of  $J_c$  is indeed a bulk effect.

#### 4.1.5. Anti-phase Boundaries in Films Grown on Vicinal Substrates

By careful preparation of the substrate surface it has been demonstrated that YBCO films may be grown on miscut substrates with a large number of anti-phase boundaries present in the crystal structure (Haage, *et al.* 1997, Habermeier, *et al.* 1998). Anti-phase and stacking faults are shown in Figure 4.10.

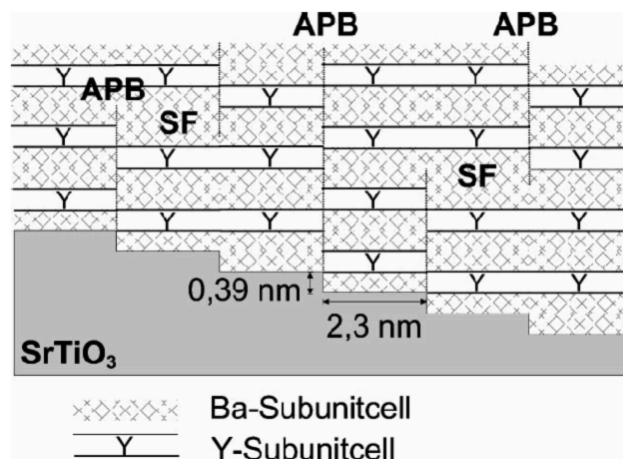


Figure 4.10 Schematic diagram of stacking faults (SF) and anti-phase boundaries (APB) in YBCO grown on a  $9.46^\circ$  miscut  $\text{SrTiO}_3$  substrate. From Jooss, *et al.* (2000).

This is achieved by careful annealing of the substrates. The effect is particularly marked for substrates miscut at  $9.46^\circ$  when one unit cell of YBCO corresponds to three steps on the substrate surface. The presence of APBs (Jooss, *et al.* 2000) in the film results in a dramatic enhancement in  $J_c$ . The critical current in the  $c$ -axis crossing  $\mathbf{T}$  direction in such films is similar to that seen in plane in the best quality  $c$ -axis orientated films (Haage, *et al.* 1997, Jooss, *et al.* 1999).

By the deposition of an iron-garnet film on an YBCO film it is possible to optically measure, using the Faraday effect, the magnitude and distribution of critical currents flowing in a thin film of YBCO (Jooss, *et al.* 1998). Jooss *et al.* (1999, 2000) have used this Magneto-Optical (MO) technique to extensively study the penetration of flux into films grown on vicinal substrates with high densities of APBs. Jooss *et al.* have observed a characteristic filamentary penetration of flux into the film along the APBs. Such a characteristic filamentary flux penetration is shown in Figure 4.11 for a film grown on a  $37.5^\circ$  mis-cut annealed substrate supplied to me by Peter Czerwinka of the University of Nottingham. This film was grown using the same technique as that employed by Habermeier *et al.*

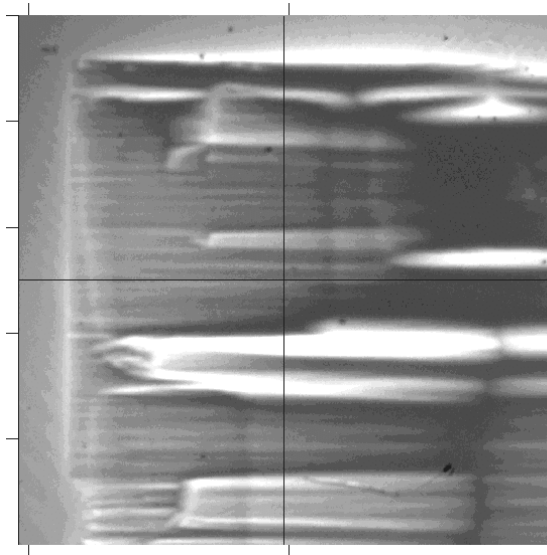


Figure 4.11 Filamentary flux penetration in a film of YBCO grown on a  $37.5^\circ$  mis-cut substrate in an 8 mT field (Jooss 2000). Dark areas correspond to the Meissner phase and light areas to the areas where flux has penetrated.

The  $37.5^\circ$  off-axis film, when studied by the author, did not show any vicinal channelling effect in  $J_c(\theta)$  measurements, this is shown in Figure 4.12. As this sample was grown using a similar annealing process as the films studied by Jooss it is very likely that the APBs introduced by the substrate annealing step act to strongly pin flux vortices thus suppressing the vortex channelling effect. Interestingly, the force-free peak, expected at  $\theta=37.5^\circ$ , cannot be seen in this data suggesting that the enhancement in  $J_c$  caused by the APBs is larger than that found in the force-free geometry.

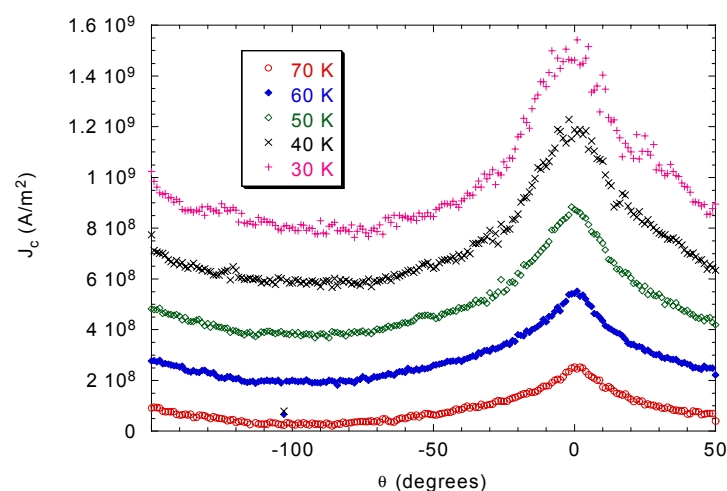


Figure 4.12  $J_c(\theta)$  measurements performed on a  $\mathbf{T}$  track cut on a  $37.5^\circ$  vicinal film. The data was obtained in a field of 1 T in the  $\phi=0^\circ$  geometry. In a vicinal film with no anti-phase boundaries present, a minimum is expected at  $\theta=0^\circ$ .

## 4.2. Sample and Measurement Details

### 4.2.1. Sample Sources and Characterisation

The measurements described in this thesis were performed on on-axis laser ablated YBCO films prepared by Dr G. Gibson. The films were grown on substrates 12 mm x 3 mm supplied by Crystal G.M.B.H. The alignment and phase purity of the films was confirmed by both rocking curve and pole figure X-Ray measurements. No  $c$ -axis growth was detectable in any of the films apart from those grown on the most vicinal,  $20^\circ$ , substrates. As is discussed in Chapter 2 the films did exhibit characteristic pin holes visible in AFM images.

The critical importance of the absence of anti-phase boundaries in observing vortex channelling has already been discussed. Although APBs can be imaged using high resolution electron microscopy (HREM) this method gives a snapshot of one particular area of a film. In order to look for APBs one film from the batch, sample Z324B grown on a  $6^\circ$  vicinal substrate was imaged magneto-optically by Dr Ch. Jooss of the University of Göttingen.

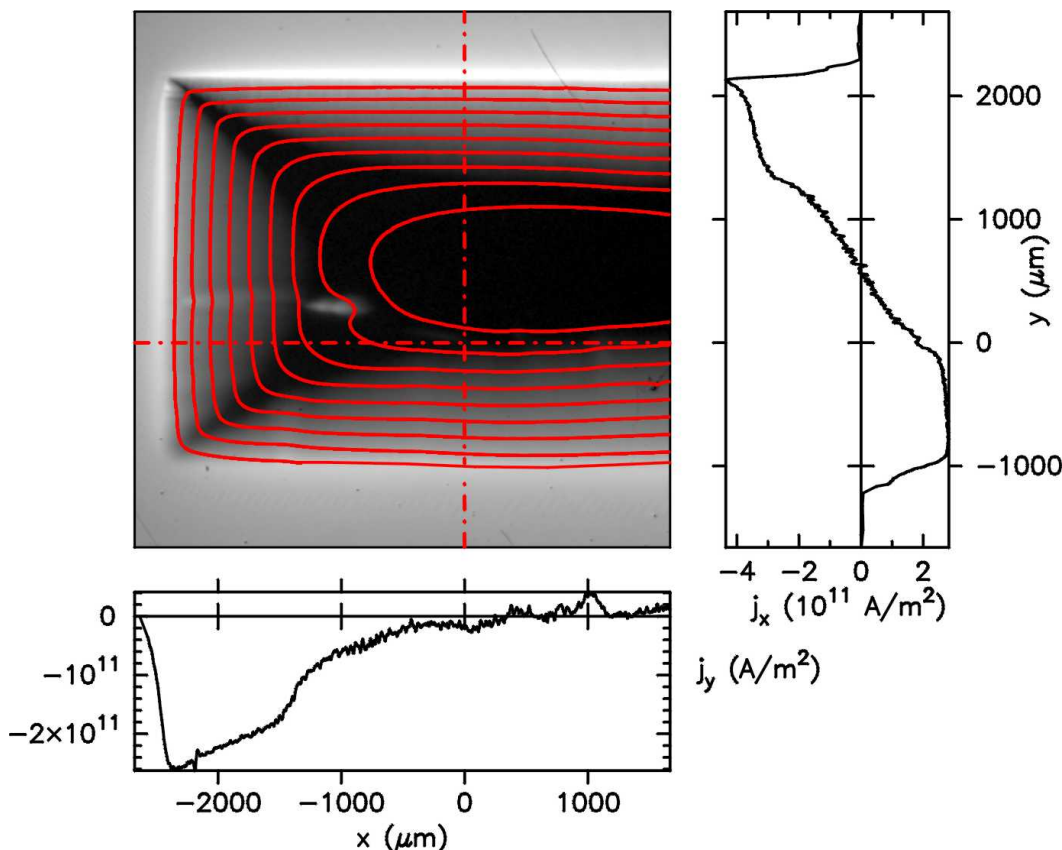


Figure 4.13  $6^\circ$  MO image prepared by Dr Ch. Jooss of the University of Göttingen. The local values of  $j$  has been determined using the inverse Biot-Savart law (Jooss, et al. 1998). The results shown are with an applied field of 32 mT (Zero field cooled) at 4.2 K.

The MO images of this film show none of the filamentary flux penetration characteristic of APB. It is also possible to see the anisotropy in the critical current density between the **L**

direction (across the page) and the **T** direction (down the page). The current flow penetrates further onto the film when flowing in the ‘difficult’ **T** direction. Also noticeable is anisotropy between current flowing in the upper and lower half of the film. This has been attributed (Jooss 2000) to interaction between the applied field and the tilt of the cuprate planes.

#### 4.2.2. Processing

The films were patterned using the CAM 24 mask described in Chapter 3. Each film had, therefore, 3 **T** and 3 **L** tracks, each 100  $\mu\text{m}$  long and 10  $\mu\text{m}$  wide. The thickness of the films, which were patterned by ion milling, was measured by wet etching a step which was then measured using an AFM. Due to the unavailability of the ion milling apparatus one film, Z324A was wet etched rather than ion milled. This results in a less well defined track edge, however, comparisons between data obtained from different tracks on the same film should still be valid. The  $T_c$  values of the films were measured and found to be in the range 88K-90K. This is, as is discussed in Chapter 3, slightly lower than that seen in the best quality *c*-axis oriented films.

#### 4.2.3. FIB Milling

In order to look for any possible effect of the track width on the channelling minimum one sample, Z324A a film grown on a  $6^\circ$  mis-cut substrate was focussed ion beam (FIB) milled. One **T** track was thinned from 10  $\mu\text{m}$  to nominally 2  $\mu\text{m}$  using the FIB. The FIB process, in which material is ablated using accelerated gallium ions has the disadvantage that gallium implantation extends some distance from the cut creating a wider region in which superconductivity is suppressed. Additionally during imaging gallium ions contaminate the entire surface of the track being examined. This gallium contamination can depress  $T_c$  and affect the electrical properties of the superconductor, as shown in Figure 4.14.

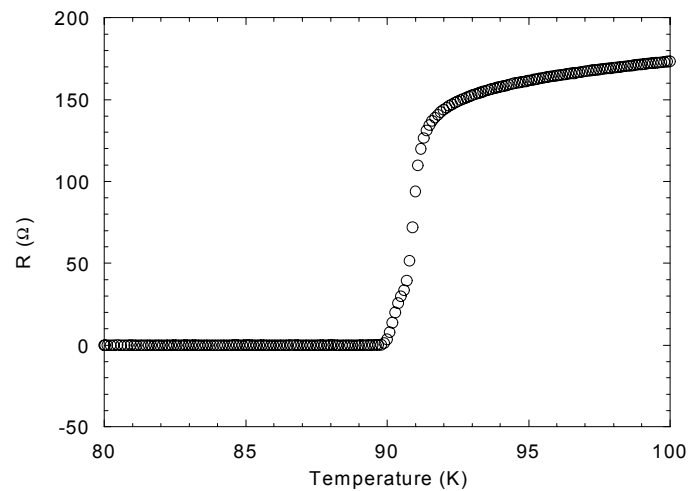


Figure 4.14 Characteristic ‘foot’ developed in an RT transition after FIB milling.

To minimise the consequences of this imaging of the track as kept to the minimum required to accurately focus the beam, position the cut and produce one image of the cut after milling.

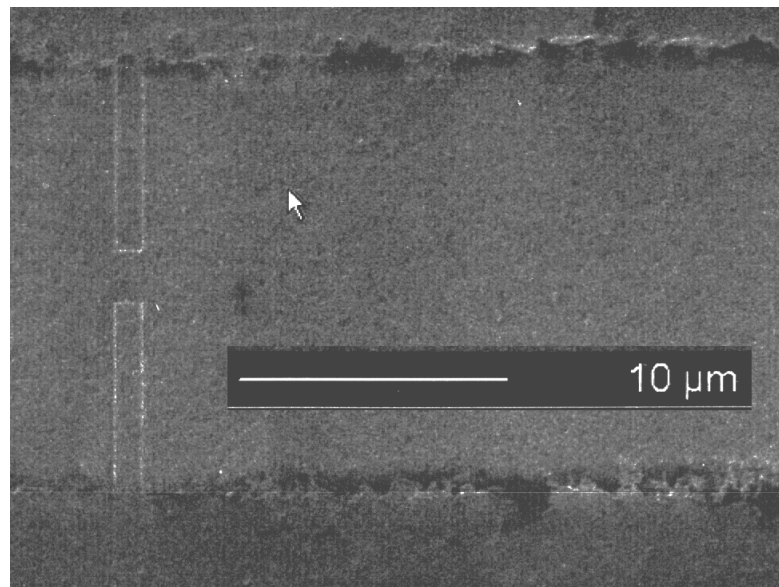


Figure 4.15 Image of a current track showing the FIB cuts used to narrow the track.

### 4.3. $J_c(\theta)$ Measurements

#### 4.3.1. Introduction

Berghuis *et al.* (1997) recorded the  $J_c(\theta)$  behaviour on a vicinal film grown on a  $6^\circ$  substrate. The results presented in that paper are only from measurements made in the  $\phi=0^\circ$  geometry. The aim of this thesis was to extend these measurements over a range of samples in order to confirm them and allow further deductions about the angular dependence of the FLL to be made. Initial measurements were therefore aimed at confirming the channelling effect in samples with different miscut angles. During the course of this thesis it was, unfortunately,

not possible to obtain further supplies of films grown by a sputtering process. The films measured in this Chapter were prepared by PLD. It is unfortunate that no systematic comparison of vicinal films grown by these two methods was possible given the intimate link between film microstructure and critical current properties (Dam, *et al.* 1999).

Figure 4.16 shows the channelling minima for  $2^\circ$ ,  $4^\circ$ ,  $10^\circ$  and  $20^\circ$  vicinal films at 1 T and 40 K. In this data, as the field has been swept at  $\phi=0^\circ$ , the prominent peak observed in the data is coincident with the force-free geometry.

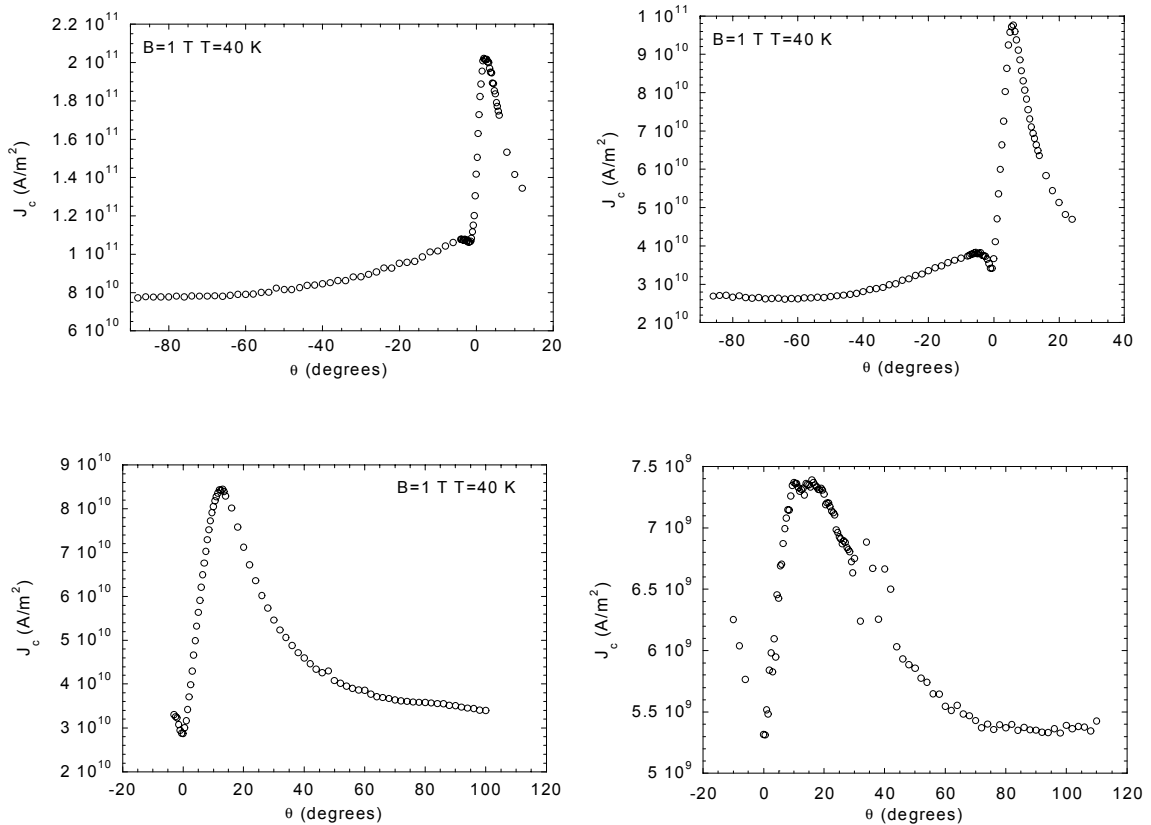


Figure 4.16 Clockwise from top left, the channelling minima at  $\phi=0$  observed in  $J_c(\theta)$  data recorded from  $2^\circ$ ,  $4^\circ$ ,  $20^\circ$  and  $10^\circ$  films.

From the results available it is possible to observe that these PLD films show the same channelling behaviour as the earlier, sputtered films. This would tend to suggest that, as is indicated by the MO result shown in Figure 4.13, these PLD films did not contain a high density of APBs. Qualitatively it is possible to observe that the channelling minimum deepens with increasing vicinal angle. Using Equation (4.4) the pinning force per unit length opposing the movement of the vortex strings may be calculated for each case, this is shown in Table 4.1. Ideally this value should not change between films of differing vicinality that are otherwise identical.

The determination of  $I_c$  is subject to very small experimental errors, any experimental noise is rapidly evident in the plots obtained due to the large number of data points acquired. Most of the uncertainty in determining  $J_c$  is due to uncertainty in calculating the cross sectional areas of the track. The track width is accurate to  $\pm 0.5 \mu\text{m}$  and the thickness to  $\pm 10 \text{ nm}$ . The uncertainty in the thickness is large because there is evidence that the vicinal films studied have a thin non superconducting layer between the substrate and the superconductor. This is evidenced by the fact that very thin films are not superconducting. The dimensions of the tracks measured in this section were  $200 \text{ nm} \times 10 \mu\text{m}$  so the errors amount to some 5%. Although this error is large, it is systematic and need only be taken into account when comparing values of  $J_c$  between samples.

Miscut Angle	Pinning force per unit length ( $10^6 \text{ Nm}^{-1}$ )
20°	3.8
10°	10 (+/- 5%)
4°	4.9
2°	7.0

Table 4.1 Pinning forces per unit length opposing movement of vortex strings in the cuprate planes.

This value is similar to that obtained from the Berghuis data, at 40K  $f_{p, \text{str}} \sim 8 \times 10^6$  (+/- 5%)  $\text{Nm}^{-1}$ . It is also worth noting that a similar value is deduced from string dragging measurements in Chapter 6. The variation in values of the pinning force, given these values were recorded at the same fields and temperatures are probably due to physical variations between the films.

As the substrate miscut angle increases, if all other factors remain constant, the critical current density on a **T** track would be expected to tend towards that observed for currents flowing along the  $c$ -axis. A  $90^\circ$  vicinal film is an  $a$ -axis oriented film, such films are observed to exhibit critical currents in T tracks considerably smaller than those observed in  $c$ -axis films Herzog (1997). The critical current with a 1 T field applied at  $\theta=90^\circ$  is shown in the figure below for these films. For comparison data from the  $6^\circ$  vicinal films measured by Berghuis, *et al.* (1997), and the  $c$ -axis oriented film (equivalent to a vicinal film with  $\theta_v=0^\circ$ ) described in Chapter 6 are included.

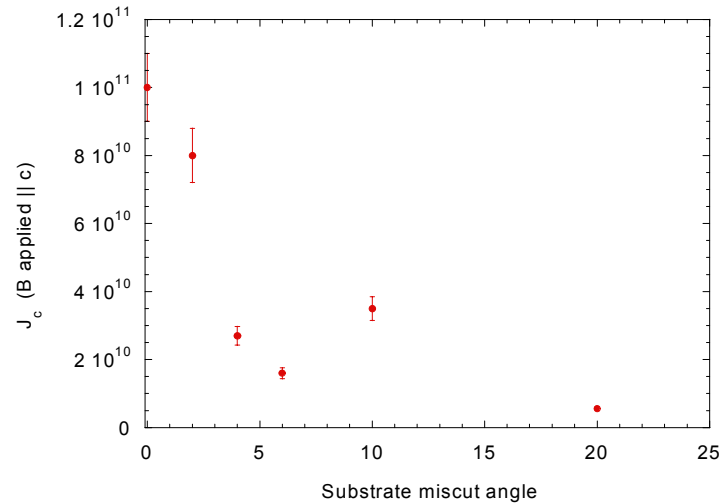


Figure 4.17 Plot of the variation of critical current density in a  $\mathbf{T}$  track (1 T field parallel to  $c$ -axis, 40 K) against the miscut angle of the substrate on which the film was grown.

While this data shows the general trend of decreasing critical current with increasing vicinal angle there is considerable variation between samples. Enough samples and experimental time were not available to make a systematic study of the relationship between the growth conditions and the absolute critical current values of the films. Both the data in Figure 4.17 and Table 4.1 would tend to suggest that there is some variation in the microstructure of the different films measured. Caution must therefore be exercised in making quantitative comparisons between the absolute values of  $J_c$  in different films.

Relating the microstructure of a film to the pinning and critical current behaviour observed in measurements on it is a difficult problem. Dam, *et al.* (1999) have been able to clearly demonstrate that the predominate source of pinning in  $c$ -axis films is due to growth induced dislocations. As the growth observed in vicinal films is different, step flow rather than spiral, the nature of the pinning centres in vicinal films remains an open question. It is clear however that introducing APBs has the potential to greatly increase  $J_c$ .

#### 4.3.2. $2^\circ$ Vicinal Film

A two degree vicinal film would be expected to show a less striking vortex channelling effect than a  $6^\circ$  vicinal film since, from equation (4.5), the force density on the vortex strings is  $J_c B \sin \theta_v$ . Indeed, the behaviour might be expected to tend towards that observed in  $c$ -axis films which appear to exhibit no vicinal channelling effect.

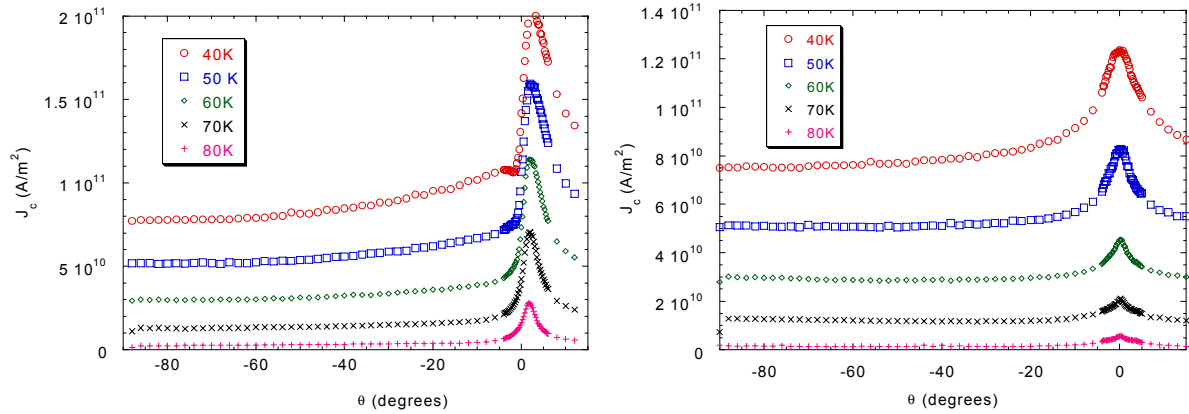
$J_c(\theta)$  at Varying Temperatures

Figure 4.18  $J_c(\theta)$  behaviour measured on a  $\mathbf{T}$  track in sample Z336B. The left plot shows behaviour at  $B=1$  T and  $\phi=0^\circ$ , the right plot behaviour at  $B=1$  T and  $\phi=90^\circ$ .

From the variation with temperature of  $J_c(\theta)$  measurements shown in Figure 4.18 it is possible to make several observations. In the measurements at  $\phi=0^\circ$ , as with the data recorded by Berghuis, the channelling dip is suppressed at higher temperatures. This is consistent with the idea of a temperature dependent cross-over from a kinked lattice to a rectilinear lattice. There is no channelling dip visible in the  $\phi=90^\circ$  data. At  $\phi=90^\circ$  the field is aligned with the cuprate planes at  $\theta=0^\circ$  and a channelling effect has been observed in more vicinal films. It is possible however that the dip would appear at lower temperatures than those recorded.

Figure 4.19 shows the  $J_c(\theta)$  data for various temperatures scaled for comparison. In each case  $n_{j_c} = J_c(\theta)/J_c(90^\circ)$ .

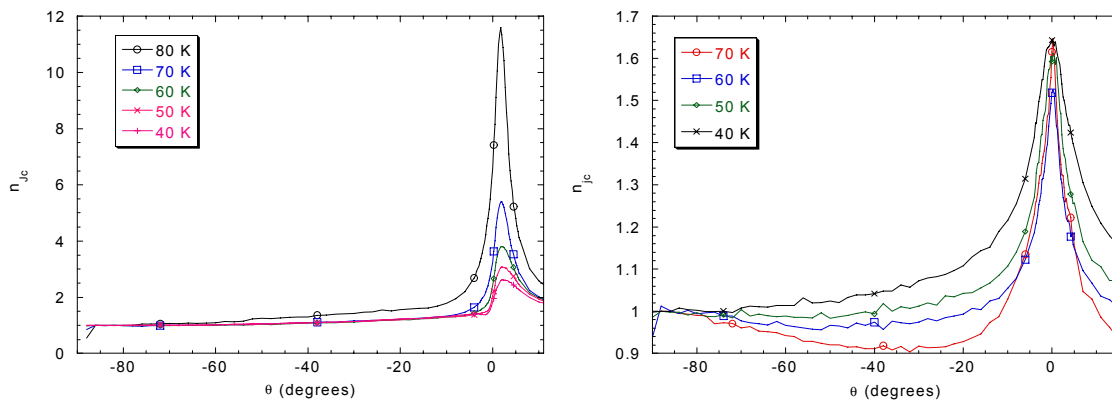


Figure 4.19  $J_c(\theta)$  behaviour measured on a  $\mathbf{T}$  track in sample Z336B. The left plot shows behaviour at  $B=1$  T and  $\phi=0^\circ$ , the right plot behaviour at  $B=1$  T and  $\phi=90^\circ$ , the data is scaled so that  $n_{j_c} = J_c(\theta)/J_c(90^\circ)$ .

Taking the  $\phi=0^\circ$  data we can see that the 80 K data exhibits a large peak at  $\theta=2^\circ$ . This peak corresponds to the force free orientation since at  $\theta=2^\circ$  the applied field is parallel to the

current. As the temperature is reduced a minimum developed at  $\theta=0^\circ$ . This minimum which corresponds to vortex channelling is not sharp but extends a distance either side of  $\theta=0^\circ$ . If the simple assumption is made that in the absence of the cross-over to the kinked lattice the lower temperature plots would approach the  $T=80$  K data, it is possible to quantify the effect of the 2D-3D cross-over.

Unfortunately in the  $\phi=90^\circ$  case the  $T=80$  K data exhibited too much noise to make a clear comparison. Interestingly though while there is a clear temperature dependence of the critical current at larger values of  $\theta$  the variation at  $\theta=0^\circ$  is much smaller. There is also evidence for enhanced pinning at  $\theta=-90^\circ$ , this could well be due to pinning by twin boundaries.

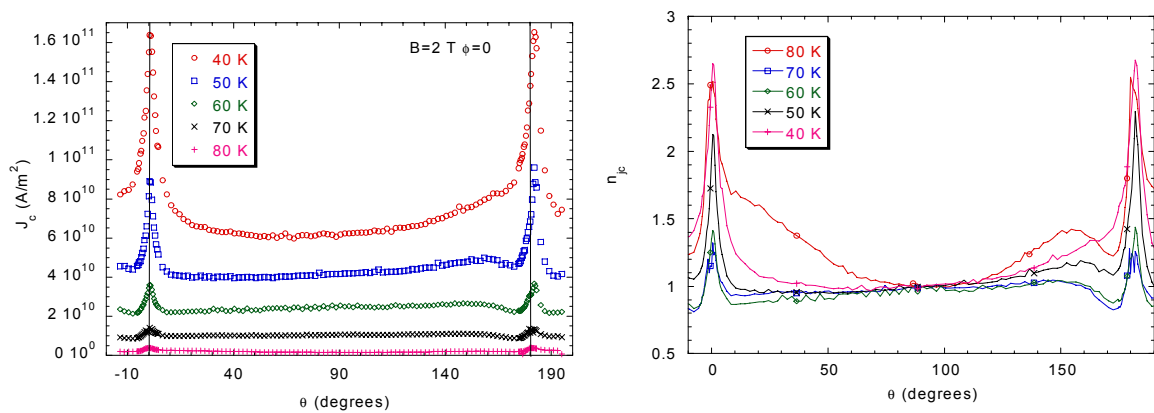


Figure 4.20  $J_c(\theta)$  behaviour measured at  $B=2$  T and  $\phi=0^\circ$  on an **L** track in sample Z336A. The right hand plot shows the same data scaled so that  $n_{jc}=J_c(\theta)/J_c(90^\circ)$ . Visible, at left, is the shift in the  $J_c(\theta)$  peak caused by surface pinning.

Data recorded on an **L** track shows no evidence of channelling, as would be expected since there is never a component of the Lorentz force on strings acting along the  $a$ - $b$  planes. There is however evidence of surface pinning. Here the field is swept perpendicularly to the current, the peaks would therefore be expected to occur at  $\theta=0^\circ$  and  $180^\circ$  (field parallel to planes). Any surface pinning effect would introduce extra pinning at a  $2^\circ$  displacement, which is observed in the shift of the  $\theta=180^\circ$  peak in Figure 4.20.

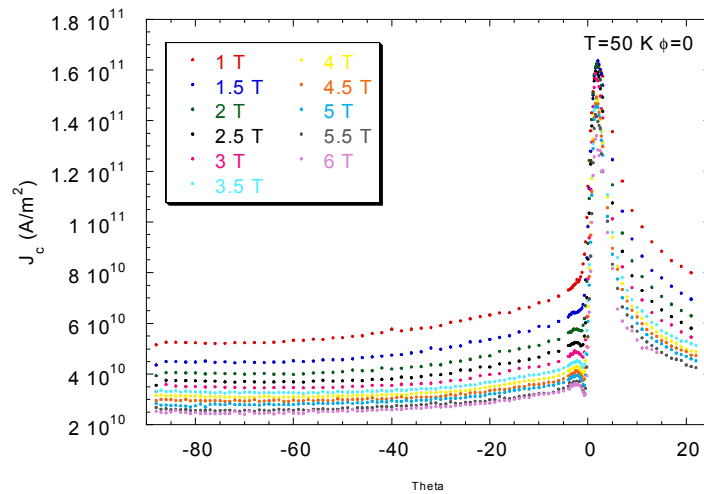
$J_c(\theta)$  at Varying Fields

Figure 4.21  $J_c(\theta)$  data recorded on a  $\mathbf{T}$  track on sample Z336B at 50 K and  $\phi=0^\circ$ .

In Figure 4.21 and Figure 4.22 the evolution of the channelling minimum with field may be seen in a  $\mathbf{T}$  track. At 50 K the dip can be seen to develop fully at higher fields. Even where no minimum is apparent the force pinning peak is clearly altered becoming asymmetric due to the depression of the critical current on one side of the peak.

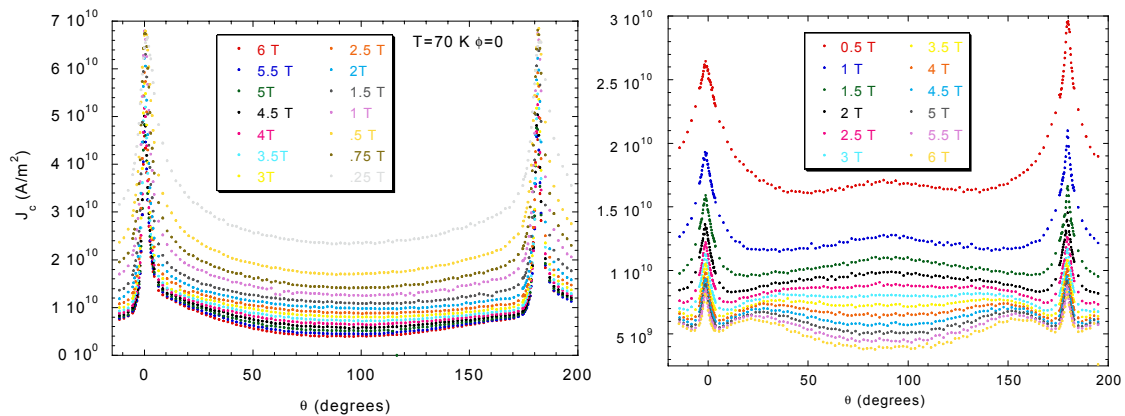


Figure 4.22  $J_c(\theta)$  data recorded in a  $\mathbf{T}$  track on sample Z336B at 70 K. The left plot shows data for  $\phi=0^\circ$ , the right for  $\phi=90^\circ$ .

At higher temperatures, it can be seen that the effect of vicinal channelling is apparent at  $\phi=0^\circ$ , but not at  $\phi=90^\circ$ . The difference between the  $\theta=0^\circ$  and  $\theta=180^\circ$  peaks is interesting, the peaks are of different heights, yet surface pinning would tend to introduce a shift in the peak position.

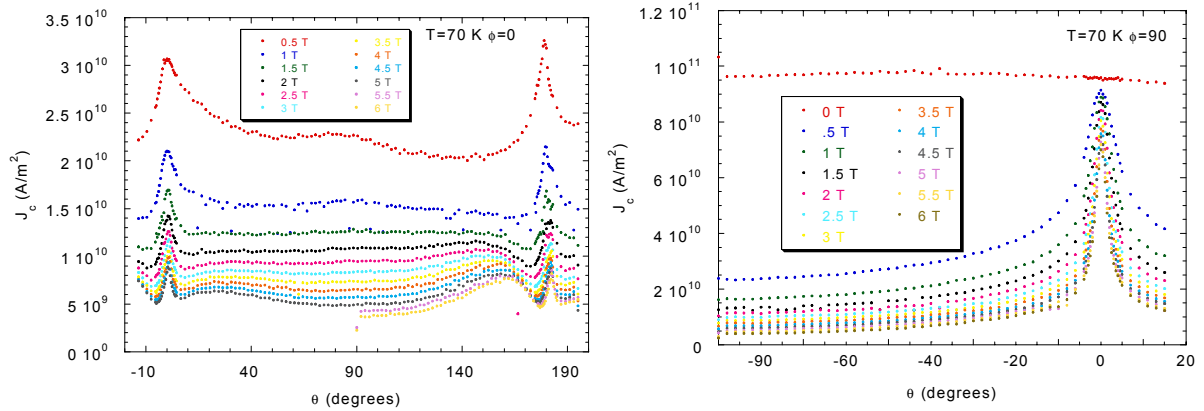


Figure 4.23  $J_c(\theta)$  data recorded in a **L** track on sample Z336A at 70K in the  $\phi=0^\circ$  geometry (left) and the  $\phi=90^\circ$  geometry (right).

Figure 4.23 shows data recorded on a **L** track for comparison. In both cases  $J_c$  peaks when the field is parallel to the  $a$ - $b$  planes. At  $\phi=0^\circ$  the peaks are again at the intrinsic pinning geometry and the peak at  $\phi=90^\circ$  is in the force free geometry.

#### 4.3.3. $4^\circ$ Film

##### $J_c(\theta)$ at Varying Temperatures

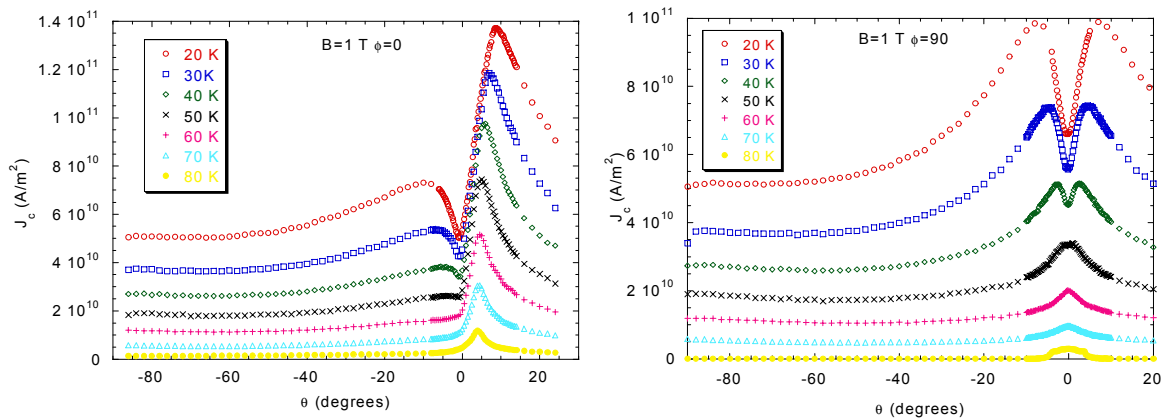


Figure 4.24  $J_c(\theta)$  data recorded on a **T** track in sample Z335A. The left plot shows data recorded at  $\phi=0^\circ$ , the right plot data recorded at  $\phi=90^\circ$ .

$J_c(\theta)$  measurements on a film grown on a  $4^\circ$  vicinal substrate show a more noticeable vortex channelling effect than those on the  $2^\circ$  film. This is as expected since for any given string pinning force a  $4^\circ$  film will exhibit a smaller  $J_c$  than a  $2^\circ$  film. Figure 4.25 shows these results replotted as before.

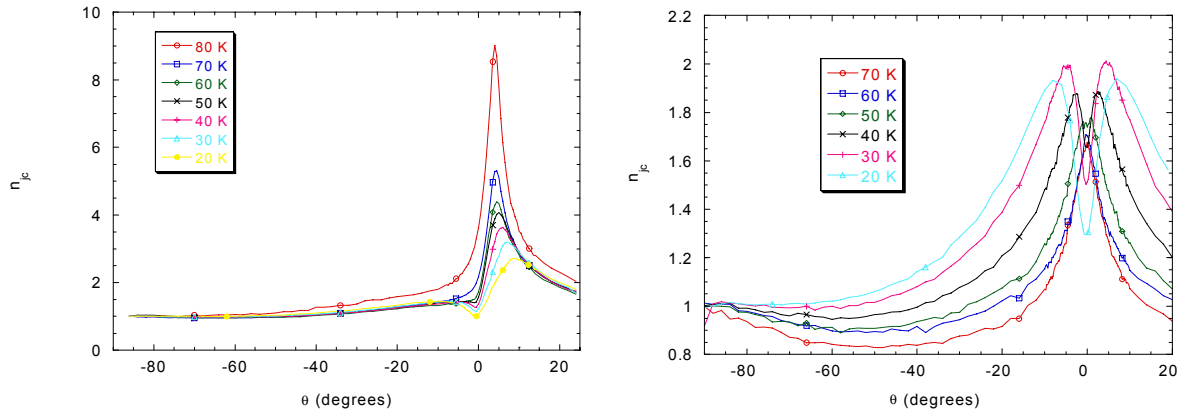


Figure 4.25  $J_c(\theta)$  plots recorded in sample Z335A ( $4^\circ$  vicinal) on a  $\mathbf{T}$  track at 1 T replotted as a proportion of the value of  $J_c$  at  $\theta=90^\circ$ . The left hand results were recorded with  $\phi=0^\circ$ , the right with  $\phi=90^\circ$ .

In contrast to the  $2^\circ$  results the channelling in the  $\phi=90^\circ$  geometry is noticeable at 40K and below. At  $\phi=0^\circ$  and  $\phi=90^\circ$  the channelling minimum suppresses the force free and intrinsic pinning peaks respectively. Again, considering the rescaled data at  $\phi=0^\circ$  the effect of the cross-over extends further than the channelling minimum itself leading to a distinctly anisotropic peak.

### $J_c(\theta)$ at Varying Fields

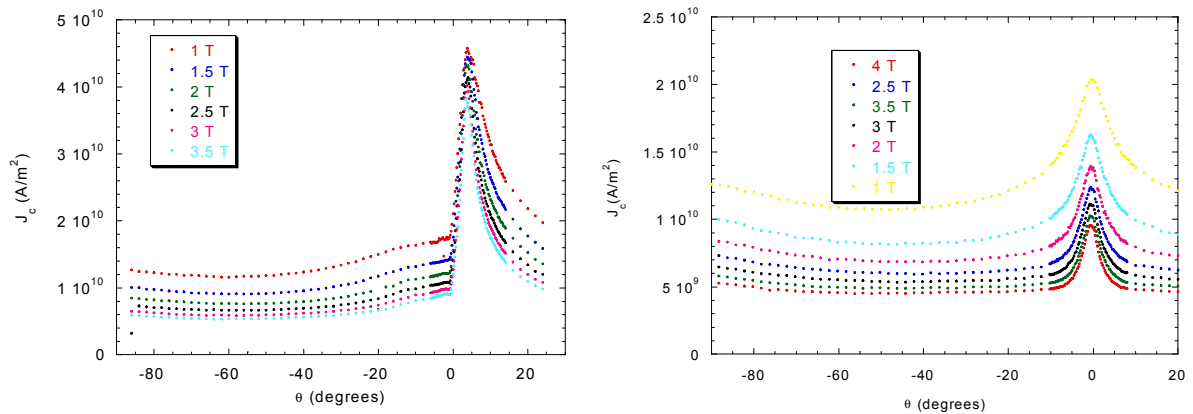


Figure 4.26  $J_c(\theta)$  measurements performed on a  $\mathbf{T}$  track at 60K in sample Z335A ( $4^\circ$  vicinal). The left hand data was recorded with  $\phi=0^\circ$  that on the right was recorded with  $\phi=90^\circ$

No particularly striking variation in the  $J_c(\theta)$  behaviour with field is apparent in Figure 4.26. There is no channelling minimum visible at  $\phi=90^\circ$  over a wide range of applied fields.

#### 4.3.4. $10^\circ$ Film

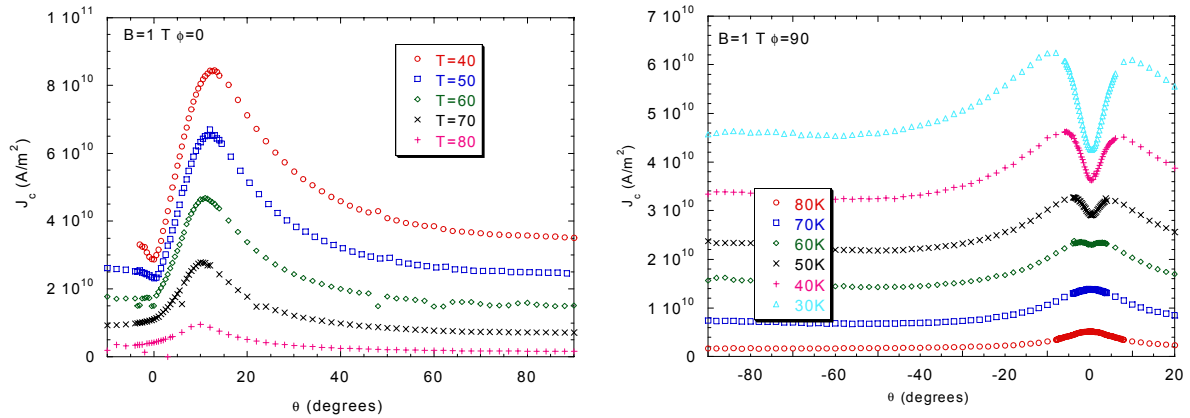


Figure 4.27  $J_c(\theta)$  data recorded on sample Z333A ( $10^\circ$  vicinal) in a  $\mathbf{T}$  track. The left hand plot shows data recorded at  $\phi=0^\circ$ , the right hand plot data recorded at  $\phi=90^\circ$ .

Again, as the vicinal angle increases, the temperature at which channelling becomes noticeable also increases in the  $\phi=90^\circ$  geometry.

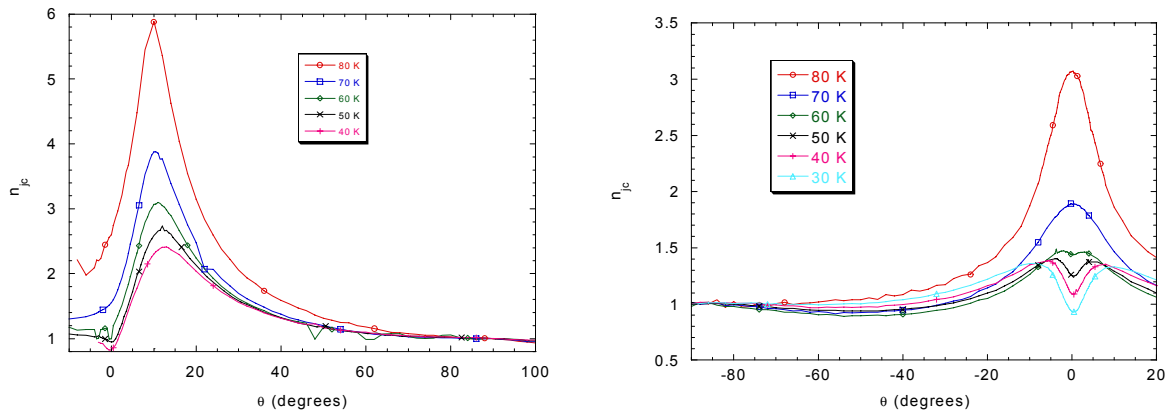


Figure 4.28  $J_c(\theta)$  data recorded on sample Z333A ( $10^\circ$  vicinal) in a  $\mathbf{T}$  track. The left hand plot shows data recorded at  $\phi=0^\circ$ , the right hand plot data recorded at  $\phi=90^\circ$ . The plots are rescaled with  $n_{j_c}=J_c(\theta)/J_c(90^\circ)$

#### 4.4. $J_c(\phi)$ Measurements

If the applied magnetic field is rotated in  $\phi$  at a constant value of  $\theta$  the vortex structure will remain constant. Only the direction of the Lorentz forces on the flux elements will change. By taking  $J_c(\theta)$  at the pinning peak for varying values of  $\phi$  it is possible to examine how changing the Lorentz force direction affects the critical current density. The ‘force-free’ contribution to the enhancement of the critical current must also be considered when calculating the pinning forces, however at  $\theta=0^\circ$  it has been predicted that the pinning forces are the same in both the

$\phi=0^\circ$  and  $\phi=90^\circ$  geometries.  $J_c(\theta)$  sweeps at varying  $\phi$  were therefore performed on a  $10^\circ$ ,  $4^\circ$  and a  $2^\circ$  vicinal film. These results are shown in the following Figures.

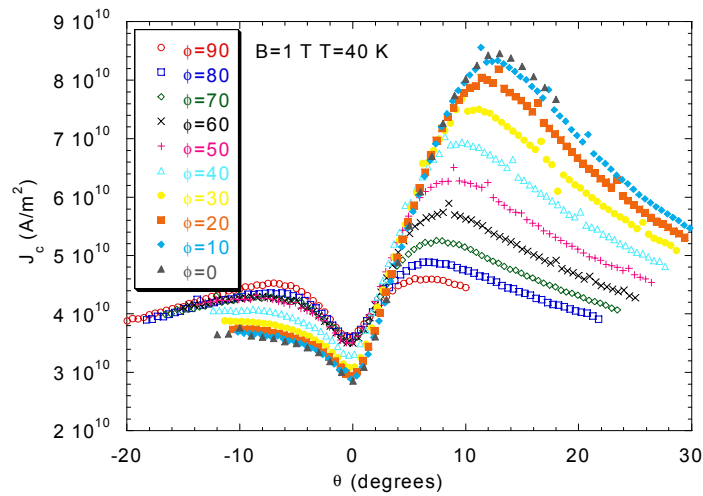


Figure 4.29  $J_c(\theta)$  data recorded at 1 T and 40K on sample Z334A ( $10^\circ$  vicinal film) as the value of  $\phi$  is swept.

In Figure 4.29 it can be seen that at  $\phi=0^\circ$  the prominent force free peak is present at about  $\theta=10^\circ$ . The shift of the peak is probably due to the combination of the reduction in the Lorentz force, due to the force free geometry, and a reduction in the pinning force density in the string-pancake regime. Examining  $\theta=0^\circ$  it is possible to observe that the critical current density is larger in the  $\phi=90^\circ$  geometry than the  $\phi=0^\circ$  geometry. The same observations may be made from the data from a  $4^\circ$  vicinal film shown in Figure 4.30.

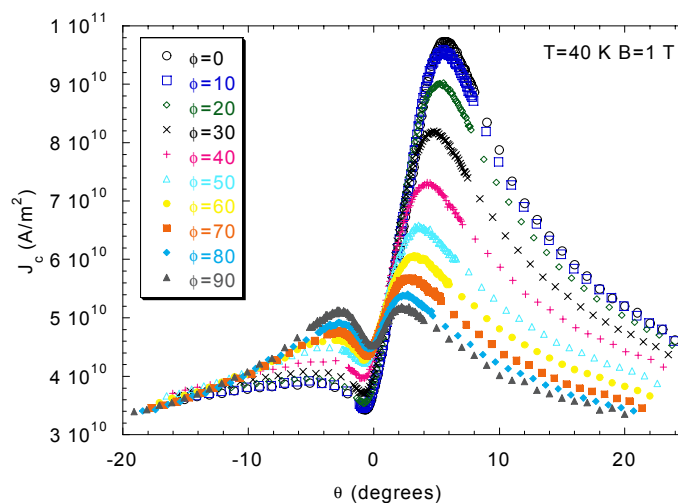


Figure 4.30  $J_c(\theta)$  data recorded at 40 K and 1T on sample Z335A ( $4^\circ$  vicinal film).

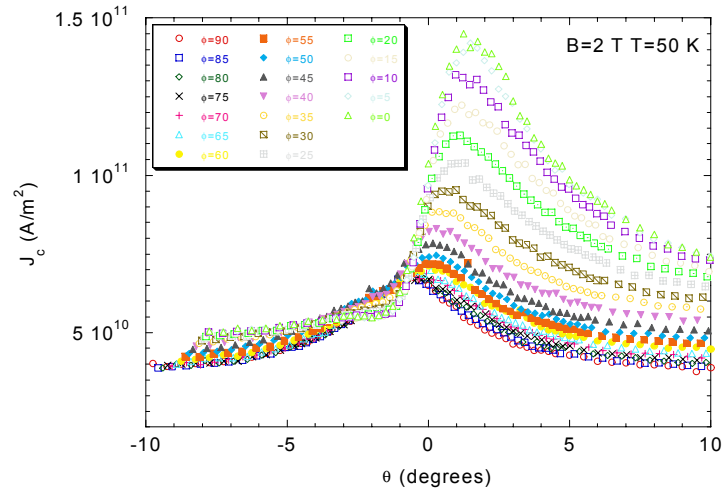


Figure 4.31  $J_c(\theta)$  data recorded at 50 K and 2 T on sample Z336B ( $2^\circ$  vicinal film).

In the data from a  $2^\circ$  film shown in Figure 4.31 the channelling minimum is only visible in the  $\phi=0^\circ$  geometry and it is shifted slightly from  $\theta=0^\circ$ .

To quantify the effect of changing  $\phi$ , the ratio  $J_c(0^\circ)/J_c(90^\circ)$  ( $r_\phi$ ) has been plotted for the three films. This is shown in Figure 4.32.

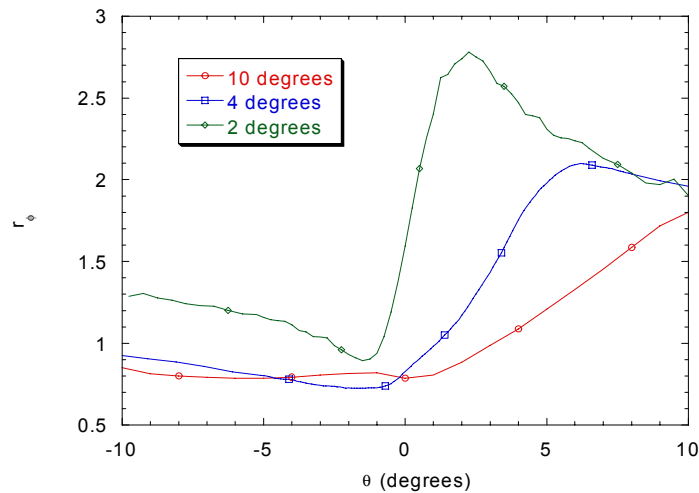


Figure 4.32 Value of the ratio  $r_\phi=J_c(0^\circ)/J_c(90^\circ)$  plotted near the channelling minimum for measurements on a  $\mathbf{T}$  track at 40 K and 1 T in a  $2^\circ$ ,  $4^\circ$  and a  $10^\circ$  vicinal film. (The  $2^\circ$  data was recorded at 2 T and 50 K)

In the  $2^\circ$  results the force free peak and the channelling minimum are very close together which may explain the shift and suppression of the channelling minimum. In the  $4^\circ$  and  $10^\circ$  films, however, the critical current density at  $\theta=0^\circ$  is larger in the  $\phi=90^\circ$  orientation than in the  $\phi=0^\circ$  orientation. The force directed along the a-b plane is expected to be given by Equation (4.5) in both cases. The enhancement of  $J_c$  at  $\phi=90^\circ$  could be due to the force on the vortex strings in

the  $c$ -axis direction depicted in Figure 4.9. The intrinsic pinning force may, in some way, enhance the pinning of the flux lines against movement inside the  $a$ - $b$  planes.

At  $\phi=90^\circ$  the vortex strings cross the entire width of the track, perhaps providing more scope for pancakes to be introduced due to interactions with crystallographic defects. As the string pinning force is much weaker than the pancake pinning force, only a small number of defects could have a large effect.

#### 4.5. $J_c(B)$ Measurements

The variation of the critical current with  $\phi$  at  $\theta=0^\circ$  noted in the previous section is interesting given that calculations of the Lorentz force on the strings would suggest that the two orientations should exhibit the same critical current values. Moreover the  $2^\circ$  vicinal film shows a different behaviour, at  $\theta=0^\circ$  the  $\phi=0^\circ$  value is larger than the  $\phi=90^\circ$  value. This is in contrast to the clear relationship shown for the  $4^\circ$  and  $10^\circ$  vicinal sample. To further investigate this discrepancy the variation of critical current with field was measured on a  $2^\circ$  vicinal film, this is shown in Figure 4.33.

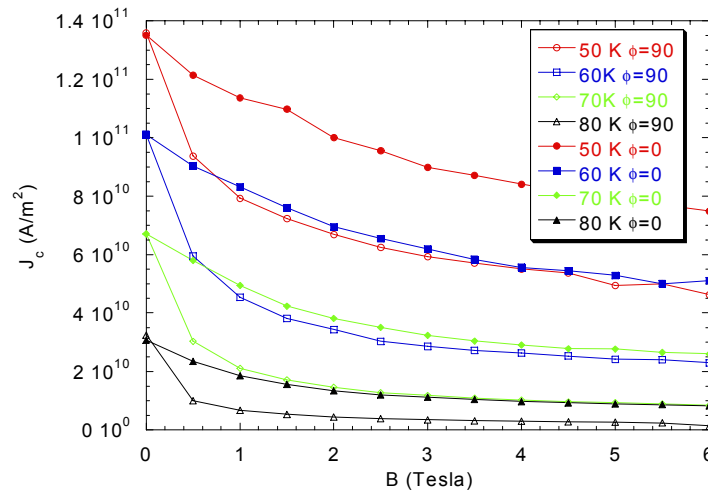


Figure 4.33 Variation of critical current with applied field at  $\theta=0^\circ$  with the applied field rotated in  $\phi$ . Open symbols correspond to  $\phi=90^\circ$ , closed symbols to  $\phi=0^\circ$ .

The effective component of the Lorentz force is the same whether the strings are orientated at  $\phi=0^\circ$  or  $\phi=90^\circ$ . In the former case the volume pinning force on the strings is simply  $J_c B \sin\theta_v$ . As has been discussed in Section 4.1.4 at  $\phi=90^\circ$  the component acting inside the  $a$ - $b$  plane is also given by this expression.

If, as before, we define a ratio  $r_\phi$  where  $r_\phi(\theta)=J_c(\theta,\phi=0^\circ)/J_c(\theta,\phi=90^\circ)$  it is possible to plot the field dependence of the effect of rotating the vortex strings in plane at the lock-in angle,  $\theta=0^\circ$ .

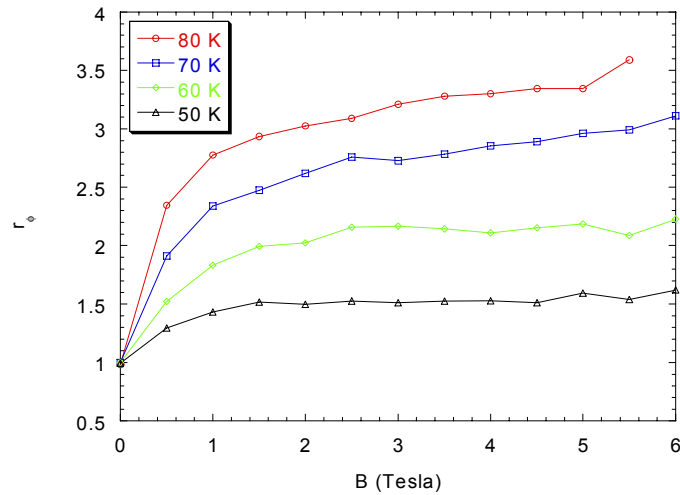


Figure 4.34 Ratio of the  $\phi=90^\circ$  channelling minimum to the  $\phi=0^\circ$  minimum at various fields and temperatures, measured at  $\theta=0^\circ$  in a  $\mathbf{T}$  track on sample Z336B ( $2^\circ$  vicinal).

From this plot we see that in the case of the  $2^\circ$  vicinal film there is a greater anisotropy at 80K, where the lattice is rectilinear than at 50K where the lattice is expected to have kinked. This may be due to the fact that at 80K it is an anisotropically cored vortex that is pinned, the pinning forces will differ depending on the direction of the Lorentz force, this is discussed in greater detail in Chapter 6. In contrast at 50K and  $\theta=0^\circ$  it is expected that the forces on the vortex strings in the channelling direction are identical.

#### 4.6. FIB Investigation of Track Width Effect

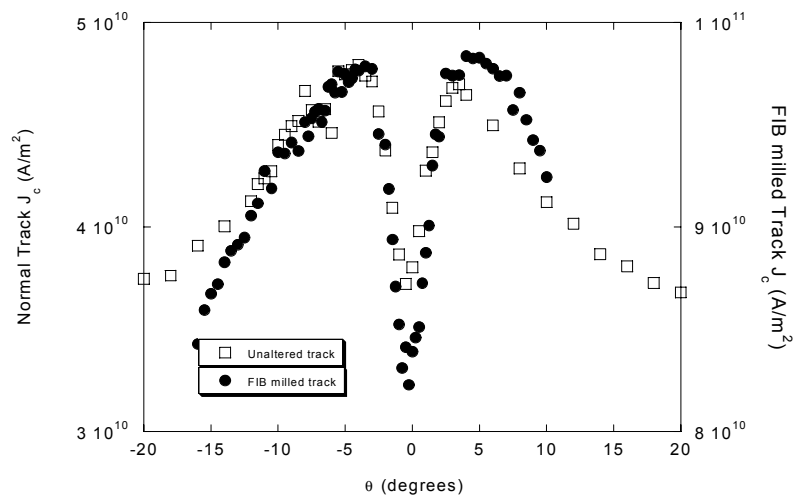


Figure 4.35 Plots of the intrinsic ( $\phi=90^\circ$ ) channelling minimum in an as prepared  $10\mu\text{m}$  wide track and a track thinned to  $\sim 2\mu\text{m}$  using an FIB.

The absolute value of the critical current in this measurement is not reliable. This is due to uncertainty in the width of the gallium damage caused in the FIB beam.

The width of the minimum is unchanged. This suggests that the width of the channelling minimum is not defined by the geometry of the sample but is rather due to an intrinsic effect. The fact that the string must lock into shorter planes in the altered track does not seem to have resulted in a noticeable widening of the channelling minimum.

However we can compare the depth of the channelling minimum with the shoulder of the peak. The minimum, as a fraction of the  $J_c$  at the shoulder, is 0.77 for the FIB milled track and 0.85 for the unaltered track. This decrease in  $J_c$  with shortening of the vortex strings is consistent with the variation in  $J_c$  with  $\phi$  discussed in Section 4.4. To draw systematic conclusions about the relationship between the track width and the  $J_c(\theta)$  behaviour would require measurements on a number of samples of varying vicinality.

#### **4.7. Discussion**

Taken as a whole the measurements presented in this chapter confirm the observation of vortex channelling by Berghuis *et al.* as a general property of YBCO films grown on mis-cut substrates rather than a curiosity particular to a single thin film sample. It appears clear that the effect should be easily observable in any vicinal film, in the  $\phi=0^\circ$ , geometry at measurements made below 80K. Many angular scaling measurements in YBCO however are made in the  $\phi=90^\circ$  geometry in order to avoid complications introduced by the force-free geometry. The results presented here show that in this geometry the channelling minimum is noticeable only at lower  $<50$  K temperatures and in films with a higher mis-cut angle. This may account for the fact that the vortex channelling effect was not observed earlier. A variation in the string vortex pinning force opposing the channelling of strings in the a-b plane has been noted. This is not systematically related to the vicinal angle suggesting that even in carefully controlled growth conditions significant variation in the pinning density in individual films occurs. The results obtained on a high angle vicinal film suggest that the high APB density observed in films grown on annealed  $\text{SrTiO}_3$  substrates can entirely suppress the vortex channelling effect and additionally lead to a significant overall enhancement of pinning and thus  $J_c$ .

Examining the channelling minimum indicates, by comparison to peaks recorded at or near  $J_c$  that it is associated with the cross-over into the string pancake state. A rectilinear Abrikosov vortex is not channelled. The width of the depression in the intrinsic or force free  $J_c$  peak that would be expected in the absence of channelling is about  $10^\circ$  either side of  $\theta=0^\circ$ . This

corresponds to the angle at which the fully developed string pancake lattice is expected to develop.

In *c*-axis films no string channelling can be directly observed, although as is discussed in Chapter 6 the string pinning force may be indirectly accessed. The intriguing possibility remains, however, that the intrinsic pinning peak observed in *c*-axis films is itself depressed to some extent by the rectilinear/string-pancake cross-over. There may therefore be scope for enhancing the pinning properties of *c*-axis films if a technique for inducing a high APB density in these films can be developed. Experiments suggest that while the pinning defect density for pancakes is high in YBCO thin films, in the absence of APB's strings are only weakly pinned.

In addition to deductions about the effect of microstructure on pinning, these measurements also shed light on the applicability of angular scaling laws developed from FLL models. Firstly the strong effect of APBs and channelling indicates that relying on such models in the presence of highly anisotropic *extrinsic* pinning cannot be justified. Secondly the indications in the Berghuis data of a cross-over into a string/pancake state, dependent both on field angle and temperature, are confirmed. This means that any successful angular scaling model must explicitly take this into account. In striking contrast to the almost pure 2D FLL behaviour in BSCCO the angular dependence of the FLL and thus  $J_c$  in YBCO is rich and difficult to model. This marks out YBCO as an 'atypical' HTS material.

Given the variation in absolute critical current density values between different samples it is not possible to directly compare  $J_c$  values between the samples measured. There is clearly scope for further investigations of the relationship between growth parameters and resultant film structure in vicinal YBCO films. At least one proposed coated conductor method, RATS, involves the employment of an effectively vicinal substrate thus such an investigation might be expected to have immediately technologically useful results.

#### **4.8. Conclusion**

The results presented in this chapter confirms the existence of the flux channelling effect in YBCO films grown on a vicinal substrate. The development of the channelling minimum is consistent with a cross-over to a regime where, below  $\sim 80$  K, at small values of  $\theta$  the FLL adopts a kinked string pancake structure. The results, underline the observation, that angular scaling models for critical current density developed from models of the FLL must be treated with caution when applied to real systems. It appears unlikely that any of the proposed scaling laws applies to the entire angular range of behaviour in YBCO.

The pinning forces on vortex string elements are clearly smaller than those on rectilinear vortices and on Abrikosov vortices. It appears clear that the results showing critical current enhancement at  $\theta=0^\circ$  in APB rich vicinal films is due to very effective pinning of vortex strings by APB's. Given the fact that the films measured for this thesis exhibited no evidence of APB's it is possible to conclude that substrate annealing is responsible for introducing a high APB density.

#### **4.9. Bibliography**

- Aomine, T., T. Nishizaki, F. Ichikawa, T. Fukami, T. Terashima and Y. Bando (1994). Physica B **194**: 1613-1614.
- Berghuis, P., F. Baudenbacher, R. Herzog, R. Somekh, A. M. Campbell, J. E. Evetts and G. Wirth (1996). Proc. 8th IWCC in Superconductors, World Scientific, Singapore.
- Berghuis, P., E. DiBartolomeo, G. A. Wagner and J. E. Evetts (1997). Physical Review Letters **79**(12): 2332-2335.
- Blatter, G., M. V. Feigelman, V. B. Geshkenbein, A. I. Larkin and V. M. Vinokur (1994). Reviews Of Modern Physics **66**(4): 1125-1388.
- Blatter, G., Geshkenbein, V.B. and Larkin, A.I. (1992). Phys. Rev. Lett. **68**(6): 875-878.
- Chaudhari, P., R. H. Koch, R. B. Laibowitz, T. R. McGuire and R. J. Gambino (1987). Physical Review Letters **58**(25): 2684-2686.
- Clem, J. R. (1991). Physical Review B-Condensed Matter **43**(10 PtA): 7837-7846.
- Clem, J. R. (1998). Superconductor Science & Technology **11**(10): 909-914.
- Dam, B., J. M. Huijbregtse, F. C. Klaassen, R. C. F. van der Geest, G. Doornbos, J. H. Rector, A. M. Testa, S. Freisem, J. C. Martinez, B. Stauble-Pumpin and R. Griessen (1999). Nature **399**(6735): 439-442.
- Dinger, T. R., T. K. Worthington, W. J. Gallagher and R. L. Sandstrom (1987). Physical Review Letters **58**(25): 2687-2690.
- Haage, T., J. Zegenhagen, J. Q. Li, H. U. Habermeier, M. Cardona, C. Jooss, R. Warthmann, A. Forkl and H. Kronmuller (1997). Physical Review B-Condensed Matter **56**(13): 8404-8418.
- Habermeier, H. U., T. Haage, J. Zegenhagen, R. Warthmann and C. Jooss (1998). Superconductor Science & Technology **11**(10): 929-934.
- Herzog, R. (1997). Critical Currents in YBCO thin films. Materials Science and Metallurgy, University of Cambridge.

- Hosseinali, G. S., R. M. Schalk, H. W. Weber, A. Ponniger, S. Proyer and P. Schwab (1994). Physica B **194**: 2357-2358.
- Huijbregtse, J. M., B. Dam, R. C. F. van der Geest, F. C. Klaassen, R. Elberse, J. H. Rector and R. Griessen (2000). Physical Review B **62**(2): 1338-1349.
- Iye, Y., S. Nakamura and T. Tamegai (1989). Physica C **159**: 433-438.
- Iye, Y., S. Nakamura, T. Tamegai, T. Terashima, K. Yamamoto and Y. Bando (1990). Physica C **166**(1-2): 62-70.
- Iye, Y., T. Tamegai, T. Sakakibara, T. Goto, N. Miura, H. Takeya and H. Takei (1988). Physica C **153**: 26-31.
- Jakob, G., M. Schmitt, T. Kluge, C. Tomerosa, P. Wagner, T. Hahn and H. Adrian (1993). Physical Review B-Condensed Matter **47**(18): 12099-12103.
- Jooss, C. (2000). Private Communication.
- Jooss, C., R. Warthmann, A. Forkl and H. Kronmuller (1998). Physica C **299**(3-4): 215-230.
- Jooss, C., R. Warthmann and H. Kronmuller (2000). Physical Review B **61**(18): 12433-12446.
- Jooss, C., R. Warthmann, H. Kronmuller, T. Haage, H. U. Habermeier and J. Zegenhagen (1999). Physical Review Letters **82**(3): 632-635.
- Kes, P. H., J. Aarts, V. M. Vinokur and C. J. van der Beek (1990). Phys. Rev. Lett. **64**(9): 1063-1066.
- Lawrence, W. E. and S. Doniach (1970). Proceedings of the 12th International Conference on Low Temperature Physics, Kyoto, Keigaku, Tokyo.
- Mechin, L., P. Berghuis and J. E. Evetts (1998). Physica C **302**(2-3): 102-112.
- Nishizaki, T., T. Aomine, I. Fujii, K. Yamamoto, S. Yoshii, T. Terashima and Y. Bando (1991a). Physica C **185**: 2259-2260.
- Nishizaki, T., T. Aomine, I. Fujii, K. Yamamoto, S. Yoshii, T. Terashima and Y. Bando (1991b). Physica C **181**(4-6): 223-232.
- Palstra, T. T. M., B. Batlogg, R. B. Vandover, L. F. Schneemeyer and J. V. Waszczak (1989). Applied Physics Letters **54**(8): 763-765.
- Ravi Kumar, G., M. R. Koblishka, J. C. Martinez, R. Griessen, B. Dam and J. Rector (1994). Physica C **235-240**: 3053-3054.
- Roas, B. L., L. Schultz and G. Saemannishenko (1990). Phys. Rev. Lett. **64**(4): 479.
- Schalk, R. M., G. S. Hosseinali, H. W. Weber, Z. H. Barber, P. Przyslupski, J. E. Evetts, A. Ponniger, P. Schwab, S. Proyer, A. Kochemasov and D. Bauerle (1993). Cryogenics **33**(3): 369-374.

- Schalk, R. M., H. W. Weber, Z. H. Barber, P. Przyslupsky and J. E. Evetts (1992). Physica C **199**(3-4): 311-320.
- Tachiki, M. and S. Takahashi (1989a). Solid State Communications **72**(11): 1083.
- Tachiki, M. and S. Takahashi (1989b). Solid State Communications **70**(3): 291-295.
- Tachiki, M., S. Takahashi and K. Sunaga (1993). Physical Review B-Condensed Matter **47**(10): 6095-6105.
- Yeshurun, Y., A. P. Malozemoff, T. K. Worthington, R. M. Yandroski, L. Krusinbaum, F. H. Holtzberg, T. R. Dinger and G. V. Chandrashekar (1989). Cryogenics **29**(3A): 258-262.

## 5. Measurements on De-oxygenated Vicinal YBCO Films

*In the previous chapter, a cross-over model of the flux line lattice (FLL) has been discussed. In that model, the angles at which the FLL changes form are related to the  $c$ -axis coherence length and the anisotropy ratio in the superconductor. To further examine this model experiments were performed with de-oxygenated YBCO films. It has been proposed that de-oxygenation, as well as suppressing  $T_c$  and  $J_c$ , leads to a greater anisotropy in the superconducting parameters. Initial measurements on a de-oxygenated YBCO film indicated that the vortex channelling effect was more pronounced in de-oxygenated films. To investigate this more systematically a matched pair of films were grown. One film was optimally oxygenated and the second de-oxygenated, giving a  $T_c=51$  K. By comparing  $J_c(\theta)$  results from fully and partially de-oxygenated films it is possible to see how the predictions of the cross-over model compare with experiment in a more anisotropic system.*

### 5.1. Introduction

#### 5.1.1. Effect of De-oxygenation in YBCO

The structure of  $\text{YBa}_2\text{Cu}_3\text{O}_{7-\delta}$  (YBCO) consists of superconducting cuprate planes separated by blocking layers. The blocking layers in YBCO, in contrast to most other HTS contain cuprate chains. It has been suggested that these chains are responsible for the reduced anisotropy in YBCO as compared to other HTS. It is possible to vary the oxygen concentration in YBCO by annealing under varying oxygen partial pressures. As is discussed in Section 3.1.3 it is, thus, possible to produce thin YBCO films with different levels of oxygenation.

The oxygen atoms in the cuprate chains are the most mobile and it is these sites that are depopulated when  $\delta$  increases. With underdoping a reduction in the critical transition temperature and the critical current density of the material is observed. It appears, however, to be the case that the empty oxygen sites do not enhance pinning in the material (Christen and Feenstra 1991, Ossandon, *et al.* 1992), the pinning in a thin film being already near optimal. In addition to effects on the superconducting properties of the material as  $\delta$  increases above  $\sim 0.5$  YBCO undergoes a transition from an orthorhombic to a tetragonal structure. This is reflected in an increasing  $c$ -axis length.

During annealing it has been observed that oxygen moves preferentially along defects and along the  $a$ - $b$  planes. This may mean that vicinal films, where the edges of short  $a$ - $b$  planes are exposed, are more easily annealed than  $c$ -axis oriented films.

With reduced oxygen doping YBCO exhibits a reduced critical temperature,  $T_c$ , and critical current density,  $J_c$ . Some authors have reported little change in the value of the Ginzburg-Landau superconducting anisotropy parameter,  $\epsilon=1/\gamma=\xi_c/\xi_{ab}$ , for small values of  $\delta < 0.2$  (Ossandon, *et al.* 1993). It is clear that the anisotropy does increase at larger values (Cava, *et al.* 1990, Hou, *et al.* 1994).

It is difficult to assess the oxygen contribution in YBCO thin films since any mass changes are extremely small. In contrast, in bulk samples techniques such as thermogravimetric analysis may be employed to determine  $\delta$ . Although Raman microscopy can indicate oxygenation, this is a local measurement and does not yield the average oxygenation of the film. For this reason the oxygenation is often inferred from the recorded  $T_c$ . The plot below, reproduced from Chapter 3, shows a relationship between  $\delta$  and  $T_c$ .

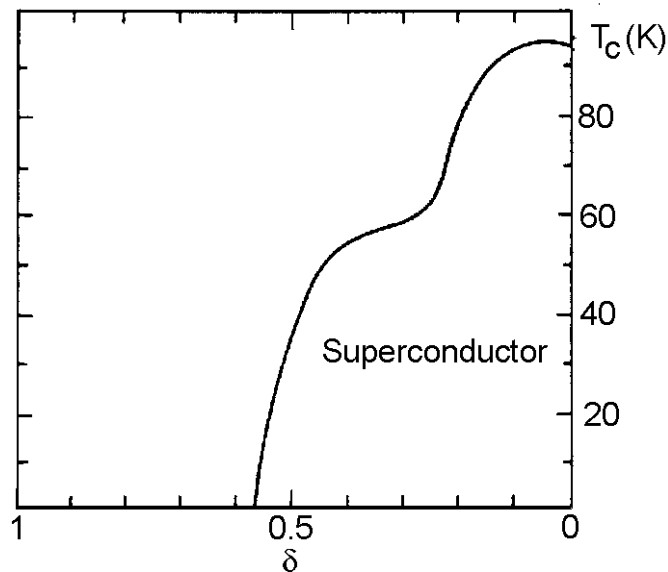


Figure 5.1 Variation of  $T_c$  with oxygenation in  $YBa_2Cu_3O_{7-\delta}$  (Cyrot and Pavuna 1995)

Factors other than oxygenation affect the  $T_c$  of a sample, therefore a value for  $\delta$  obtained in this way is an estimate. It is possible to determine the value of  $\delta$  from the variation in the  $c$ -axis length in thin films (Ye and Nakamura 1993, Farnan, *et al.* 2001). However, the exact value of  $\delta$  is not required for a qualitative discussion of the effect of de-oxygenation on the FLL anisotropy in YBCO.

### 5.1.2. FLL anisotropy in de-oxygenated YBCO

In the previous chapter the vicinal channelling effect was discussed in the context of a cross-over from a Abrikosov to a string pancake lattice. This 3D to ‘quasi’ 2D cross-over is characterized by the ratio  $\xi_c/d$ . The string pancake lattice is ‘quasi’ 2D since it contains Josephson string vortices and does not obey the Kes law, as for a purely 2D FLL. Although there is some variation in the c-axis length and thus the interlayer spacing,  $d$ , with oxygenation, the variation in the coherence length is proportionately larger.

Deak *et al.* (1995) identified a cross-over into a 2D lattice structure in de-oxygenated YBCO in magnetisation measurements. They, on the basis of these measurements, deduced the relationship between the anisotropy parameter and  $\gamma$  shown in Figure 5.2. It can be seen from Figure 5.2 that there is significant uncertainty in the measurements, but their results certainly confirm the idea that anisotropy increases with underdoping.

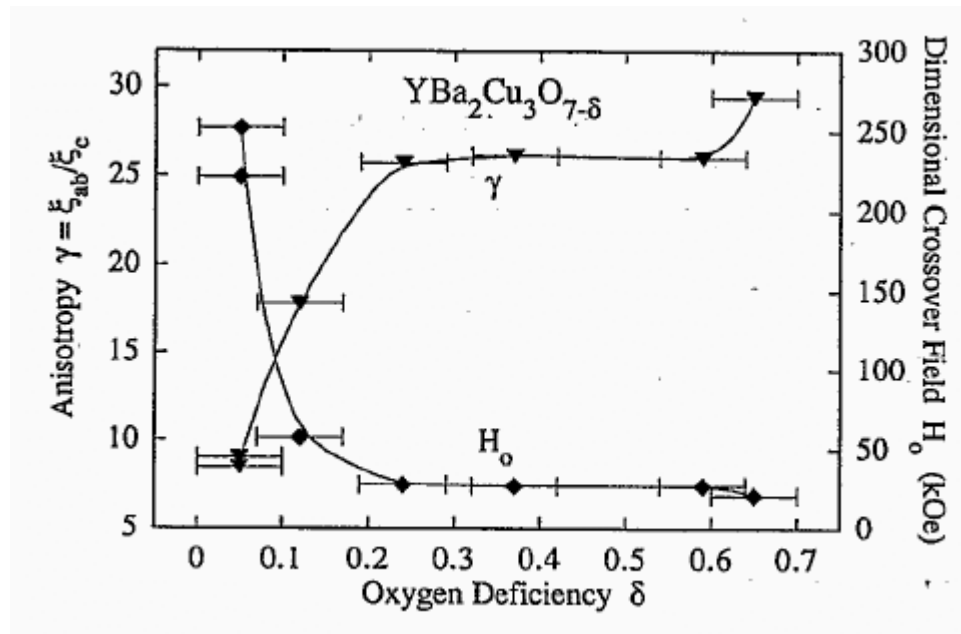


Figure 5.2 Relationship between de-oxygenation,  $\delta$ , and the G-L anisotropy parameter,  $\gamma=1/\epsilon$ , deduced by Deak, et al. (1995) from magnetisation measurements on thin YBCO films.

Other groups have reported a cross-over to a 2D lattice structure with increasing anisotropy (Moreno and Bekeris 2000b, Moreno and Bekeris 2000a), in this case it is suggested that the cross-over is associated with reduced pinning. As has been discussed in Chapter 2 it is difficult to apply results that appeal to a particular thermodynamic model of the FLL to thin film measurements in the presence of strong pinning.

Herzog (1997) performed magnetic field angularly dependent critical current measurements in c-axis orientated YBCO films. He observed smaller values of critical current and that  $J_c(\theta)$  behaviour consistent with a 2D lattice persisted at higher temperatures.

The cross-over model defines the angle,  $\theta_2$ , for cross-over into the string pancake state as (Blatter, *et al.* 1994, pp 1286):

$$\tan(\theta_2) = \epsilon \quad (5.1)$$

and the cross-over temperature  $T_{cr}$  is reached when  $\xi_c > d/\sqrt{2}$ .

Since the equation for  $T_{cr}$  yields 80 K for fully oxygenated YBCO it is reasonable to predict that in de-oxygenated YBCO with a shorter c-axis coherence length  $T_{cr}$  is larger than  $T_c$ . In this case the string pancake state will exist for all values of  $\theta$  less than  $\theta_2$ .

Assuming that a critical transition temperature of 51 K corresponds to  $\delta \sim 0.4$  in the de-oxygenated sample,  $\theta_2$  would be predicted to be smaller than that in fully oxygenated YBCO,  $\sim 3^\circ$ . Interestingly, therefore, this model predicts that the kinked string pancake vortex will exist over a smaller range of angles. The distorted FLL occurring for  $\theta < \theta_1$  where  $\tan \theta_1 = d/\xi_{ab}$  will, however, persist over a greater range of angles as the a-b plane coherence length,  $\xi_{ab}$ , should be relatively unchanged in de-oxygenated YBCO and the interlayer spacing,  $d$ , will increase.

## 5.2. Sample Preparation and Characterisation

### 5.2.1. Sample Preparation

The 200 nm thick films were prepared by Laser Ablation by Roman Rössler of the University of Linz. Sample 200630 was optimally oxygenated, while sample 210600 was de-oxygenated by reducing the oxygen partial pressure during annealing.

The substrates used both had a  $10^\circ$  miscut, and were 10mm by 10mm. The larger substrate size allowed 9 tracks to be patterned using the lithography method described in Chapter 3. After patterning the film contained six **T** tracks and 3 **L** tracks.

### 5.2.2. RT data

The two samples were characterised by performing RT measurements on both a **T** and an **L** track for each film. These measurements showed that the optimally oxygenated sample had a zero resistance  $T_c$  of 90 K, and that for the **L** track the de-oxygenated sample had a  $T_c$  of 51 K. These transitions are shown in Figure 5.3. From the transition shown in Figure 5.1 we may estimate that the de-oxygenated sample had  $\delta \sim 0.4$ .

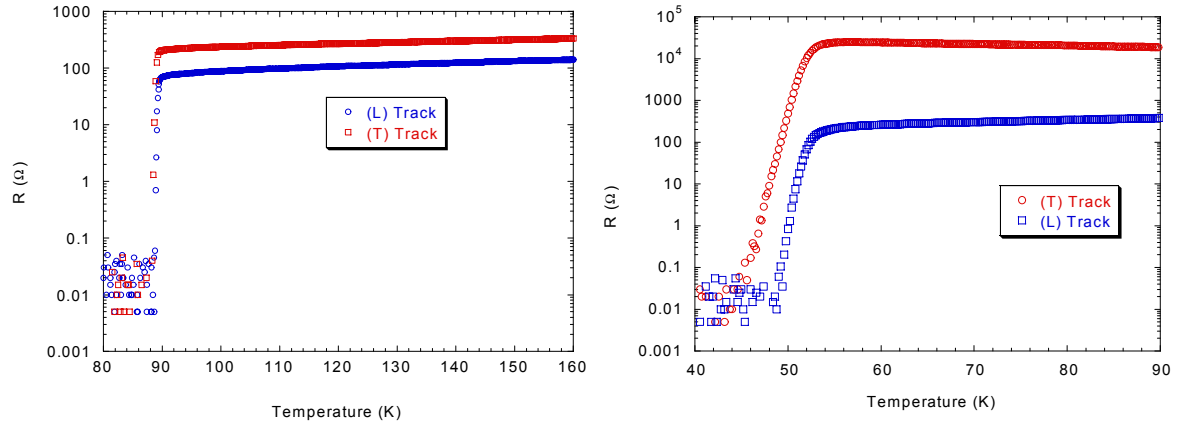


Figure 5.3 Shown on the left is the resistive transition for the optimally oxygenated film, and on the right the transition for the de-oxygenated film. Transitions are shown for both tracks running parallel to the  $a$ - $b$  planes  $\mathbf{L}$  and tracks crossing the vicinal steps  $\mathbf{T}$ .

The  $RT$  transition for the optimally oxygenated film is as expected, with a larger resistance present in the  $\mathbf{T}$  track due to the normal state anisotropy present in the superconductor. At 100 K the anisotropy between the  $\mathbf{L}$  and  $\mathbf{T}$  track is a factor of three. The de-oxygenated sample shows a significantly more marked normal state anisotropy, the  $\mathbf{T}$  track resistance being a factor of 50 greater at 90 K. The resistance of the  $\mathbf{T}$  track also shows a semiconductor-like increase with decreasing temperature close to  $T_c$ . The width of the transition in the de-oxygenated sample is larger than that in the optimally oxygenated film. An increase in the transition width with de-oxygenation has been widely reported (Osquiguil, *et al.* 1992, Ye and Nakamura 1993, Wu, *et al.* 1998, Farnan, *et al.* 2001).

The resistivity in the  $\mathbf{L}$  tracks,  $\rho_L$ , and  $\mathbf{T}$  tracks,  $\rho_T$ , is related to the  $c$ -axis resistivity,  $\rho_c$ , by the Equation (5.2) (Zahner, *et al.* 1998), the resistivity in the  $a$ - $b$  planes,  $\rho_{ab}$ , being equal to  $\rho_L$ . The substrate miscut angle is denoted as  $\theta_v$ .

$$\rho_c = \frac{\rho_{(T)} - \rho_{(L)} \cos^2 \theta_v}{\sin^2 \theta_v} \quad (5.2)$$

This can be rewritten to allow the resistivity and therefore the resistance anisotropy between the  $a$ - $b$  planes and the  $c$ -axis direction,  $\gamma_\rho$ , to be related to that between the  $\mathbf{T}$  and  $\mathbf{L}$  tracks,  $\gamma_{TL}$ .

$$\gamma_\rho = \frac{\gamma_{TL} - \cos^2 \theta_v}{\sin^2 \theta_v} \quad (5.3)$$

The normal state resistance anisotropy for the optimally and de-oxygenated samples at 100 K and 90 K respectively may therefore be calculated using Equation (5.3):

	$\gamma_{TL}$	$\gamma_{\rho}$
Optimally Oxygenated	3	66
De-oxygenated	50	1600

Table 5.1 Resistivity anisotropies for the optimally and de-oxygenated YBCO samples measured for this chapter.

From these results it can be seen that de-oxygenation has a striking effect on the normal state resistance anisotropy of YBCO. The normal state resistivity anisotropy at 100 K is consistent with values observed in single crystals (Datta 1992).

### 5.3. Results

The measurement geometry used for the measurements described in this chapter is the same as that in the previous and the same notation is used. For the convenience of the reader a fold out diagram depicted the various angles and directions in the measurement is provided in Appendix B.

#### 5.3.1. $J_c(\theta)$ at varying temperatures

The figure below shows  $J_c(\theta)$  measurements on both the optimally and de-oxygenated films at the same reduced temperature, these measurements were performed on 10 micron wide tracks, as in the previous chapter. To attempt to provide a useful comparison the measurements were performed at the same reduced temperature,  $t$ , where  $t=T/T_c$ .

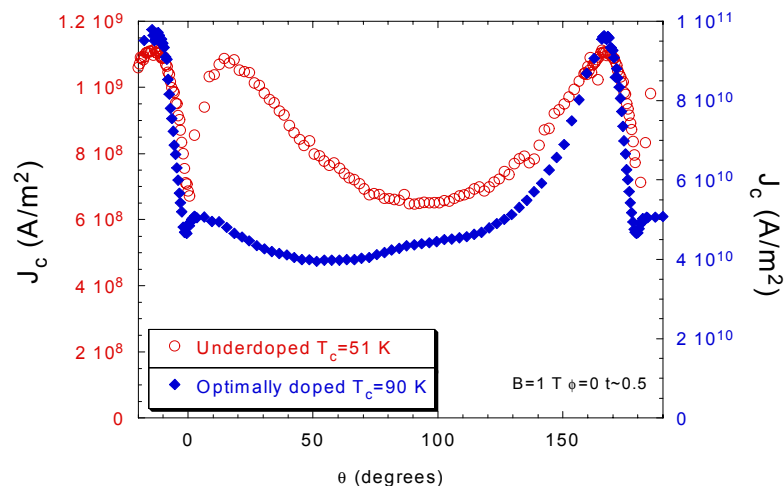


Figure 5.4  $J_c(\theta)$  plot from data recorded on a  $\mathbf{T}$  track for both the optimally oxygenated sample (200630) and the de-oxygenated sample (210600). This data was recorded at a reduced temperature,  $t$ , of 0.5, a field of 1 T and in the  $\phi=0^\circ$  geometry.

Clearly, therefore, vortex channelling is present in de-oxygenated YBCO films as well as optimally oxygenated samples.

It is interesting to note from the Figure that the shape of the channelling dip in the two cases is quite different. Figure 5.5 shows how this minimum develops in the  $\phi=0^\circ$  configuration at varying temperatures for both films.

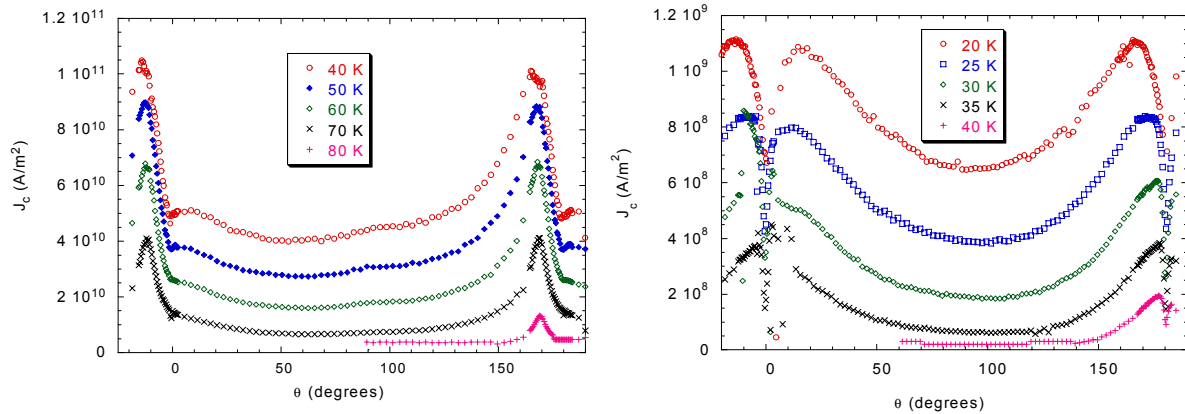


Figure 5.5  $J_c(\theta)$  measurements on  $\mathbf{T}$  tracks at 1 T and  $\phi=0^\circ$  on an optimally doped (left) and an under doped (right) YBCO sample.

The channelling minimum in the fully oxygenated sample develops as the temperature is reduced below  $T_{cr}$ . The minimum affects the force-free peak over a wide angular range leading to a very anisotropic peak. In contrast in the de-oxygenated film the effect of the channelling configuration is restricted to smaller range about  $\theta=0^\circ$ . Additionally the channelling minimum in the de-oxygenated film is fully developed for both lower temperatures and those close to  $T_c$ . The evolution of the channelling minimum in both cases is shown more clearly in Figure 5.6. Here the data sets from Figure 5.5 are shown rescaled to the value of  $J_c$  at  $\theta=90^\circ$ . This allows the way the channelling minimum vary with temperature to be examined.

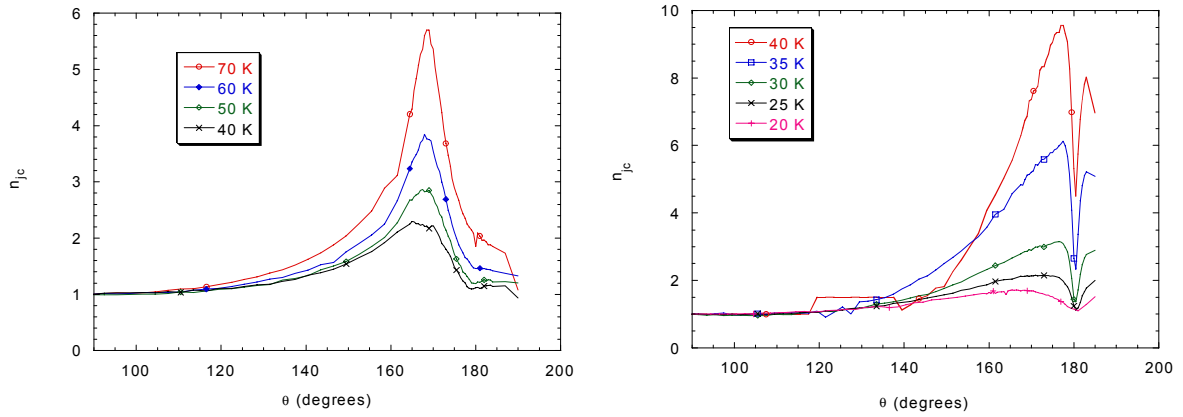


Figure 5.6  $J_c(\theta)$  measurements on  $\mathbf{T}$  tracks at 1 T and  $\phi=0^\circ$  on an optimally doped (left) and an under doped (right) YBCO sample replotted as a function of  $n_{j_c}$ , where  $n_{j_c}(\theta)=J_c(\theta)/J_c(90^\circ)$ .

In contrast to results observed in both this, and the previous chapter, on fully oxygenated samples the channelling minimum in de-oxygenated YBCO appears more pronounced.

The variation in the channelling minimum at  $\phi=90^\circ$  is shown in Figure 5.7 below,

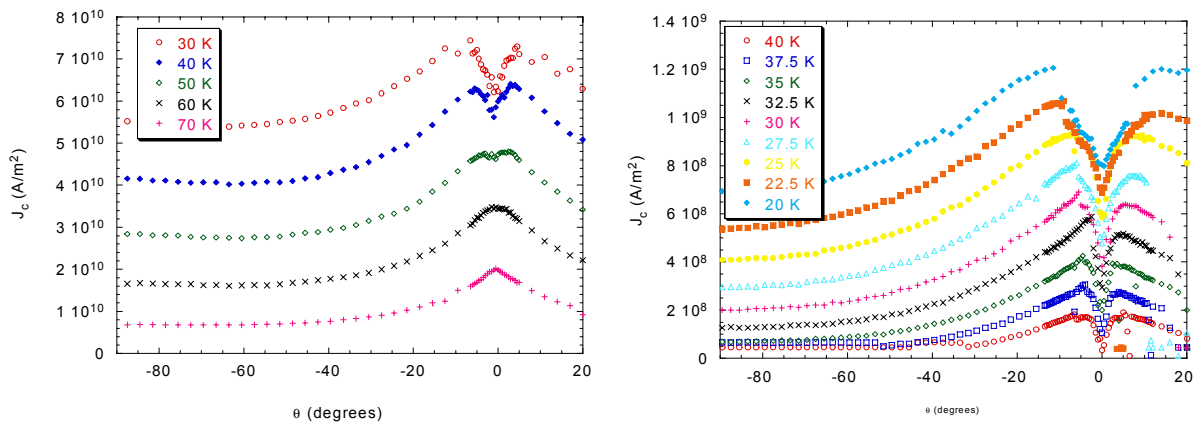


Figure 5.7  $J_c(\theta)$  measurements on  $\mathbf{T}$  tracks at 1 T and  $\phi=90^\circ$  on an optimally doped (left) and an under doped (right) YBCO sample.

The  $\phi=90^\circ$  data may also be rescaled as before, this is shown in Figure 5.8:

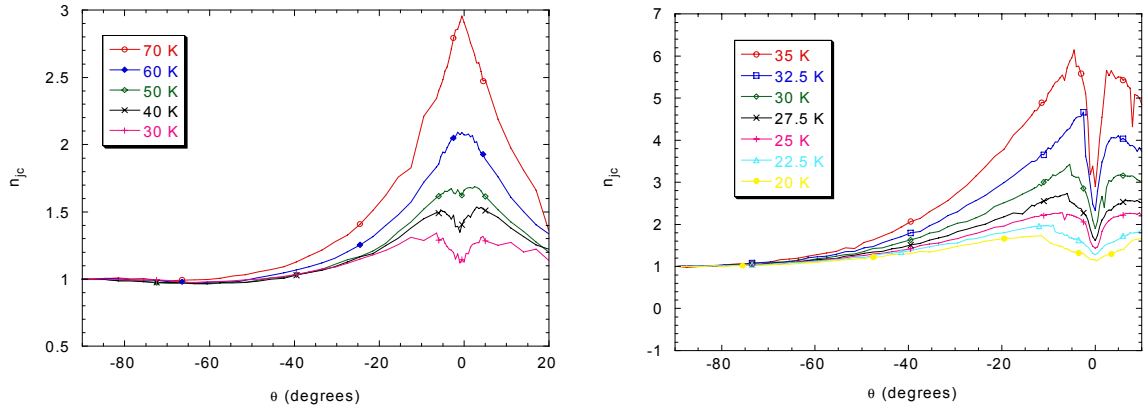


Figure 5.8  $J_c(\theta)$  measurements on  $\mathbf{T}$  tracks at 1 T and  $\phi=0^\circ$  on an optimally doped (left) and an under doped (right) YBCO sample replotted as a function of  $n_{j_c}$ , where  $n_{j_c}(\theta)=J_c(\theta)/J_c(90^\circ)$ .

In all these plots it appears that although the channelling minimum may be subjectively deeper its influence extends over a smaller angular range. This is consistent with the prediction given in Section 5.1.2 even if the result appears somewhat counter intuitive.

### 5.3.2. $J_c(\theta)$ in varying applied fields

The measurements presented in Figures 5.9 and 5.10 show how the  $J_c(\theta)$  behaviour varies with field in both the fully and partially oxygenated samples at  $\phi=0^\circ$  and  $\phi=90^\circ$ .

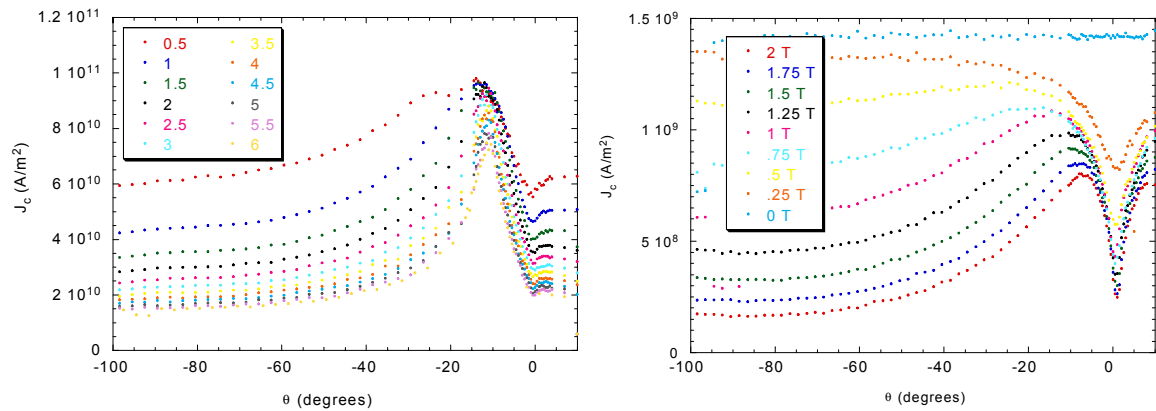


Figure 5.9  $J_c(\theta)$  measurements on  $\mathbf{T}$  tracks in the  $\phi=0^\circ$  geometry on an optimally doped (left) and an under doped (right) YBCO sample. These measurements were performed at  $t=0.4$ .

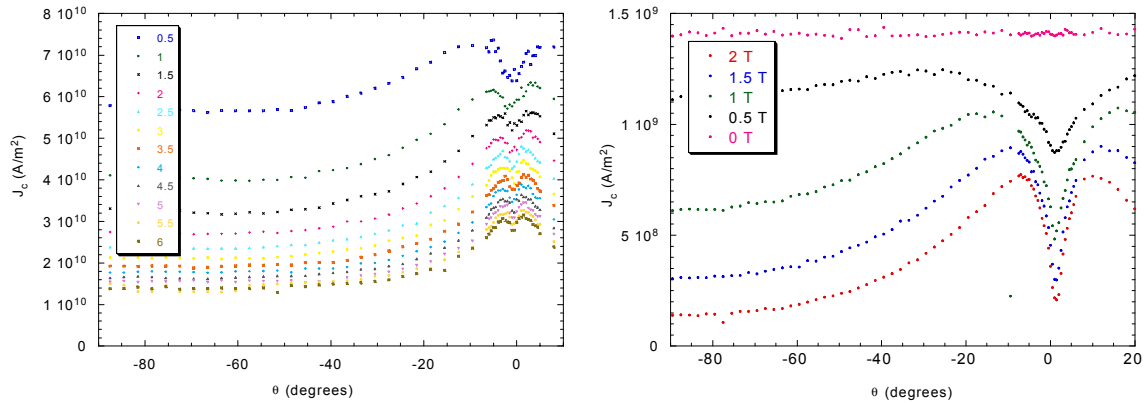


Figure 5.10  $J_c(\theta)$  measurements on  $\mathbf{T}$  tracks in the  $\phi=90^\circ$  geometry on the optimally doped (left) and the under doped (right) YBCO sample. These measurements were performed at  $t=0.4$ .

Again, in these measurements the more pronounced channelling minimum in de-oxygenated YBCO may be observed. In the underdoped sample the minimum is present at a range of fields, providing further evidence that channelling is an intrinsic effect rather than a peculiarity of a particular sample.

#### 5.4. Discussion

From the results obtained it is clear that de-oxygenated YBCO does appear to exhibit a larger superconducting anisotropy. The anisotropy is not, however, such that the material starts exhibiting entirely 2D Kes law behaviour. It seems therefore reasonable to assume that the cross-over model of the behaviour of the FLL in YBCO is still applicable.

The channelling minimum in de-oxygenated films exhibit a different variation with field and temperature than that in an optimally oxygenated sample. In addition although  $J_c$  is depressed considerably in the minimum the effect of the channelling dip appears to have less effect on the rest of the  $J_c(\theta)$  characteristic in de-oxygenated films. This is perhaps linked to the narrower window of  $\theta$  in which the fully developed kinked pancake string lattice is expected.

From the results obtained the prediction that  $T_{cr}$  in YBCO is larger than  $T_c$  appears to be valid; it is certainly larger than 40 K. The channelling minimum is well developed at all temperatures, rather than becoming more pronounced with decreasing temperature as observed in measurements on fully oxygenated films.

## 5.5. Conclusions

The results shown in this chapter suggest that de-oxygenation of YBCO increases the superconducting anisotropy, and that this increase is manifested in the magnetic field angular dependent behaviour of the FLL and thus the critical current anisotropy.

The rather counter intuitive prediction of equation (5.1), that a material with increased anisotropy will exhibit a fully developed string/pancake lattice over a smaller range of  $\theta$ , appears consistent with the  $J_c(\theta)$  results obtained. The channelling minimum is more prominent than that seen in optimally oxygenated films yet the rest of the  $J_c(\theta)$  characteristic appears less affected.

## 5.6. Bibliography

- Blatter, G., M. V. Feigelman, V. B. Geshkenbein, A. I. Larkin and V. M. Vinokur (1994). Rev. Mod. Phys. **66**(4): 1125-1388.
- Cava, R. J., A. W. Hewat, E. A. Hewat, B. Batlogg, M. Marezio, K. M. Rabe, J. J. Krajewski, W. F. Peck and L. W. Rupp (1990). Physica C **165**(5-6): 419-433.
- Christen, D. K. and R. Feenstra (1991). Physica C **185**: 2225-2226.
- Cyrot, M. and D. Pavuna (1995). Introduction to Superconductivity and High- $T_c$  materials. Singapore, World Scientific.
- Datta, T. (1992). Oxide Superconductors: Physical Properties. Concise Encyclopedia of Magnetic and Superconducting Materials. J. E. Evetts. Oxford, Pergamon
- Deak, J., L. F. Hou, P. Metcalf and M. McElfresh (1995). Phys. Rev. B. **51**(1): 705-708.
- Farnan, G. A., M. P. McCurry, D. G. Walmsley, Z. Z. Li and H. Raffy (2001). Supercon. Sci. Technol. **14**(3): 160-167.
- Herzog, R. (1997). Critical Currents in YBCO thin films. Thesis - Materials Science and Metallurgy, University of Cambridge.
- Hou, L. F., J. Deak, P. Metcalf and M. McElfresh (1994). Phys. Rev. B. **50**(10): 7226-7229.
- Moreno, A. J. and V. Bekeris (2000a). Physica C **329**(3): 178-184.
- Moreno, A. J. and V. Bekeris (2000b). Physica Status Solidi B. **220**(1): 597-601.
- Osquiguil, E., M. Maenhoudt, B. Wuyts and Y. Bruynseraede (1992). Appl. Phys. Lett. **60**(13): 1627-1629.
- Ossandon, J. G., J. R. Thompson, D. K. Christen, B. C. Sales, H. R. Kerchner, J. O. Thomson, Y. R. Sun, K. W. Lay and J. E. Tkaczyk (1992). Phys. Rev. B. **45**(21): 12534-12547.

- Ossandon, J. G., J. R. Thompson, D. K. Christen, Y. R. Sun, B. C. Sales, H. R. Kerchner, J. E. Tkaczyk and K. W. Lay (1993). Appl. Supercon. **1**(3-6): 371-380.
- Wu, K. H., M. C. Hsieh, S. P. Chen, S. C. Chao, J. Y. Juang, T. M. Uen, Y. S. Gou, T. Y. Tseng, C. M. Fu, J. M. Chen and R. G. Liu (1998). Japan. J. Appl. Phys. **37**(8): 4346-4355.
- Ye, J. H. and K. Nakamura (1993). Phys. Rev. B. **48**(10): 7554-7564.
- Zahner, T., R. Stierstorfer, R. Rossler, J. D. Pedarnig, D. Bauerle and H. Lengfellner (1998). Physica C **298**(1-2): 91-94.

## 6. Critical current measurements on c-axis films

*It has been shown in the previous two chapters that there is strong evidence that the structure adopted by the flux line lattice (FLL) in  $\text{YBa}_2\text{Cu}_3\text{O}_{7-\delta}$  (YBCO) depends on the angle,  $\theta$ , between the applied field and the superconducting cuprate planes. If this angle is held constant and the field rotated about an axis normal to the cuprate planes, the structure of the FLL will remain constant, while the direction of the Lorentz force on the vortex lines changes. Measurements of the critical current density,  $J_c$ , with respect to this rotation angle,  $\phi$ , thus probe pinning behaviour while excluding effects due to changes in the structure of the FLL. If the value of  $\theta$  is small, such that the FLL adopts the kinked, string/pancake, state, the variation in  $J_c$  seen with  $\phi$  must be due to pinning of the string vortex segments. If  $\theta$  is large then the change in pinning is due to the shape of the Abrikosov vortex cores. In this chapter high resolution measurements of the variation of  $J_c$  with this second angle  $\phi$  have been made on thin (120 nm) YBCO films. A simple model is proposed to explain this variation in terms of dragging of vortex strings by the vortex pancake elements. The increase in  $J_c$  at large  $\theta$  is modelled in terms of the Ginzburg Landau angular scaling parameter  $\epsilon_\theta$ .*

### 6.1. Introduction

#### 6.1.1. Previous measurements

Previous measurements of the critical current versus field angle behaviour in *c*-axis oriented YBCO thin films have been reviewed in Chapter 4. The majority of experiments have concentrated on determining the variation of critical current with the *tilt* angle between the applied field and the cuprate planes,  $\theta$ . With a two-axis goniometer it is possible to *rotate* the applied field,  $\phi$ , about the *c*-axis at constant  $\theta$ . This means that although the direction of the Lorentz force changes, the structure of the FLL will remain constant. Figure 6.1 defines the angles  $\phi$  and  $\theta$  for measurements on *c*-axis orientated films.

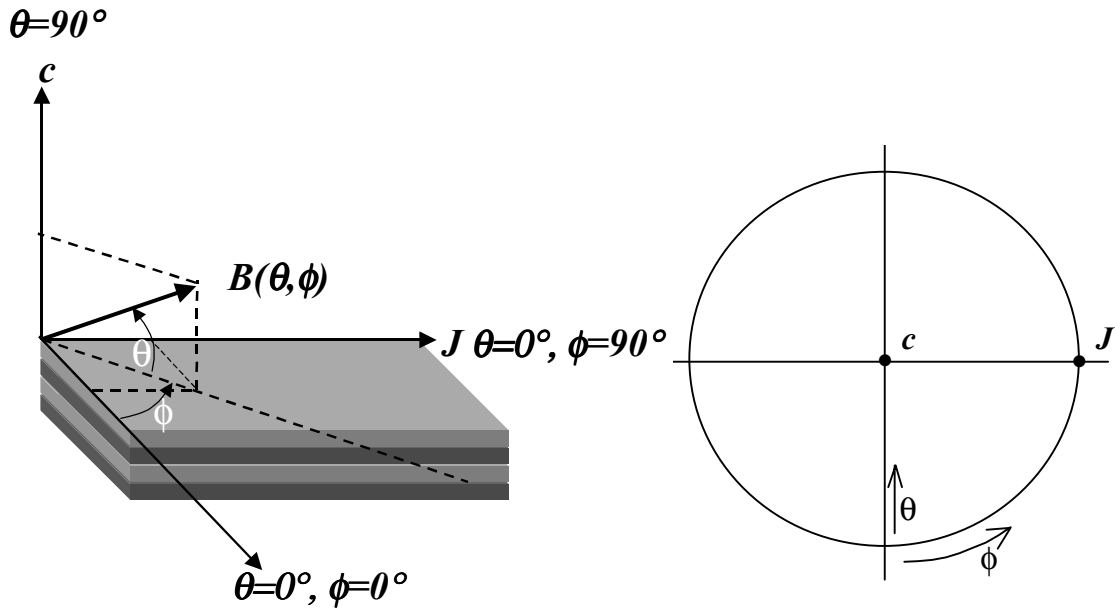


Figure 6.1 (left) Definition of the field angles  $\theta$  and  $\phi$  with respect to a current flowing in a  $c$ -axis film. (right)  $\theta$  and  $\phi$  shown on a pole figure.

Nishizaki *et al.* (1993, 1991a, 1991b) measured the  $\phi$  dependence of  $J_c$ . They attributed the difference between  $J_c(\theta)$  measurements at  $\phi=0^\circ$  and  $\phi=90^\circ$  to the changing Lorentz forces on the vortex string elements. At  $\theta=0^\circ$  the  $J_c(\phi)$  variation itself was attributed to an anisotropy of the volume pinning force rather than the change in the direction and magnitude of the Lorentz forces on the strings. They, for  $\theta=0^\circ$ , fitted their results to the following equation where  $A_p$  is a ‘pinning force parameter’

$$J_c(\phi) = \frac{A_p}{B|\sin \phi| + A_p/J_c(\phi=0)} \quad (6.1)$$

The same group has, however reported entirely 2D behaviour in measurements on YBCO thin films at low  $< 40$  K temperatures (Aomine, *et al.* 1994). In the 2D model (discussed in Chapter 7) only the pancake density is important and, as this does not change with  $\phi$ , the critical current should not alter either. The volume pinning force approach implies collective pinning which is unlikely given the generally strong pinning and high defect density observed in YBCO films (Dam, *et al.* 1999).

Herzog (1997) modelled the  $\phi$  dependence of  $J_c$  in terms of the forces on an individual extended pancake vortex. He arrived at the dependence given by equation (6.2).

$$J_c(\theta, \phi) = \frac{1}{\sqrt{\frac{\cos^2 \phi}{J_c^2(\theta, 90)} + \frac{\sin^2 \phi}{J_c^2(\theta, 0)}}} \quad (6.2)$$

This equation is derived from one particular model of the pinning potential, it would seem difficult to apply such a model to a system where a variety of pinning potentials exist. This model also fails to consider the effect of pinning forces on vortex strings.

These two models only considered the variation of  $J_c$  in a geometry where in principle the vortex lines are entirely string like. In this geometry ( $\theta=0^\circ$ ) the Lorentz force on the strings is always in the strongly pinned  $c$ -axis direction and reduces from a maximum at  $\phi=0^\circ$  when the field is perpendicular to the current direction to the force free configuration at  $\phi=90^\circ$  when the applied field is parallel to the current direction. At  $\theta=0^\circ$  it would seem likely that the critical current is proportional to the Lorentz force which varies as  $\cos\phi$ . Naturally this picture will be complicated by the more involved flux line behaviour associated with the force free regime at  $\theta=0^\circ$  and  $\phi=90^\circ$ .

Herzog (1997) separately considered the enhancement in  $J_c$  due to vortex strings in terms of pinning of the string by point defects. Experimental data was unfortunately only obtained for  $\theta=20^\circ$  in a de-oxygenated film and Herzog concluded that there was no clear evidence that this enhancement was due to string dragging.

Both Herzog and Nishizaki concentrated on considering the  $J_c(\phi)$  dependence at  $\theta=0^\circ$  (that is parallel to the cuprate planes). This treatment has the disadvantage that at  $\theta=0^\circ$ ,  $\phi=90^\circ$  the force free regime is achieved. To attempt to avoid the complications entailed with such measurements this chapter describes  $\phi$  measurements performed at a variety of values of  $\theta$ . This has the added advantage that alignment errors become obvious if successive plots of  $J_c(\phi)$  are considered.

The change in the structure of the vortex lattice with  $\theta$  in YBCO is discussed in Chapter 2. As the tilt angle between the applied field and the cuprate planes decreases it is expected that the flux lines become more anisotropic. At an angle  $\theta_1$ , which is temperature dependent, the flux lines start to become distorted ( $\theta_1 \sim 35^\circ$  at  $t=0$  in YBCO). At an angle  $\theta_2$  ( $\sim 11^\circ$  in YBCO) cross-over into a kinked string pancake lattice is expected to take place. It follows, therefore, that if the angle  $\theta$  is fixed and the field line rotated in  $\phi$  the only possible cause of a change in the critical current is change in the magnitude and direction of the Lorentz force. To quantify the effect of this rotation the ratio  $r_\phi(\theta) = J_c(\theta, \phi=90^\circ) / J_c(\theta, \phi=0^\circ)$  may be defined. The nature of the  $J_c(\phi)$  dependence will change as the FLL crosses over from a rectilinear Abrikosov lattice into a kinked string pancake lattice state.

### 6.1.2. $J_c(\phi)$ dependence of an Abrikosov lattice

For values of  $\theta$  greater than  $\theta_1$  an Abrikosov lattice is expected. In order to consider the variation of  $J_c$  with  $\phi$  on an Abrikosov lattice, we need to be able to determine the magnitude of the Lorentz force at any particular value of  $\phi$  and  $\theta$ . This is given by  $J_c B \sin \alpha$  where  $\alpha$  is the angle between the applied field and the current direction. From Figure 6.1 we can see that this may be calculated by considering a right angled spherical triangle of sides  $\theta$ ,  $90^\circ - \phi$  and  $\alpha$ . The law of cosines may be used to write  $\cos(\alpha) = \sin(\phi) \cos(\theta)$ . We may then write the Lorentz force on the flux line in terms of  $\phi$  and  $\theta$ :

$$F_L(\theta, \phi) = J_c B \sqrt{1 - \sin^2 \phi \cos^2 \theta} \quad (6.3)$$

Three simple cases of equation (6.3) are that at  $\theta = 0^\circ$  we have  $F_L = J_c B \cos \phi$ , at  $\phi = 90^\circ$  the Lorentz force density is given by  $F_L = J_c B \sin \theta$  and that at  $\phi = 0^\circ$  and all values of  $\theta$  the expression is  $F_L = J_c B$ . If the pinning is constant we would expect that the critical current will always increase as  $\phi$  is swept towards  $90^\circ$  since the Lorentz force is decreased. For  $\theta = 0^\circ$  and  $\phi = 90^\circ$  the force free regime is reached.

In the previous section the ratio  $r_\phi$  was introduced to quantify the variation in critical current between  $\phi = 0$  and  $\phi = 90$  where  $r_\phi(\theta) = J_c(\theta, \phi = 90^\circ) / J_c(\theta, \phi = 0^\circ)$ . If the only factor affecting the critical current density is the reduction in the Lorentz force as the force free regime is approached, it is possible to write the following expression for  $r_\phi$  as a function of  $\theta$ :

$$r_\phi(\theta) = 1 / \sin \theta \quad (6.4)$$

In addition to this effect both the anisotropy of the core and any anisotropy of the pinning potential will also affect the  $\phi$  dependence of  $J_c$ . The force balance equation states that at the critical current density  $\mathbf{J}_c \times \mathbf{B} = \mathbf{F}_p$  thus if the pinning force decreases the critical current will decrease. The ratio  $r_\phi$  will depend on the relative magnitude of these contributions of the force balance equation.

The core of an Abrikosov vortex in a uniaxially anisotropic material is elliptical for any orientation other than  $\theta = 90^\circ$ . The vortex core has a radius of  $\xi_{ab}$  in one axis and  $\epsilon_\theta \xi_{ab}$  in the other, where  $\epsilon_\theta$  is the anisotropy parameter defined in Chapter 2.. At  $\phi = 0^\circ$ ,  $F_L = JB$  for any value of  $\theta$  and the Lorentz force is directed perpendicular to the flux line, along the shorter axis. At  $\phi = 90^\circ$  the Lorentz force is directed along the longer axes of the core and its magnitude is  $JB \sin \theta$ . This is shown in Figure 6.2

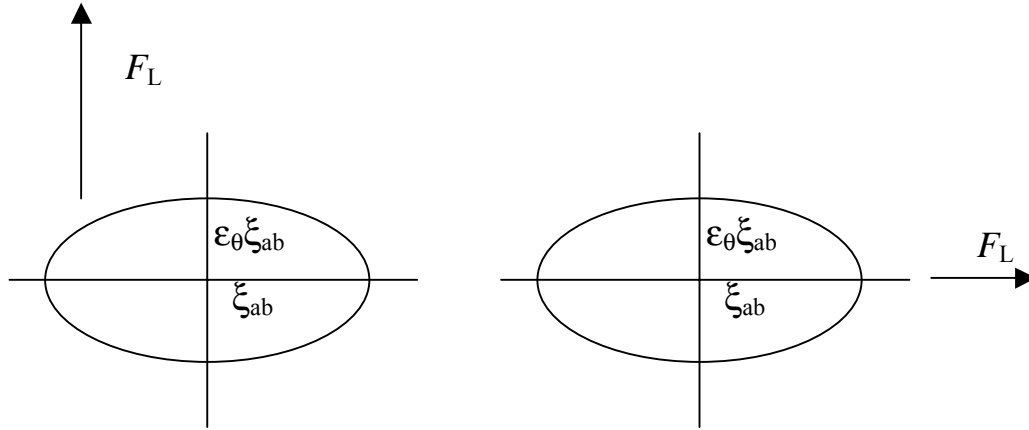


Figure 6.2 Direction of the Lorentz force on a tilted flux line at  $\phi=0^\circ$  (left) and  $\phi=90^\circ$  (right)

In YBCO the anisotropy parameter,  $\epsilon$ , is  $\sim 0.2$  and therefore the core anisotropy at any value of  $\theta$  will be given by Equation 2.37. This change in the size of the core would be expected to have an effect on the interaction between individual vortices and the pinning centres. In YBCO the predominant source of pinning is that due to interactions between the vortex cores and material defects.

The size of the vortex core has a strong effect on the interaction of the vortex with pinning centres. The only difference between the  $\phi=0^\circ$  and  $\phi=90^\circ$  orientations is the direction of the Lorentz force with respect to the vortex core. The difference in the pinning force between  $\phi=0^\circ$  and  $\phi=90^\circ$  should, therefore, be proportional to the anisotropy parameter. As  $\xi_{ab}$  and  $\epsilon_\theta \xi_{ab}$  would be expected to exhibit the same temperature dependence the effect on the pinning due to the anisotropy of the core should not have a significant temperature dependence. Following this argument, to take into effect the rotation of the Lorentz force direction between  $\phi=0^\circ$  and  $\phi=90^\circ$ , equation (6.4) may be rewritten as the following relation:

$$r_\phi = \epsilon_\theta / \sin\theta \quad (6.5)$$

When  $\phi=0^\circ$  the Lorentz force flux line is at least partially in the strong intrinsic pinning direction whereas in the  $\phi=90^\circ$  case the flux line is pushed perpendicularly to the strong pinning direction. This suggests a smaller pinning force at  $\phi=90^\circ$ . However, the flux lines are rectilinear in nature only when the  $c$ -axis  $\xi_c$  is of the order of the interlayer spacing,  $d$ . As has been discussed in Chapter 4 intrinsic pinning is only significant for vortices that are small enough to be localised in the blocking layers, that is when  $\xi_c < d$ .

### 6.1.3. $J_c(\phi)$ dependence of a string-pancake lattice

For values of  $\theta < \theta_2$  the flux lines are expected to enter a kinked string/pancake state. The force on each flux line will be a combination of that on the flux pancakes and that on the flux

strings. The force on the flux pancakes will stay constant with rotation in  $\phi$  as the system is isotropic in the  $a$ - $b$  plane. The Lorentz force on each string element will always be directed in the intrinsically pinned  $c$ -axis direction (Tachiki, *et al.* 1989, Tachiki, *et al.* 1993) with a magnitude varying as  $\cos\phi$ .

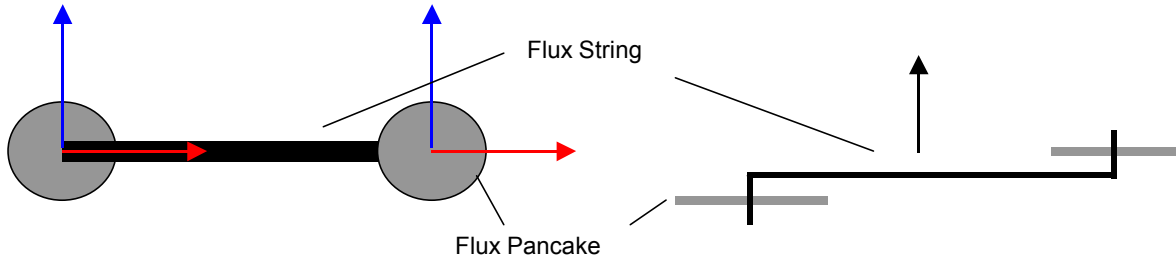


Figure 6.3 Views along the  $c$ -axis (left) and  $a$ - $b$  plane (right) of a pair of vortex pancakes coupled by a Josephson string element. The Lorentz force direction on the pancakes is shown on the left for magnetic fields at  $\phi=0^\circ$  (red) and  $\phi=90^\circ$  (blue). The Lorentz force on the string (black) is directed along the  $c$ -axis and varies in magnitude as  $\cos\phi$ .

At  $\phi=0^\circ$  the Lorentz force on the flux pancakes is along the flux lines and the critical current will be expected to be solely dependent on pancake pinning. The following force balance equation may therefore be written, where  $D$  is the film thickness and  $f_{p,pc}$  is the pinning force per unit length on the pancake vortices:

$$j_c \Phi_0 D = f_{p,pc} D \quad (6.6)$$

At  $\phi=90^\circ$ , however, for the pancakes to move transverse to the strings the strings must be ‘dragged’ along inside the  $a$ - $b$  planes. Results from vicinal films (Berghuis, *et al.* 1997, Chapter 4) already indicate that the pinning force density on a string moving in the  $a$ - $b$  planes is significantly smaller than that for a pancake.

We can therefore postulate the following force balance equation for a kinked vortex line at  $\phi=90^\circ$  assuming the pinning is strong and that the Lorentz force on the strings is small compared with the intrinsic pinning. The pinning force on each flux line will comprise a pancake contribution and a vortex string contribution:

$$j_c \Phi_0 D = f_{p,pc} D + f_{p,str} \frac{D}{\tan\theta} \quad (6.7)$$

Here  $f_{p,pc}$  is the pancake pinning force per unit length,  $f_{p,str}$  the string pinning force per unit length for movement in the  $a$ - $b$  plane,  $D$  the film thickness and  $\Phi_0$  the flux quantum. The  $D/\tan\theta$  term takes into account the variation in string length with  $\theta$ .

For the case of  $\theta$  very close to  $0^\circ$  the situation will again break down since the flux structure is expected to consist exclusively of strings which are either solely intrinsically pinned or alternatively in the force free configuration. It is difficult to predict the behaviour in this regime, however it is quite possible that rather than pancakes being totally eliminated variation in the structure of the material will lead to a number of remnant pancakes even at  $\theta=0^\circ$ . If the pancake pinning is significantly larger than the string pinning these remnant pancakes will still produce the majority of the pinning force on each line.

YBCO is relatively isotropic compared to other HTS materials. BSCCO, for example, exhibits entirely two dimensional behaviour and only the pancake density contributes to  $J_c$ . The ratio  $r_\phi$  is expected to be always equal to one in these materials except very close to  $T_c$ . Measurements on BSCCO are discussed in the following chapter.

The Figure below shows the predicted behaviour of  $r_\phi$  for the two models discussed in this chapter, considering force free effects only, equation (6.4) and force free and core anisotropy contributions combined ( $\epsilon=0.2$ ), equation (6.5). Also shown is the expected behaviour for a purely 2D superconductor.

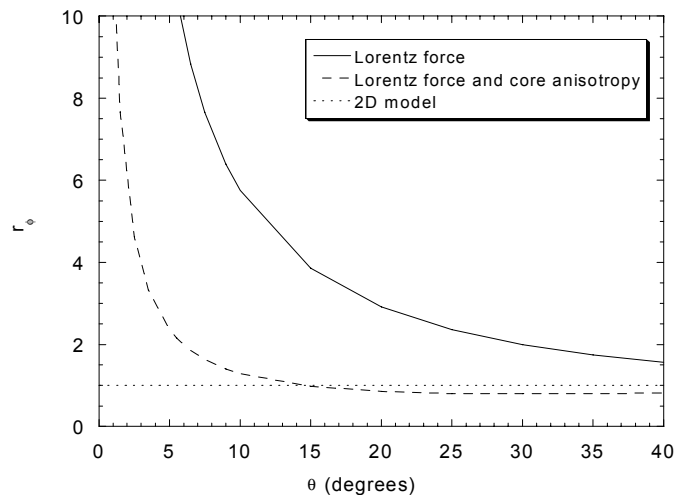


Figure 6.4 Schematic showing the expected behaviour of  $r_\phi$  taking into account purely the change in the magnitude of the Lorentz force, taking into account the Lorentz force and the core anisotropy and finally the expected behaviour for a 2D superconductor.

## 6.2. Sample Details

Good quality  $c$ -axis films for device applications have been grown in Cambridge using off-axis pulsed laser deposition. These films have a uniform surface and a reproducible  $T_c$  of 88-

89K (Santiso, *et al.* 1998). The measurements described in this chapter were performed on such a *c*-axis orientated film grown on a SrTiO<sub>3</sub> substrate. This film, run number Y1034, was 120nm thick. The  $T_c$  was a little depressed, 86.5 K compared to the best quality films probably due to slight oxygen overdoping.

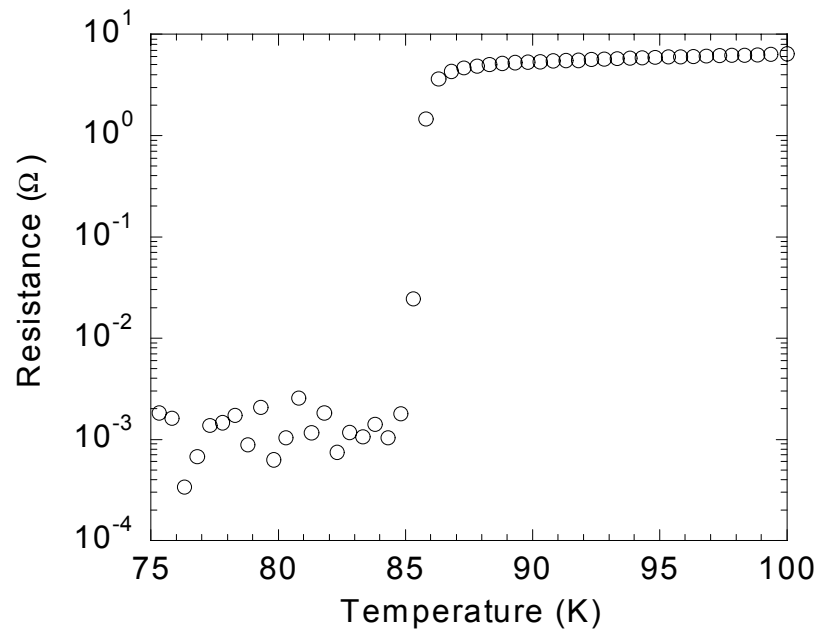


Figure 6.5 Resistance versus temperature measurement on sample Y1034.

The film was prepared by etching tracks 500 μm long and 10 μm wide as previously described. The critical current,  $J_{c1}$ , was determined using a voltage criterion of  $5 \times 10^7$  μV this corresponds to an  $E$  field of  $1 \times 10^{-3}$  Vm<sup>-1</sup>. Figure 6.6 shows the variation of critical current with field for a field applied parallel to the *c*-axis.

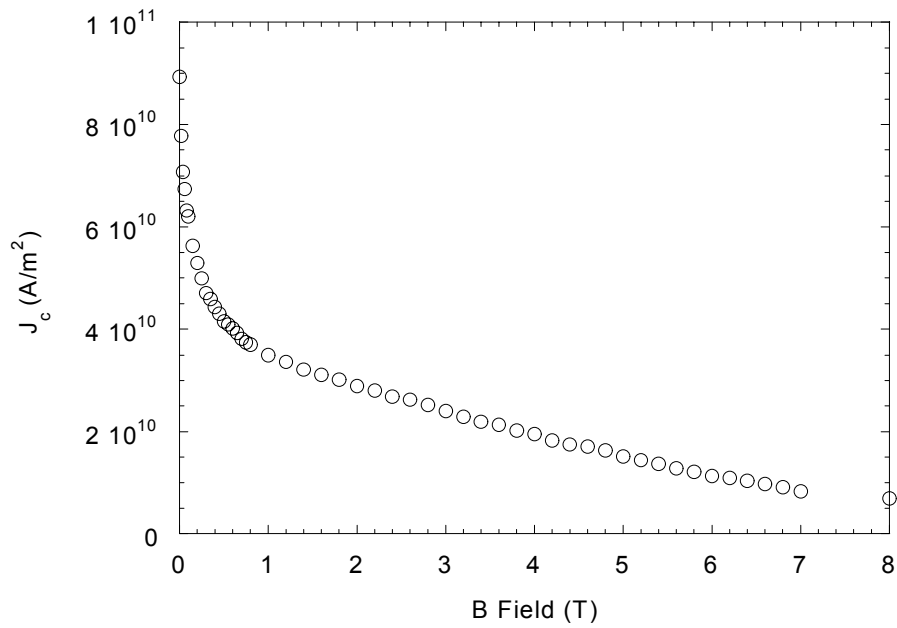


Figure 6.6 Variation of critical current with field (sample Y1034, 60K)

### 6.3. Results and Discussion

#### 6.3.1. Results

The variation of the critical current density with the rotation angle  $\phi$  was measured at various values of  $\theta$  at 1 T and 40, 60 and 80 K. These data sets are presented in Figures Figure 6.7, Figure 6.8, Figure 6.9 below. There is no sharp transition apparent as the value of  $\theta$  moves into the expected string pancake regime.

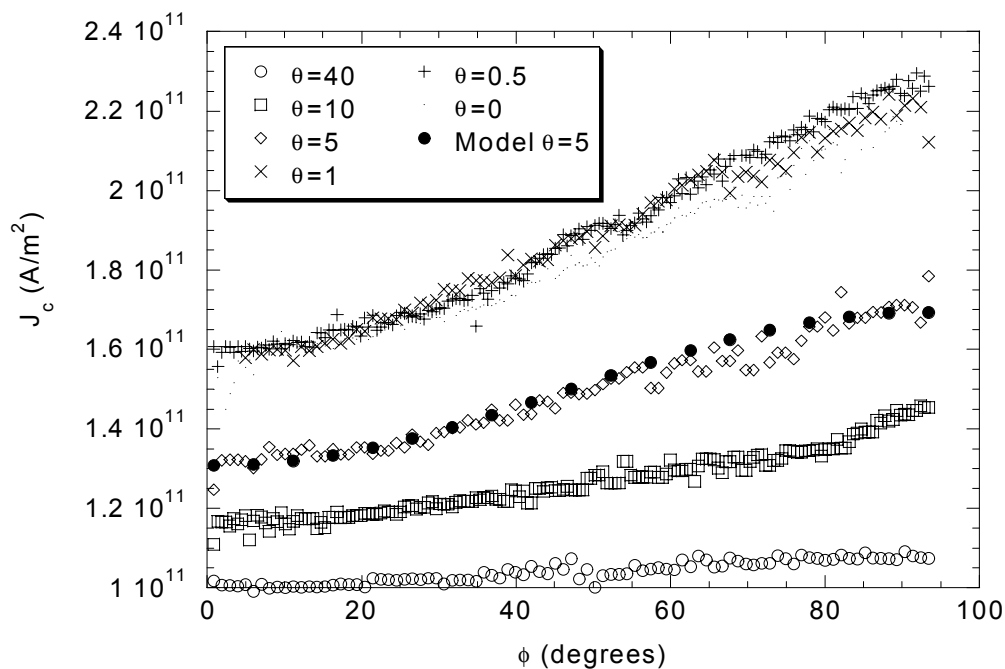


Figure 6.7  $J_c(\phi)$  scans at 40K and 1T showing the fit from equation (6.8) at  $\theta=5$ .

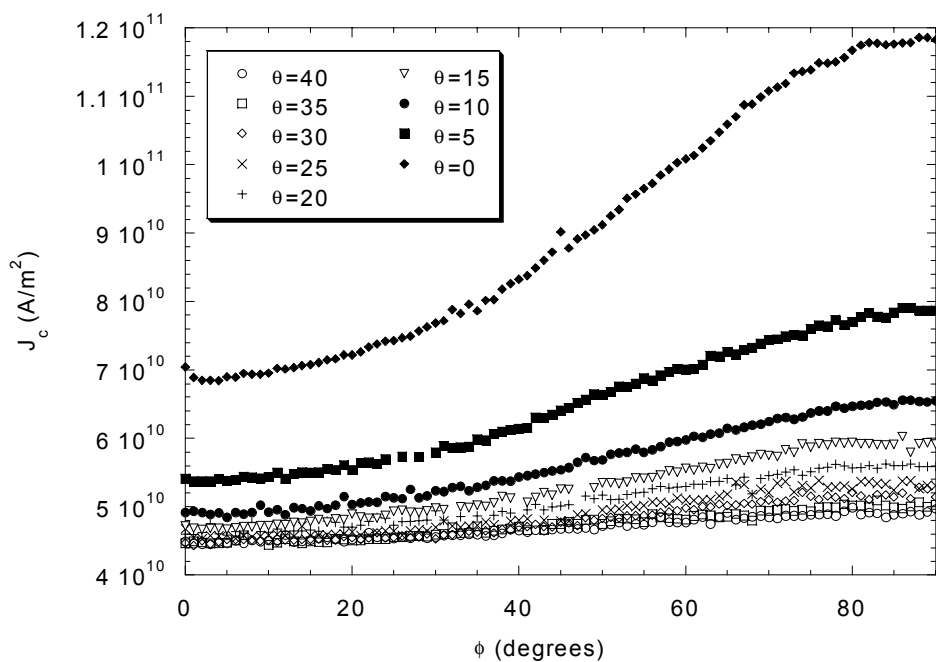


Figure 6.8  $J_c(\theta)$  scans at 60 K and 1 T

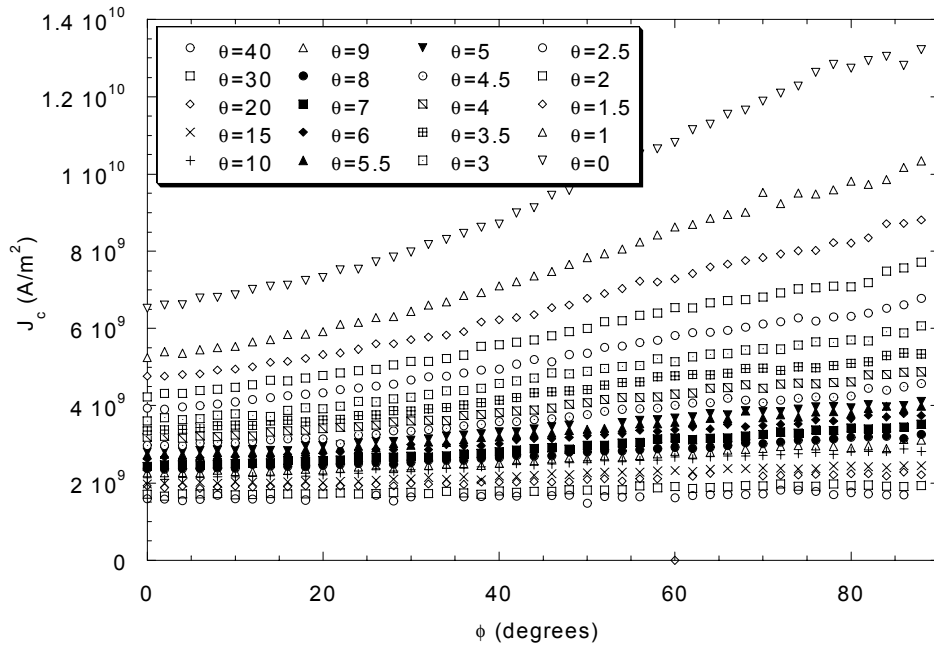


Figure 6.9  $J_c(\theta)$  scans at 80 K and 1 T

6.3.2. Variation of pinning force with  $\phi$

To quantify the increase of critical current between  $\phi=0^\circ$  and  $\phi=90^\circ$  the ratio  $r_\phi = J_c(\phi=90^\circ)/J_c(\phi=0^\circ)$  may be plotted against the tilt angle  $\theta$ . This is shown in the figure below:

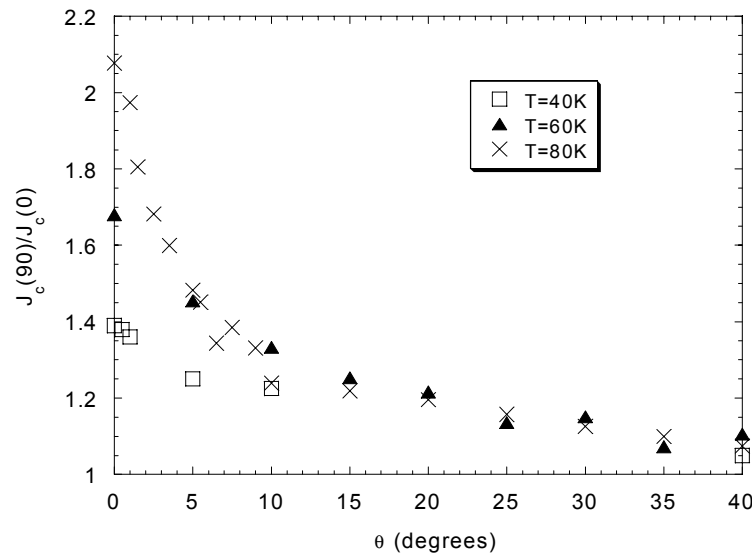


Figure 6.10 Variation of  $r_\phi$  with  $\theta$  at various temperatures.

Several observations may be made from Figure 6.10. It is clear that YBCO, even at lower temperatures and small values of  $\theta$  does not exhibit purely two dimensional behaviour. Such a

material would exhibit a value of  $r_\phi=1$  for all  $\theta$  since only the  $c$ -axis field component is significant. As the temperature is reduced the ratio does appear to reduce toward the 2D limit. The plots only diverge at small  $\theta$ , this may be indicative of the cross-over into the string pancake regime. Any analysis of the pinning forces in terms of strings and pancakes is clearly only valid at small  $\theta$ . Such an analysis will also be unreliable for very small  $\theta$  where the force free regime is entered.

We can now consider the results in terms of the three FLL structures discussed in section 6.1.3. At large  $\theta$  the FLL is expected to consist of elliptically cored Abrikosov vortices, below  $\theta_2$  and  $T_{cr}$  the FLL is expected to enter a kinked flux line regime. Very close to  $\theta=0^\circ$  the flux pancakes disappear and as the applied field is rotated in  $\phi$  the force free regime is approached.

#### Abrikosov Lattice $\theta > \theta_1$

As the temperature dependence of both the G-L parameters is similar, a weak variation with temperature of the  $\phi$  dependence would be expected in the 3D regime. This is indeed observed for large values of  $\theta$  in Figure 6.10.

For the case of an Abrikosov vortex, at constant  $\theta$  the Lorentz force will be of magnitude  $JB$  at  $\phi=0^\circ$  and  $JB\sin\theta$  at  $\phi=90^\circ$ . If this is the only effect on the critical current density the relationship  $J_c(90)=J_c(0)/\sin\theta$  will apply. The figure below shows how this model compares with the  $T=80$  K data. Neglecting the region close to  $\theta=0^\circ$ , any variations from this are due to the change in the direction of the Lorentz force on the vortex lines.

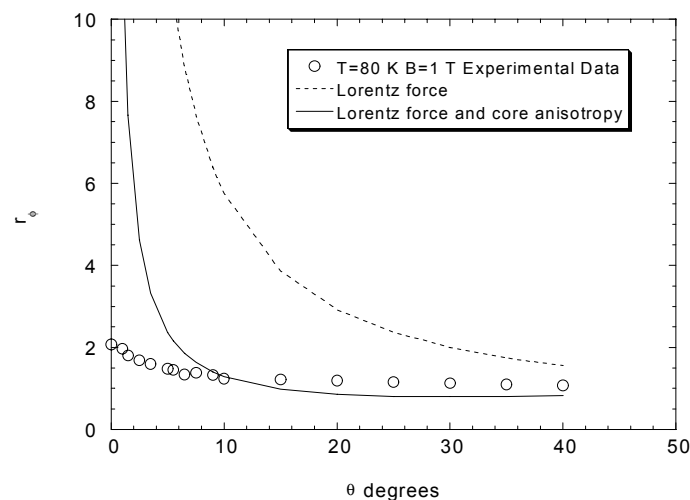


Figure 6.11 Predicted behaviour of  $r_\phi$  compared to that observed at 80 K in the  $c$ -axis film measured.

Clearly the critical current is not purely dependent on the cross product  $J \times B$ . Figure 6.2 shows that the size of the vortex core parallel to the direction of the Lorentz force is reduced by a factor  $\epsilon_\theta$  at  $\phi=0^\circ$  as compared to  $\phi=90^\circ$ . In the strong pinning regime the pinning force on individual flux lines may be considered. If the pinning anisotropy, as  $\phi$  is rotated, is due to the anisotropy of the vortex core the reduction in pinning force at  $\phi=90^\circ$  would be expected to be equal to  $\epsilon_\theta$ . This is also shown in Figure 6.11 assuming  $\epsilon=0.2$ .

In the measurements described the only change between the measurement at  $\phi=0^\circ$  and that at  $\phi=90^\circ$  is the direction of the Lorentz force developed on the flux lines. It is therefore possible to account for the  $\phi$  variation in the critical current in terms of the predicted anisotropy of the vortex core, except for small values of  $\theta$ . Indeed, if the assumption that the pinning force anisotropy is proportional to the anisotropy of the vortex core is valid this measurement provides a simple method of determining the anisotropy parameter in YBCO.

For small  $\theta$  the measured values of critical current do not follow this prediction. The behaviour of the flux line lattice in the force free regime is difficult to model. Although  $T_{cr}$  is 80K and therefore no string pancake transition is expected this prediction itself is based on experimental measurements of the anisotropy parameter and the coherence lengths. These measurements exhibit a large experimental error.

### **Kinked vortex lines $\theta < \theta_2$**

Given the geometry accessed in the experiments described it is reasonable to attribute the increase in the pinning force and thus  $J_c$  at  $\phi=90^\circ$  to the effect of dragging vortex strings through the material. The exception to this is the  $\theta=0^\circ$ ,  $\phi=90^\circ$  orientation where, if all pancakes are eliminated, the flux lines are in the force free configuration.

For intermediate values of  $\phi$  the string pinning force will not act on the entire length of the string, as the string is free to move along itself, the string will only be pinned for motion perpendicular to itself. The force acting on the vortex strings will thus vary as  $\sin\phi$ . In addition the effective cross section of the string will decrease as  $\phi$  increases. This will lead to a change in the pinning force density varying as  $\sin^2\phi$ , assuming for simplicity an inverse relationship between pinning force and the cross sectional width of the string. Thus:

$$j_c \Phi_0 = f_{p,pc} + f_{p,str} \frac{\sin^2 \phi}{\tan \theta} \quad (6.8)$$

The fit to equation (6.8) is shown in Figure 6.7. From this we can estimate that  $f_{p, \text{str}} = 8 \times 10^{-6} \text{ Nm}^{-1}$  at 40K and 1T for the film studied. We also obtain, for the pancake pinning force density,  $f_{p, \text{pc}} = 3 \times 10^{-4} \text{ Nm}^{-1}$ . These values are determined from the macroscopic critical current  $J_c$  and therefore represent average pinning forces per unit length in the material. This value may be compared to those determined from measurements on vicinal films. At 25 K and 1 T Berghuis et al (1997) found that  $f_{p, \text{str}} = 8 \times 10^{-6} \text{ Nm}^{-1}$ . It is likely however, that there is wide variation in the pinning force density depending on the exact film growth method employed.

This model is expected to be valid for  $\theta < \theta_1$  except at very small  $\theta$  where the length of vortex string between pancakes is large and flux cross-over and cutting will occur. At  $\theta = 90^\circ$  this corresponds to the intrinsic pinning peak at  $\phi = 0^\circ$  and the force free peak at  $\phi = 90^\circ$ . This breakdown regime appears to have been reached at  $\theta \sim 1^\circ$  in Figure 6.10. For the rectilinear FLL ( $\theta > \theta_1$ ) a  $\phi$  dependence will also be expected due to the anisotropy of the vortex cores.

Figure 6.10 shows the variation in the ratio  $J_c(\phi = 90^\circ)/J_c(\phi = 0^\circ)$  against  $\theta$  at various temperatures. A temperature dependence in  $r_\phi$  begins to appear at about  $15^\circ$ . The kinked vortex lattice is expected to be fully developed at  $\theta_2 = \tan \epsilon$ , which is about  $10^\circ$ . These results suggest that the temperature dependence of the pancake pinning force density and that for the string pinning force densities are different.

### Lock-In

Applying a simple interpretation at  $\theta = 0^\circ$  is not possible since the flux line is, both in the Abrikosov model and the string-pancake model, parallel to the current. The critical current behaviour in this force free orientation is not readily analysable.

### 6.3.3. $J_c(B)$ Measurements

Figure 6.6 shows how the  $J_c(B)$  behaviour changes with  $\phi$ .

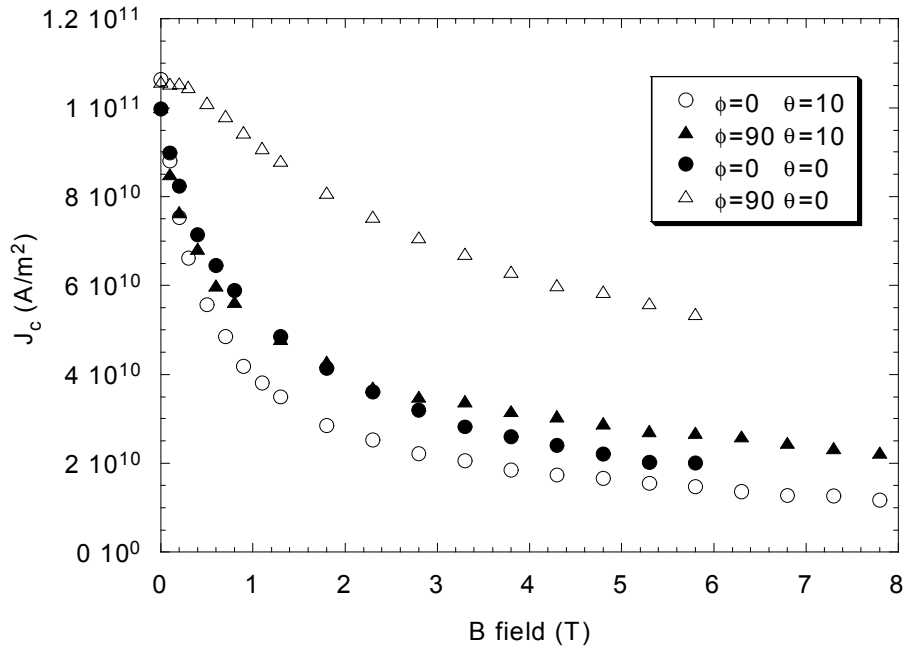


Figure 6.12  $J_c(B)$  curves for various field directions, 60 K

The  $J_c(B)$  variation for the force free orientation is distinctly different from that at other field orientations. The smaller variation in  $J_c$  is as expected.

#### 6.4. Conclusion

The rotation of the applied field in  $\phi$  at a constant angle,  $\theta$ , with respect to the a-b planes allows critical current measurements to be performed with a constant lattice structure. When interpreting critical current results in this geometry it is crucial to ensure that the change in the Lorentz force when the field and current are not perpendicular is taken into account. Results obtained in this geometry are consistent with the theoretically predicted transition from an Abrikosov lattice state to a kinked string-pancake vortex lattice.

For an Abrikosov lattice the critical current variation change between  $\phi=0^\circ$  and  $\phi=90^\circ$  can be modelled taking into account both the change in the Lorentz force with  $\phi$  and the anisotropy of the vortex core. The variation of  $r_\phi$  with  $\theta$  is consistent with a anisotropy parameter of about 0.2.

For smaller values of  $\theta$  the ratio  $r_\phi$  acquires a temperature dependence. In the string pancake regime the increase in  $J_c$  at  $\phi=90^\circ$  is due to the dragging of vortex strings by vortex pancakes. The vortex string pinning density obtained from this model is consistent with those measured on vicinal films.

By carefully choosing the experimental geometry it is therefore possible to observe the pinning of vortex string elements on  $c$ -axis orientated as well as thin films grown on vicinal substrates. Away from the kinked vortex lattice regime the variation in critical current is due to the rotation of the Lorentz force direction about an anisotropic vortex cores.

The results presented in this chapter are consistent with a cross-over from an Abrikosov like FLL to a kinked vortex lattice. As is the case with vicinal films this means that any model of the angular dependence of  $J_c$  must take into account these two regimes. Neither the anisotropic Ginzburg Landau model nor the kinked string pancake model is sufficient to account for the full range of behaviour observed.

## 6.5. Bibliography

- Aomine, T., T. Nishizaki, F. Ichikawa, T. Fukami, T. Terashima and Y. Bando (1994). Physica B **194**: 1613-1614.
- Berghuis, P., E. DiBartolomeo, G. A. Wagner and J. E. Evetts (1997). Phys. Rev. Lett. **79**(12): 2332-2335.
- Dam, B., J. M. Huijbregtse, F. C. Klaassen, R. C. F. van der Geest, G. Doornbos, J. H. Rector, A. M. Testa, S. Freisem, J. C. Martinez, B. Stauble-Pumpin and R. Griessen (1999). Nature **399**(6735): 439-442.
- Herzog, R. (1997). Critical Currents in YBCO thin films. Materials Science and Metallurgy, University of Cambridge.
- Nishizaki, T., T. Aomine, I. Fujii, K. Yamamoto, S. Yoshii, T. Terashima and Y. Bando (1991). Physica C **185**: 2259-2260. Physica C
- Nishizaki, T., T. Aomine, I. Fujii, K. Yamamoto, S. Yoshii, T. Terashima and Y. Bando (1991). Physica C **181**(4-6): 223-232. Physica C
- Nishizaki, T., F. Ichikawa, T. Fukami, T. Aomine, T. Terashima and Y. Bando (1993). Physica C **204**(3-4): 305-314.
- Santiso, J., A. Moya and F. Baudenbacher (1998). Supercon. Sci. Technol. **11**(5): 462-466. .
- Tachiki, M. and S. Takahashi (1989). Solid State Comm. **70**(3): 291-295.
- Tachiki, M., S. Takahashi and K. Sunaga (1993). Phys. Rev. B **47**(10): 6095-6105.

## 7. Critical Current Anisotropy in Thin Film $\text{Bi}_2\text{Sr}_2\text{CaCu}_2\text{O}_{8+x}$

*Results obtained from measurements on de-oxygenated YBCO films indicate that increasing anisotropy results in a significantly more pronounced vortex ‘string’ channelling effect. This proposed anisotropy relationship was investigated by experiments using the very anisotropic  $\text{Bi}_2\text{Sr}_2\text{CaCu}_2\text{O}_{8+x}$  material. The angular critical current measurements indicated, however, that this material obeys the ‘Kes’ law and no string channelling effect could be observed. From this observation it is possible to deduce that the critical current is not dependent on any Josephson string vortices that may be present. This would tend to suggest that at the temperatures and fields considered the proposed crossing lattice theory does not provide a better description of critical current density anisotropy in BSCCO than the two-dimensional pancake model.*

### 7.1. The Flux Line Lattice in BSCCO

#### 7.1.1. Structure and superconducting properties of BSCCO

The  $\text{Bi}_2\text{Sr}_2\text{CaCu}_2\text{O}_{8+x}$  material (BSCCO) exhibits one of the largest superconducting parameter anisotropies among the high  $T_c$  oxides. The superconducting mass anisotropy parameter (Gor'kov and Melik-Barkhudarov 1963, Blatter, *et al.* 1994)  $\gamma$ , which is defined as  $\gamma^2 = (m_c/m_a)$  where  $m$  is the effective mass of the charge carriers, has been measured as having a value between 50 and 200 (Farrell, *et al.* 1989, Chikumoto, *et al.* 1992, Martinez, *et al.* 1992, Blatter, *et al.* 1994). By comparison  $\gamma$  in YBCO is placed between 5 and 7. The normal state resistivity of BSCCO is equally highly anisotropic (Martin, *et al.* 1988). Table 7.1 compares various characteristic parameters in oxide superconductors,  $d$  is the spacing between superconducting planes,  $\xi$  is the Ginzburg-Landau coherence length at 0 K,  $\rho$  is the normal state resistivity and  $\gamma$  is the mass anisotropy parameter. The subscripts  $a$ - $b$  and  $c$  indicate values measured in the  $a$ - $b$  plane and the  $c$ -axis direction respectively. It should be noted that YBCO, although it has a similar value of  $d$  to BSCCO, exhibits a markedly smaller anisotropy. This is possibly due to the cuprate chains found in YBCO.

Superconductor	$d$ (nm)	$\xi_{a-b}$ (nm)	$\xi_c$ (nm)	$\rho_c/\rho_{a-b}(300K)$	$\gamma$
YBa <sub>2</sub> Cu <sub>3</sub> O <sub>7-<math>\delta</math></sub>	1.2	$\sim 1$	$\sim 0.2$	29	5-7
Bi <sub>2</sub> Sr <sub>2</sub> CaCu <sub>2</sub> O <sub>8+x</sub>	1.5	$\sim 1$	$\sim 0.02$	$\sim 110$	50-200
(Pb,Bi) <sub>2</sub> Sr <sub>2</sub> Ca <sub>2</sub> Cu <sub>3</sub> O <sub>10-x</sub>	1.8				30-60
Tl <sub>2</sub> Ba <sub>2</sub> Ca <sub>2</sub> Cu <sub>3</sub> O <sub>10-y</sub>	1.9				3-4

Table 7.1 Layer spacing, normal state and superconducting anisotropy parameters for various oxide superconductors. (Datta 1992, Hardy, et al. 1994, Matsubara, et al. 1992, Blatter, et al. 1994) Wide variations exist in quoted values for  $\xi$  and  $\gamma$  mainly due to the difficulties found in measuring these parameters in the  $c$  direction. It is also difficult to obtain precise values for  $H_{c2}$  since this is very large in high  $T_c$  materials and flux creep hinders its extraction from  $I$ - $V$  measurements using the Bardeen-Stephen model.

It can be seen from Table 7.1 that Bi<sub>2</sub>Sr<sub>2</sub>CaCu<sub>2</sub>O<sub>8+x</sub> is particularly anisotropic. As the  $c$ -axis coherence length is much smaller than the interlayer spacing,  $d$ , the material should exhibit clearly two dimensional behaviour. The exception to this will be temperatures very close to  $T_c$  since as  $T \rightarrow T_c$  the G-L coherence length,  $\xi \rightarrow \infty$ .

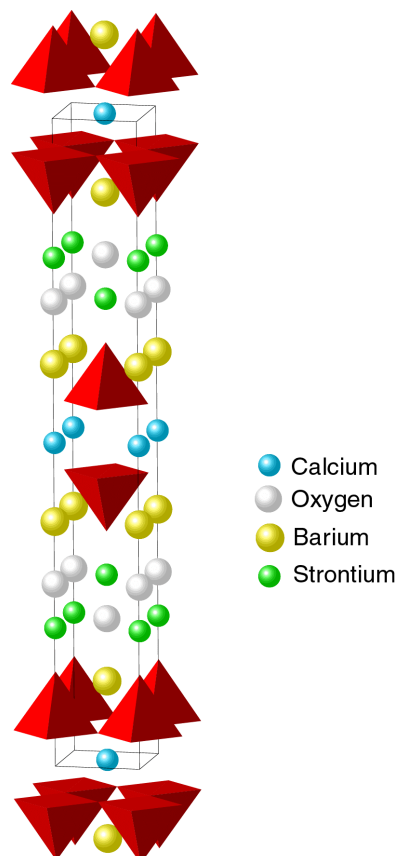


Figure 7.1 In BSCCO 2212 there is no cuprate chain layer, it is thought that the presence of this layer accounts for the lower level of superconducting anisotropy in YBCO. In this diagram oxygen is present at the apices of the red pyramids and the centre of their bases contains a copper atom. Diagram after Shaked, et al. (1994) and Weber (1999).

### 7.1.2. Angular Dependent Resistivity and Critical Current in BSCCO

Resistive transition measurements on BSCCO indicated that the material's transport properties were insensitive to a magnetic field applied parallel to the crystallographic  $a$ - $b$  planes (Iye, *et al.* 1989). Additionally it has been observed that the angle between the current and applied field has no effect on resistivity measurements (Raffy, *et al.* 1991), this suggests that there is no force-free effect in BSCCO.

This phenomenon was studied by Kes *et al.* who proposed that due to its high anisotropy BSCCO is best described as a layered material with very small or no order parameter in the intercalated layers between the conducting cuprate planes (Kes, *et al.* 1990). Kes deduced that BSCCO is in effect 'magnetically transparent' to the component of field applied parallel to the planes. Thus if  $\theta$  is the angle between the applied field and the cuprate planes we can write the Kes law stating that:

$$J_c(B, \theta) = J_c(B \sin \theta, 90) \quad (7.1)$$

This field independence of  $J_c$  for fields parallel to the  $a$ - $b$  planes was confirmed by Schmitt *et al.* (1991) for fields up to 7 T, as shown in Figure 7.2.

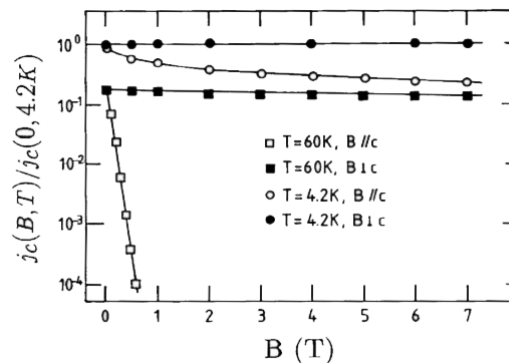


Figure 7.2 Critical current measurements on a  $c$ -axis BSCCO 2212 thin film showing field independence for fields parallel to the  $a$ - $b$  plane (Schmitt, *et al.* 1991).

There is therefore strong experimental evidence for treating BSCCO as a stack of superconducting layers separated by a non-superconducting intercalated layer. This structure has been considered by Lawrence and Doniach (1970). Given the two dimensional nature of the flux line lattice in BSCCO it seems likely that the Abrikosov lattice in BSCCO breaks down into the lattice of *pancake vortices* suggested by Clem (1991) (Chapter 2).

In the Lawrence and Doniach model the superconducting layers are Josephson coupled. In single crystals, with current flow along the  $c$ -axis, an *intrinsic Josephson effect* has been experimentally observed (Kleiner, *et al.* 1992, Kleiner and Muller 1994). No convincing evidence for the intrinsic Josephson effect has been observed in the much less anisotropic

YBCO material. Some evidence has been observed for the intrinsic Josephson effect in deoxygenated, and therefore more anisotropic, YBCO (Wang, *et al.* 2000). The existence of the intrinsic Josephson effect provides further experimental evidence for the two-dimensional nature of BSCCO.

Although there is extensive evidence for a pancake structure in BSCCO the nature of the coupling between the flux pancakes has been the subject of much theoretical investigation. In the limit of an extremely two-dimensional superconductor, however, it is predicted that the pancakes are magnetically coupled into stacks parallel to the  $c$ -axis (Clem 1998). The component of the field parallel to the planes is unscreened and has no effect on the FLL structure or the critical current density.

A string/pancake lattice where the string and pancake vortex elements are not joined in contiguous flux lines has also been suggested. In the *crossing lattice* model the material contains two separate, but magnetically interacting, lattices (Koshelev 1999).

If the string/pancake lattice in BSCCO consists of string and pancake flux line elements in contiguous lines (as is the case in YBCO at small  $\theta$ ) or the crossing lattice, the vortex channelling effect observed in YBCO would also be expected in BSCCO. At  $\theta=0^\circ$  in a vicinal film only Josephson strings will be present which will not be pinned by their interaction with flux pancakes due to either to line energy or magnetic interactions.

As has already been noted, it is not directly possible to observe the motion of Josephson vortex strings, except in films grown on vicinal substrates. However in Chapter 6 it has been discussed how the existence of string elements will be reflected in the variation of  $J_c$  with  $\phi$  at constant  $\theta$ .

## **7.2. Sample Description**

The preparation and patterning of samples has been discussed in Chapter 3. The superconducting films available for this measurement consisted of 120 nm thick layers of BSCCO 2212 grown on  $10^\circ$  miscut SrTiO<sub>3</sub> substrates. The orientation of the films was confirmed both by four circle XRD analysis and by high resolution electron microscopy.

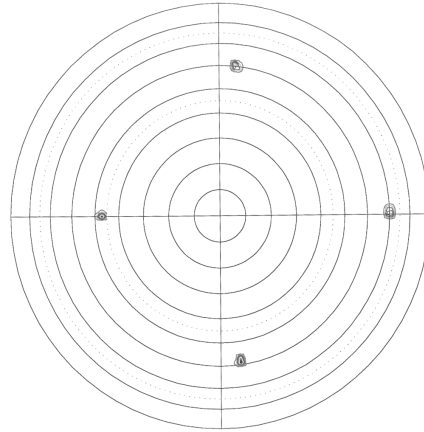


Figure 7.3 A (115) pole figure from a 120 nm thick BSCCO film grown on a 10° miscut STO substrate.

Current tracks both parallel, **L**, and perpendicular, **T**, to the vicinal steps were patterned using Ar-ion milling. The tracks were 120 nm thick, 500  $\mu\text{m}$  long and of width 20, 10 or 5  $\mu\text{m}$ . The geometry of measurements on a **T** track is shown in Figure 7.4.

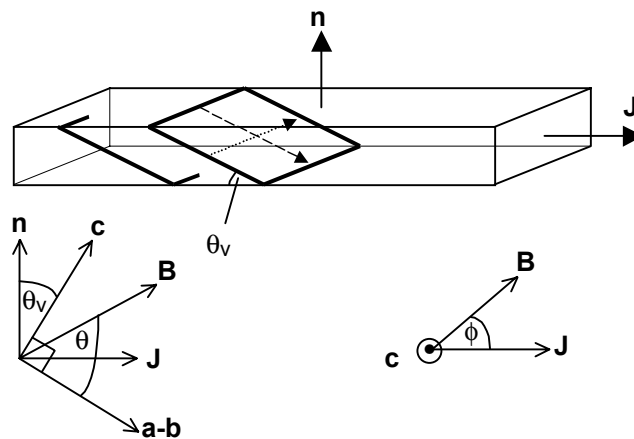


Figure 7.4 Geometry of measurements on a **T** track. The angle  $\theta$  is that between the applied field and the cuprate planes. The angle  $\phi$  is the rotation of the field about the  $c$ -axis. The dashed line corresponds to  $\theta=0^\circ$ ,  $\phi=0^\circ$  and the dotted line to  $\theta=0^\circ$ ,  $\phi=90^\circ$ . The angle  $\theta_v$  is the miscut (vicinal) angle of the substrate.

To ensure that the **T** tracks were not being ‘shorted’ by  $c$ -axis impurities, the resistivities of both **L** and **T** tracks were measured. If the **L** and **T** tracks are well aligned the  $a$ - $b$  and  $c$  axis resistivities may be deduced from  $\rho_{(L)}$  and  $\rho_{(T)}$  (Zahner, *et al.* 1998) using equation (7.2). Here  $\rho_{a-b}$ ,  $\rho_c$ ,  $\rho_{(L)}$  and  $\rho_{(T)}$  are the resistivities measured in the  $a$ - $b$  plane,  $c$ -axis, **L** track and **T** track directions respectively and  $\theta_v$  is the vicinal tilt angle: The  $a/b$  anisotropy is neglected and  $\rho_{a-b} = \rho_{(L)}$  as currents flowing in an **L** track do not cross between cuprate planes.

$$\rho_c = \frac{\rho_{(T)} - \rho_{(L)} \cos^2 \theta_v}{\sin^2 \theta_v} \quad (7.2)$$

For sample L3 at 100 K this yields  $\rho_{a-b}=1 \times 10^{-4} \Omega\text{cm}$  and  $\rho_c=6 \times 10^{-1} \Omega\text{cm}$ . These values are consistent with values measured on  $c$ -axis single crystals (Crommie, *et al.* 1990). Resistivities measured at 300K on similarly grown films have also been found to be consistent with single crystal values (Zahner, *et al.* 1998). The resistive transition is shown in Figure 7.5 (1  $\mu\text{A}$  current), it is comparatively wide compared to those observed on high quality  $c$ -axis orientated films.

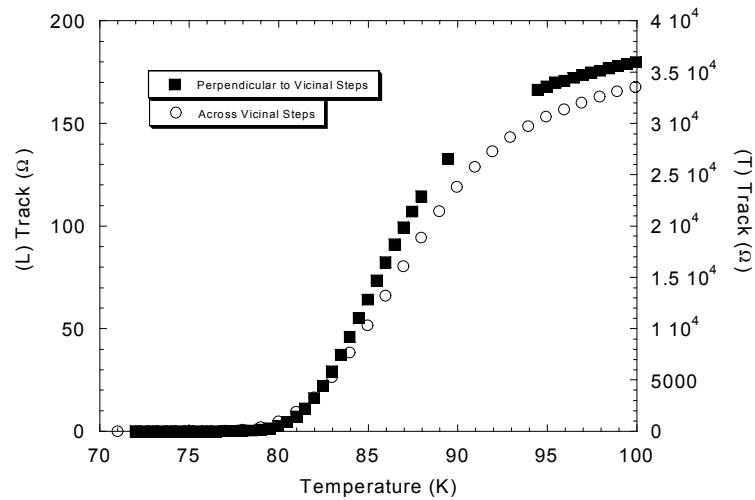


Figure 7.5 Resistance versus Temperature plot on parallel, **L**, and step crossing tracks, **T**.

It can be seen in Figure 7.6 that the critical current anisotropy is significantly smaller than the resistivity anisotropy. This is unsurprising since resistivity combines additively whereas the measured critical current density will depend on the weakest link in the current path.

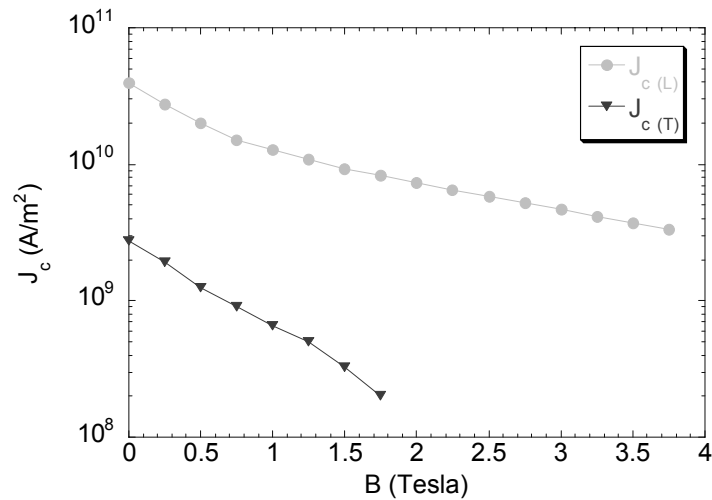


Figure 7.6 Critical current for, **T**, and, **L**, tracks, with field applied normal to the film surface. ( $T=40$  K)

Experimentally it was found to be much harder to obtain low noise results in measurements on **T** tracks than on **L** tracks. This was due to the smaller absolute values of the critical current measured on T tracks. Nonetheless, as can be seen from Figure 7.11 and Figure 7.12, the noise is small enough for the  $J_c(\theta)$  behaviour to be clearly discerned.

## 7.3. Results

### 7.3.1. RT measurements

Figure 7.7 shows resistive transitions, with a current of 1  $\mu$ A, in fields applied parallel and perpendicular to the  $c$ -axis. As expected from the Kes law the RT curve shows little change with field applied parallel to the  $a$ - $b$  planes and significant variation with field applied in the  $c$ -axis direction. On a **T** track, however, current must flow along the  $c$ -axis to pass between cuprate planes, this geometry is inaccessible with  $c$ -axis thin films. Nonetheless it appears that BSCCO is still ‘magnetically transparent’ to fields parallel to the  $a$ - $b$  planes in this configuration. The spread in the RT curve with field applied parallel to the  $a$ - $b$  planes is probably due to a slight misalignment of the field.

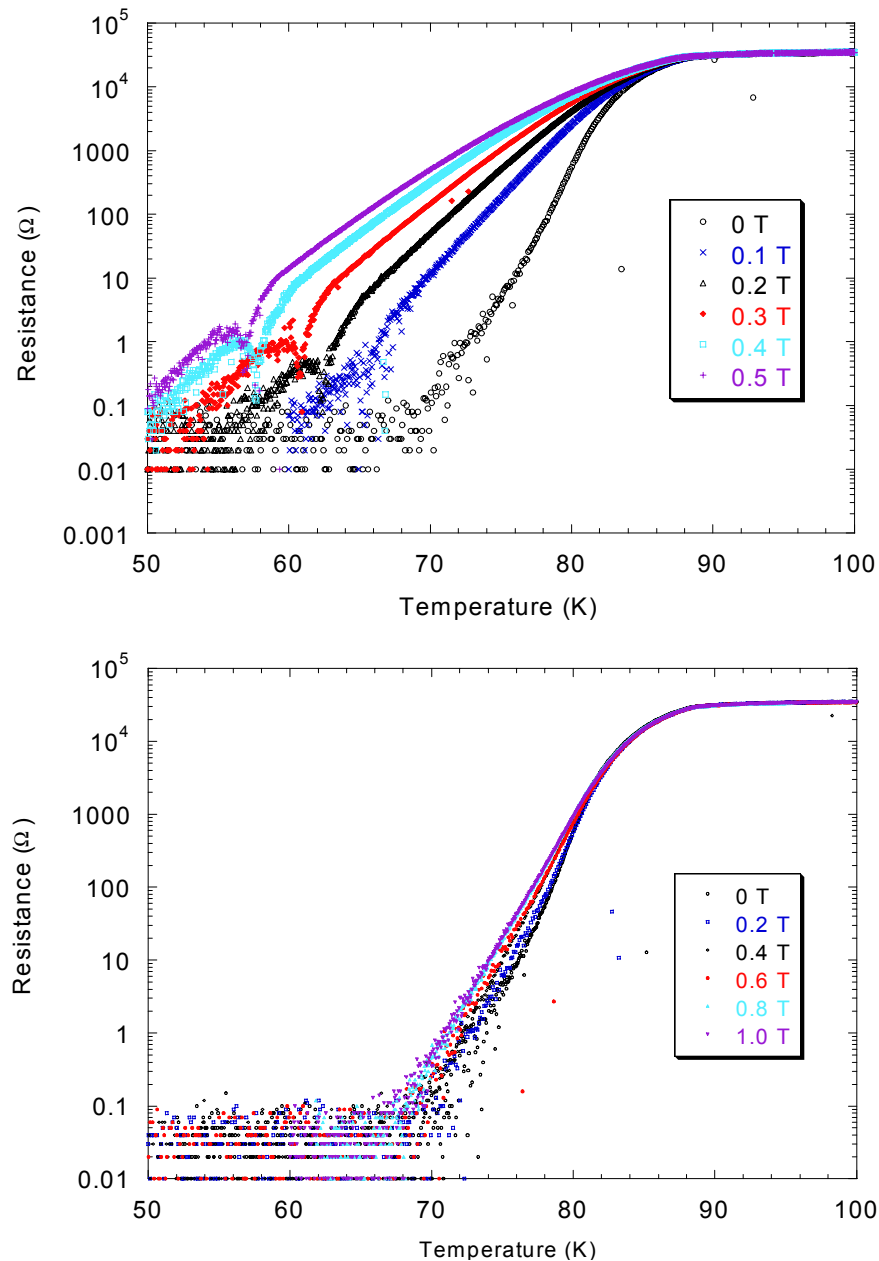


Figure 7.7 Broadening of the resistive transition in a  $\mathbf{T}$  track with field applied parallel to the  $c$ -axis (top) and in plane (bottom).

In BSCCO resistance temperature curves give an indication of the form of the temperature dependence of the flux creep activation energy. Figure 7.8 shows the  $RT$  data from Figure 7.7 in the form of an Arrhenius plot.

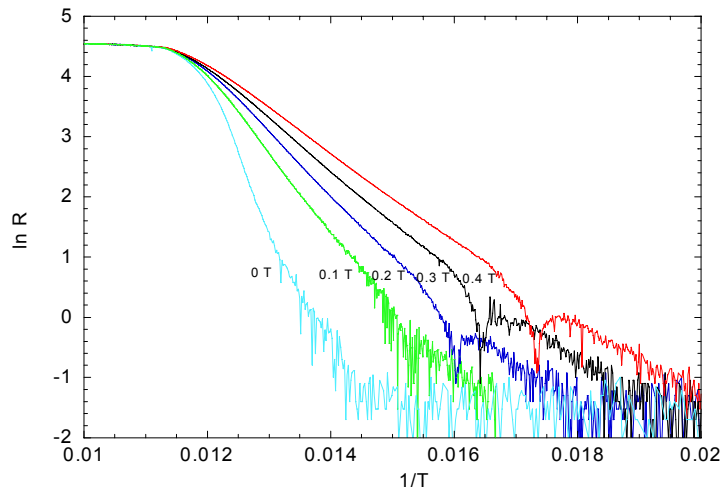


Figure 7.8 An Arrhenius plot of  $RT$  data recorded on a  $\mathbf{T}$  track with field applied parallel to the  $c$ -axis.

As would be expected the  $\ln R$  vs  $1/T$  plot is linear though the transition, again with current flow along the  $c$ -axis. The broadening of the transition would, therefore, appear to be due to thermally activated flux creep.

The  $RT$  transitions show an interesting feature, there is a noticeable dip in the resistivity near the end of the transition. A small decrease in temperature leads to a sharp decrease in the resistance. The reduction in the resistivity implies that the activation for flux creep is increased. The cause of this increase in the activation energy is not clear from the data, but may be due to some change in the structure of the FLL. Any change in the FLL that results in coupling of vortex pancakes will increase the activation energy, it is harder to depin two pancakes than one.

Measurements of the resistive transition in  $\mathbf{T}$  tracks therefore indicate that ‘magnetic transparency’ is present in BSCCO irrespective of the direction in which the current flows.

### 7.3.2. $J_c(B)$ Measurements

The critical current density as a function of field angle was measured on a  $\mathbf{T}$  track at 40K with the field swept both at  $\phi=0^\circ$  and at  $\phi=90^\circ$ . These results are shown in Figure 7.9 below.

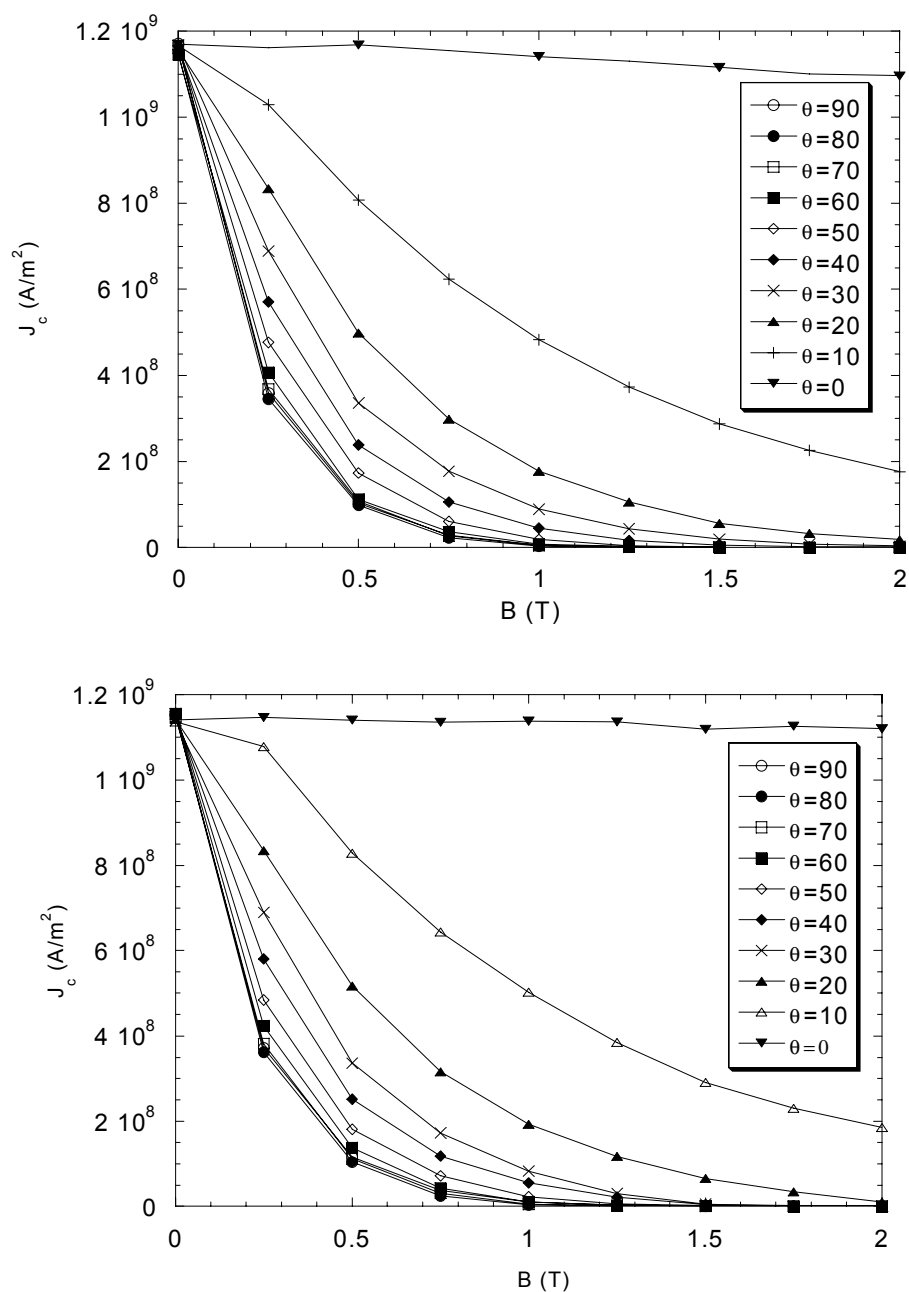


Figure 7.9  $J_c(B)$  data at 40 K on a **T** track. The top plot is data taken at  $\phi=0^\circ$  and the lower plot was taken at  $\phi=90^\circ$ .

In both sets of data there is no field dependence for  $J_c$  at  $\theta=0^\circ$  (with the field parallel to the cuprate planes). It also appears that rotating the field in the plane has no effect on the measured critical current density. These two features are as would be expected from the Kes law.

### 7.3.3. $J_c(T)$ measurements

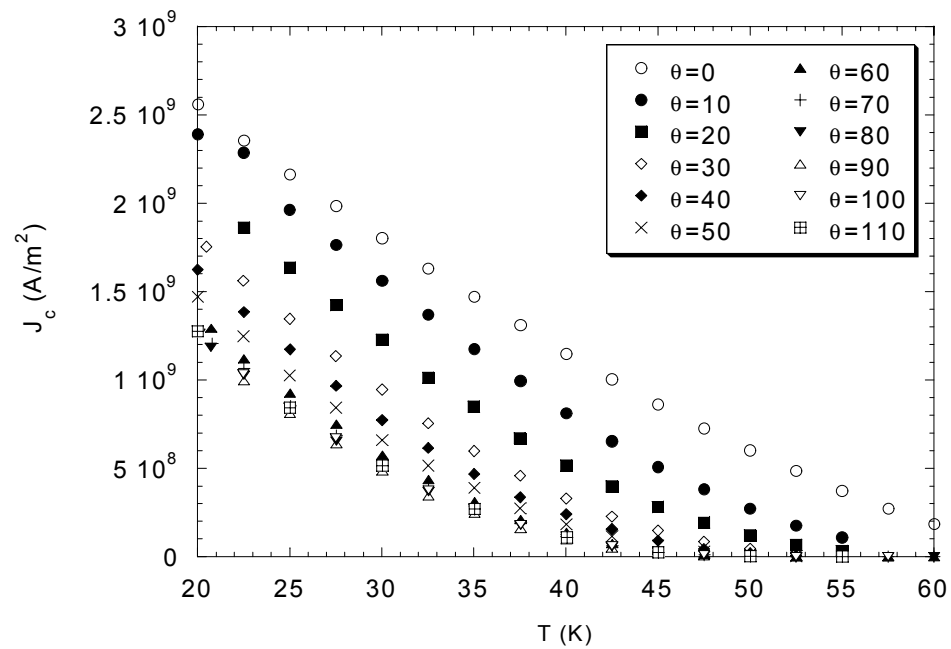


Figure 7.10 Variation of critical current density with temperature. These measurements were performed on a  $T$  track with the magnetic field swept in plane of tilt ( $\phi=0$ ,  $B=0.5$  T)

The variation of the critical current density with varying temperature is shown in Figure 7.10 with the field at various orientation with respect to the  $a$ - $b$  planes.

### 7.3.4. $J_c(\theta)$ in varying field

Critical current data was recorded on both  $\mathbf{L}$  and  $\mathbf{T}$  tracks at 20 K and various applied fields up to 1 T. This is shown in Figure 7.11. Experimentally it was found that data recorded on the  $\mathbf{L}$  track exhibited lower noise than that observed on the  $\mathbf{T}$  track. Nonetheless the important characteristics of the behaviour may be observed. The plots at different applied fields converge for  $\theta=0^\circ$ . This is in accordance with the Kes law, since any field applied parallel to the cuprate planes has no effect on  $J_c$ .

Additionally, unlike measurements performed on YBCO films, there is no detectable peak in the force-free geometry. Given the nature of the vortex lattice in BSCCO this is unsurprising. The direction of the vortex elements are parallel to the  $a$ - $b$  planes and the  $c$ -axis irrespective of the angle of the applied field.

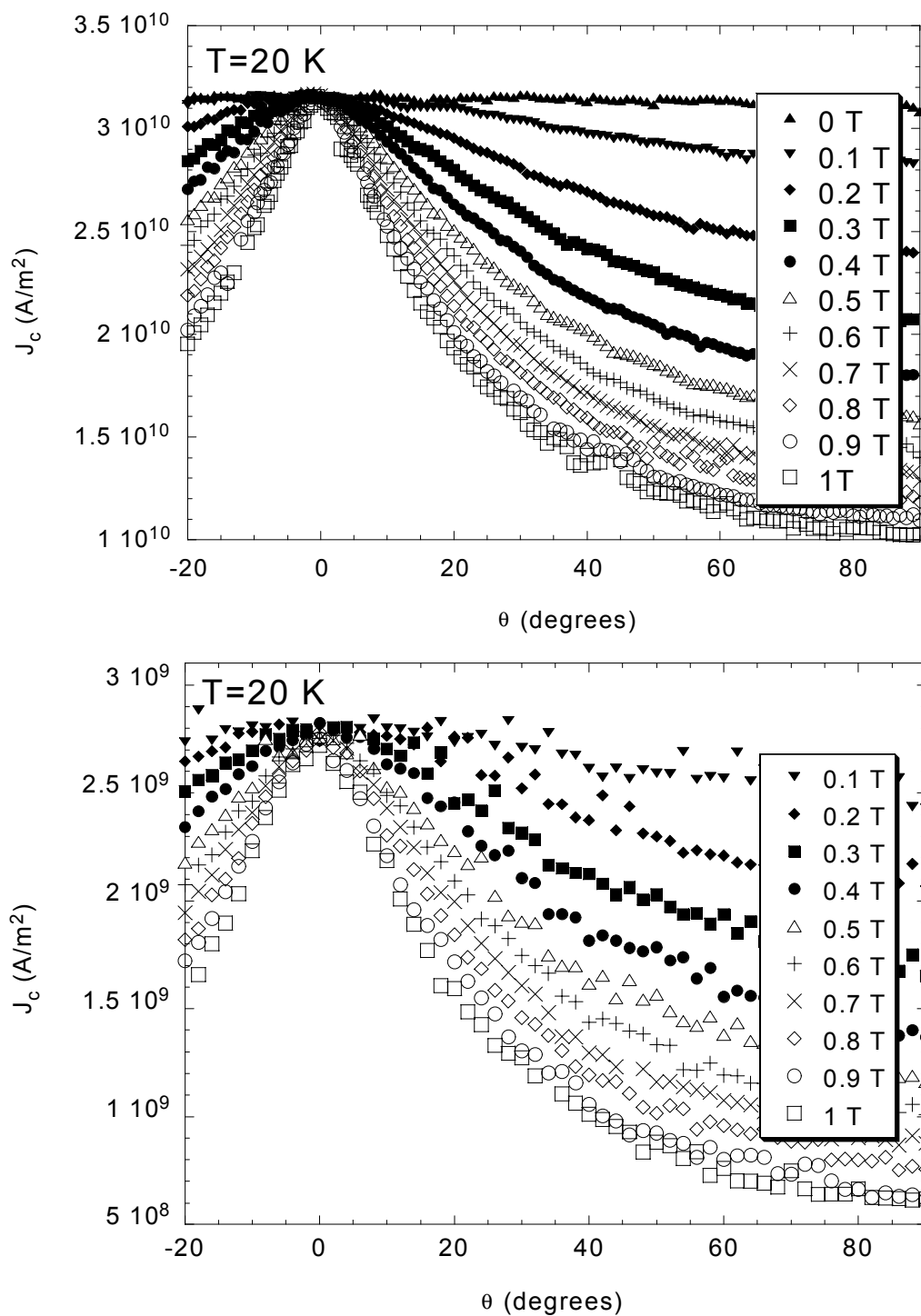


Figure 7.11.  $J_c(\theta)$  plots, field swept in plane of the tilt direction ( $\phi=0^\circ$ ,  $T=20$  K). The top data was measured on an **L** track, the lower data on a **T** track.

### 7.3.5. $J_c(\theta)$ at varying temperatures

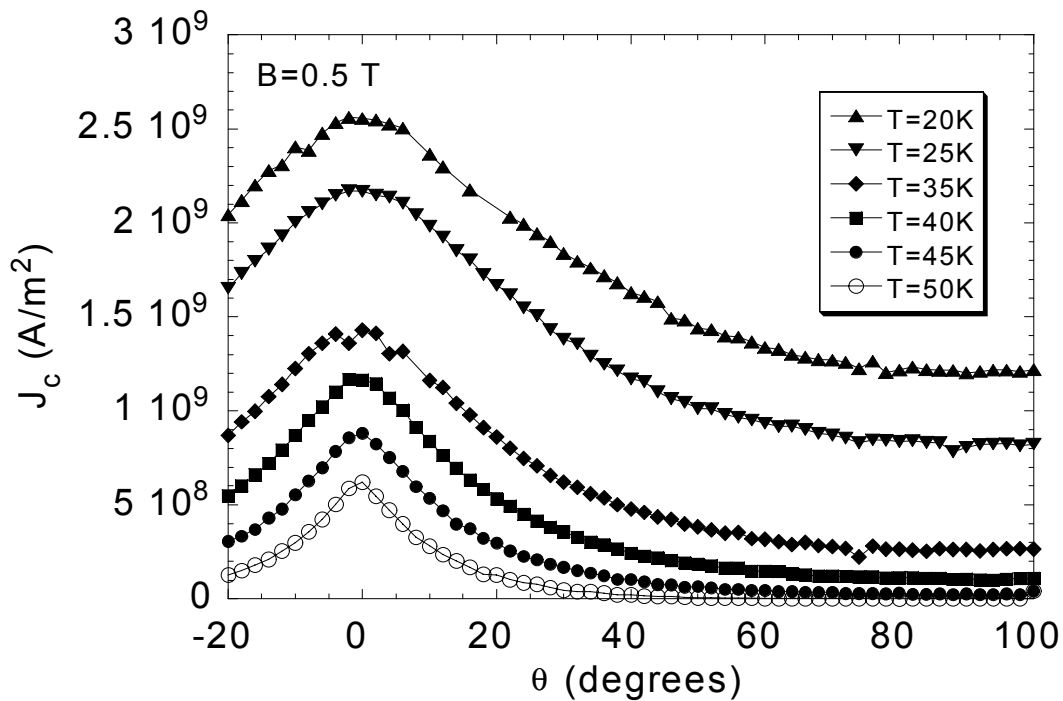


Figure 7.12  $J_c(\theta)$  data at varying temperatures on a **T** track.

Figure 7.12 shows the variation of the  $J_c(\theta)$  dependence with temperature. The peak in the critical current density at  $\theta=0^\circ$  remains over the entire temperature range studied. This is in contrast to YBCO where at higher temperatures the prominent channelling peak is suppressed. Data was not recorded close to  $T_c$  where two-dimensional behaviour is expected to break down. Experimentally it was found difficult to record the very small critical current values at these elevated temperatures. Additionally, it can be seen from the  $RT$  data recorded on the sample that at 60K and above a resistive state is entered for all but the smallest fields.

### 7.3.6. $J_c(\phi)$ data

The plot below shows the effect of various values of  $\phi$  on  $J_c(\theta)$  measurements. Here it is possible to confirm the expected two-dimensional behaviour.

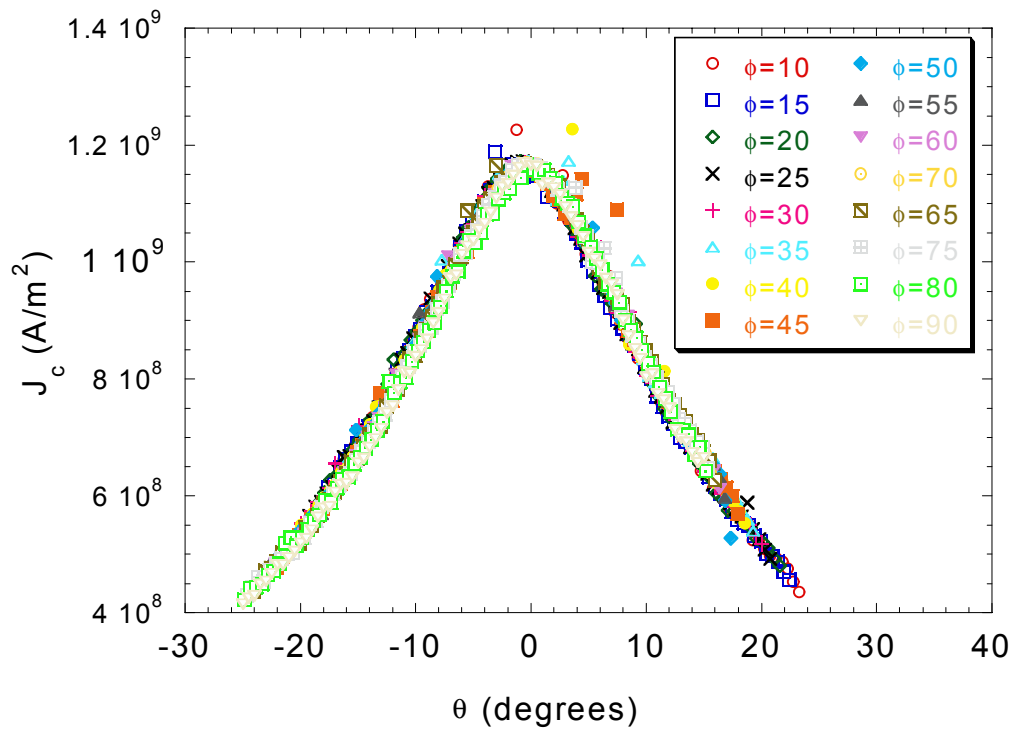


Figure 7.13 Variation of the critical current with the field angle,  $\theta$ , recorded at various values of the field rotation angle,  $\phi$ . This data was recorded at 40 K and 0.5 T.

This plot is further evidence that the rotation of the applied magnetic field in  $\phi$  has no effect on the critical current density. There is no change in the critical current density at constant  $\theta$  as the field is rotated in  $\phi$ . This corresponds to  $r_\phi=1$  as was predicted for a two-dimensional superconductor in the previous chapter.

#### 7.4. Discussion

Figure 7.14, below, shows the data presented in Figure 7.11 replotted against the  $c$ -axis component of the magnetic field for both an **L** and a **T** track. As would be expected for a material obeying the Kes law, it is clear that there is no distinction between tilting the applied field and varying the magnitude of a field applied parallel to the  $c$ -axis of the material.

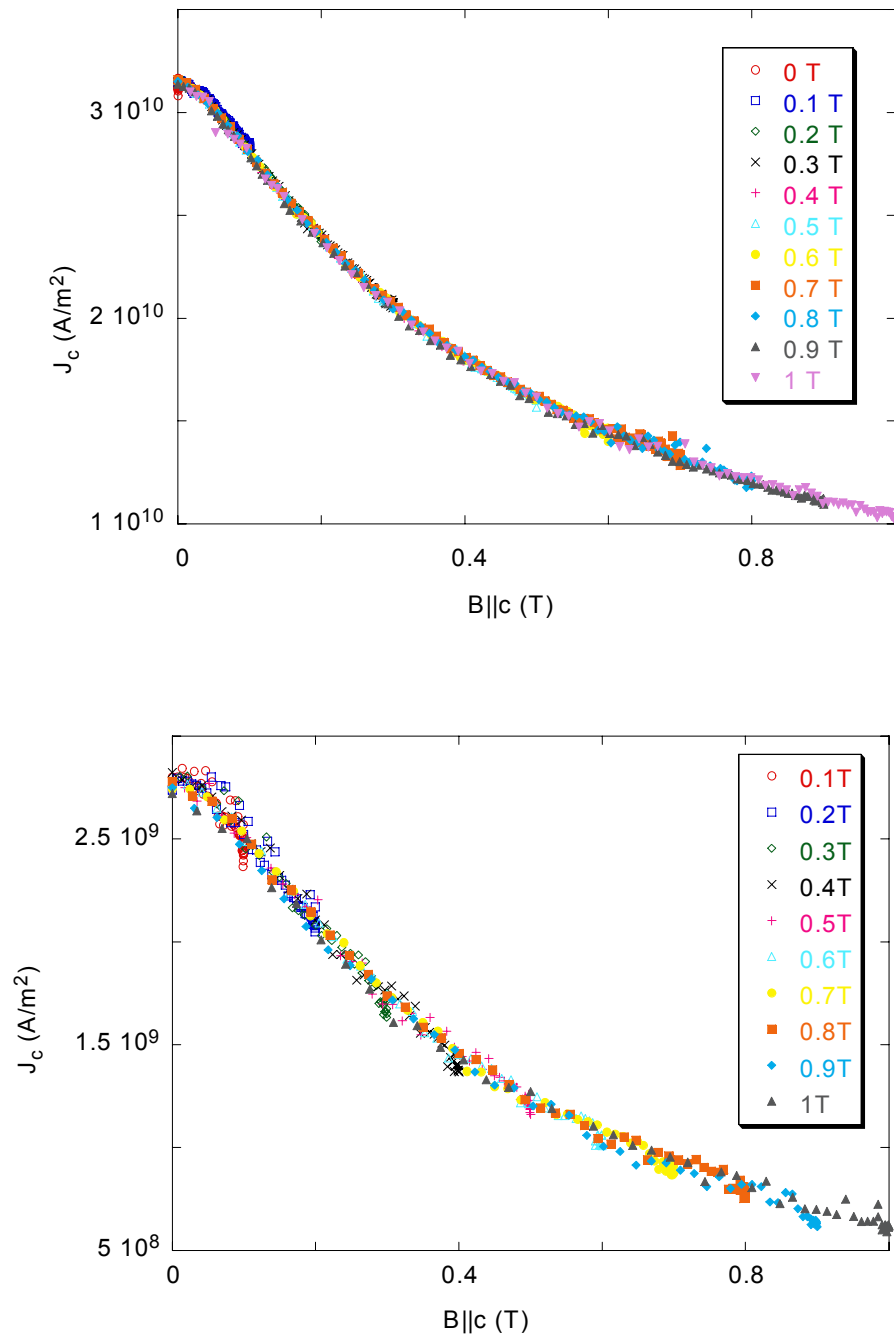


Figure 7.14 Rescaled  $J_c(\theta)$  data showing adherence to the Kes law for measurements made on a **L** track (top) and a **T** track (bottom).

The measurements on BSCCO grown on vicinal substrates are consistent with the simple 2D scaling law proposed to explain the angular dependence of  $J_c$  in highly anisotropic cuprate superconductors (Kes, *et al.* 1990). Only the component of the field perpendicular to the cuprate planes has an effect on current transport, this appears to be the case even when there is a significant  $c$ -axis component to the current transport.

However as vicinal films have been used further observations may be made. It is possible to state on the basis of experimental evidence that there is no force free effect in BSCCO. This is not possible from measurements made on  $c$ -axis films, as the force free geometry is the same as the geometry for which the  $c$ -axis component of the applied field is at a minimum. The absence of the string channelling effect indicates that the joined string/pancake lattice suggested for YBCO is not present in BSCCO.

The question remains however of the presence of Josephson strings in the blocking layers. Several authors have discussed the crossing lattice model in the context of BSCCO (Koshelev 1999). The crossing lattice model still retains strings localised in the blocking layers of the superconductor, these strings are weakly magnetically coupled to the pancake stacks. In measurements on a **T** track there is current flowing between cuprate planes. This current would be expected to interact with vortex strings, if present, between the planes. This would be expected to give rise to a deviation from the Kes law.

Although no evidence for anything other than 2D behaviour has been observed in these measurements, the  $c$ -axis coherence length is expected to become larger than  $d$  close to  $T_c$ . A dimensional cross-over in the structure of the FLL would therefore be expected close to  $T_c$ . Critical current measurements were not made close to  $T_c$  it is practically difficult to measure these very small values. However, the  $RT$  curve shown in Figure 7.7 does provide some information about flux motion. It is possible that the dip in  $RT$  is connected to a change in the structure in the FLL. This may be a transition between a chain like string/pancake structure and the separated crossing lattice.

## **7.5. Conclusion**

Although the results obtained agree with existing two dimensional models of the FLL in BSCCO it is clear that the pancake coupling of the FLL in BSCCO is quite different to the coupling between pancakes in the small angle string/pancake regime in YBCO. No evidence has been found that a Lorentz force exerted on the Josephson strings has an effect on  $J_c$ . This could be interpreted to imply the lack of Josephson strings in these materials and that the pancake coupling is mainly magnetic (Clem 1998). This would also seem to exclude the perpendicular lattice of Josephson vortices predicted by some authors.

The use of a film grown on a vicinal substrate allows the peak in the  $J_c(\theta)$  measurements to be unambiguously attributed to the variation in the  $c$ -axis oriented component of the applied

field. No evidence has been observed that the force free orientation, surface pinning or extrinsic pinning centres substantially affect the  $\theta$  dependence of  $J_c$  in BSCCO.

It is also possible that the pinning of the strings is so weak that the pinning of pancakes is always dominant, even for  $B||a-b$  where there are expected to be very few, if any, pancakes present. It is, therefore, not possible to exclude the possibility of a crossing lattice of Josephson strings. Indeed the resistivity transition data does indicate the possibility of a lattice structure changeover at temperatures close to  $T_c$ .

## 7.6. Bibliography

- Blatter, G., M. V. Feigelman, V. B. Geshkenbein, A. I. Larkin and V. M. Vinokur (1994). Rev. Mod. Phys. **66**(4): 1125-1388.
- Chikumoto, N., M. Konczykowski, N. Motohira and K. Kishio (1992). Physica C **199**(1-2): 32-36.
- Clem, J. R. (1991). Phys. Rev. B **43**(10 PtA): 7837-7846.
- Clem, J. R. (1998). Supercon. Sci. Technol **11**(10): 909-914.
- Crommie, M. F., A. Y. Liu, M. L. Cohen and A. Zettl (1990). Phys Rev B- **41**(4): 2526-2529.
- Datta, T. (1992). Oxide Superconductors: Physical Properties. Concise Encyclopedia of Magnetic and Superconducting Materials. J. E. Evetts. Oxford, Pergamon
- Farrell, D. E., S. Bonham, J. Foster, Y. C. Chang, P. Z. Jiang, K. G. Vandervoort, D. J. Lam and V. G. Kogan (1989). Phys. Rev. Lett. **63**(7): 782-785.
- Gor'kov, L. P. and T. K. Melik-Barkhudarov (1963). Sov. Phys. JETP **18**: 1031.
- Hardy, V., A. Maignan, C. Goupil, J. Provost, C. Simon and C. Martin (1994). Supercon. Sci. Technol. **7**(3): 126-132.
- Iye, Y., S. Nakamura and T. Tamegai (1989). Physica C **159**: 433-438.
- Kes, P. H., J. Aarts, V. M. Vinokur and C. J. van der Beek (1990). Phys. Rev. Lett. **64**(9): 1063-1066.
- Kleiner, R. and P. Muller (1994). Phys. Rev. B **49**(2): 1327-1341.
- Kleiner, R., F. Steinmeyer, G. Kunkel and P. Muller (1992). Phys. Rev. Lett. **68**(15): 2394-2397.
- Koshelev, A. E. (1999). Phys. Rev. Lett. **83**(1): 187-190.
- Lawrence, W. E. and S. Doniach (1970). Proceedings of the 12th International Confernece on Low Temperature Physics, Kyoto, Keigaku, Tokyo.
- Martin, S., A. T. Fiory, R. M. Fleming, L. F. Schneemeyer and J. V. Waszczak (1988). Phys. Rev. Lett. **60**(21): 2194-2197.

- Martinez, J. C., S. H. Brongersma, A. Koshelev, B. Ivlev, P. H. Kes, R. P. Griessen, D. G. Degroot, Z. Tarnavski and A. A. Menovsky (1992). Phys. Rev. Lett. **69**(15): 2276-2279.
- Matsubara, I., H. Tanigawa, T. Ogura, H. Yamashita, M. Kinoshita and T. Kawai (1992). Phys. Rev. B **45**(13): 7414-7417.
- Raffy, H., S. Labdi, O. Laborde and P. Monceau (1991). Phys. Rev. Lett. **66**(19): 2515-2518.
- Schmitt, P., P. Kummeth, L. Schultz and G. Saemannschenko (1991). Phys. Rev. Lett. **67**(2): 267-270.
- Shaked, H., P. M. Keane, J. C. Rodriguez, F. F. Owen, R. L. Hitterman and J. D. Jorgenson (1994). Crystal Structures of the High-Tc Superconducting Copper-Oxides. Amsterdam, Elsevier Science B.V.
- Wang, H. B., J. Chen, K. Nakajima, T. Yamashita, P. H. Wu, T. Nishizaki, K. Shibata and N. Kobayashi (2000). Phys. Rev. B **61**(22): R14948-R14951.
- Weber, S. (1999). <http://www.nirim.go.jp/~weber/gallery/HighTc/HighTc.html>.
- Zahner, T., R. Stierstorfer, R. Rossler, J. D. Pedarnig, D. Bauerle and H. Lengfellner (1998). Physica C **298**(1-2): 91-94.

## 8. Conclusions and Further Work

### 8.1. Conclusions

It is clear from the measurements of the critical current anisotropy, presented in this thesis, that the variation of critical current density with applied field in  $\text{YBa}_2\text{Cu}_3\text{O}_{7-\delta}$  is complex. The vortex channelling effect, first observed by (Berghuis, *et al.* 1997) is striking. By confirming these measurements it has been shown that the channelling effect is indeed a genuine intrinsic effect, and not due to the characteristics of any particular experimental sample.

The confirmation of this effect is significant. It means that no simple scaling law can successfully describe the  $J_c(\theta)$  behaviour in  $\text{YBa}_2\text{Cu}_3\text{O}_{7-\delta}$ . Both the Kes law, which it is demonstrated applies well to results from BSCCO, and the anisotropic Ginzburg-Landau model do not predict vortex channelling. The results obtained appear to fit relatively well with the prediction in (Blatter, *et al.* 1994, pp. 1286) of a field angle dependent cross-over from a three dimensional rectilinear FLL to a kinked lattice of strings and pancakes. The effect of the transition to the string pancake state in  $\text{YBa}_2\text{Cu}_3\text{O}_{7-\delta}$ , is to suppress the peaks in  $J_c$  which occur due to intrinsic pinning and the force free geometry. The pinning force density for movement of strings in the cuprate plane is considerably less than that on vortex pancake elements. When the FLL is entirely string-like this reduced pinning leads to the observed channelling minimum.

Although the channelling effect cannot be directly observed in  $c$ -axis  $\text{YBa}_2\text{Cu}_3\text{O}_{7-\delta}$  films the results presented here show that the pinning force density for vortex strings extracted indirectly, by measuring string dragging, in measurements on  $c$ -axis films are consistent with those from channelling measurements. Additionally, by observing  $J_c(\phi)$  behaviour in  $c$ -axis films it is possible to observe the cross-over into the string pancake regime. In the 3D region the  $J_c(\phi)$  behaviour is well explained by considering the anisotropy of the vortex cores using the anisotropic Ginzburg-Landau model.

Vortex channelling itself is observed since the pinning on vortex strings inside the  $a$ - $b$  planes is weaker than the pancake pinning density. It has been possible to compare the current anisotropy results obtained from films grown on un-annealed substrates, where measurements suggest a low density of anti-phase boundaries (APB), with those from films with a high APB density. This allows the observation to be made that the enhancement in critical current

density observed in APB rich samples must be due to very much enhanced vortex *string* pinning.

The lattice cross-over model predicts for de-oxygenated  $\text{YBa}_2\text{Cu}_3\text{O}_{7-\delta}$  that the angular cross-over will occur at all temperatures below  $T_c$  and this is indeed observed. Intriguingly, the counter intuitive prediction, that the range of  $\theta$  for which the kinked lattice is fully developed reduces with increasing anisotropy, appears to be confirmed.

Measurements of  $J_c(\theta)$  on vicinal  $\text{Bi}_2\text{Sr}_2\text{CaCu}_2\text{O}_8$  provide a highly anisotropic comparison to  $\text{YBa}_2\text{Cu}_3\text{O}_{7-\delta}$ . Here the predictions of the Kes law for a highly anisotropic superconductor are closely followed by the observed  $J_c(\theta)$  behaviour. No evidence for the predicted crossing lattice is observed, the purely 2D model appears to well describe the data. Measurements on a vicinal film have allowed the peak in  $J_c(\theta)$  to be unambiguously identified with a minimum in the  $c$ -axis component of the applied magnetic field. There is, however, some evidence from the measured  $RT$  transitions of a change in the FLL structure at temperatures close to  $T_c$ . Enough data was not collected to be certain that this feature is not an experimental artefact.

The ability to separate contributions to  $J_c(\theta, \phi)$  behaviour, and from this deduce the FLL structure, provided by measurements on vicinal films underlines this as a powerful experimental technique for probing the structure and pinning of the FLL in HTS materials.

## 8.2. Further Work

The vortex channelling effect is one manifestation of the complex behaviour of the FLL in YBCO. In contrast to more high anisotropic materials, such as  $\text{Bi}_2\text{Sr}_2\text{CaCu}_2\text{O}_8$ , the angularly dependence of  $J_c$  is difficult to quantitatively model. One prerequisite to further work in this field is further study of the growth of  $\text{YBa}_2\text{Cu}_3\text{O}_{7-\delta}$  films on vicinal substrates. The experimental evidence discussed in the thesis show that the critical current anisotropy is highly sensitive to the morphology of the film. In the string/pancake regime the vortex strings are more weakly pinned, the evidence suggests that this is not the case when a high density of anti-phase boundaries are present. It would be crucial to identify exactly why films grown on unannealed substrates seem to show better alignment of the vicinal steps. Research is currently ongoing to correlate Magneto-Optical measurements, HREM structure studies and  $J_c(\theta)$  behaviour in vicinal films grown on as supplied and vicinal substrates.

The clear change in the critical current anisotropy in  $\text{YBa}_2\text{Cu}_3\text{O}_{7-\delta}$  with deoxygenation could be usefully studied further through a systematic study of films with progressively increasing and well established levels of de-oxygenation. The difference in behaviour between de-

oxygenated  $\text{YBa}_2\text{Cu}_3\text{O}_{7-\delta}$  and  $\text{Bi}_2\text{Sr}_2\text{CaCu}_2\text{O}_8$  is striking, measurements on HTS compounds with intermediate anisotropies might allow the point of transition from the quasi 2D kinked string pancake lattice found in  $\text{YBa}_2\text{Cu}_3\text{O}_{7-\delta}$  to the pure 2D pancake lattice in BSCCO to be identified.

In this thesis it has been assumed that, at the relatively large fields used, the microscopic direction of the flux lines is near parallel to the applied field. As has been discussed in Section 2.4.3 this is not expected for very thin samples of superconductor in small fields. It would therefore be interesting to investigate whether the  $J_c(\theta)$  behaviour seen in this thesis, where a marked angular dependence is evident, disappears for this case.

### **8.3. Bibliography**

- Berghuis, P., E. DiBartolomeo, G. A. Wagner and J. E. Evetts (1997). Physical Review Letters **79**(12): 2332-2335.
- Blatter, G., M. V. Feigelman, V. B. Geshkenbein, A. I. Larkin and V. M. Vinokur (1994). Reviews Of Modern Physics **66**(4): 1125-1388.

## Appendix A - List of samples studied

The table below specifies the sources of the samples I studied during my PhD project.

Film	Description (all films were YBCO grown on SrTiO <sub>3</sub> unless otherwise stated)	Source
8722	Sputtered de-oxygenated films 0,2,4 and 6° vicinality	A. Bramley, Cambridge
8880	Sputtered de-oxygenated films 0,2,4 and 6° vicinality	A. Bramley, Cambridge
Linz 1	PLD 10° vicinal BSCCO film	R. Rössler, Linz
Y1034	PLD <i>c</i> -axis film	E. Tarte, Cambridge
Linz 3	PLD 10° vicinal BSCCO film	R. Rössler, Linz
Z323	PLD 6° vicinal film	G. Gibson, Cambridge
Z324 A + B	PLD 6° vicinal films	G. Gibson, Cambridge
Z333A	PLD 10° vicinal film	G. Gibson, Cambridge
Z334 A+B	PLD 20° vicinal films	G. Gibson, Cambridge
Z335 A+B	PLD 4° vicinal films	G. Gibson, Cambridge
Z336 A+B	PLD 2° vicinal films	G. Gibson, Cambridge
Linz 4	PLD 15° BSCCO film	R. Rössler, Linz
210600	PLD, de-oxygenated 10° vicinal film	R. Rössler, Linz
200630	PLD 10° vicinal film	R. Rössler, Linz
nott 37.5	PLD 37.5° vicinal film on annealed SrTiO <sub>3</sub> substrate	P. Czerwinka, Nottingham

## Appendix B

The diagrams opposite reproduce, from top to bottom, Figures 4.4, 4.5 and 6.1 from the main text.

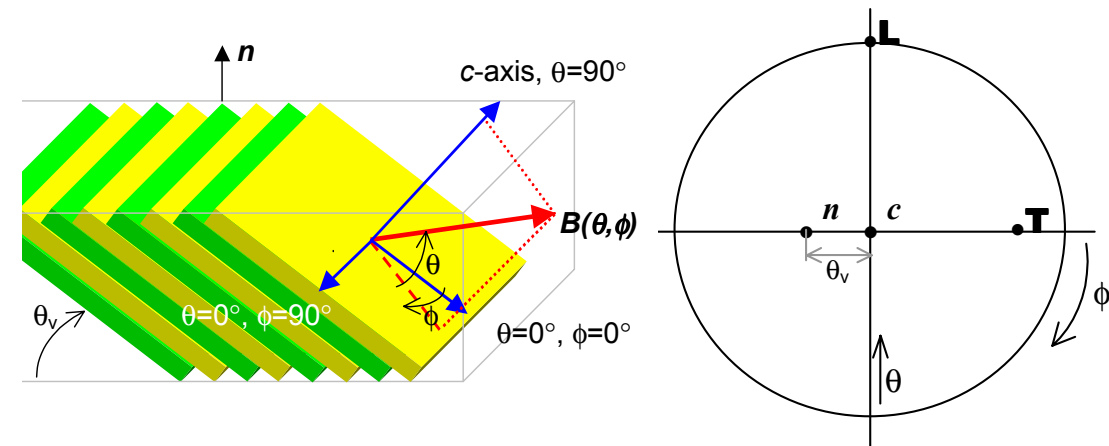


Figure 4.4 On the left is shown the geometry of a measurement on a vicinal film. The right hand diagram is a pole figure showing the definitions of  $\theta_v$ ,  $\theta$  and  $\phi$  and the direction of current flow in **T** and **L** tracks. Also shown are the vectors, **n**, normal to the surface of the film and the *c*-axis direction.

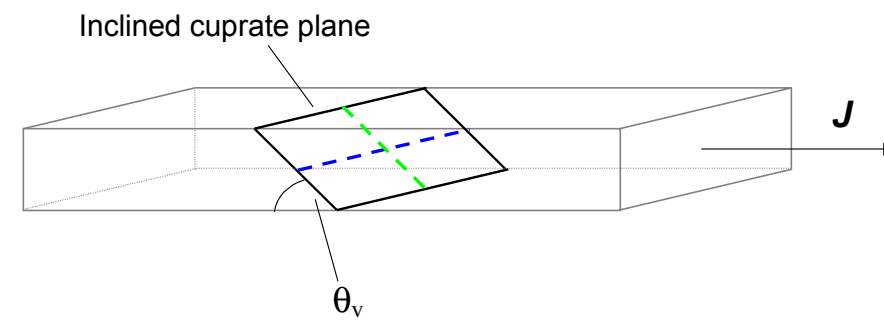


Figure 4.5 Cross-section of a **T** track showing the orientation of the vicinal steps. The green and blue lines indicate the orientation of the applied field at  $(\theta=0^\circ, \phi=0^\circ)$  and  $(\theta=0^\circ, \phi=90^\circ)$  respectively.

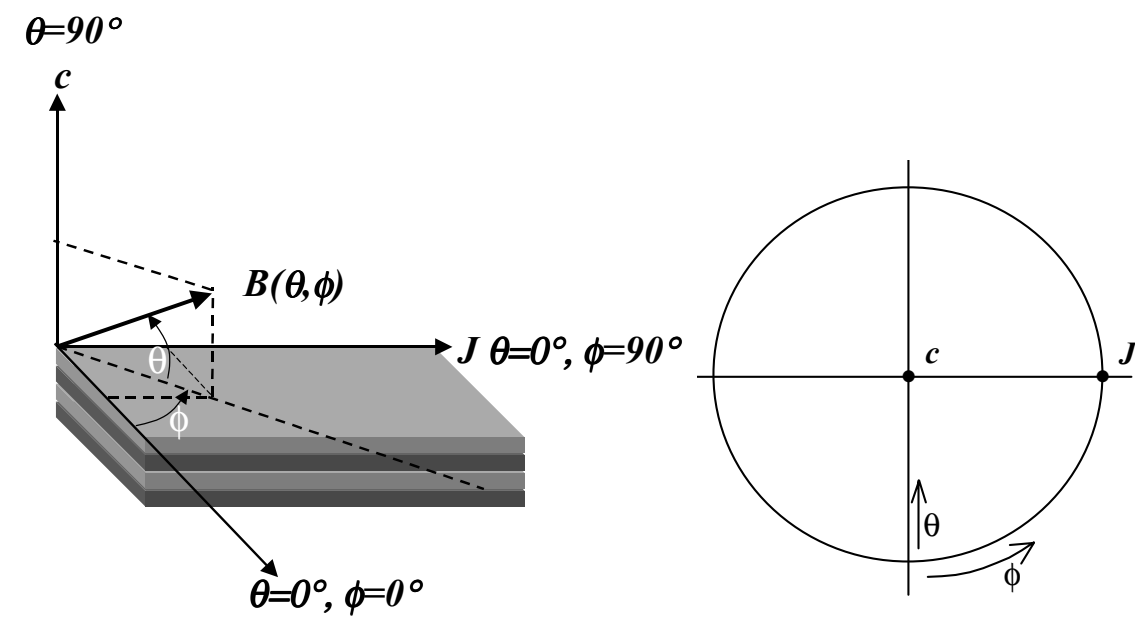


Figure 6.1 (left) Definition of the field angles  $\theta$  and  $\phi$  with respect to a current flowing in a *c*-axis film. (right)  $\theta$  and  $\phi$  shown on a pole figure.

Cut off  
This bit!

## Appendix C – Publications

The following list consists of journal and conference papers published. Those marked with an asterisk are reproduced in this Appendix.

- Durrell, J.H.**, G. Gibson, Z.H. Barber, J.E. Evetts, R. Rossler, J.D. Pedarnig, and D. Bauerle, *Dependence of critical current on field angle in off-c-axis grown Bi2Sr2CaCu2O8 film*. Applied Physics Letters, 2000. **77**(11): p. 1686-1688. \*
- Durrell, J.H.**, R. Herzog, P. Berghuis, A.P. Bramley, E.J. Tarte, Z.H. Barber, and J.E. Evetts, *Determination of pinning forces on vortex lines in YBa2Cu3O7- delta*. Superconductor Science & Technology, 1999. **12**(12): p. 1090-1093. \*
- Latif, A., W.E. Booij, **J.H. Durrell**, and M.G. Blamire, *Real time resistometric depth monitoring in the focused ion beam*. Journal of Vacuum Science & Technology B, 2000. **18**(2): p. 761-764.
- Bauerle, D., J.D. Pedarnig, R. Roessler, C. Stockinger, W. Markowitsch, W. Lang, **J.H. Durrell**, and J.E. Evetts, *Pulsed-laser deposition and characterization of high-temperature superconducting films*. Proc SPIE IX International Conference on Laser-Assisted Microtechnology (LAM 2000), 2000.
- Tsaneva, V.N., C. Christou, **J.H. Durrell**, G. Gibson, F. Kahlmann, E.J. Tarte, Z.H. Barber, M.G. Blamire, and J.E. Evetts, *Plasma optical emission studies during HTSC thin film deposition process optimisation*. Conference Series- Institute of Physics, 2000. **167**(VOL 2): p. 61-64.
- Rutter, N.A., B.A. Glowacki, **J.H. Durrell**, J.E. Evetts, H.t. Lintelo, R. De Gryse, and J. Denul, *Formation of native cube textured oxide on a flexible NiFe tape substrate for coated conductor applications*. Conference Series- Institute of Physics, 2000. **167**(VOL 1): p. 407-410.
- Blamire, M.G., B.S. Teo, **J.H. Durrell**, N.D. Mathur, Z.H. Barber, J.L.M. Driscoll, L.F. Cohen, and J.E. Evetts, *Strain-induced time-dependent magnetic disorder in ultra-thin La0.7Ca0.3MnO3 films*. Journal of Magnetism and Magnetic Materials, 1999. **191**(3): p. 359-367.
- Durrell, J.**, G. Hauchecorne, J. Bok, J. Bouvier, A.C. Boccara, J.P. Contour, and J.P. Roger, *Study of the birefringence by optical reflectivity in YBa2Cu3O7 and its variation with a superconducting current*. Physica C, 1997. **282**: p. 1025-1026.

## Dependence of critical current on field angle in off-*c*-axis grown $\text{Bi}_2\text{Sr}_2\text{CaCu}_2\text{O}_8$ film

J. H. Durrell,<sup>a)</sup> G. Gibson, Z. H. Barber, and J. E. Evetts

*Department of Materials Science and IRC in Superconductivity, University of Cambridge, Pembroke Street, Cambridge CB2 3QZ, United Kingdom*

R. Rössler, J. D. Pedarnig, and D. Bäuerle

*Institut für Angewandte Physik, Johannes-Kepler-Universität Linz, 4040 Linz, Austria*

(Received 5 April 2000; accepted for publication 24 July 2000)

Critical current measurements for varying angles of applied field have been performed on  $\text{Bi}_2\text{Sr}_2\text{CaCu}_2\text{O}_8$  thin films grown on  $10^\circ$  vicinal (001) substrates. Measurements were performed on current tracks orientated both parallel (L) and transverse (T) to the vicinal steps. No Josephson vortex channeling effect was observed, in contrast to results previously obtained on both oxygenated and deoxygenated  $\text{YBa}_2\text{Cu}_3\text{O}_{7-\delta}$  films grown on vicinal substrates. In addition, no force-free peak was observed when the applied field was parallel to the current. This provides experimental evidence that there is a difference between the pancake coupling mechanism in  $\text{YBa}_2\text{Cu}_3\text{O}_{7-\delta}$  at small field angles where Josephson vortices are present and that in  $\text{Bi}_2\text{Sr}_2\text{CaCu}_2\text{O}_8$ . © 2000 American Institute of Physics. [S0003-6951(00)04237-6]

In contrast to the relatively isotropic  $\text{YBa}_2\text{Cu}_3\text{O}_{7-\delta}$  (YBCO) material  $\text{Bi}_2\text{Sr}_2\text{CaCu}_2\text{O}_{8+x}$  (BSCCO) has a large anisotropy in both its superconducting and normal state properties. The structure of the flux line lattice in YBCO depends strongly on temperature and on the angle of the applied magnetic field. In contrast BSCCO, due to the large spacing between cuprate layers, exhibits two-dimensional behavior over all field angles and temperatures (except for  $T/T_c \sim 1$ ).<sup>1</sup> A simple scaling law, proposed by Kes *et al.*, successfully describes the behavior of BSCCO;  $j_c(B, \theta) = j_c(B \sin \theta, 90)$  [Eq. (1)], where  $\theta$  is the angle between the applied field and the cuprate planes.<sup>2</sup> This strongly suggests that the structure of the flux line lattice (FLL) in BSCCO is that of flux “pancakes” lying inside the cuprate planes.<sup>3</sup> A similar pancake structure is envisaged in YBCO for fields applied nearly parallel to the cuprate planes. The flux pancakes in YBCO appear to be linked by Josephson string vortices that behave in some ways like conventional Abrikosov vortices.<sup>4</sup> Angular  $j_c(\theta)$  measurements performed on YBCO films grown on vicinal (miscut) substrates have demonstrated that it is possible to channel Josephson vortices inside the intercalated layers<sup>5</sup> and thus calculate a volume pinning force for the vortex strings. In contrast, in highly anisotropic materials such as BSCCO it is expected that the pancakes are predominantly weakly magnetically coupled,<sup>6</sup> although a perpendicular lattice of Josephson vortices is still present.<sup>7</sup> We have performed  $j_c(\theta)$  measurements on 120 nm thick BSCCO films grown on  $10^\circ$  vicinal (001)  $\text{SrTiO}_3$  substrates and observe no channeling effect over a range of fields and temperatures. This strongly suggests that the pancake coupling in BSCCO is very different from that in YBCO. It is important to note that these experimental observations can only be made using vicinal films. The “channeling” effect

only occurs in vicinal films, in addition the “force-free” and “intrinsic” peaks are superimposed in *c*-axis films.

BSCCO films were grown by pulsed laser deposition on  $10^\circ$  vicinal (001)  $\text{SrTiO}_3$  substrates.<sup>8</sup> The films were characterized by x-ray diffraction and the half maximum width of the (0010) peak was found to be less than  $1^\circ$ . In addition, transmission electron microscopy analysis confirmed that the films consisted purely of epitaxial 2212 phase. Current tracks  $500 \times 20 \mu\text{m}^2$  were patterned both parallel (L) and transverse (T) to the vicinal steps using photolithography and Ar ion milling. The sample was mounted in a two-axis goniometer<sup>9</sup> inserted in an 8 T cryostat. Resistance measurements using a four point geometry were employed to determine the critical current density,  $j_c$ , using a voltage criterion of  $0.5 \mu\text{V}$  for a range of temperatures,  $T$ , fields,  $B$ , and applied field angles  $\theta$ ,  $\phi$ . The angles  $\theta$  and  $\phi$  define tilt with respect to the *c* axis and rotation in the *a*-*b* plane, they are derived from experimental angles  $\theta_e$  and  $\phi_e$  which are defined in terms of the normal and surface of the film.

Figure 1 shows the geometry of the measurement on a

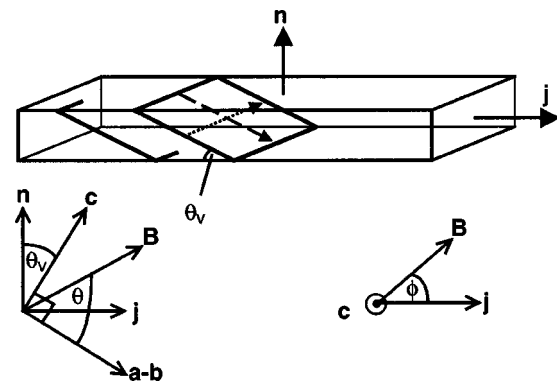


FIG. 1. Experimental geometry for current flowing in a track crossing the cuprate planes.  $\theta$  is the angle between the cuprate planes and the applied field,  $\phi$  is the angle of rotation of the plane in which  $\theta$  is swept. The dashed line corresponds to  $\theta=0^\circ$ ,  $\phi=0^\circ$  and the dotted line to  $\theta=0^\circ$ ,  $\phi=90^\circ$ .

<sup>a)</sup> Author to whom all correspondence should be addressed; electronic mail: jhd25@cam.ac.uk

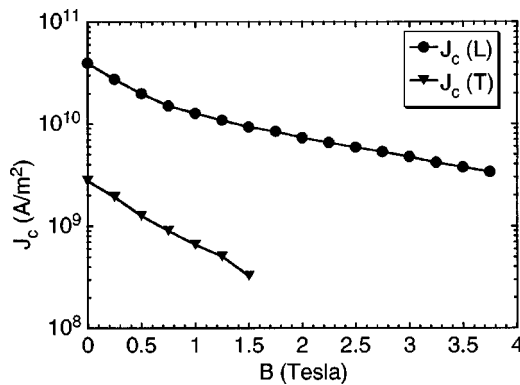


FIG. 2. Variation of the critical current density ( $j_c$ ) on a (T) track with applied field at 20 K. The field is applied parallel to the  $c$  axis of the material

track running transverse to the vicinal steps. The angle  $\theta$  is defined as that between the cuprate layers and the applied field,  $\theta=0^\circ$  corresponds to the applied field being parallel to the cuprate planes. The angle  $\phi$  defines the plane in which  $\theta$  is swept with respect to the current direction. To illustrate this the diagram indicates the field direction at  $\theta=0^\circ$ ,  $\phi=0^\circ$  (dashed line), and  $\theta=0^\circ$ ,  $\phi=90^\circ$  (dotted line).

It has previously been shown that the normal state resistivity of the (T) track is considerably higher than that measured on the (L) track.<sup>10</sup> This is attributed to the combination of  $a-b$  and  $c$ -axis transport experienced by a current flowing along a (T) track. It is possible to estimate  $\rho_{a-b}$  and  $\rho_c$  given the vicinal angle of the film. The values obtained for  $\rho_{a-b}$  and  $\rho_c$  on these films are consistent with those seen in single crystal  $\text{Bi}_2\text{Sr}_2\text{CaCu}_2\text{O}_8$ .<sup>10</sup>

Measurements of  $j_c(B)$  in both orientations were made, as shown in Fig. 2. At 20 K and zero field  $j_c(T)=3 \times 10^9 \text{ A/m}^2$  and  $j_c(L)=4 \times 10^{10} \text{ A/m}^2$ . The  $j_c(L)$  value is directly comparable to measurements made on  $c$ -axis BSCCO films grown under similar conditions for which a  $j_c$  at 20 K and zero field of  $1 \times 10^{11} \text{ A/m}^2$  was measured. This indicates that the tracks are well aligned parallel and perpendicular to the vicinal steps and that the current transport in a (L) track is within  $a-b$  planes as for current flow in a conventional  $c$ -axis orientated film. The  $j_c$  for a (T) orientated track is lower since the current must flow in the  $c$  direction in order to cross between  $a-b$  planes. It has been demonstrated in YBCO that for a particular vicinal substrate orientation (corresponding to a vicinal angle of  $9.46^\circ$ ) pinning enhancement by antiphase boundaries occurs.<sup>11</sup> This is manifested by values of  $j_c(T)$  similar to those found in  $c$ -axis films. This effect is not observed in these BSCCO films.

Angular  $j_c$  measurements were performed on both track orientations for a range of applied fields and temperatures. Figure 3 shows measurements of  $j_c$  on a (T) track with varying  $\theta$  at 0.5 T,  $\phi=0^\circ$ , and a range of temperatures. The inset in Fig. 3 shows the results from an identical geometry experiment performed on a (T) track from a  $10^\circ$  vicinal YBCO film at 1 T and 40 K. Both the channeling minima (at  $\theta=0^\circ$ ) and the partially suppressed force free peak (at  $\theta=10^\circ$ ) can be seen. At the channeling minimum the Josephson strings move due to a Lorentz force parallel to the planes  $JB \cos \theta_v$ . It is clear that, in the BSCCO measurement, the characteristic Josephson string channeling minimum is absent. In addition the prominent force-free<sup>12</sup> peak at  $\theta=10^\circ$

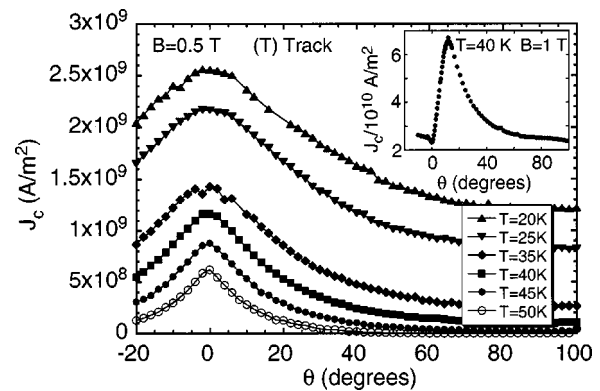


FIG. 3. Angular dependence of the critical current density at 0.5 T and varying temperatures.  $\theta$  is swept with  $\phi$  held at  $0^\circ$ . The inset shows the results of the same measurement performed on a YBCO film grown on a  $10^\circ$  miscut (001) substrate. The partially suppressed peak at  $10^\circ$  on the inset figure is due to the force-free effect.

corresponding to  $B$  parallel to  $j$  is absent in BSCCO. It is important to note that the angle at which the critical current minimum occurs in YBCO corresponds to a  $j_c$  maximum in the measurements on BSCCO.

Figure 4 shows the variation in the  $j_c$  versus  $\theta$  behavior with field for both a (L) track [Fig. 4(a)] and a (T) track [Fig. 4(b)]. The insets in the figures show the same  $j_c$  data plotted against the resolved component of the field parallel to the  $c$  axis. It can be seen from these plots that there is excellent agreement between the angular  $j_c$  data obtained and the scaling law given by Eq. (1). Interestingly, the scaling law works just as well for the (T) track, where the limiting factor on  $j_c$  would be expected to be the  $c$ -axis critical current.

It was also observed that varying  $\phi$ , that is rotating the plane in which ( $\theta$ ) is swept, has no effect on the  $j_c(\theta)$  be-

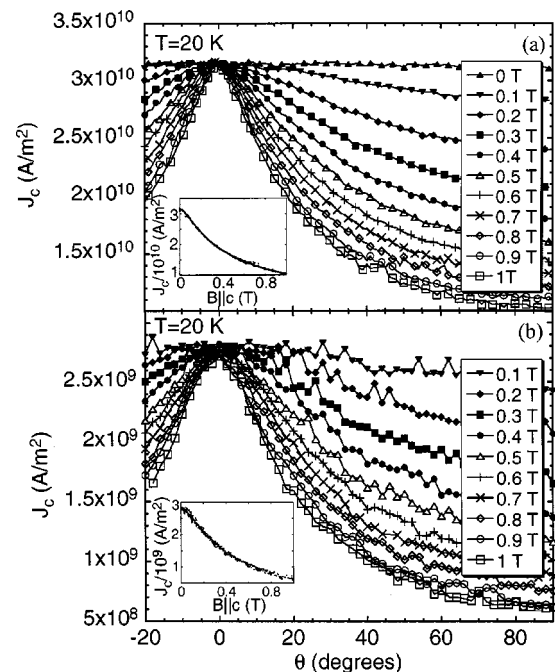


FIG. 4. Main figure shows the variation of critical current with field angle for varying applied fields and 20 K. (a) shows results from a measurement performed on a (L) track and (b) shows results from a (T) track. The insets show the same data sets plotted against the  $c$ -axis component of the applied field.

havior for both (T) and (L) tracks. This contrasts strongly with observed behavior in YBCO where rotating the direction of the Lorentz force on the vortex strings has a clear effect on  $j_c$  particularly in the string/pancake regime.<sup>13</sup>

Thus, measurements on BSCCO grown on vicinal substrates is consistent with the simple two-dimensional (2D) scaling law proposed to explain the angular dependence of  $j_c$  in highly anisotropic cuprate superconductors.<sup>2</sup> Only the component of the field perpendicular to the cuprate planes has an effect on current transport, this appears to be the case even when there is a significant  $c$ -axis component to the current transport.

We conclude that although the results obtained agree with existing 2D models of the FLL in BSCCO, it is clear that the pancake coupling of the FLL in BSCCO is quite different from the coupling between pancakes in the small angle string/pancake regime in YBCO. No evidence has been found that a Lorentz force exerted on the Josephson strings has an effect on  $j_c$ . This could be interpreted to imply the lack of Josephson strings in these materials and that the pancake coupling is mainly magnetic.<sup>6</sup> It is also possible that the pinning of the strings is so weak that the pinning of pancakes is always dominant, even for  $B\parallel a-b$  where there are expected to be very few, if any, pancakes present.

This work is supported by the European Community TMR network "SUPERCURRENT," the Austrian "Bundesministerium für Bildung, Wissenschaft und Verkehr" and by the Engineering and Physical Sciences Research Council.

- <sup>1</sup>P. Schmitt, P. Kummeth, L. Schultz, and G. Saemann-Ischenko, *Phys. Rev. Lett.* **67**, 267 (1991).
- <sup>2</sup>P. H. Kes, J. Aarts, V. M. Vinokur, and C. J. van der Beek, *Phys. Rev. Lett.* **64**, 1063 (1990).
- <sup>3</sup>J. R. Clem, *Phys. Rev. B* **43**, 7837 (1991).
- <sup>4</sup>G. Blatter, M. V. Feigelman, V. B. Geshkenbein, A. I. Larkin, and V. M. Vinokur, *Rev. Mod. Phys.* **66**, 1125 (1994).
- <sup>5</sup>P. Berghuis, E. DiBartolomeo, G. A. Wagner, and J. E. Evetts, *Phys. Rev. Lett.* **79**, 2332 (1997).
- <sup>6</sup>J. R. Clem, *Supercond. Sci. Technol.* **11**, 909 (1998).
- <sup>7</sup>A. E. Koshelev, *Phys. Rev. Lett.* **83**, 187 (1999).
- <sup>8</sup>S. T. Li, A. Ritzer, E. Arenholz, D. Bäuerle, W. M. Huber, and H. Langfellner, *Appl. Phys. A: Mater. Sci. Process.* **63**, 427 (1996).
- <sup>9</sup>R. Herzog and J. E. Evetts, *Rev. Sci. Instrum.* **65**, 3574 (1994).
- <sup>10</sup>T. Zahner, R. Stierstorfer, R. Rössler, J. D. Pedarnig, D. Bäuerle, and H. Lengfellner, *Physica C* **298**, 91 (1998).
- <sup>11</sup>C. Jooss, R. Warthmann, and H. Kronmüller, *Phys. Rev. B* **61**, 12433 (2000).
- <sup>12</sup>A. M. Campbell and J. E. Evetts, *Adv. Phys.* **21**, 199 (1972).
- <sup>13</sup>J. H. Durrell, R. Herzog, P. Berghuis, A. P. Bramley, E. J. Tarte, Z. H. Barber, and J. E. Evetts, *Supercond. Sci. Technol.* **12**, (1999).

# Determination of pinning forces on vortex lines in $\text{YBa}_2\text{Cu}_3\text{O}_{7-\delta}$

J H Durrell, R Herzog, P Berghuis, A P Bramley, E J Tarte,  
Z H Barber and J E Evetts

Department of Materials Science and Metallurgy and IRC in Superconductivity,  
University of Cambridge, Pembroke Street, Cambridge CB2 3QZ, UK

Received 7 July 1999

**Abstract.** The structure adopted by the flux line lattice (FLL) in  $\text{YBa}_2\text{Cu}_3\text{O}_{7-\delta}$  (YBCO) depends strongly on the angle ( $\theta$ ) between the applied field and the superconducting cuprate planes. If this angle is held constant and the field rotated about an axis normal to the cuprate planes, the structure of the FLL remains constant, while the direction of the Lorentz force on the vortex lines changes. Measurements of the critical current density ( $j_c$ ) with respect to this rotation angle ( $\phi$ ) thus probe pinning behaviour while excluding effects due to changes in the structure of the FLL. If the value of  $\theta$  is small, such that the FLL adopts the kinked (string–pancake) state, the variation in  $j_c$  seen with  $\phi$  must be due to the behaviour of the string vortex segments. High-resolution measurements of the variation of  $j_c$  with this second angle  $\phi$  have been made on thin (120 nm) YBCO films. A simple model is proposed to explain this variation in terms of dragging of vortex strings by the vortex pancake elements. From this model and experimental data an estimate has been made for the value of the pinning force density on vortex strings for motion in the  $a$ – $b$  planes. This estimate is in agreement with values found for the string pinning force density found in earlier measurements on YBCO films grown on vicinal-cut substrates.

## 1. Introduction

There is no model of the variation of the flux line lattice (FLL) structure with the angle between the applied field and the cuprate planes ( $\theta$ ) in  $\text{YBa}_2\text{Cu}_3\text{O}_{7-\delta}$  (YBCO) which successfully describes the whole range of variation of the critical current density  $j_c(\theta, \phi)$ . Two main models have been developed to describe the FLL lattice in cuprate superconductors, one two dimensional (2D) in nature and the second three dimensional (3D) in nature.

It is possible to view more highly anisotropic superconductors, such as  $\text{BaSr}_2\text{Ca}_2\text{CuO}_2$ , as a 2D structure of layered superconducting and non-superconducting material [1]. In this case it is only the component of the applied field in the  $c$ -direction which is significant and a flux line always passes perpendicularly through the  $a$ – $b$  plane. Flux elements passing through the  $a$ – $b$  plane (pancakes) are linked by weak Josephson vortices (strings) which run parallel to the  $a$ – $b$  plane [2]. The FLL therefore adopts a kinked structure. At low temperatures, some success has been obtained in applying this model to the behaviour of YBCO. The flux strings are strongly intrinsically pinned for motion in the  $c$ -axis direction by the layered structure of the superconductor [3, 4]. When the applied field runs exactly parallel to the  $a$ – $b$  planes ‘lock-in’ to a totally string state is expected [5]. The peak observed in  $j_c(\theta, \phi)$  at  $\phi = 0^\circ$  with  $j$  perpendicular to  $B$  [6] is due to this strong intrinsic pinning effect. The angular behaviour of the FLL in YBCO has also been interpreted in

terms of the 3D Ginzburg–Landau (GL) model by introducing anisotropic GL parameters [7].

It has been suggested that in YBCO the FLL exhibits behaviour which changes from 2D to 3D as the field angle,  $\theta$ , is varied [8]. Thus the FLL in  $\text{YBa}_2\text{Cu}_3\text{O}_{7-\delta}$  (YBCO) may exist in one of four configurations [9]. The form of the FLL in an external magnetic field is dependent on three parameters: the ratio  $d/\xi_{ab}$  where  $d$  is the superconducting layer spacing and  $\xi_{ab}$  the  $a$ – $b$  plane GL coherence length, the GL anisotropy parameter  $\varepsilon$  ( $\xi_c = \varepsilon\xi_{ab}$ ) and the angle between the applied  $B$  field and the  $a$ – $b$  plane,  $\theta$ . At large values of  $\theta$  the lattice is rectilinear. However, the shape of a tilted vortex core is anisotropic owing to the anisotropy of the GL coherence lengths  $\xi_{ab}$  and  $\xi_c$ . For  $\theta$  less than some critical value  $\theta_1$  the rectilinear vortex lattice is distorted. The value of  $\theta_1$  is given by  $\tan \theta_1 = d/\xi_{ab}$ . At smaller values of  $\theta$  a kinked vortex lattice forms. The angle at which the ‘kinked’ vortex lattice is fully developed,  $\theta_2$ , is governed by the condition  $\tan \theta_2 = \varepsilon$ . For  $T/T_c = 0$   $\theta_1 = 35^\circ$  and  $\theta_2 = 11^\circ$ . The kinked vortex state is suppressed entirely at a critical temperature  $T_{cr}$  which is 80 K for YBCO.

It has been shown, by measurements on films grown on vicinal-cut substrates, that the pinning force for motion of vortex strings in the  $a$ – $b$  plane is smaller than the pinning force on vortex pancakes [9]. In a  $c$ -axis oriented thin film it is not possible, with an in-plane current, to directly apply a Lorentz force on vortex strings in any direction other than the strongly pinned  $c$ -direction.

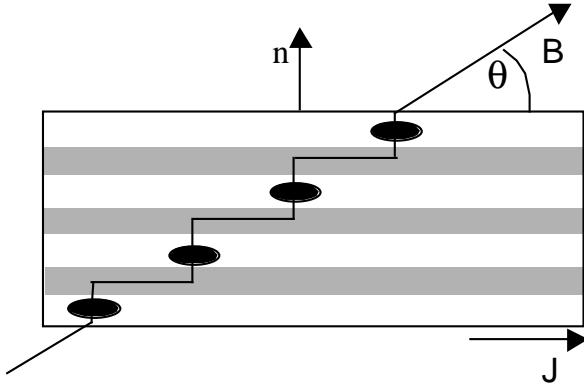


**Figure 1.** A kinked vortex line in a  $c$ -axis film. The angle  $\theta$  is the angle between the  $a$ - $b$  plane and the applied field. The angle  $\phi$  corresponds to rotation of the applied  $B$  field around the normal to the film surface  $n$ . The orientation shown in the diagram corresponds to  $\phi = 90^\circ$ .

Given the complex behaviour of the FLL with variations in  $\phi$ , angular measurements at constant  $\theta$  would be expected to provide a simpler insight into the pinning of the FLL.

Measurements made by keeping  $\theta$  constant and rotating  $\phi$  (see figure 1) have shown that when the pancakes move perpendicularly to the string direction,  $\phi = 90^\circ$ ,  $j_c$  is increased and this increase has been attributed to the vortex strings [10].

In order to gain a good understanding of the properties of the FLL in high-temperature superconductors the present work has concentrated on attempting to determine the flux pinning forces on the string and pancake elements of the FLL.

## 2. Experimental configuration

Angular critical current measurements were performed using a two-axis goniometer mounted in an Oxford Instruments 8 T cryostat [11]. All four experimental parameters are controlled by computer. Temperature stability is accurate to the order of 20 mK. A microstepping motor controller is employed so that, once systematic angular offsets are taken into account, the angular precision attainable is better than  $0.1^\circ$  [12].

The YBCO films studied were deposited by either on-axis dc sputtering or pulsed laser deposition onto  $\text{SrTiO}_3$  substrates. Current tracks were patterned using optical lithography and argon ion milling. Finally Au/Ag contacts were sputtered onto the films to provide contacts for performing four-point resistance measurements.

The experimental geometry used is shown in figure 1. It is important to note that when performing an angular scan in  $\phi$  at constant  $\theta$  the structure of the vortex line remains constant. In the case, as shown, of a kinked vortex line, as  $B$  is rotated the direction of the Lorentz force changes. The force on each flux pancake rotates in the  $a$ - $b$  plane about the normal to the planes  $n$ . The force on the vortex string elements is always in the  $c$ -axis direction. There is no force on the strings due to the component of  $j$  parallel to the flux strings.

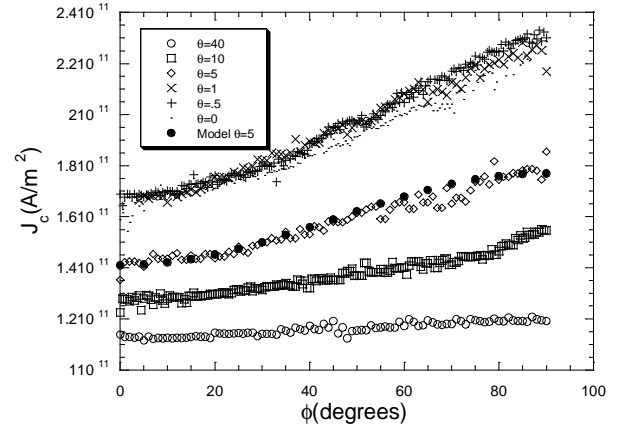


**Figure 2.** Variation of  $j_c$  with  $\phi$  at several values of  $\theta$ ,  $B = 1$  T,  $T = 40$  K.

## 3. Results and discussion

### 3.1. $c$ -Axis films

For the fully kinked FLL ( $\theta < \theta_2$ ) the pinning force per unit length on a vortex line may be resolved into a force on the vortex pancakes which is independent of  $\phi$  and an out-of-plane force on the string vortices which is opposed by the strong intrinsic pinning force. As the intrinsic pinning force is relatively strong only the force on the pancakes produces motion of the vortex line.

The  $\phi$  dependence of the critical current density,  $j_c$ , for small  $\theta$  observed in figure 2 cannot be due to a variation of the pancake pinning force density with  $\phi$  as, averaged over the film, pinning forces in the  $a$ - $b$  plane on flux pancakes may be considered to be isotropic. At  $\phi = 0^\circ$  the pancakes move in the direction of the strings and there is no further contribution to the total pinning force. At  $\phi = 90^\circ$ , in order for the vortex line to move, the flux pancakes must drag the vortex strings in the  $a$ - $b$  plane. It has been previously demonstrated that there is a pinning force acting to oppose such channelling of vortex strings in the  $a$ - $b$  plane [9]. We can therefore postulate the following force balance equation for a kinked vortex line at  $\phi = 90^\circ$ :

$$j_c \Phi_0 D = f_{p,pc} D + f_{p,str} \frac{D}{\tan \theta} \quad (1)$$

where  $f_{p,pc}$  is the pancake pinning force per unit length,  $f_{p,str}$  the string pinning force per unit length for movement in the  $a$ - $b$  plane,  $D$  the film thickness and  $\Phi_0$  the flux quantum.

For intermediate values of  $\phi$  the string pinning force will not act on the entire length of the string, as the string is free to move along itself; the string will only be pinned for motion perpendicular to itself. The force acting on the vortex strings will thus vary as  $\sin \phi$ . In addition the effective cross section of the string will decrease as  $\sin \phi$  increases. This will lead to a change in the pinning force density varying as  $\sin \phi$ . Thus

$$j_c \Phi_0 = f_{p,pc} + f_{p,str} \frac{\sin^2 \phi}{\tan \theta}. \quad (2)$$

The fit to equation (2) is shown in figure 2. From this we can estimate  $f_{p,str} = 8 \times 10^{-6} \text{ N m}^{-1}$  at 40 K and 1 T for the

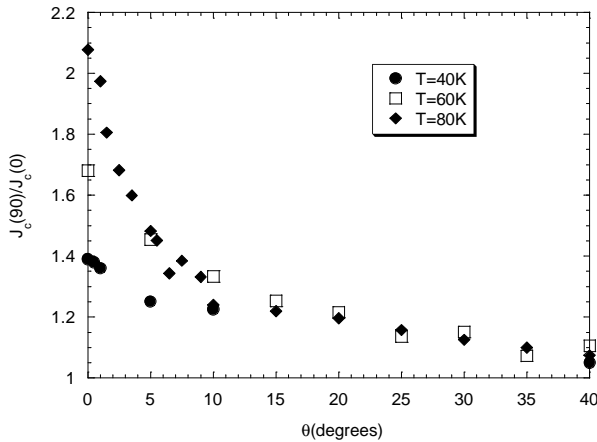


**Figure 3.** The ratio between  $j_c(\phi = 90^\circ)$  and  $j_c(\phi = 0^\circ)$  plotted against  $\theta$  for varying temperature.

film studied. We also obtain, for the pancake pinning force density,  $f_{p,pc} = 3 \times 10^{-4} \text{ N m}^{-1}$ .

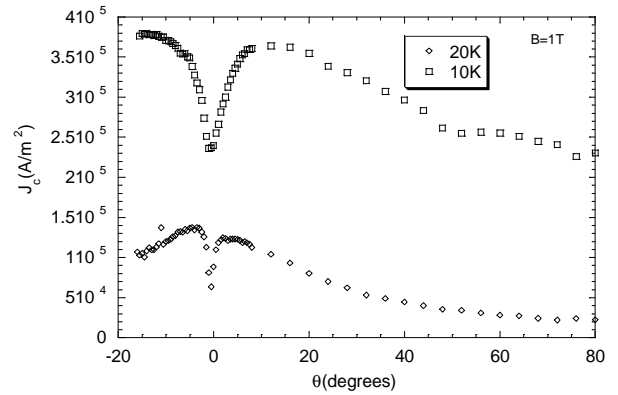
This model is expected to be valid for  $\theta < \theta_2$  except at very small  $\theta$  where the length of vortex string between pancakes is large and flux crossover and cutting will occur. At  $\phi = 90^\circ$  this corresponds to the intrinsic pinning peak at  $\phi = 0$  and the force free peak at  $\phi = 90^\circ$ . This breakdown regime appears to have been reached at  $\theta \sim 1^\circ$  in figure 2. For the rectilinear FLL ( $\theta > \theta_1$ ) a  $\phi$  dependence will also be expected owing to the anisotropy of the vortex cores.

Figure 3 shows the variation in the ratio  $j_c(\phi = 90^\circ)/j_c(\phi = 0^\circ)$  against  $\theta$  at various temperatures. It is useful to compare the  $\theta$  variation in the  $\phi$  dependence with what would be expected from the 3D and 2D models of the FLL. The Kes model [1] states that it is only the  $c$ -axis component of the applied field that is significant; thus 2D behaviour implies no  $\phi$  variation and thus  $j_c(\phi = 90^\circ)/j_c(\phi = 0^\circ)$  is always equal to unity. This is not seen, even at the small values of  $\theta$  where the kinked vortex lattice is expected. This has been explained in terms of string dragging; it would be expected that the deoxygenated YBCO and more anisotropic cuprate materials would show more 2D behaviour. It can also be seen from the plot that as temperature decreases the behaviour more nearly approaches the 2D model. At very small values of  $\theta$  flux cutting occurs which limits the maximum contribution of string dragging to the enhanced  $j_c$  at  $\phi = 90^\circ$ .

As the temperature dependences of both the GL parameters are similar, a weak variation with temperature of the  $\phi$  dependence would be expected in the 3D regime. This is indeed observed for large values of  $\theta$ .

### 3.2. Vicinal films

A vicinal substrate has the (001) planes running at an angle to its surface. Measurements using vicinal films allow behaviour obscured by the high symmetry of the experimental configuration when using  $c$ -axis films to be studied. It has been shown that with  $B$  parallel to the  $a$ - $b$  planes, if there is a component of the Lorentz force that is directed along the  $a$ - $b$  planes, string channelling occurs. This results in a local minimum in  $j_c$  at  $\phi = 0$ .



**Figure 4.** The string channelling effect in deoxygenated vicinal YBCO ( $T_c = 65 \text{ K}$ ,  $B = 1 \text{ T}$ ).

Figure 4 shows measurements made using a deoxygenated  $6^\circ$  vicinal film ( $T_c = 65 \text{ K}$ ). The relative magnitude of the minimum is much larger. This indicates that the pinning of string elements in deoxygenated vicinal films is much weaker, in this case by at least 2 orders of magnitude.

The string pinning force per unit string length,  $f_{p,str}$ , is given by the following equation, where  $\theta_c$  is the angle of the vicinal cut [9]:

$$f_{p,str} = j_{c,str} \Phi_0 \sin \theta_c. \quad (3)$$

Using equation (3) it is possible to estimate the value of the string pinning force density in the vicinal films studied. A value for  $f_{p,str}$  of  $8 \times 10^{-6} \text{ N m}^{-1}$  may be taken from measurements on fully oxygenated vicinal films [9]. This is in agreement with the value obtained at  $T = 40 \text{ K}$  from the analysis of string dragging in a  $c$ -axis film above. An equivalent value at  $T = 20 \text{ K}$  for a deoxygenated film from figure 4 is  $8 \times 10^{-8} \text{ N m}^{-1}$ . It is not possible, however, to eliminate the possibility of residual pancakes even at the lock-in angle. The string pinning force may, therefore, be weaker than calculated.

### 4. Conclusion

High-resolution angular measurements of the variation in  $j_c$  as the angle  $\phi$  is varied in YBCO have been performed. For the kinked FLL the enhancement in  $j_c$  at  $\phi = 90^\circ$  has been interpreted in terms of dragging of vortex strings by vortex pancakes. A simple model to describe the  $\phi$  dependence of the pinning force for kinked vortex lines in  $c$ -axis YBCO has been developed from this interpretation.

The magnitude of the pinning of vortex strings for motion in the  $a$ - $b$  plane measured on  $c$ -axis YBCO has been compared with that previously measured using films grown on vicinal-cut substrates. The values obtained from these two different experimental observations are in good agreement.

The change observed in the  $\phi$  dependence as the field angle,  $\theta$ , changes is attributed to the transition from a rectilinear regime through a kinked regime with vortex string dragging enhancing  $j_c$  to, at very small  $\theta$ , a flux-cutting regime where no further enhancement of  $j_c$  is possible. This variation has been interpreted in terms of models of the  $\theta$  dependence of the structure of the FLL.

## Acknowledgments

This work was partly supported by the European Community TMR network 'SUPERCURRENT' under contract no CT98-0189 and by the Engineering and Physical Sciences Research Council.

## References

- [1] Kes P H, Aarts J, Vinokur V M and van der Beek C J 1990 *Phys. Rev. Lett.* **64** 1063–6
- [2] Clem J R 1991 *Phys. Rev. B* **43** (10 Part A) 7837–46
- [3] Tachiki M and Takahashi S 1989 *Solid State Commun.* **70** 291–5
- [4] Tachiki M, Takahashi S and Sunaga K 1993 *Phys. Rev. B* **47** 6095–105
- [5] Feinberg D and Villard C 1990 *Phys. Rev. Lett.* **65** 919–22
- [6] Roas B L, Schultz L and Saemannishenko G 1990 *Phys. Rev. Lett.* **64** 479
- [7] Blatter G, Geshkenbein V B and Larkin A I 1992 *Phys. Rev. Lett.* **68** 875–8
- [8] Blatter G, Feigelman M V, Geshkenbein V B, Larkin A I and Vinokur V M 1994 *Rev. Mod. Phys.* **66** 1125–388
- [9] Berghuis P, DiBartolomeo E, Wagner G A and Evetts J E 1997 *Phys. Rev. Lett.* **79** 2332–5
- [10] Nishizaki T, Ichikawa F, Fukami T, Aomine T, Terashima T and Bando Y 1993 *Physica C* **204** 305–14
- [11] Herzog R and Evetts J E 1994 *Rev. Sci. Instrum.* **65** 3574–6
- [12] Herzog R 1997 Critical currents in YBCO thin films *Thesis* University of Cambridge, Cambridge